Natural Resources Canada | Ressources naturelles Canada

GEOLOGICAL SURVEY OF CANADA
OPEN FILE 8349

Iron-oxide and alkali-calcic alteration, skarn, and epithermal mineralizing systems of the Grenville Province: the Bondy gneiss complex in the Central Metasedimentary Belt of Quebec as a case example — a field trip to the 14th Society for Geology Applied to Mineral Deposits (SGA) biennial meeting

L. Corriveau, O. Blein, F. Gervais, P.H. Trapy, S. De Souza, and D. Fafard

2018

Canada

GEOLOGICAL SURVEY OF CANADA
OPEN FILE 8349

Iron-oxide and alkali-calcic alteration, skarn, and epithermal mineralizing systems of the Grenville Province: the Bondy gneiss complex in the Central Metasedimentary Belt of Quebec as a case example — a field trip to the 14th Society for Geology Applied to Mineral Deposits (SGA) biennial meeting

L. Corriveau[1], O. Blein[2], F. Gervais[3], P.H. Trapy[3], S. De Souza[4], and D. Fafard[4]

[1] Geological Survey of Canada, Natural Resources Canada, 490 de la Couronne, Québec, Quebec G1K 9A9 Canada
[2] BRGM, Georessources Division, 3, avenue Claude-Guillemin, 45060 Orléans cedex 2 – France
[3] Polytechnique Montréal, Department of Civil, Geological and Mining Engineering, 2500, chemin de Polytechnique, Montréal, Quebec H3T 1J4 Canada
[4] Département des sciences de la Terre et de l'atmosphère, Université du Québec à Montréal, 201, avenue du Président-Kennedy, Montréal, Quebec H2X 3Y7 Canada

2018

Permanent link: https://doi.org/10.4095/311230
This publication is available for free download through GEOSCAN (http://geoscan.nrcan.gc.ca/).

Recommended citation

Corriveau, L., Blein, O., Gervais, F., Trapy, P.H., De Souza, S., and Fafard, D., 2018. Iron-oxide and alkali-calcic alteration, skarn, and epithermal mineralizing systems of the Grenville Province: the Bondy gneiss complex in the Central Metasedimentary Belt of Quebec as a case example — a field trip to the 14th Society for Geology Applied to Mineral Deposits (SGA) biennial meeting; Geological Survey of Canada, Open File 8349, 136 p. https://doi.org/10.4095/311230

Publications in this series have not been edited; they are released as submitted by the author.

14th SGA Biennial Meeting
Quebec City, Canada
August 20-23, 2017

MINERAL RESOURCES TO DISCOVER

EXCURSION GUIDEBOOK FT-02

Iron-oxide and alkali-calcic alteration, skarn, and epithermal mineralizing systems of the Grenville Province: the Bondy gneiss complex in the Central Metasedimentary Belt of Quebec as a case example

Louise Corriveau, Olivier Blein, Félix Gervais, Pierre-Henry Trapy, Stéphane De Souza, and David Fafard

SGA QUÉBEC 2017 FIELD TRIPS COMMITTEE

Chair
Michel Houlé

Co-chair
Anne-Aurélie Sappin

Guidebook Publication
Anne-Aurélie Sappin
Michel Houlé
Claude Dion
André Tremblay

SGA QUÉBEC 2017 FIELD TRIP FT-02 GRENVILLE

Organisors
Louise Corriveau
Félix Gervais
Olivier Blein
Alain Cayer
Jocelyn Pelletier

Leader
Louise Corriveau

SGA QUÉBEC 2017 / FT-02 Grenville guidebook

Cover photo: Amphibolite and garnetite within the Breccia Trail mineral occurrence, Bondy gneiss complex, Grenville Province, Quebec.

Photo: *O. Blein (BRGM)*

Table of Contents

Foreword

This geological field trip guidebook describes the iron oxide and alkali-calcic alteration system, and associated epithermal, IOCG and affiliated mineralization of the Bondy gneiss complex in the southwestern Grenville Province (Québec, Canada). Additional transects across its host terrane, the Central Metasedimentary Belt, and the adjacent Morin Terrane provide an overview of the tectono-magmatic events and styles of magma emplacement in the region. Field attributes of the complex are those of metasomatic systems metamorphosed to granulite facies. Mineral parageneses and rock types markedly contrast with non-metamorphosed IOCG deposits, the most significant difference being the development of widespread garnetites, and orthopyroxene, garnet and biotite-rich gneisses at the expense of magnetite-rich alteration types. Mineralization rarely leads to gossan on outcrops. Consequently, we emphasize the field protocols for the identification and exploration of such metamorphosed hydrothermal systems and the genetic linkages among the varied alteration types and styles of mineralization. Thousands of xenoliths in a lamprophyre dyke also offer a 3D perspective on the Grenvillian lithosphere. The outcrops described are show cased in public awareness brochures and are the object of geological rallies in the Papineau-Labelle wildlife reserve. Enjoy!

Cette excursion géologique porte sur le système minéralisateur à oxydes de fer et altération alcali-calcique du complexe gneissique de Bondy et ses indices de type IOCG et épithermaux du sud-ouest de la province de Grenville (Québec, Canada). Des coupes additionelles à travers son terrane hôte, la ceinture métasédimentaire centrale, et le terrane de Morin plus à l'est en cadrent le contexte tectono-magmatique et les divers styles de mise en place de magmas. Les attributs de terrain du complexe sont ceux de systèmes métasomatiques métamorphisés au faciès des granulites. Ses paragenèses minérales et ses types de roches contrastent nettement avec ceux des gîtes IOCG non métamorphisés de par le développement de grenatites et de gneiss riches en orthopyroxène, grenat ou biotite au détriment des types d'altération usuelle riche en magnétite. Comme les affleurements minéralisés sont rarement rouillés, une attention particulière est portée aux protocoles de terrain pour identifier et explorer ces systèmes et les liens génétiques entre leurs divers types d'altération et de minéralisation. Des milliers de xénolites dans un dyke de lamprophyre offrent également une perspective 3D sur la lithosphère grenvillienne. Les affleurements décrits font l'objet de brochures de vulgarisation scientifique et de rallyes géologiques dans la réserve faunique Papineau-Labelle. Amusez-vous!

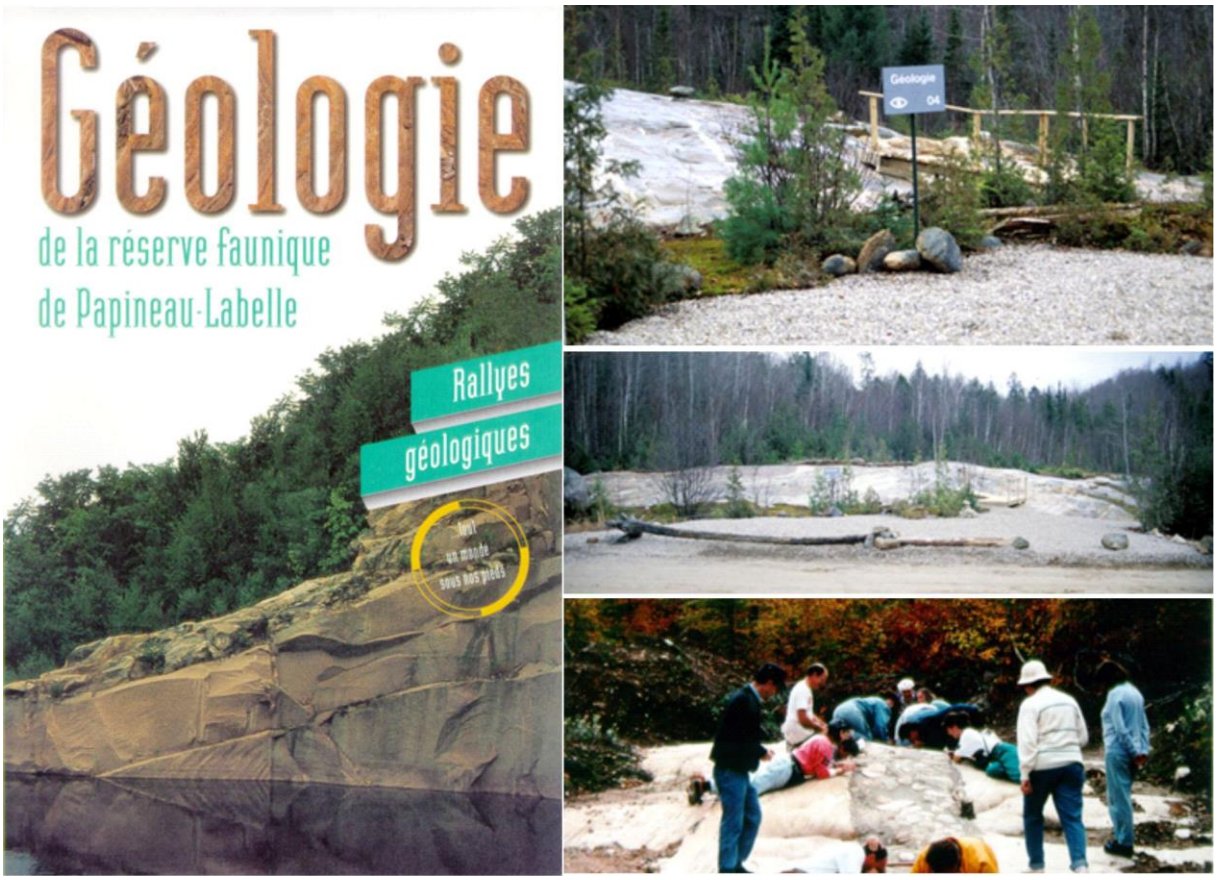

Programme

Day 1, Tuesday August 15th – Miller graphite and syntectonic magma emplacement of the Chevreuil intrusive suite in the Quartzite domain and Nominingue-Chénéville deformation corridor.

8H00: Departure at 8:00 from Quebec City.
11H00: Miller graphite deposit and lunch.
13H00: Departure for Lake Chevreuil west of Duhamel.
13H30: Outcrops along Lake Chevreuil road: syntectonic subvertical sheet intrusions (monzonite, diorite), Nominingue-Chénéville deformation zone, and zones of magma mingling, country rock assimilation and formation of skarns.
15H00: Outcrop along road 34 in the Papineau-Labelle wildlife reserve. Typical outcrop of the Quartzite domain with polyphase deformation prior to and concurrently with emplacement of the Chevreuil intrusive suite. Overview of regional geology.
16H00: Departure for Mont-Laurier.

Day 2, Wednesday August 16th –Bondy gneiss complex (east sector) and Lac Harvey showing: Alteration mapping as vector to mineralization.

8H00: Departure from Mont-Laurier
8H30: Papineau-Labelle wildlife reserve, driving along Road 3 as far as Lac Michaud road. Turn left and follow the road until you reach Stop 1.
9H00: Outcrops along the main road: metamorphosed metasomatized mafic to felsic rocks *(hydrothermally altered tuffs*).
14H30: Short walk to a garnetite unit with magnetite and chalcopyrite (*argillic or sericitic alteration of a K-Fe altered unit*) and associated orthopyroxene-biotite gneiss (*K-Fe altered unit*) and layered amphibolite (*metavolcanic rocks*). The area may have cameras installed by hunters.
15H30: Walk-back to the car and return to Road 3, turn right on Road 3 and then right again unto the road for Lac Harvey and the Lac Harvey prospect: biotite-rich garnetites with magnetite and chalcopyrite and associated orthopyroxene-biotite gneiss (*varieties of K-Fe altered unit*) and layered amphibolite (*metavolcanic rocks*).
17H00: Return to Mont-Laurier.

Day 3, Thursday August 17th –Bondy gneiss complex (west sector), Rivard dyke and if time permit, Kar-Ha-Kon intrusion: field attributes and lithogeochemical signature of metamorphosed iron oxide alkali-calcic alteration systems and associated mineralization, nature of the lithosphere at 1.07 Ga, style of emplacement of K-alkaline magmas and vertically layered mafic intrusions.

8H00: Departure from Mont-Laurier
8H30: Arrival at the Papineau-Labelle wildlife reserve and drive along Road 3, including on top of an esker, turning on road for lakes Coindrelle etc. keeping on the road that reach Lake Clouthier.
9H30: Driving by a quartzite cut by an amphibolite dyke and short stop at quartzofeldspathic and aluminous gneisses at the margin of the Bondy gneiss complex. Northeast is a tourmalinite unit with kornerupine-bearing veins among aluminous gneisses (access uncertain).
10H00: Driving south to intersection for Lake Clouthier among Bondy gneisses and a layered garnetiferous amphibolite (*mafic metavolcanic*).
10H15: White Na-Mg-Al gneiss with kornerupine, tourmaline, orthopyroxene, cordierite and phlogopite among plagioclase dominant gneisses (*chloritized HT Ca-Fe alteration facies among albitites*). Head back north for the intersection with the old road to Lake Clouthier.
11H00: Three hours walk and outcrop observation along a 2.2 km trail: Na-Mg-Al gneiss, sillimanite, biotite, garnet, cordierite, orthopyroxene gneisses (*HT to LT K-Fe alteration facies and phyllic to argillic alteration*), laminated quartzofeldspathic gneiss (*K-altered rhyolite*).
14H30: The Rivard dyke
15H30: Return to road 3, turn left for the Kar-Ha-Kon vertically layered intrusion.
17H00: Return to Mont-Laurier.

Day 4 - Friday August 18th

8H00: Departure from Mont-Laurier
8H05: Marble tectonite with calc-silicate and mafic enclaves.
9H30: Summary of regional geology near Gand Remous.
12H00: Lacoste gneisses.
13H00: Labelle deformation zone.
14H30: The Morin anorthosite.
16H30: End of fieldtrip.

Health, safety and access

Most of the fieldtrip sites are located in the beautiful Papineau-Labelle wildlife reserve, within a two-hour drive from Montréal or Ottawa (Figs. 1, 2). The Bondy gneiss complex and most sites visited are in the less accessible and most nondeveloped parts of the reserve. The sites are accessible by trucks and four-wheel drive along dirt roads, and via short walks along former, overgrown, roads. They are less than two hours travel time from a hospital or medical facility under normal travelling conditions by cars including our walks along 2.2 km trail(s) (4.4 km return).

Versions of this fieldtrip have been run for the Friends of the Grenville, the Geological Association of Canada and Mineralogical Association of Canada, and graduate students at INRS and Laval University since 1995. As for any geological field work, **participants should be aware that the fieldtrip can present significant safety hazards,** including those stemming from relative remoteness, deteriorating road and fieldtrip conditions due to inclement weather, branches poking the eyes or falling dead trees, slips and falls on uneven potentially slippery terrain, falling or rolling rocks, insect bites or stings and potential ensuing allergies, wildlife encounters and flying rock chips from hammering to name a few.

Responsibilities. Fieldtrip preparation was as thorough as possible (e.g. driving the roads, sweeping outcrops and marking trails). During the trip, leaders will take all reasonable care for ensuring the safety of the participants. However, each participant is responsible for acting in a manner that is safe for themselves and their co-participants and must be vigilant and self-reliant in terms of safety awareness. Participant responsibility includes

1. advising one of the organisors if there is a need to be away from the group momentarily or if you feel exhausted or ill,
2. using the appropriate personal protective equipment and field gear,
3. staying hydrated, covered (hat, long sleeves, insect repellent, sun screen; creek water is unsafe),
4. attending safety meetings
5. complying with departure times in the morning and at each stop.

Accidents may require of every one to deal with difficult situations. Considerable degree of vigilance and a good health is required to be able to safely participate in the trip. Additional risks may stem from foreign participants inexperience of Canadian bush, road conditions and wildlife. During the trip, leaders may have to take decisions based on particular local conditions and arrangements. In all such cases, the safety and health of all participants and leaders will be of paramount consideration. Impaired or dangerous to one self or others, participants may not be allowed to join in the fieldtrip.

Road conditions can be at time difficult. Conditions can vary along a single road and can change rapidly due to inclement weather. Trees can fall unexpectedly blocking your way in or your way out. Heavy rain can lead to bridge collapses, ravines and loose rocks and boulders in the middle of the road. Be prepared accordingly, you may have to move a very large tree out of the way or fill holes with gravel to get back. Ultimately, access to fieldtrip sites may not be possible.

Logging is active in the reserve and no car announces the arrival of a truck as is done is some countries. One must remain vigilant for fast moving logging trucks and cars (as well as for deers that abound in the reserve).

Wildlife abounds. Bears, deers, moose, wolfs are most common. Please do not forget that all these animals can be dangerous especially if they feel threatened (i.e. if you behave as if they were pets or if you think that having a selfies with them in the background is a necessity, endangering your life, that of others, and the life of the animal). Mosquitoes, black flies, no-see-ums and deer flies can be numerous. They will be most annoying if you were dark colour clothes and perfume. Be aware that non-Canadians can be particularly sensitive to local insects with unexpected allergic reactions. Please refer to the Papineau-Labelle wildlife reserve web site for basic health and safety measures.

Outcrops along former roads are becoming overgrown with lichens, moss, bushes and trees. They may be difficult to find. They are flat or very irregular, partly covered by lichen or sand and gravel, and with very hard rocks. Wet or dry, they can be slippery. Chips during sampling can be a safety hazard. Please use all precautions required by your varied activities. In addition, some of the outcrops are part of a geological rally for the visitors of the wildlife reserve. We would be grateful if you could refrain from sampling outside of areas planned to this effect in order to leave the outcrops as nice as possible and avoid accidents. The Geological Survey of Canada has a large sample collection that can be borrowed for research. Thank you for your cooperation.

Appropriate field gear. Participants must bring: comfortable hiking boots, a light daypack for hiking (25l or less), their medication (if any), appropriate clothing (e.g. lightweight PALE COLOUR, long-sleeve shirt and pants, socks appropriate for hiking), absolutely waterproof jacket and rain pants (Gore-Tex or equivalent), personal sunscreen, at least one non-cotton (wool/fleece, NOT down) insulating layer, a hat, sunscreen, insect repellent, safety glasses, and work gloves. A mosquito net, a whistle and telescoping trekking poles can also be useful.

Papineau-Labelle wildlife reserve. The reserve is crown land managed by the SEPAQ where the concept of sustainable development applies to all activities. Hence one can camp, fish, observe wildlife, hunt, walk, and pick berries as well as harvest timber (logging) and conduct mineral exploration and mining. All these varied activities are regulated so is access. Restrictions may apply and great opportunities arise all time in the reserve, please make sure

to visit the reserve web site for up-dates prior to making your plans and accessing the land (see http://www.sepaq.com/rf/pal/). In addition, mineral claims may be active in the area. Please comply with regulations. Don't forget to bring the Papineau-Labelle wildlife reserve road map and again please beware when driving in the reserve, deers, mooses and logging trucks abound. Lodging is available in the wildlife reserve and can be reserved at http://www.sepaq.com/rf/pal/. The reserve is an ideal setting to bring large groups of students as cottages hosting 15 to 20 people are available and relatively inexpensive (Fig. 2). You can also decide to answer the geo-quiz of our geological rallies in Tremblay et al. (1993, 1996) and visits our geosites (Fig. 1).

Figure 1. The public awareness geological sites were realized by the Centre d'interprétation de la Géologie du Grenville in collaboration with the INRS project *Si la Terre m'était contée* (Tremblay et al. 1993, 1996).

Figure 2. The view at the Lake Sept-Frères; our favourite cottage for graduate students and Friends of Grenville fieldtrips.

Acknowledgements

The authors are greatly indebted to Kintavar Exploration Inc. and Canada Carbon for their enthusiastic logistical support of this fieldtrip, and to Canada Carbon and Richmond Minerals for permission to access and publish information on their respective properties (Miller graphite deposit; Bondy gneiss complex EM1, EM2, Lac Harvey, Bing and Breccia Trail showings). An internal GSC review of this field guide by Pedro Acosta-Góngora is greatly appreciated.

Regional data for this trip was largely acquired in the 1990s through a Geological Survey of Canada regional mapping project and an Industrial Partnership Program project with KWG Resources Inc. Many Ph.D. and M.Sc. theses were attached to these projects and those that followed through a DIVEX-funded project to Louise Corriveau and a Richmond Minerals-funded project to Lyal Harris. We acknowledge the very hard work and the novel research of these graduate students. Our work and that of our various collaborators build upon the previous mapping and research undertaken in the area. These are acknowledged through citation in the text and listed in the references.

The authors also acknowledge

1. Alain Cayer, Jocelyn Pelletier, Steven Lauzier, David Fafard, Pedro Acosta-Góngora, Nicolas-Piette Lauzière and Roman Hanes for their logistical assistance prior to and during the trip,
2. Anita Demers and Joé Bélanger for their in depth knowledge of the Papineau-Labelle wildlife reserve,
3. Michel Houlé and Anne-Aurélie Sappin as chairs of the SGA 2017 fieldtrip committee,
4. Valérie Bécu as SGA 2017 logistical coordinator,
5. Marco Boutin for his GIS assistance, and
6. Nicolas-Piette-Lauzière, Christopher Lambert and Hartwig Frimmel for some photos included in this guidebook.

We also thank the logging company active in the reserve for upgrading the road to Lake Clouthier as we were preparing the trip. They made it possible for us to drive through difficult sections and reach outcrops for this fieldtrip.

Canada Carbon Inc. and SL exploration granted access to the Miller deposit and logistical support for fieldwork to S. De Souza and his students. Jean David (Ministère de l'Énergie et des Ressources naturelles du Québec) is sincerely acknowledged for conducting the LA-ICP-MS U-Pb zircon analyses at the GEOTOP radiogenic isotopes laboratory and for providing the associated geochronological data for the Miller deposit. Jean-François Hélie and Agnieszka Adamowicz from the GEOTOP kindly helped with the acquisition of the $\delta^{13}C$ values for the Miller deposit. De Souza's research was subsidized in part by Mitacs. Claudie Lefebvre-Fortier provided assistance for fieldwork during an NSERC undergraduate research internship.

We are also in debt to our mentors and our colleagues, Tony Davidson, Otto van Breemen, Léopold Nadeau and Lyal Harris, as well as to all Friends of the Grenville for sharing their knowledge with us through our undergraduate and graduate studies and subsequently through our career. We are also in debt to Sunil Gandhi, a pioneer on the identification and characterization of prospective IOCG settings across Canada, and to Gilles Allard and Michel Gauthier who have traced the path for the study of metamorphosed hydrothermal systems in the Grenville Province.

Fieldtrips shape our understanding of geology and is one of the most effective mean to transfer knowledge among colleagues including among colleagues within a same organization. None of the many Friends of Grenville and GAC-MAC fieldtrips that made us who we are would have happened without the dedication of our former fieldtrip leaders. They prepared these trips adding weeks of volunteer work to their very busy schedules in a very altruist way. Those among them who worked for surveys could count on support from their managers. For this fieldtrip, the first author wants to acknowledge Yves Michaud, Kathleen Lauzière, Valérie Bécu and Patrick Mercier-Langevin who helped us make this fieldtrip happen beyond the call of duty. Research scientist dedication and ability to share their knowledge, and manager vision and thrust were paramount to the Geological Survey of Canada celebrating its 175th anniversary this year.

Collaboration between Canadian federal, provincial and territorial surveys, academia and private sector is a must for the diversification of exploration in Canada. Key ingredients made this fieldtrip of the Society of Geology applied to mineral deposits possible:

1. The ability to acquire extensive geological information on the IOCG districts of the Great Bear magmatic zone through extensive collaboration, including with the Northwest Territories Geological Survey, Fortune Minerals, First Nations governments and A.H. Mumin.
2. The means to develop effective mapping and exploration tools and geological models for IOCG deposits and apply them to high-grade metamorphic terranes of the Grenville Province through extensive national and international collaborations including with Patrick Williams.
3. The support of private sector through their interest in our work, in kind contributions to our projects including Richmond Minerals, and help in organizing this fieldtrip. For the latter we thank again Kintavar Inc.

Extended abstract

The 2017 Society for Geology Applied to Mineral Deposits (SGA) FT-02 field trip is taking place in the east-central part of the Central Metasedimentary Belt of Quebec, Grenville Orogen. The trip is an opportunity to ponder the nature of gneiss complexes in the belt, the pathways and styles of magma emplacement at deep crustal levels, the development of skarn, magma mingling and assimilation zones, and the origin of graphite deposits. The field trip also provides an overview of the architecture and Grenvillian and pre-Grenvillian tectono-magmatic evolution of the Central Metasedimentary Belt in Quebec (Grenville Province) through sedimentation, volcanism, hydrothermal activity, magma emplacement, metamorphism, and deformation. It illustrates the rheological contrast across the different domains of Mont-Laurier area of the Central Metasedimentary Belt as recorded by styles of magma emplacement and extent of deformation of dyke swarms and intrusions. Participants will also see for themselves, in a puzzle mode, what the lower lithosphere looked like 1070 m.y. ago. On the agenda are:

- the cupriferous hydrothermal system of the Bondy gneiss complex,
- the Rivard minette dyke and its xenoliths,
- the sheet like monzonite and diorite intrusions of the Nomininguе-Chénéville deformation zone, their skarn and zones of country rock assimilation and magma mingling;
- the Quartzite domain (eastern half of the CMB-Q),
- the marble typical of the western Marble domain of the CMB-Q and of the Morin Terrane,
- the Labelle shear zone that border the CMB-Q with the Morin Terrane,
- the Morin anorthosite, and
- the Miller graphite prospect.

Additional sites or alternative ones if a road is closed are:

- vertically layered mafic intrusions,
- the Rolleau K-alkaline ultramafic stock.

The Mont-Laurier area comprises two main metasedimentary domains dominated respectively by marble and quartzite. These overlie a series of granulite-facies gneiss complexes that includes the 1.38-1.35 Ga volcano-plutonic Bondy gneiss complex regionally metasomatized prior to granulite facies metamorphism at 1.2 Ga. The gneiss complexes are interpreted as juvenile island-arc to back-arc components built on a thinned Laurentian margin substrate. Northward these gneiss complexes record a continental arc setting.

The Bondy gneiss complex exhibits an exceptional array of metasomatic rocks metamorphosed to granulite facies as well as several mineral occurrences and prospects with a large realm of metal associations. Previous to our work, such quartzofeldspathic gneiss complexes in the region were mapped as an undifferentiated assemblage of charnockitic and related intrusive rocks, granulites, and quartzofeldspathic gneisses of uncertain origin. They were considered sterile. This field trip provides an overview of the volcanic host and the metasomatic rocks at granulite facies. Road conditions make it difficult to access the main mineralization sites (i.e. the Breccia trail, EM1, etc.). In any case, the complex remains significantly underexplored.

Field attributes of this iron oxide and alkali-calcic hydrothermal system, its epithermal alteration zones, IOCG and affiliated skarn and epithermal mineralization metamorphosed to granulite facies markedly contrast with non-metamorphosed analogues in terms of mineral parageneses. The most significant difference is the development of widespread garnetites, and biotite, garnet and orthopyroxene-rich gneisses at the expense of magnetite-rich alteration types. The destabilization of magnetite and hematite through metamorphic reactions sensitive to oxygen fugacity impacts the effectiveness of geophysical exploration in that the large magnetic anomalies typical of IOA and IOCG deposits may not occur at granulite facies. In contrast, geochemical tools will remain effective. To this effect, the composition of metamorphosed metasomatic rocks of the Bondy gneiss complex are compared with those of iron oxide alkali-calcic alteration systems and their deposits from the Great Bear magmatic zone and the Andes. This comparison contributes to a better understanding of the genetic linkages among the varied alteration types and styles of mineralization in such mineral systems, and the field protocols for their identification and exploration once metamorphosed at high grade. A particular emphasis is put on parageneses and textures of the gneisses and their leucosomes. The latter are generally not deformed and both the gneiss and their leucosomes are sharply cut by non-deformed mafic dykes. Premetamorphic mafic intrusions and intrusive breccias now at granulite facies are also visited.

Vertically layered mafic intrusions, mafic-to-felsic sheets of the Chevreuil intrusive suite (1.17-1.16 Ga) and coeval mafic and mafic-felsic dykes with magma-mingling textures intrude the gneiss complexes and the marble and quartzite domains across the entire CMB-Q including along its northern boundary. All ages obtained on intrusions and dykes of this suite fall within the 1.17-1.16 Ga age range (Corriveau and van Breemen 2000; Corriveau 2013; Davis and Nantel 2016). One monzodiorite dated at 1189.7±1.1 Ma was included wihtint he Chevreuil suite (Davis and Nantel 2010). The latter is foliated and recristallized and may be more representative of a suite of mafic rocks that have been emplaced after peak metamorphism but metamorphosed to amphibolite facies. These mafic rocks predate the Chevreuil suite.

The vertically layered mafic intrusions of the Chevreuil suite contain local nickel-copper mineralization. These intrusions are commonly emplaced at fault intersections of deformation zones. The faults are interpreted as magma conduits that tapped directly mafic reservoirs in the lower

crust during renewed orogenesis at 1.17 Ga following granulite facies metamorphism at 1.19 Ga (Corriveau and van Breemen 2000; Corriveau 2013). Mafic magmas show no field evidence of mixing with intermediate to felsic magmas. In contrast, along the main deformation corridors of the belt are series of steeply dipping sheet-like intrusions of monzonite, diorite and locally gabbro with abundant zones of mafic-felsic magma mixing and mingling. Some sheets intruded marble units and led to the formation of skarns and to extensive country-rock assimilation. Magma emplacement was syntectonic and the intrusive rocks commonly appear gneissic. This gneissic fabric is an artefact of magma flow, crystal segregation and subsolidus deformation. These sheets and coeval mafic and felsic dykes cut the gneisses and are not migmatized. Host gneisses have deformed leucosomes and an amphibolite-facies metamorphic imprint. They are interpreted as having been pervasively deformed and retrograde to amphibolite facies based on regional geology and relics of high-temperature conditions (Boggs and Corriveau 2004). The Chevreuil suite is spatially distinct but coeval with the onset of the Morin anorthosite-mangerite-charnockite suite (1.165-1.135 Ga) that led to the emplacement of the Morin anorthosite to the east of the Central Metasedimentary Belt. Volume of magmas and styles of magma emplacement of both suites are significantly distinct.

The Kensington-Skootamatta potassic alkaline suite (1.09-1.07 Ga) consists of ultramafic to felsic nested plutons and minette lamprophyre dykes that record magma ascent by fracture propagation along dykes and entrapment by marble to form plutons. In the Rivard dyke, repeated delamination of wall rocks during magma ascent resulted in the incorporation of xenoliths that reveal the nature and composition of the lithosphere at 1.07 Ga from at least a depth of 70 km. In addition to recording the presence of Chevreuil intrusive suite and typical gneisses of the region at depth, the xenoliths provide evidence for abundant quartzite interpreted to be older than 1.4 Ga, massive pyrrhotite, high-temperature mylonites and potassic-alkaline ultramafic units.

The integration of xenolith, surface geology, and seismic data provides 4D mapping elements that were used to propose an evolutionary model of the Central Metasedimentary Belt in Quebec.

Notes

Chapter 1: Introduction

Geological processes leave a field record laden with mappable attributes useful to interpret the nature and evolution of geological systems with a reasonable degree of confidence. Optimizing field mapping tools significantly enlarge prognostication capabilities and toolboxes for efficient geological mapping and exploration. This guidebook reviews the geology of the northern half of the Central Metasedimentary Belt in the southwest Grenville Province and highlights some of its key outcrops. In particular, it reviews the geology of the Mont-Laurier area in the province of Québec, Canada.

The visited area transects one of the large supracrustal belts in the Grenville Province. The belt was metamorphosed to granulite facies at 1.19 Ga and subsequently reactivated at amphibolite facies. Crustal domains (marble/quartzite/ felsic gneiss) reacted differently to successive orogeneses preserving a record of each event. The strain windows are tracked down through the style of emplacement and extent of deformation of 1.165 Ga, 1.08 Ga and 1.06 Ga intrusive suites. Extent of deformation delineates areas that escaped deformation and those that were reactivated after 1.19 Ga. The belt also hosts a well exposed volcanic-hosted polymetallic iron oxide and alkali-calcic alteration system that evolved to epithermal mineralization prior to being metamorphosed to granulite facies. Records of magma emplacement in deformation zones at 1.17-1.16 Ga and nature of the lithosphere at 1.07 Ga are also well exposed. Collectively the geology of the discrete orogenic time windows, the variety of geological and metallogenic settings, the abundant ultramafic to felsic, mantle (?) and lower crust xenoliths in a lamprophyre dyke, the deep level of erosion, and the proximity to large urban centres (Montréal and Ottawa) make the Mont-Laurier area a superb and easily accessible outdoor laboratory to study deep crustal processes and continental tectonics.

The geology described in this guidebook helps appreciate mapping and exploration challenges in high-grade metamorphic terranes and understand how under-explored the Grenville Province is. Chapter 2 addresses the need for adapted megascopic criteria to recognize hydrothermal systems at granulite facies and reviews some key elements of the mapping protocols that were used to map the area. It also reviews the basis for alteration mapping as a vector to mineralization within iron oxide alkali-calcic alteration systems and the model it is based upon. More information is provided in Corriveau (2013), Corriveau and Spry (2014), and Bonnet and Corriveau (2007a, b). The chapter sets the stage for understanding the why and how:

1. basic field observation can lead to the recognition of metamorphosed hydrothermal systems,
2. mineral parageneses of metamorphosed alteration zones provide in situ information on chemical changes that vector to mineralization,
3. ore deposit models developed for low to medium-grade metamorphic terranes is applied to high-grade metamorphic terranes.

Chapter 3 summarizes the geology and the tectonic evolution of the Central Metasedimentary Belt in Québec, taking excerpts from Corriveau (2013) bulletin of the Geological Survey of Canada (GSC). The bulletin furthers the description of observation for the evolution and 4D architecture of the belt provided in Corriveau and Morin (2000) and Corriveau and van Breemen (2000). It also provides a complete list of reference for the area. This guidebook (Chapters 4 to 10) further describes and illustrates the lithodemic units and the structural geology of the belt and is met to complement the bulletin. The information is in part based on new outcrops cleaned after the original GSC project.

Outcrops described herein also illustrate a great variety of styles of magma emplacement, including sheet-like intrusions in deformation zones, vertically-layered mafic intrusion, and zones of magma mingling, country rock assimilation and formation of skarns. We combine information on styles of magma emplacement and extent of subsequent deformation to highlight that recognition of strain partitioning at regional scale helps discover tectonic windows that escaped repeated reactivation during the series of orogeneses that affected the Grenville Province. Such windows not only provide a record of early granulite-facies metamorphism but they also indicate that mineralization zones within the Bondy gneiss complex largely escaped repeated remobilization. The trip thus provides participants with a unique opportunity to walk across such a mineralized system from paleo-depth to paleo-surface but at granulite facies and to see its regional context.

Eighty percent of the world Precambrian terranes are metamorphosed to high grade (62% at amphibolite facies, 25% at granulite facies; Goodwin 1996). The state of current knowledge on gneiss complexes in the Grenville Province poses the question as to how poorly metal endowed is the so-called Boring Billion. Without appropriate tools and knowledge base for exploring high-grade metamorphic terranes, is it even possible to talk about secular changes in metal endowment in the Precambrian. Is the term Boring Billion more evocative of what some may consider high-grade metamorphic terranes to be: boring gneisses?

The guidebook updates previous versions of this field trip prepared for the Geological Association of Canada and the Friends of Grenville (Corriveau et al. 1989, 1995; Corriveau and Rivard 1997). It complements other guidebooks for the Central Metasedimentary Belt in Québec (Gauthier et al. 1988, 2004; Sharma et al. 1993; Tremblay et al. 1993, 1996, 1997; Kretz 1997; Sharma and Singhroy 1997; Davidson et al. 2002).

Chapter 2: Geological tools for mapping and exploring high-grade metamorphic terranes

2.1 Context

The ability to identify the presence of hydrothermal systems at granulite facies is paramount to the discovery of metamorphosed SEDEX, volcanogenic massive sulphide (VMS), epithermal, porphyry, iron oxide copper-gold (IOCG), IOA, and albitite hosted U and U-Au-Co deposits (Corriveau and Spry 2014). Field indicators such as cordierite-anthophyllite rocks and meta-exhalites have helped identified and explored metamorphosed hydrothermal systems for decades (Vallance 1967; Froese 1985; Schreurs and Westra 1985; Allard and Carpenter 1989; Sheepers and Cornell 1990; Bernier and MacLean 1993; Gauthier 1993; Spry et al. 2000). From these, a much better understanding of the entire spectrum of metamorphosed alteration types associated with volcanic-hosted massive sulphide deposits have been acquired (Froese 1998; Bonnet and Corriveau 2007 a, b; Theart et al. 2010 and references therein). In the process, as carbonate, potassic, sericitic, argillic and advanced argillic alteration were recognized new deposits and new examples of metamorphosed deposit types were discovered (e.g. Ravenelle et al. 2010) while the origin of other metamorphosed ore deposits were being reinterpreted (e.g. Challenger gold deposit; McFarlane et al. 2007).

Until now high-grade metamorphic terranes where metasedimentary rocks abound appear to be the most endowed in mineral deposits. Examples include 1) Broken Hill and Cannington in the Mount Isa inlier, Australia, 2) Aggeneys and Gamsberg in the Namaqua-Natal Province in South Africa, 3) Balmat-Edwards in the Grenville Province, 4) Kholodnina in Russia, and 5) Roberto in Canada (Corriveau and Spry 2014 and references therein). Many VMS deposits metamorphosed at high grades occur in metasedimentary-rich volcanic belts such as those in the Baltic Shield (Zinkgruvan, Vihanti and Pyhäsalmi deposits) and in the Namaqua-Natal Province (Prieska, Areachap and Copperton deposits) (Hedstroem et al. 1989; Weihed and Eilu 2005; Bailie et al. 2010; Theart et al. 2010). In contrast deposits hosted by felsic rocks have remained long absent in the geological record (porphyry, high-sulphidation VMS, epithermal, and IOCG deposits). Hydrothermally altered volcanic rocks hosting deposits have also been initially mapped as metasedimentary rocks such as at the Challenger Au deposit in Australia (Tomkins and Mavrogenes 2002). Is a preferential distribution of significant ore deposits within sedimentary rocks a matter of erosion levels or increased fertility of sedimentary basin or does it portray our collective ability to recognize their settings and potential deposit models, and explore them with tools applicable to none or little metamorphosed terranes?

In gneiss terranes the valuable knowledge of geodynamic settings, volcanic-facies and synvolcanic structures that control volcanism and hydrothermal activity (Gibson and Galley 2007) is not readily available to develop exploration strategies. Geological criteria applicable to exploration of high-grade metamorphic gneiss terranes outside of known deposits have to be developed, expertise of hydrothermal systems at upper-amphibolite and granulite facies gained, and the preservation paradigm may have to fall or at least the view that high-grade metamorphic terranes only contained deeply formed parts of the crust need to be revized (see Figure 1 of Bonnet and Corriveau 2007a). Such a change of paradigm guides current research in the Grenville Province with the result that recent field-based research and protolith studies have revealed volcanic belts, extensive hydrothermal systems, subvolcanic intrusions and synvolcanic faults among undifferentiated felsic to mafic gneiss terranes (Moore and Waters 1990; Araujo et al. 1995; Blein et al. 2004; Corriveau and Bonnet 2005; Puffer and Gorring 2005; also Table 1.1 in Bonnet and Corriveau 2007b and references therein).

2.2 Mineral potential of Grenvillian high-grade metamorphic terranes

Upper amphibolite to granulite facies volcanic belts and hydrothermal systems of the Grenville Province remained nonrecognized and undifferentiated within gneiss complexes largely until this millennium (Corriveau and van Breemen 2000; Blein et al. 2004; Slagstad et al. 2004; Corriveau and Bonnet 2005; Roy et al. 2006; Gower 2007), even those in the extension of the well-endowed Archean greenstone belts documented to be prospective since the seventies (Allard 1978, 1979; Faure 2007). They too remained long elusive until the work of Cadéron et al. (2005) and Roy et al. (2006). Even today, nowhere is the lack of metamorphosed ore deposits in high-grade metamorphic terranes most startling than in the Grenville Province. This is due in part to:

1. difficulties in recognizing volcanic protoliths and synvolcanic intrusions and having them grouped as a variety of orthogneisses,
2. recrystallization and deformation of original hydrothermal mineral and textural features,
3. unusual mineralogy of hydrothermal alteration zones at amphibolite to granulite facies, and
4. common resemblance of metamorphosed metasomatic rocks with metasedimentary rocks (Corriveau and Spry 2014) or orthogneisses (this work; P.H. Trapy unpublished data 2017).

2.3 Mineral potential for metamorphosed volcanic-hosted mineral systems

The Grenville Orogen was largely built through successive

continental magmatic arcs; back-arc development was also common (Rivers 1997; McLelland et al. 2013) as reviewed in Chapter 3. Arc-related volcanic rocks and the hydrothermal systems they host have now been recognized among previously undifferentiated gneiss complexes along the entire province (e.g. 1.4 Ga Bondy gneiss complex, Canyon Domain, Calumet deposit host, Montauban Group, 1.5 Ga Musquaro-LaRomaine belt; 1.2 Ga Banded complex; Williams 1992; Corriveau and van Breemen 2000; Bernier and MacLean 1993; Blein et al. 2003, 2004; Corriveau and Bonnet 2005; Dunning and Indares 2010; Corriveau 2013; Hindemith et al. 2017). Some may have formed in juvenile arcs subsequently accreted to Laurentia (Dickin 2000). Hence the Grenville Province should have a potential for any arc-related deposit types, including:

1. volcanic hosted-massive sulphide,
2. epithermal and mesothermal gold-silver,
3. porphyry Cu/Mo/Au,
4. iron-oxide copper-gold (IOCG), iron oxide apatite (IOA), albitite hosted U and Au-Co,
5. volcanic-hosted U,
6. SEDEX, and
7. magmatic Ni-Cu-PGE deposits

(Gauthier and Chartrand 2005; Corriveau et al. 2007; Gower 2007).

The orogen also contains the metamorphosed extensions of the Archean Abitibi greenstone belt but its chains of large mining camps currently end at the Grenville Front. The orogen also hosts the extension of the Labrador Trough and its iron-formations (Gross 1996). Over its continent-scale length, this orogen has only three world-class ore deposits: Mount Wright (Fe oxides), Tio (Fe-Ti oxides) and Balmat-Edwards (SEDEX or MVT) (de Lorraine 2001; Perreault and Hébert 2003; Corriveau et al. 2007). These deposits are hosted within metasedimentary belts rich in quartzite, marble and iron-formations, and in an anorthosite massif. Again all these units are texturally and mineralogically distinctive and their parent rock-types are known.

Currently discovered IOA and IOCG mineral occurrences and deposits in the Grenville Orogen are in:

1. SE Missouri district in the Granite-Rhyolite Province of USA (which extends into the Grenville as a component of the Pinwarian arc; Gower et al. 2008; Slagstad et al. 2009; McLelland et al. 2013),
2. Adirondacks Highlands (Valley et al. 2011),
3. the Kwyjibo REE-rich IOA deposit, lac Marmont IOA prospect and other mineral occurrences in the Manitou district (Clark et al. 2003, 2005, 2010; Perreault and Lafrance 2015),
4. Grenville Highlands of New Jersey (e.g. Edison magnetite mine; Puffer and Gorring 2005), and
5. Bondy gneiss complex (Corriveau 2013; Blein and Corriveau 2017; this work).

Other settings are also being explored for IOCG potential across the province (e.g. Charbonneau and Robillard 2016).

Orogenic belts with several phases of metamorphism or intrusive activity are subject to renewed circulation of fluids and remobilization of sulphides, metals or sulphide melts creating new styles of mineralization (e.g. Williams 1990; Frost et al. 2002; Williams and Smith 2003; Wanhainen et al. 2005; Sparks et al. 2007, Tomkins 2007; Tomkins et al. 2007; Aleinikoff et al. 2016; Day et al. 2017; Hofstra et al. 2017). For example in the presence of Bi melt- and fluid-driven scavenging of metals from host rocks or pre-existing deposits can lead to secondary dispersion or re-concentration of metals in particular gold (Ciobanu et al. 2006; Acosta-Góngora et al. 2015).

2.4 Iron oxide alkali-calcic alteration systems and their IOCG and affiliated deposits

2.4.1 Overview

The IOCG deposit type and its spectrum of affiliated deposits remain a research and exploration challenge for many geologists because of the intrinsic complexities of alteration and mineralization processes and the extraordinary range of deposits formed (Williams et al. 2005; Corriveau and Mumin 2010; Groves et al. 2010). In addition views diverge widely on which deposits should be included within the IOCG deposit type and what key elements control their genesis (Hitzman et al. 1992; Pollard 2000, 2006; Williams et al. 2005; Pirajno 2009; Corriveau et al. 2010, 2016; Groves et al. 2010). Conjectures will not disappear once ore systems hosting IOCG and affiliated deposits are metamorphosed, deformed and part of the ore remobilized to the upper-amphibolite and granulite facies, as exemplifies by the protracted history of the Aitik deposit (Sweden) and host terrane where both porphyry- and IOCG-type mineralization have been documented (Weihed 2003; Weihed et al. 2005; Wanhainen et al. 2005; Wanheinen and Martinsson 2010).

In recent years, alteration, brecciation and mineralization footprints of iron oxide and related alkali-calcic alteration (IOAA) systems have been mapped much more extensively (Mumin et al. 2010; Xavier et al. 2010; Ehrig et al. 2012, 2017; Schlegel and Heinrich 2015; Slack et al. 2016). In the process case examples have arisen on how metasomatic growth of these systems can lead to iron oxide copper–gold ± Co- and Bi-rich variants (IOCG), iron oxide–apatite ± REE-rich variants (IOA), skarn, albitite-hosted U or Au-Co-U, polymetallic vein and epithermal deposits (Corriveau et al. 2016). Key districts used to illustrate these ore systems include the Olympic province and Cloncurry district in Australia, districts from northern Fennoscandia, the Central Andes and other settings of the American Cordillera, and the Canadian Great Bear magmatic zone and Grenville Province, including extension into the Granite-Rhyolite Province in the USA (Hitzman et al. 1992; Williams et al. 2005; Corriveau 2007; Porter 2010a, b; Williams 2010; Chen 2013; Slack et al. 2016; Tornos et al. 2017).

2.4.2 Prograde evolution of IOAA ore systems

Evolving fluid columns that lead to IOCG deposits alter precursor rocks intensely over hundreds of square kilometres, transforming chemically and texturally pre-existing units into a series of distinctive alteration facies (Corriveau et al. 2010, 2016 and reference therein; Corriveau 2017a, b). Where alteration is most intense, composition of alteration becomes independent of the composition of the host rocks whether they were volcanic, volcaniclastic, hypabyssal intrusive or sedimentary in origin (Fig. 2.1).

Six alteration facies characterize the evolution of an iron oxide alkali-calcic alteration system and the formation of IOCG deposits as highly saline fluid columns rise and temperatures decline (high to low temperatures: HT to LT). Each facies consists of its own paragenetic sets and their prograde evolution is regular as shown in Figure 2.2. Mineral modes can be highly variable even though the paragenetic sets are regular. They consist of:

1. Facies 1, Na (albite, scapolite; Fig. 2.1B, G);
2. Facies 2, HT Ca-Fe (amphibole, magnetite, apatite: Fig. 2.1H) and transitient Na-Ca-Fe (Fig. 2.1C);
3. Facies 3, HT K-Fe (K-feldspar, biotite, magnetite; Fig. 2.1D);
4. Facies 4, K-skarn (clinopyroxene, garnet, K-feldspar) and K-felsite (K-feldspar);
5. Facies 5, LT hydrolytic K-Fe (K-feldspar, white mica, hematite, carbonates, chlorite, barite; Fig. 2.1E); and
6. Facies 6, epithermal alteration types.

Na, HT Ca-Fe and transitional Na-Ca and Na-Ca-Fe facies are commonly early, laterally extensive, at the deepest levels of alteration systems, along fault zones and above subvolcanic intrusions. These alteration types may not be exposed or drilled into as they are not the immediate host to deposits unless replaced or brecciated and filled in by fertile alteration types and mineralized. In such cases, evidence of their occurrence may be largely obscured in large deposits and take extensive exploration to uncover them (e.g. Ehrig et al. 2017). Skarn is common in carbonate hosts at the transition between albitite and high-temperature Ca-Fe alteration facies. Na-Ca-Fe alteration facies is also a common transitional alteration facies.

Facies 1 and 2 are barren in terms of polymetallic IOCG mineralization, unless superimposed by intense HT K-Fe alteration and/or LT K-Fe^{3+}-H_2O-CO_2) alteration (Fig. 2.3). Facies 2 HT Ca-Fe hosts iron oxide-apatite (IOA) deposits. Rare-earth (REE) mineralization with high heavy to light REE ratios forms where IOA transitions to HT Ca-K-Fe or HT K-Fe alteration facies within the mineralization zone or in its vicinity (Figs. 2.3, 2.4).

The HT Ca-K-Fe alteration facies hosts Co and Bi-rich variants of IOCG deposits that are commonly dominate by arsenopyrite as sulphides (Figs. 2.3, 2.4). These facies are most extensive in sedimentary sequences with carbonate rocks; mineralization is largely stratabound (Montreuil et al. 2016b). Ductile deformation is common during the development of this and the HT Ca-Fe alteration facies.

The HT and LT K-Fe alteration facies host polymetallic magnetite- (e.g. Cloncurry deposit) and hematite-group (e.g. Olympic Dam deposit) IOCG deposits, respectively (Williams et al. 2005; Corriveau et al. 2010, 2016, 2018; Skirrow 2010; Williams 2010). Biotite-rich HT K-Fe alteration facies and associated mineralization are not associated with brecciation; mineralization can be stratabound (e.g. Zhao et al. 2017). K-feldspar-rich HT K-Fe alteration facies systematically leads to brecciation (Fig. 2.1).

Potassic skarns and associated mineralization form at the magnetite-to-hematite transition where carbonate and carbonaceous host rocks are present (e.g. Wang and Williams 2001) or in earlier-formed carbonate alteration that stem from cooling of fluids after magnetite crystallization (Mumin et al. 2010).

Facies 6 consists of silicification, and phyllic, argillic and advanced argillic alteration that leads to or are part of peripheral epithermal systems.

Figure 2.1. Alteration attributes of Great Bear mineral systems illustrating the variety of alteration facies and the common low-temperature overprints on high-temperature alteration facies. **A.** Metasiltstone grading – left to right – from weak to strong albitization and amphibole and amphibole-magnetite alteration with a K-feldspar overprint. Note that alteration is stratabound and layered selective. De Vries Lake, NWT (CQA-05-0240). **B.** Intense albitization above the roof of a diorite intrusion leading to a coarse-grained albitite resembling syenite. McLeod Lake, Port Radium-Echo Bay district, NWT. Code bars (Na-Ca-Fe-K-Fe and Na-Ca-Fe-K-Si illustrate the high Na (9.42 wt %; Corriveau et al. 2015) of this albitite. Contrasts with the fine-grained albitite in A. **C.** Transitional amphibole-magnetite-biotite alteration with patches of K-feldspar felsites developing at the expense of the earlier 'mafic' HT Ca-K-Fe alteration. Port Radium-Echo Bay district, NWT (CQA-06-0372). **D-E.** Ernest-Henry ore zones evolving from Cu-mineralized HT K-Fe alteration (K-feldspar-magnetite-chalcopyrite) to carbonate-bearing LT Ca-Fe alteration (calcite-magnetite-chalcopyrite) that is replacing earlier K-feldspar altered fragments. **F.** Amphibole-magnetite alteration of a sedimentary host similar to that of A in the South Duke sector, south of the NICO deposit. Note that early HT Ca-Fe alteration is here locally pervasively chloritized. **G.** Typical low-temperature K-Fe alteration faices with hematite-filled breccia and K-feldspar altered fragments. Ab, albite; Amp, amphibole; Bt, biotite; Cc, calcite; Ccp, chalcopyrite; Hem, hematite; Kfs, K-feldspar; Mag, magnetite; Ttn, titanite. Abbreviations in this and other figures are from Whitney and Evans (2010).

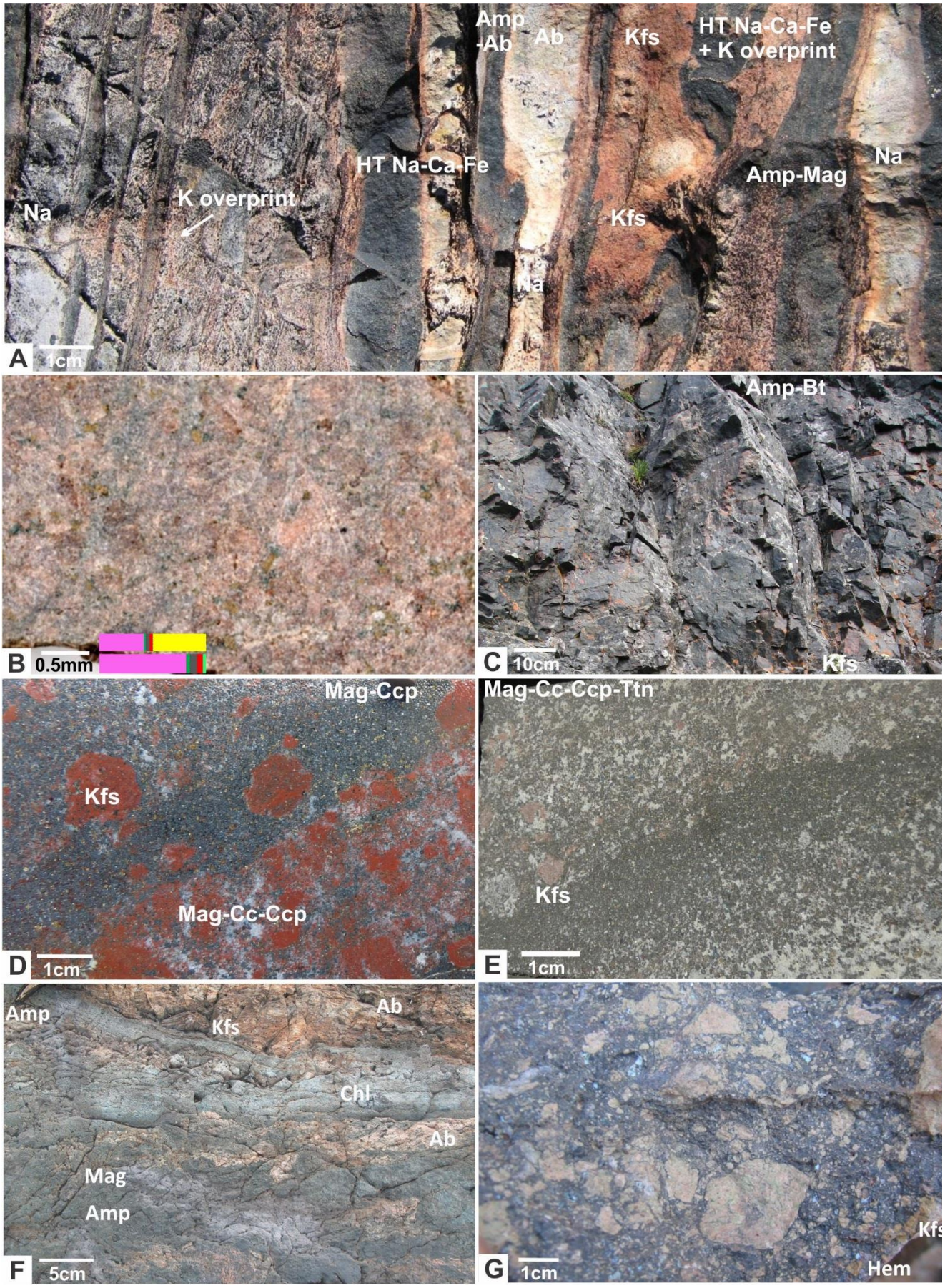
Amp
-Ab
Ab
Kfs
HT Na-Ca-Fe
+ K overprint
HT Na-Ca-Fe
Na
K overprint
Amp-Mag
Na
Kfs
Na
A
1cm
B
0.5mm
Amp-Bt
C
10cm
Kfs
Mag-Ccp
Kfs
Mag-Cc-Ccp
D
1cm
Mag-Cc-Ccp-Ttn
Kfs
E
1cm
Amp
Kfs
Ab
Chl
Ab
Mag
Amp
F
5cm
Kfs
G
1cm
Hem

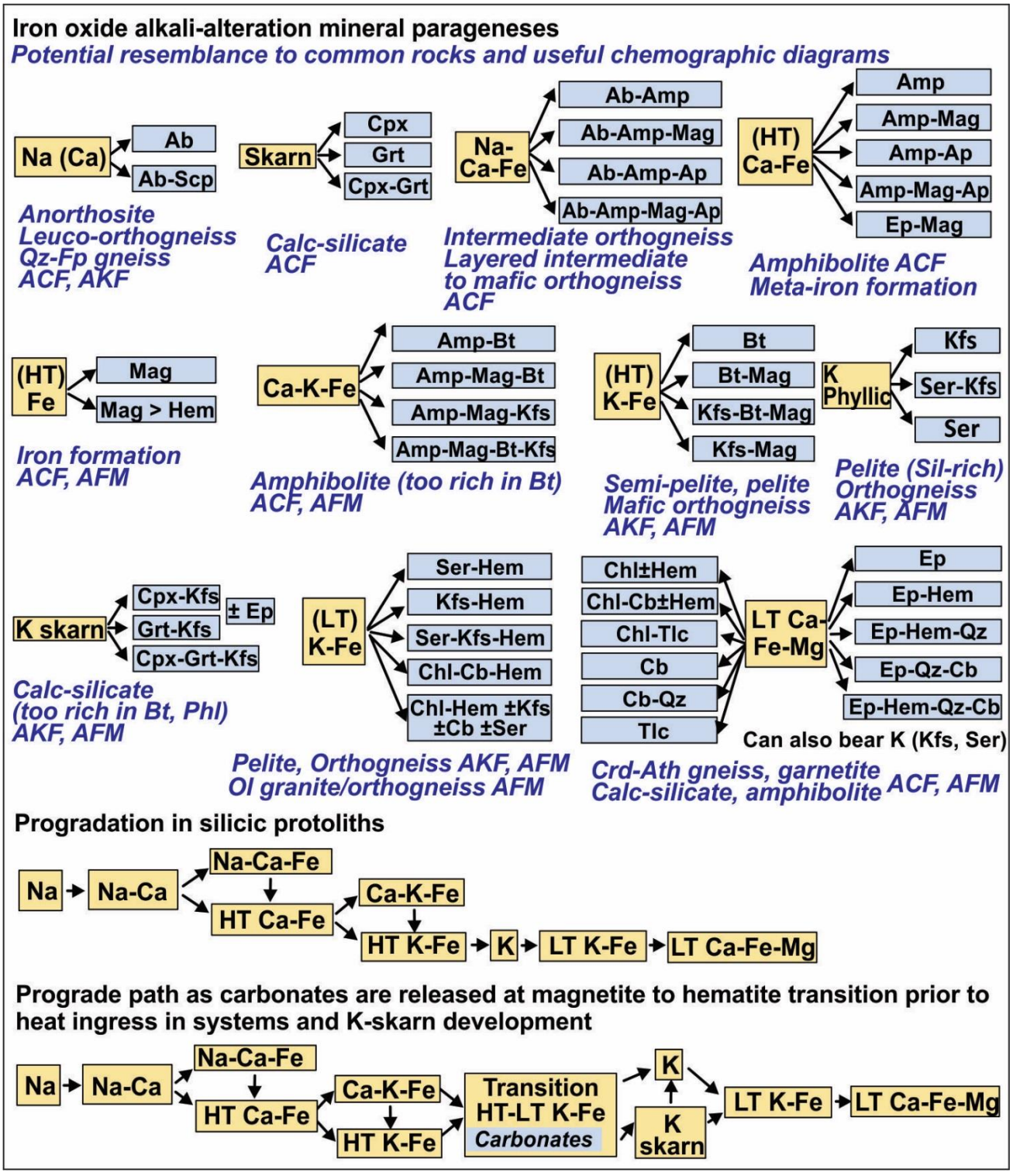

Figure 2.2. Sets of mineral assemblages characterizing each alteration facies and their prograde evolution. Each facies once metamorphosed to upper amphibolite and granulite facies can look like metamorphosed sedimentary and igneous rocks such as metapelite, semi-pelitic gneiss, amphibolite, a variety of paragneisses and orthogneisses and anorthosite.

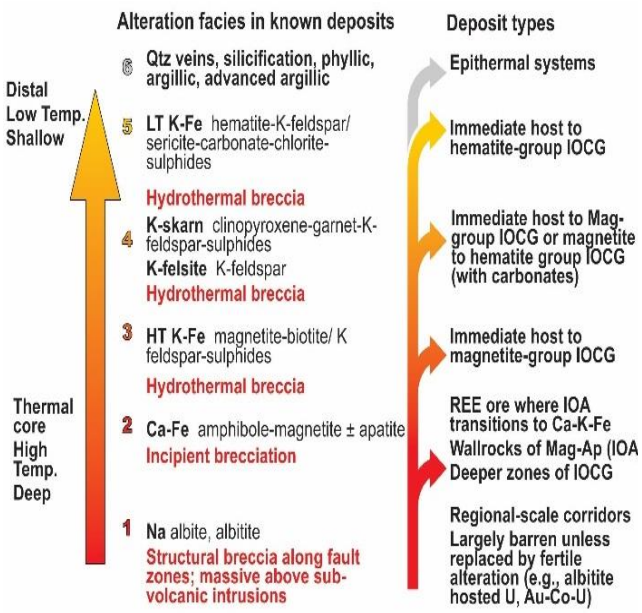

Figure 2.3. Prograde evolution of iron oxide alkali-calcic alteration systems and their deposit types (modified from Corriveau et al. 2010, 2016).

In addition to deposit formed through prograde metasomatism, overprinting of alteration types induced by active tectonics during metasomatism can lead to additional deposit types and hybrid metal associations. For example, albitites that are brought into the fluid column where it has evolved to the conditions for forming K-Fe to the epithermal facies are preferential traps for the precipitation of U and Au-Co-U. This leads to albitite-hosted U and Au-Co-U deposits. Figure 2.4 provides an overview of alteration facies hosts to Ag, Au, Fe, REE, Th, U, and sulphides. Each deposit type has its own metal association as reviewed in Corriveau et al. (2016) and Montreuil et al (2016b). In parallel each metal has its own sets of alteration facies it can precipitate in (Fig. 2.4).

2.4.3 Cationic bar codes

Each alteration facies has its distinctive molar proportions of Na, Ca, K, Fe, Mg and can thus be characterized rapidly using proportional element bar codes such as displayed in Figures 2.5 and 2.6 (Montreuil et al. 2013, 2016b; Corriveau et al., 2016). One or two of these cations dominate the molar proportions of each alteration facies in contrast to common igneous, sedimentary and metamorphic rocks which have three to four dominant cations. Rhyolites have only two dominant cation (Na and K) in the Na-Ca-Fe-K-Mg bar codes but have three dominant ones in bar codes with Al+Si; Fig. 2.6). Molar proportions do vary for a same paragenetic set due to variation in alteration intensity and protoliths but where alteration is intense the bar codes remain highly diagnostic (Figs. 2.6, 2.7).

Overprinting of alteration facies tend to re-equilibrate molar proportions of the diagnostic cations to the point that the bar codes of polyphase metasomatic rocks are similar to those of common rocks (Fig. 2.6).

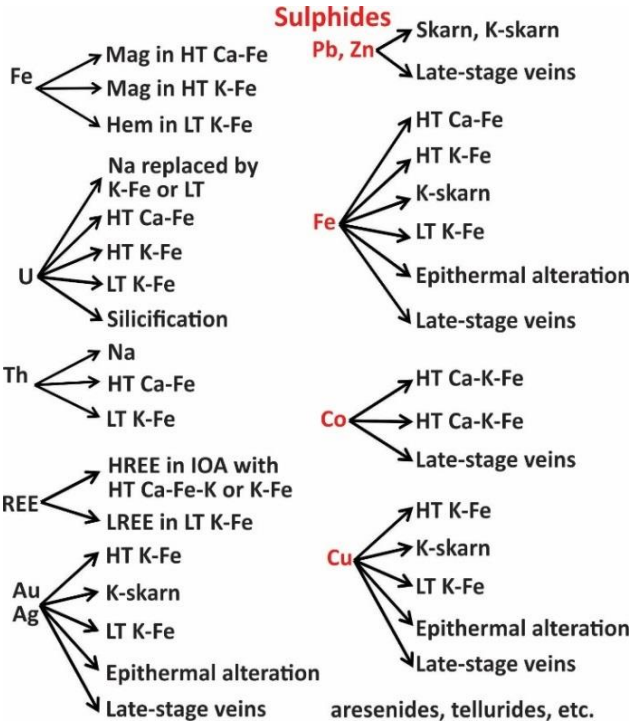

Figure 2.4. Metals and their host alteration facies modified from De Toni (2016).

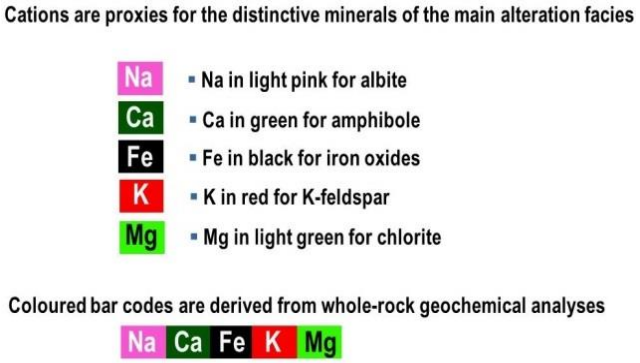

Figure 2.5. Basis for colour Na-Ca-Fe-K-Mg bar codes (Corriveau et al. 2016, 2017, 2018; Montreuil et al. 2016b; Blein and Corriveau 2017; Corriveau 2017a, b).

Such bar codes can be used to map alteration facies in a synoptic way regionally and at deposit scale (Montreuil et al. 2016b). They can be plotted within discriminant diagrams to add significant information on the evolution of the alteration facies. In addition, the bar codes footprint of iron oxide alkali-calcic alteration facies that host IOA, IOCG anad affiliate deposits can be distinguished from alteration types in other deposit types by molar proportions of (Si+Al)/10 as shown in Chapter 6 (Corriveau et al. 2017). Each deposit type has its own bar codes suites and footprint in a variety of discriminant diagrams (Fig. 2.8 and chapter 6).

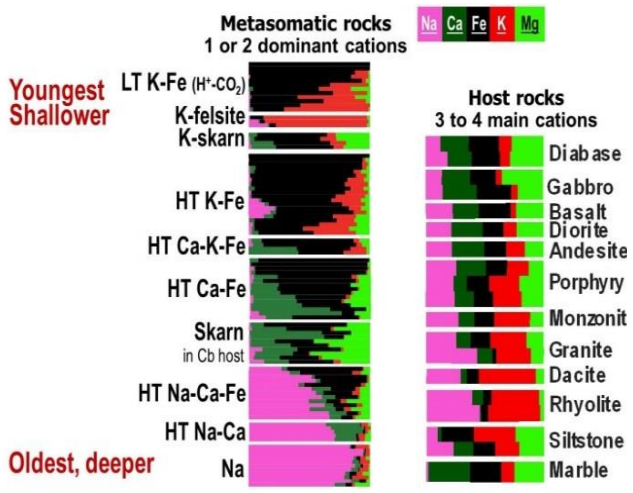

Figure 2.6. Na-Ca-Fe-K-Mg bar codes of common sedimentary, volcanic and plutonic rocks versus bar codes of IOAA metasomatites.

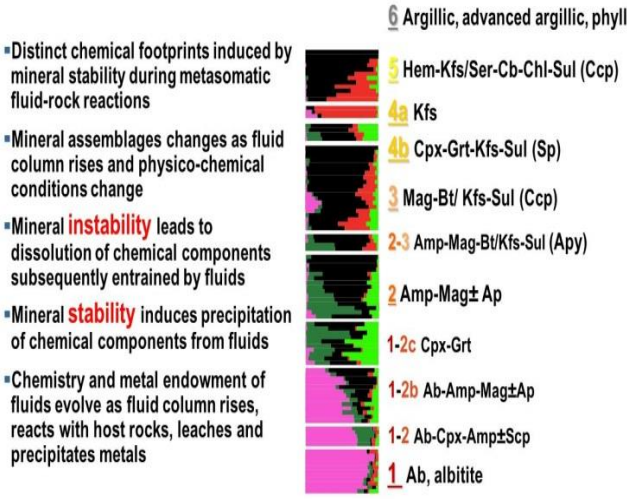

Figure 2.7. Processes leading to the diagnostic paragenetic sets following Corriveau et al. (2016) ore system model; Sul: sulphides; other mineral abbreviations in Whitney and Evans (2010).

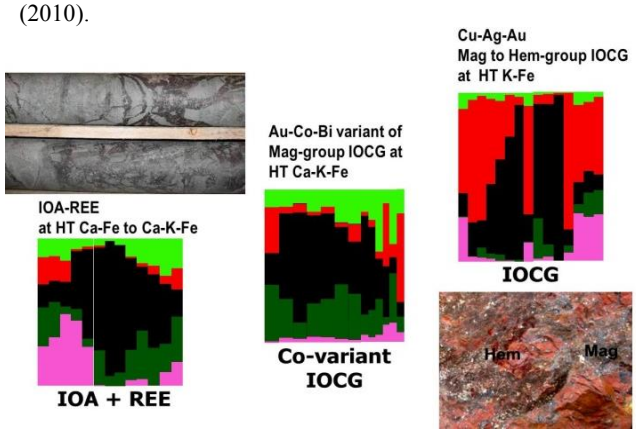

Figure 2.8. Footprint of IOA and IOCG deposits and Co-rich IOCG variants using dataset from Corriveau et al. (2015). See further examples in Corriveau et al. (2018).

2.4.4 Alteration mapping of IOAA systems

A great variety of mineral assemblages and contents, grain sizes, textures, structures, and space-time relationships of metasomatic rocks is observed at the deposit- to regional-scale in IOCG and IOA districts. This in part depends on the intensity of alteration which varies from subtle, weak, moderate, intense, or megascopically complete depending on the degree to which precursor minerals have been replaced (see definition of intensity in De Toni (2016)). Variations also depend on whether or not the textures of host rocks are preserved and new ones formed during metasomatism, the grain sizes of the metasomatites, and the spatial extent of the alteration zones.

Footprints of IOAA systems are controlled by lithospheric architecture, progradation, retrogradation, cyclical build-up and telescoping of alteration facies laterally and from depth to surface. Prograde evolution of iron oxide alkali-calcic alteration systems as fluid column ascends from large magma chambers (1 in Fig. 2.9) through the upper crust along major fault zones and splays. Repeated injection of magmas and fluids can complexifies this 'simple' prograde evolution and induced repeated cycles of some alteration facies. Subvolcanic intrusions increase heat and fluid influx and generate subsidiary hydrothermal cells (2 in Fig. 2.9). Coalescence of hydrothermal cells is observed across systems. Caldera lakes are locally observed and can include carbonate rocks (3 in Fig. 2.9). Tectonic activity and caldera collapse during the metasomatic growth of the systems can induce faulting and telescoping or superposition of alteration facies. An ignimbrite cap (4 in Fig. 2.9) can form from these large magma chambers as well as batholiths.

In systems that escaped orogenic reworking, the relatively coarse grain size of the metasomatites enables field mapping of alteration facies according to the diagnostic cations of their minerals. Doing so provides a mean to simplify the adaptation of mapping protocols of IOAA systems to high-grade metamorphic terranes. The distribution of droplets in Figure 2.9 illustrates the alteration facies that will crystallize across the path of the rising fluid columns. They provide a rapid impression of how varied, hence how apparently complex, mineral assemblages will be in such systems. Complexities further stem from variations in mineral modes due to variations of intensity of alteration and of precursor rock types, and to superposition of alteration facies. Such extreme variations of metasomatites are preserved through high grade metamorphism and become a characteristic attribute of IOAA systems that facilitates their recognition in the field.

Mapping non-metamorphosed IOAA systems is challenging but complexities are largely resolved by:

1. focusing description on paragenetic sets and applying petrological mapping concepts of metamorphic petrology to metasomatic facies,
2. qualifying alteration intensity,
3. reporting mineral assemblages and modes,
4. using a standardized terminology for veins, replacements and breccias (Fig. 2.10; De Toni 2016),

5. mapping cross-cutting and overprinting relationships among alteration facies, and
6. documenting alteration facies paragenetic affinities of mineralization assemblages.

The observed geology of the Bondy gneiss complex during this trip will show that many of the characteristics of such systems remain preserved through metamorphism. It will also highlight that the increase grain size of low-temperature metasomatic rocks helps decipher their imprint and provides a distinct series of new mappable features that can vector to mineralization.

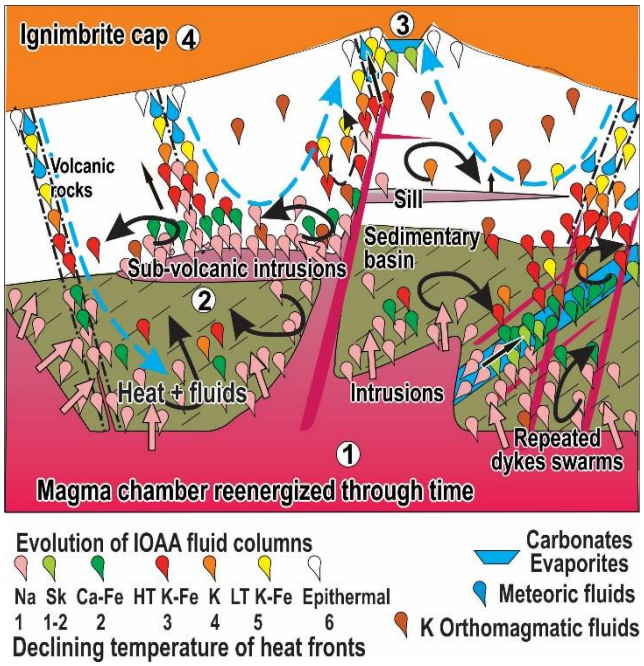

Figure 2.9. Prograde evolution of iron oxide alkali-calcic alteration systems. Numbers refering to sequence of events and alteration facies listed are described in text. Sk: skarn. Ca-Fe: high-temperature Ca-Fe.

2.5 Petrological and chemical modeling

High-grade orogenic metamorphism is largely isochemical beyond the loss of volatiles (Yardley 2012). In known deposits metamorphosed to granulite facies, the meta-alteration zones preserve the imprint of the chemical changes undergone by the protoliths during premetamorphic hydrothermal alteration (Corriveau and Spry 2014). Consequently, petrological and lithogeochemical tools to identify and quantify hydrothermal alteration associated with ore deposits can be applied to environments metamorphosed to high grades. Fine geochemical records also remain preserved at granulite facies such as the decoupling between Ca and Sr in advanced argillic alteration associated with non-metamorphosed epithermal deposits (Hikov 2004) as documented in the Bondy gneiss complex (Antonoff et al. 2010).

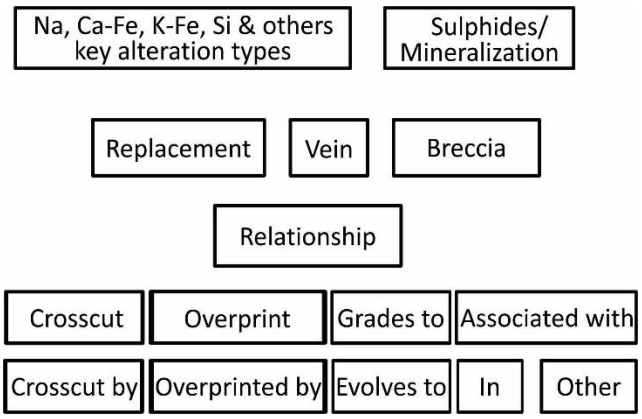

Figure 2.10. Alteration mapping framework; replacement zones, veins and breccias are described in De Toni (2016).

2.5.1 Chemographic diagrams

Generic P-T diagrams for the most common rock types and ACF, AKF, and AFM chemographic diagrams can be very useful in the field (even if simply mentally used during field observation of parageneses and mineral contents). Projecting whole-rock composition on such diagrams helps interpret stable assemblages and the mineral modes expected in various lithologies for a range of P-T conditions (Hodges and Manojlovic 1993; Bonnet and Corriveau 2007a, b; de Capitani and Petrakakis 2010; Froese 2010). In the field projecting the mineral mode proportion unto these diagrams help understand variations of composition being observed while mapping. This is turn can be used to assess the presence of variations atypical of common rocks, hence the presence of potential metasomatic rocks. In turn this recognition of mineral potential indicator rocks is paramount to effective lithogeochemical exploration (Figs. 2.11, 2.12).

2.5.2 IOAA systems at granulite facies

Mapping metamorphosed alteration zones requires an in depth understanding of the field attributes of metamorphosed metasomatic rocks (rock types, parageneses, modal mineralogy, potentially preserved textures and structures) or alternatively the ability to use mineral parageneses and mineral contents to assess the whole-rock composition of the rocks and to use these attributes, the colour of the minerals and their types to identify anomalous composition, hence potential metasomatic rocks. One way to increase available case examples is to model them based on the geochemical footprint of ore deposits.

Isochemical pressure–temperature phase-diagram sections can be modelled by a variety of software (e.g. TWEEQU, Thermocalc and Theriak–Domino; de Capitani and Petrakakis 2010; Holland and Powell 2011) to assess the stable and transient mineral assemblages, their modal mineralogy and mineral composition as a function of pressure, temperature and whole-rock composition. Trapy et al. (2015) have modelled such diagrams for IOCG footprints

at granulite facies using representative samples of alteration facies from the Great Bear magmatic zone in Canada (Figs. 2.13-2.17). Results are summarized in the next section based on unpublished phase diagrams calculated in the MnO-Na_2O-CaO-K_2O-FeO-MgO-Al_2O_3-SiO_2-H_2O-TiO_2 system using the Perple_X 6.7.5 version of December 2016 (Connolly and Petrini 2002; Connolly 2005) and the Holland and Powell thermodynamic database (Holland and Powell 1998, «tcds55» updated in 2004). The fluid content of the rocks is based on the loss on ignition of the original analyses, and calculation uses fluid evolution in the H_2O-CO_2 system of Holland and Powell (1991, 1998) assuming that H_2O prevailed. The pressure and temperature conditions imposed on modeling were those of amphibolites and granulites as defined by Spear (1993). In addition composition of the various metasomatic rocks were projected in the diagrams of Streckeisen (1976) for igneous rocks updated by Le Maître et al. (2002) to highlight the similarities and differences that may exist between the various alteration facies once metamorphosed and the gneisses derived from igneous rocks. Resemblance can be striking and further emphasize the easiness by which metamorphosed hydrothermal systems can go unnoticed.

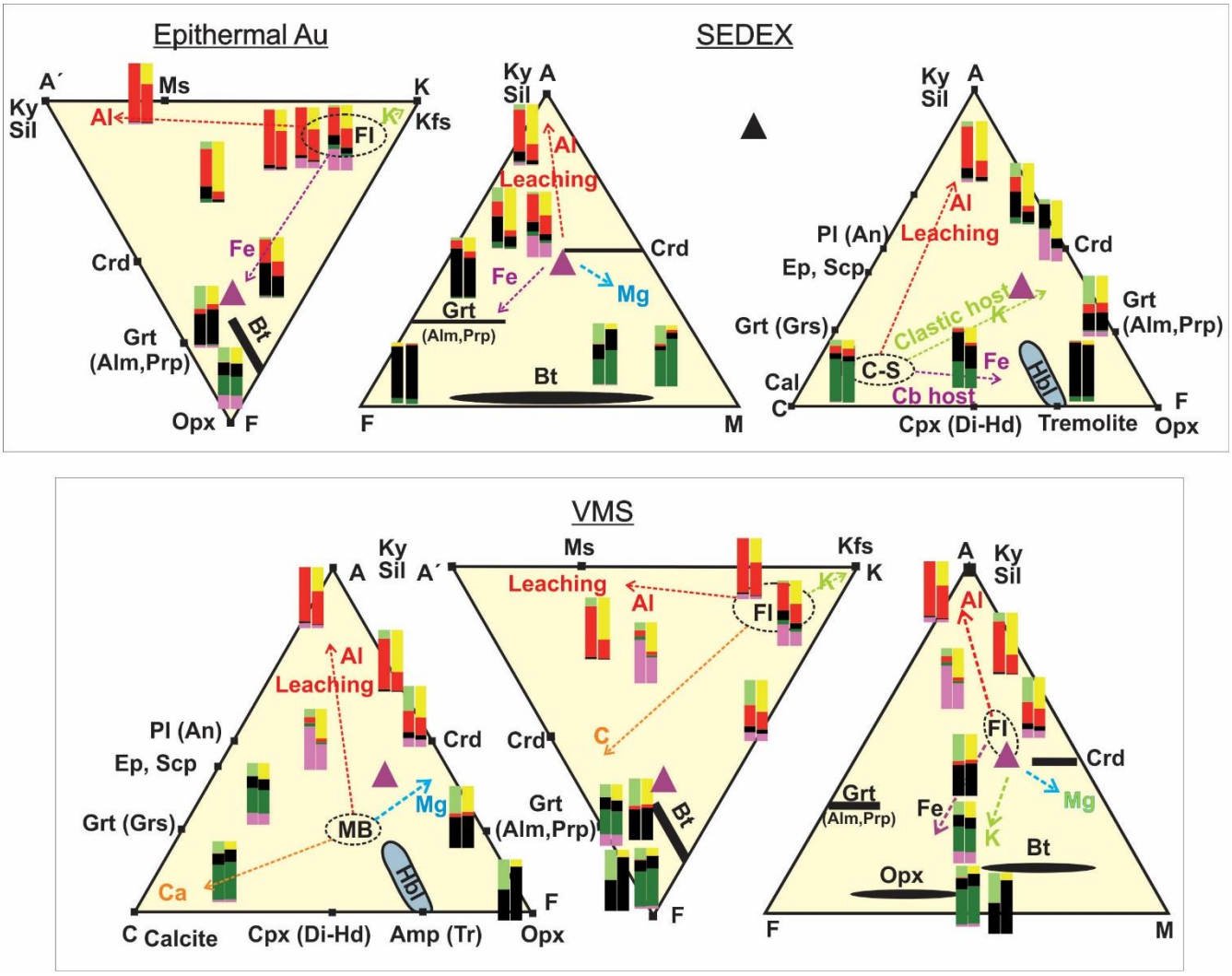

Figure 2.11. Potential chemical alteration trends on chemographic A'CF, A'KF and AFM diagrams for epithermal gold, sedimentary exhalative (SEDEX) and volcanic massive sulphide (VMS) deposits; modified from Williamson et al. (2003). AFM ($A = Al_2O_3–K_2O$, $F = FeO$, $M = MgO$), A′CF ($A' = Al_2O_3 + Fe_2O_3 – (K_2O + Na_2O)$, $C = CaO$, $F = FeO + MnO + MgO$), and A′KF ($A' = Al_2O_3 + Fe_2O_3 – (K_2O + Na_2O + CaO)$, $K = K_2O$, $F = FeO + MnO + MgO$). Bar codes represent variations in molar proportions of Na-Ca-Fe-K-Mg and Na-Ca-Fe-K-Si/8 for some representative end-members of alteration facies in epithermal, VMS and SEDEX deposits based on their distribution in the AIOCG diagram of Montreuil et al. (2013) as discussed in Chapter 6 (SEDEX not shown in Chapter 6). Location of bar codes on diagrams are approximate and used to display some key variations in Na (pink), Ca (dark green), Fe (black), K (red), Mg (green) and Si/8 (yellow). Common host rocks for each deposit types are shown (MB, metabasite; C-S, calc-silicate rock; and Fl, felsic rocks. The average composition of pelite (North American Shale Composite from Gromet et al. 1984) is used to represent metapelites (triangle) for discussion. These diagrams should be refined based on currently available geochemical databases and mineral assemblages modelled in depth for better understanding the footprints of metamorphosed ore deposits. Examples can be found in Bonnet et al. (2005), Bonnet and Corriveau (2007) and Trapy (2018).

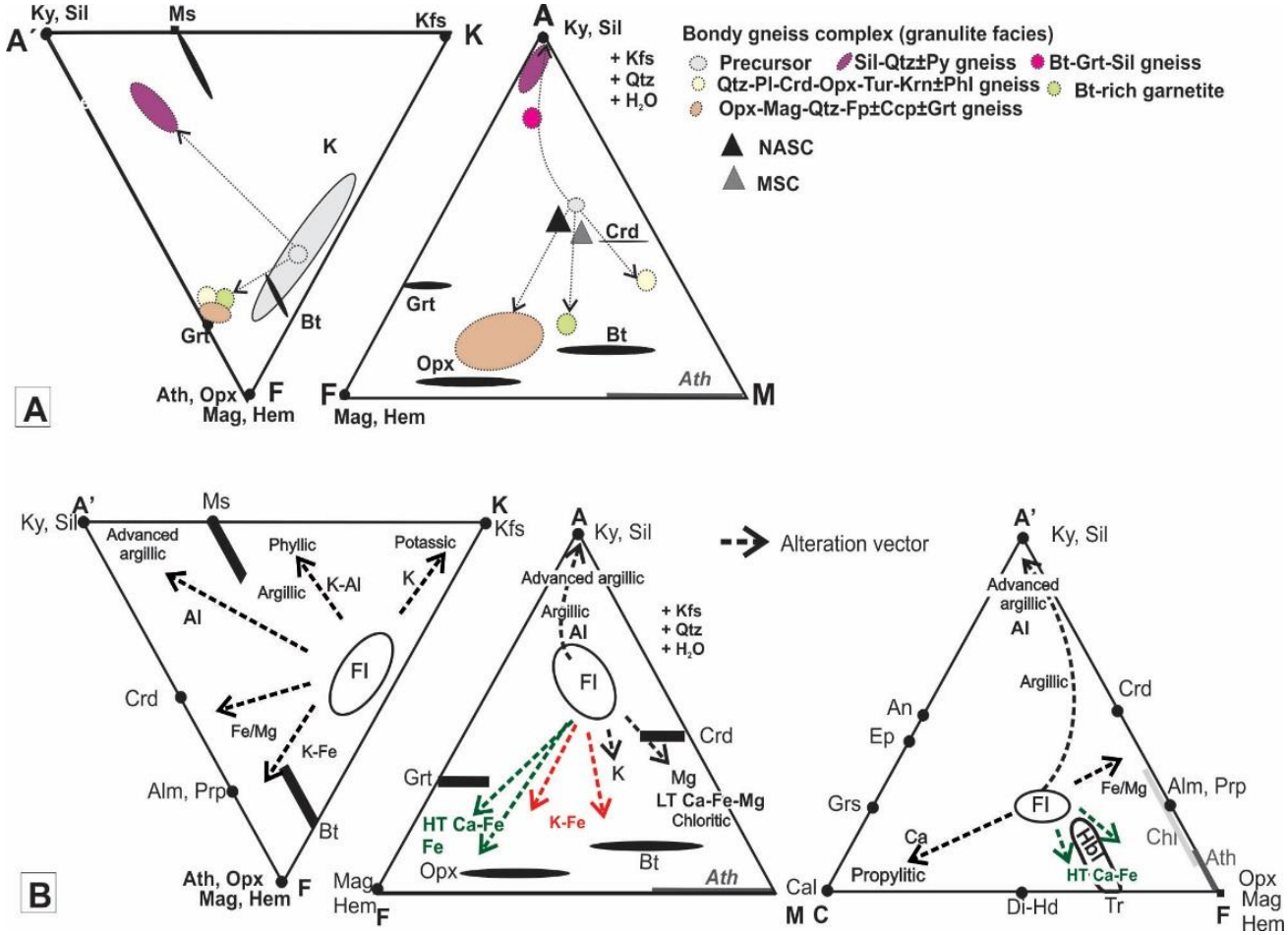

Figure 2.12. AFM, A'CF, A'KF diagrams modified from Corriveau and Spry (2014). **A.** Bondy gneiss complex. **B.** Inferred trends for IOAA to epithermal systems. See Figure 2.11 for details about the AFM, A'CF and A'KF diagrams.

The lithogeochemical, mineral assemblages and mineral chemistry signatures of iron oxide and alkali-calcic alteration systems will have geophysical and/or analytical responses that can be detected by a variety of methods both at the deposit and regional scales including prognostication of rock physical properties with petrological modelling based on whole-rock composition (Connolly and Petrini 2002; Kelley et al. 2006).

2.5.3 Modeled Na and HT Na-Ca-Fe facies

In high-grade metamorphic terranes, polyphase deformation can juxtapose regional-scale Na against fertile K-Fe alteration facies as observed in the Great Bear magmatic zone and the Bondy gneiss complex. During the development of the systems, the Na facies is commonly mildly replaced by K-feldspar alteration in a variegated way at outcrop-to-system scale. Once metamorphosed to granulite facies these rocks will take on the appearance of fine-grained quartz-poor quartzofeldspathic gneisses (leucocratic paragneisses or orthogneisses). For this reason we report on Figure 2.13, Great Bear magmatic zone metasomatic rocks on Streckeisen diagrams for igneous rocks modified by Le Maître et al. (2002).

Sodic alteration can lead to very high Na contents such as those of the albitite in Figure 2.1B (9.42 wt %; Corriveau et al. 2015). This albitite falls within the field of foidite in Pearce (1996) diagram indicating that such rocks can be undersaturated in silica with respect to aluminium and alkalis. Modeling and field observations indicate that Na alteration facies at amphibolite facies (not yet modelled at granulite facies) have the following attributes:

1. leucocratic; quartz+alkali feldspar+plagioclase above 90 vol.% for most albitites;
2. composition plots in the quartz-K-feldspar-plagioclase fields of the Streckeisen diagrams for rocks at low fugacity of oxygen. Most fall within the anorthosite field, some fall in the leucogabbro, monzodiorite, quartz-monzodiorite and quartz-diorite fields;
3. composition can plot in the feldspathoidal field of the Streckeisen diagram at mid to high oxygen fugacity;
4. oligoclase to andesine plagioclase varieties, not albite;
5. clinopyroxene, hornblende, epidote, biotite, nepheline, grossular and muscovite can be accessories at low oxygen fugacity;
6. olivine, vesuvianite and wollastonite can crystallize as

accessories at mid fugacity of oxygen with nepheline significantly increasing in mode reaching a peak at 80 vol.%;
7. magnetite, hematite can crystallize at high fugacity in albitites that were hematized prior to metamorphism;
8. cancrinite and zoisite can crystallize at high oxygen fugacity;
9. partial melting may occur above ca. 700°C depending on whole-rock composition but is not common.

Albitite may host albitite-hosted U deposits prior to metamorphism. It is unclear if in such systems uranium gets transferred to melts to form uraniferous granitic pegmatites during partial melting. If so, could it migrate and be a source of Rossing-type mineralization in higher structural levels. This could explain the widespread occurrence of uranium mineralization in 1.18 Ga pegmatites in the marble domain of the Central Metasedimentary Belt.

2.5.4 Modeled HT Na-Ca-Fe facies

Once metamorphosed, metasomatic rocks of the HT Na-Ca-Fe alteration facies will share most characteristics of albitites if they were rich in albite in the first place. This facies commonly has variegated mild potassic overprints hence they may crystallize potassic minerals (biotite, K-feldspar or more rarely muscovite) as part of their assemblages once metamorphosed. Their sum of modal quartz, alkali feldspar and plagioclase will range between 75 and 90 vol. %. Ferromagnesian minerals (clinopyroxene, biotite, amphibole) can reach 20 to 25 vol. %. Garnet only reaches 10 vol. %. Plagioclase composition ranges from albite to andesine and whole-rock composition falls into the monzonite, monzodiorite, diorite and gabbro fields. These metasomatic rocks can take on the appearance of leucocratic to mesocratic heterogeneous or layered quartzofeldspathic gneisses, orthogneisses and metabasites.

The HT Na-Ca-Fe facies where the Ca-Fe component is high can have up to 70 vol. % clinopyroxene or 70 vol. % amphibole. Biotite can reach 20 vol. % and garnet 10 vol. %. These rocks will take on the appearance of amphibolites, metabasites and calc-silicate rocks once metamorphosed to amphibolite and granulite facies. Magnetite form at mid to low oxygen fugacity and hematite can form at high oxygen fugacity.

2.5.5 Modeled HT K-Fe facies

The HT K-Fe facies once metamorphosed to granulite facies will take the appearance of migmatitic granitic to syenitic gneisses with biotite-muscovite, magnetite and/or hematite and traces of clinopyroxene. Modelling and field observations indicate that HT K-Fe alteration facies at granulite facies will have the following attributes:
1. clinopyroxene, garnet, orthopyroxene, biotite can be accessories at low oxygen fugacity, magnetite, cordierite, wollastonite and rhodonite at mid fugacity and hematite at high fugacity of oxygen;
2. composition will plot in the alkali granite and alkali syenite fields of the Streckeisen diagrams for rocks at low fugacity and also in the granite field at mid to high fugacity of oxygen;
3. clinopyroxene is a stable accessory mineral that is stable at all conditions of pressure and temperature of the granulite facies;
4. partial melting may or may not occur above ca. 750-800°C depending on whole-rock composition, and induce the disappearance of biotite and the appearance of sillimanite, orthopyroxene and/or olivine;
5. above ca. 900-950°C these facies are similar to charnokites with unusual proportions in magnetite, ferro-magnesian minerals and/or garnet;
6. once metamorphosed to granulite facies quartz-rich HT K-Fe alteration facies will take the appearance of Fe-rich migmatitic paragneisses.

2.5.6 Aids to alteration mapping

Alteration mapping within the framework of the alteration-brecciation-mineralization model for IOCG systems and affiliated deposit types is a powerful predictive tool for IOCG-targeted geoscience investigations in under-explored and under-mapped terranes as well as within the most explored mineral deposit settings (Montreuil et al. 2015, 2016a, b; Hayward et al. 2016). Petrological mapping of these alteration systems can be optimized with a variety of portable field equipment. The data can significantly help sample the most appropriate rock types for lithogeochemical exploration while adding geochemical data to the explorer tool box.

Exploration geochemical methods are branching into fields unexpected a decade ago (Coker 2010), many of which are possible through analytical and modelling breakthroughs (Schmidt Mumm et al. 2010). One addition to explorer tool box is the development of field portable chemical analysis instrumentation (gamma-ray spectrometer for U, Th and K; XRF instruments for the entire spectrum of elements but Na, etc.). Based on the IOCG alteration-brecciation-mineralization model, alteration mapping complemented with systematic measurements of % K, eTh (ppm) and eU (ppm) with a portable gamma-ray spectrometer and of rock magnetic susceptibility with a magnetic susceptibility meter, and (ii) systematic staining of rock slabs allows to recognize metamorphosed IOCG systems and develop practical exploration and research strategies while conducting fieldwork both in non-metamorphosed and highly metamorphosed IOCG systems (Antonoff et al. 2010; Corriveau et al. 2010 and unpublished data). Portable XRF are most useful to characterize the entire suite of elements of metasomatic rocks and identify cryptic mineralization but these instruments remain delicate and expensive and cannot be carried in traverses during fieldwork. In contrast the gamma-ray spectrometer is very rugged, and can be carried in the field, dropped walking in the bush and packed with samples with care. It survives difficult field geology conditions and is less expensive than XRF instruments.

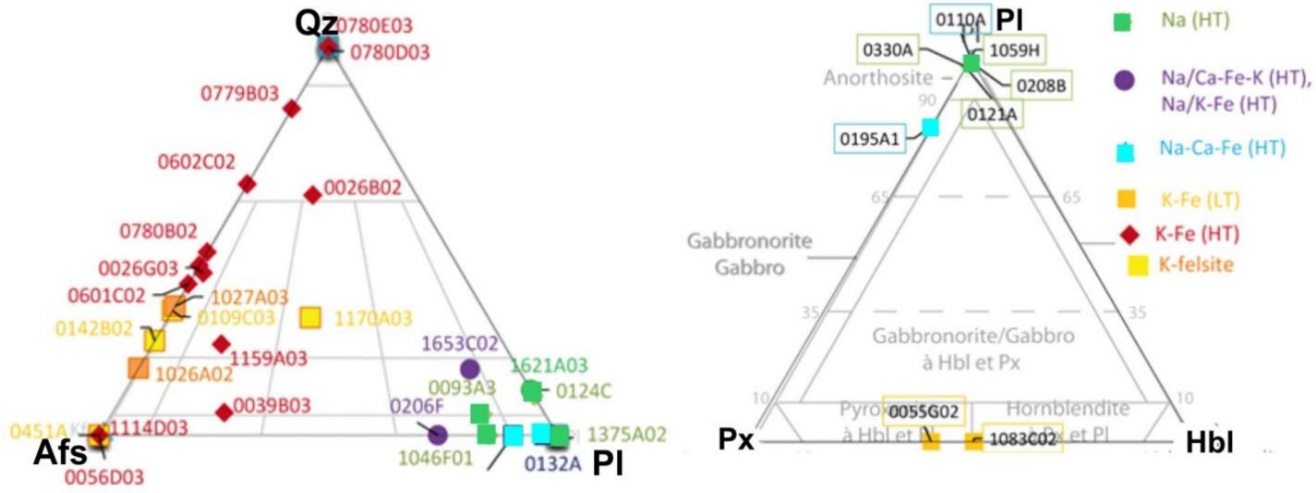

Figure 2.13. Great Bear magmatic zone metasomatic rocks plotted on Streckeisen diagrams for igneous rocks modified by Le Maître et al. (2002). These diagrams are futher discussed in Trapy (2018). **A.** Metasomatic rocks plotted on a QAFP diagram. **B.** Metasomatic rocks plotted on the diagram for gabbroic rocks. By plotting metasomatic rocks on discriminant diagram for felsic-intermediate and mafic igneous rocks, the goal is to portray that metasomatites one metamorphosed will have very similar mineral assemblages to common orthogneisses and may escape recognition even where mineral modes may differ significantly from common igneous rocks.

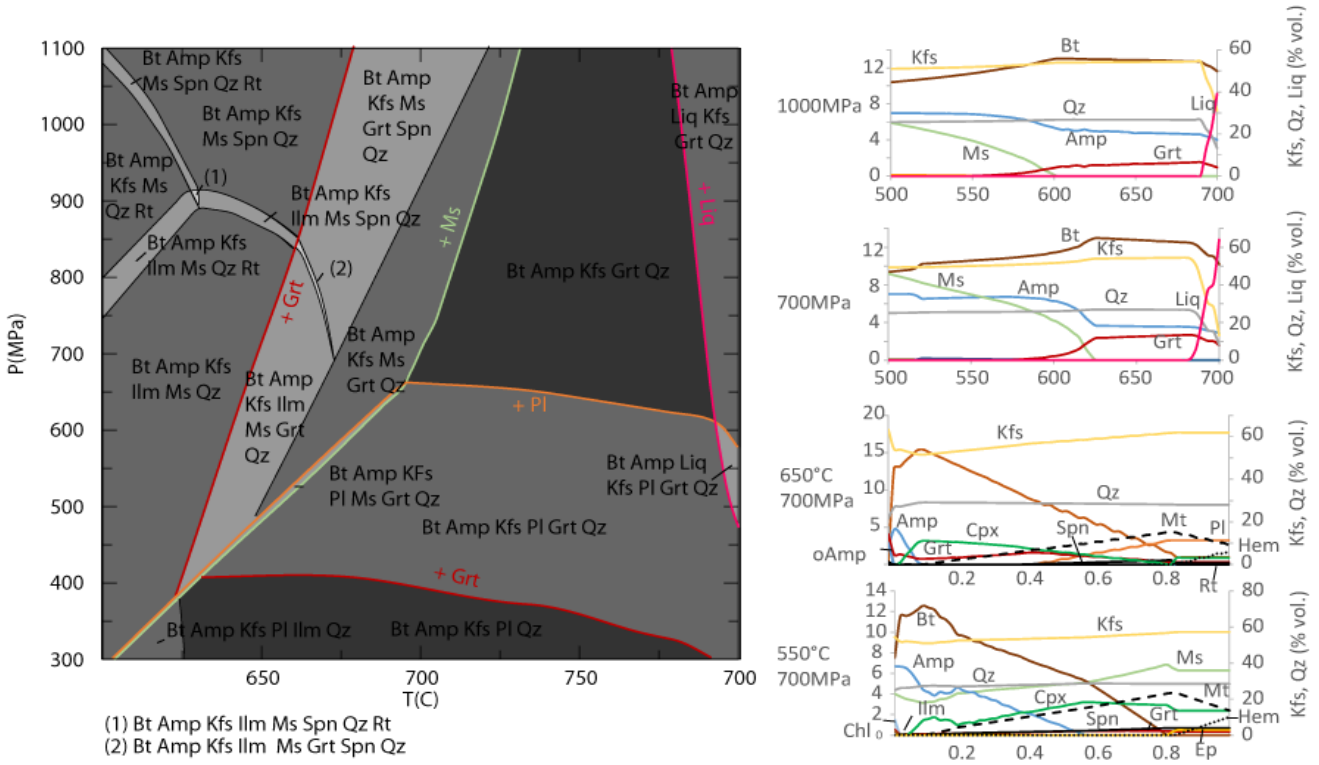

Figure 2.14. Modeled HT K-Fe metasomatite at amphibolite facies. Upper right diagrams show the variations in in mineral assemblages and modes according to increasing temperature (X axis in °C) and lower right diagrams show these variation according to increasing oxygen fugacity (X axis in Mol O_2).

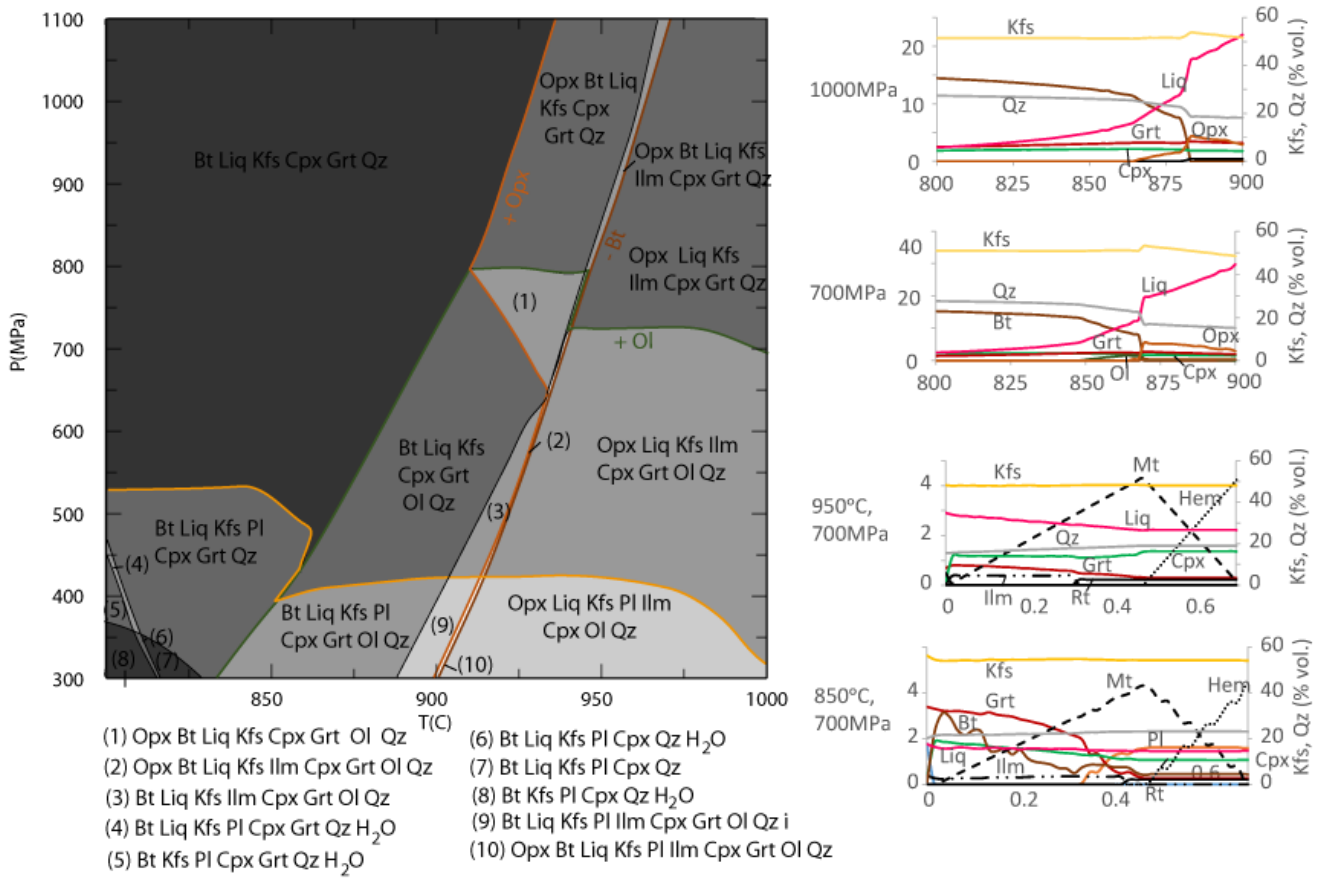

Figure 2.15. Modeled HT K-Fe metasomatite at amphibolite facies. Upper right diagrams show the variations in in mineral assemblages and modes according to increasing temperature (X axis in °C) and lower right diagrams show these variation according to increasing oxygen fugacity (X axis in Mol O_2).

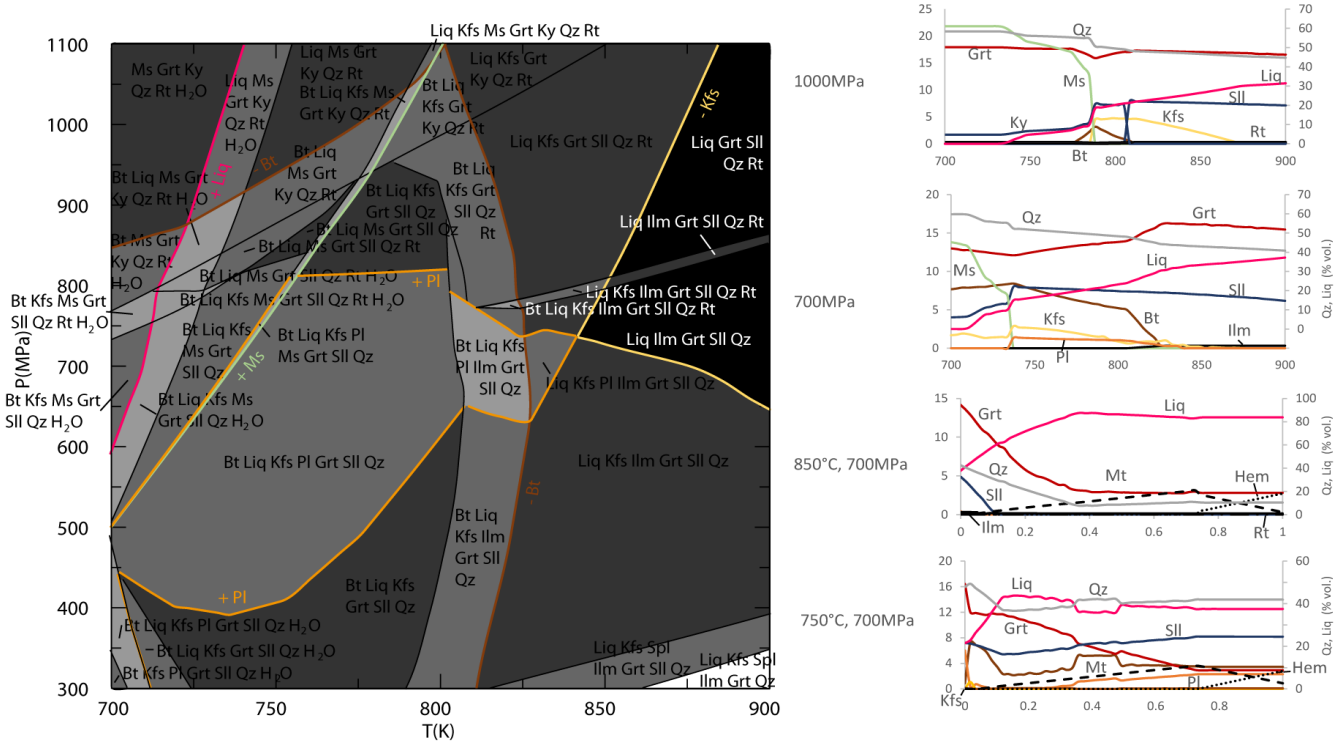

Figure 2.16. Modeled HT K-Fe metasomatite at granulite facies (sample 10-CQA-0780E03, Great Bear magmatic zone (whole-rock analysis in Corriveau et al. 2015). Upper right diagrams show the variations in in mineral assemblages and modes according to increasing temperature (X axis in °C) and lower right diagrams show these variation according to increasing oxygen fugacity (X axis in Mol O_2).

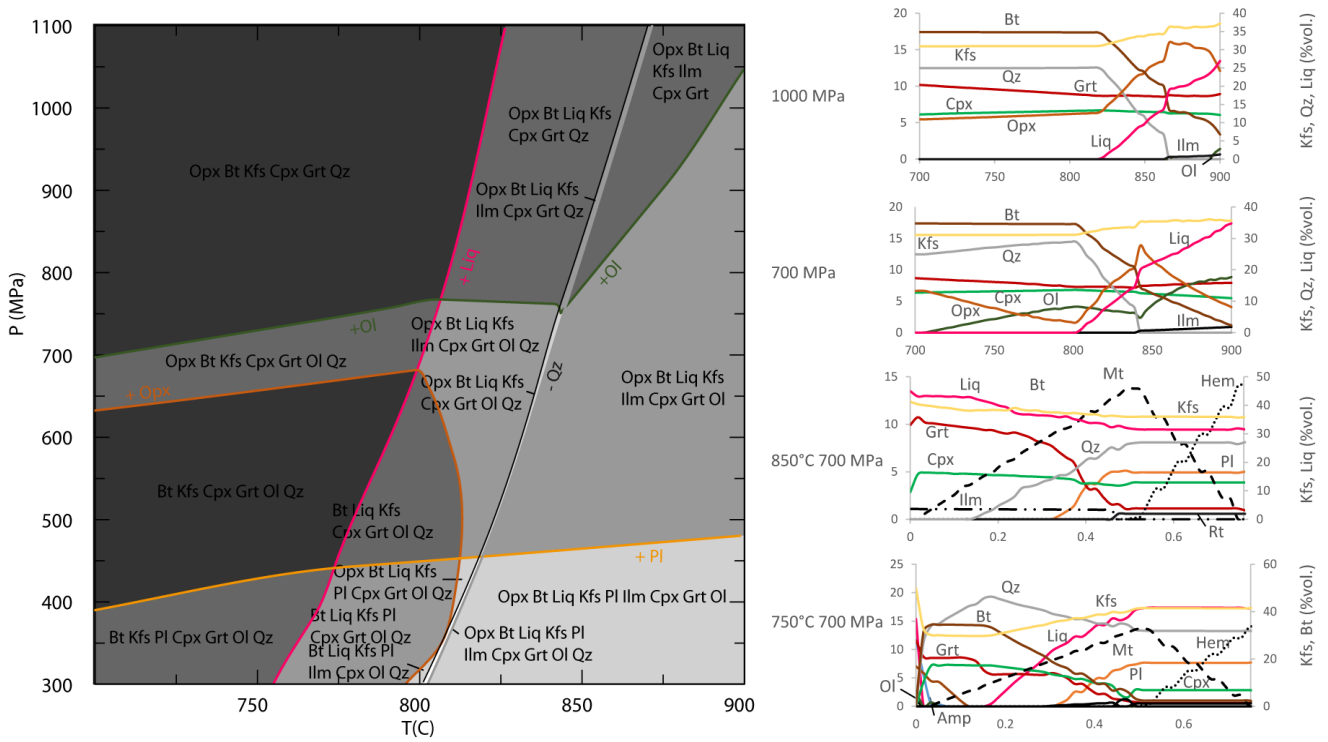

Figure 2.17. Modeled Fe-rich HT K-Fe metasomatite at granulite facies (sample 10-CQA-0601C02, Great Bear magmatic zone (whole-rock analysis in Corriveau et al. 2015). Upper right diagrams show the variations in in mineral assemblages and modes according to increasing temperature (X axis in °C) and lower right diagrams show these variation according to increasing oxygen fugacity (X axis in Mol O_2).

During field work, minor to intense potassic/sodic alteration zones and/or weak to highly significant U-Th anomalous enrichment/depletion may remain concealed among quartzofeldspathic gneisses and go unnoticed without a gamma-ray spectrometer. Variations in K/Th and U/Th ratio provide insights on hydrothermally derived element mobility and help quantify intensity of alteration in the studied hydrothermal systems. For example, zones of Th enrichment helped find rare-earth mineralization in the Great Bear magmatic zone. Consequently mapping and exploring iron oxide and alkali-calcic alteration systems is most efficient with a gamma-ray spectrometer. In fact carrying this instrument or a scintillometer is a basic health and safety measure as radiation is cryptic in the field but may become a health hazard in particular if uranium-rich alteration and mineralization zones are being sampled and transported without appropriate safety measures.

The susceptibility meter helps quantify the intensity of magnetite alteration, though magnetite coarsening (where magnetite remains stable during high-grade metamorphism) makes this issue less problematical in high-grade metamorphic terranes than in non-metamorphosed settings.

2.6 IOAA systems in Laurentia and implications for the Grenville Province

The presence of mineralized iron oxide and alkali-calcic alteration systems in the Great Bear magmatic zone (Canada), in southeast Missouri (USA), Romanet Horst (Canada) and Central Mineral Belt (Canada) emphasize the potential in Laurentia to host additional deposits including in its high-grade metamorphic terranes (e.g. Kwyjibo, Bondy; Corriveau and Clark 2005; Corriveau et al. 2007, 2014, 2016; Slack et al. 2016). Fortunately, the distinctive geological and chemical attributes of iron oxide and alkali-calcic alteration facies remain diagnostic once metamorphosed to high grades. By combining what we know of the geological attributes of non to highly metamorphosed case examples, alteration mapping protocols and chemical discrimination plots can be adapted to remain useful in exploring these ore systems across any metamorphic grades.

Metamorphism of regional-scale alteration systems that can host IOCG deposits leads to very diagnostic lithological and geochemical attributes of metamorphic rock types regardless of the nature of the precursor rocks in the altered units. The distinctive character of such alteration haloes remains once metamorphosed as displayed by the Johnnies Reward prospect and the Bondy gneiss complex (Huston and Hussey 2004; Corriveau et al. 2007; Corriveau 2013; Blein and Corriveau 2017). Within such systems, mineralization styles that are part of porphyry and epithermal systems also occur (Pollard 2000; Mumin et al. 2010; Tornos et al. 2010), hence a continuum from metamorphosed porphyry to IOCG to epithermal signatures is to be expected as documented in the Aitik deposit (Wanhainen et al. 2005), the Andes (Kreiner and Barton 2011), the Great Bear magmatic zone (Mumin et al. 2010) and the Bondy gneiss complex (Blein and Corriveau 2017).

Chapter 3: Regional geology

3.1 Tectonic setting

The development of the southwestern Grenville Province that host the Central Metasedimentary Belt in Québec (Figs. 3.1, 3.2) is part of a protracted episode of continental arc magmatism and back-arc development associated with Pinwarian (1.50-1.45 Ga), Elsonian (1.35-1.3 Ga), Elzevirian (1.28-1.20 Ga) and Shawinigan (1.19-1.14 Ga) magmatic and orogenic activities (Corrigan and Breemen 1997; Nantel and Pintson 2002a; Blein et al. 2003; Wodicka et al. 2004; Dunning and Indares 2010; McLelland et al. 2013; Augland et al. 2015; Hindemith et al. 2017). The geological record of SE Laurentia between 1.6 Ga to 1.2 Ga lacks outboard passive-continental margin sequences. Worldwide, such sequences are typically preserved in thrust belts during collisional orogeny. Their absence in the province further support the existence of an active margin prior to arc accretion to Laurentia (Shawinigan orogeny) and continental collision (Grenvillian orogeny).

3.1.1 Pinwarian continental arc

The Pinwarian arc developed from 1.50 to 1.45 Ga and is typical of Proterozoic continental magmatic arc with calc-alkaline volcanic and granitoid belts that locally evolved to A-type granites. It formed the Britt-Pinware terrane in Canada and the early magmatic belt of the Granite-Rhyolite Province of the USA (Gower et al. 2008; Slagstad et al. 2009; McLelland et al. 2013; Augland et al. 2015).

A well exposed arc-parallel, more than 60 km long volcanic belt is exposed in the eastern Grenville Province (Corriveau and Bonnet 2005). The volcanic rocks consists of mafic to felsic, 1.50-1.46 Ga, calc-alkaline volcanic and volcaniclastic rocks and one exposed subvolcanic mafic intrusion among extensive coeval to subsequent plutons (van Breemen and Corriveau 2005; Bonnet et al. 2005). The plutons are part of a series of batholiths that extend for hundreds of kilometres to the east of the Wakeham Group into the Pinware terrane sensus-stricto (Gower et al. 2008) as well as to the west of the Wakeham Group (Gobeil et al. 2003). All units are gneissic but tectonic windows preserve excellent volcaniclastic textures across the Musquaro-La Romaine volcanic belt. A series of cupriferous, high-sulphidation VMS-type alteration systems have been discovered along the belt but remain significantly under explored (Corriveau and Bonnet 2005; Bonnet et al. 2005). The Musquaro-La Romaine belt displays prograde metamorphism from low amphibolite to granulite facies and many field attributes of volcaniclastic rocks and argillic and advanced argillic alteration zones resemble those of the more deformed units of the Bondy gneiss complex visited during this trip and help interpret the Bondy system as illustrated in Day 3 section.

In the western Grenville Province, Muskoka domain 1.48-1.43 Ga dioritic to granodioritic orthogneisses is calc-alkaline, mantle-derived continental arc magmas (Timmermann et al. 1997; Nadeau and van Breemen 1998; McMullen 1999; Slagstad et al. 2004). Magmatism evolved to A-type granites (e.g. in the Granite-Rhyolite Province, Muskoka domain) in and behind the active continental arc where it was undergoing intra-arc and back-arc extension, around 1.47 Ga. This extension may be due to period of rollback, slab breakoff, or delamination of lithosphere resulting in ascent of asthenosphere at the base of the crust. Iron oxide-apatite and iron oxide-copper gold deposits occur in the Granite-Rhyolite Province.

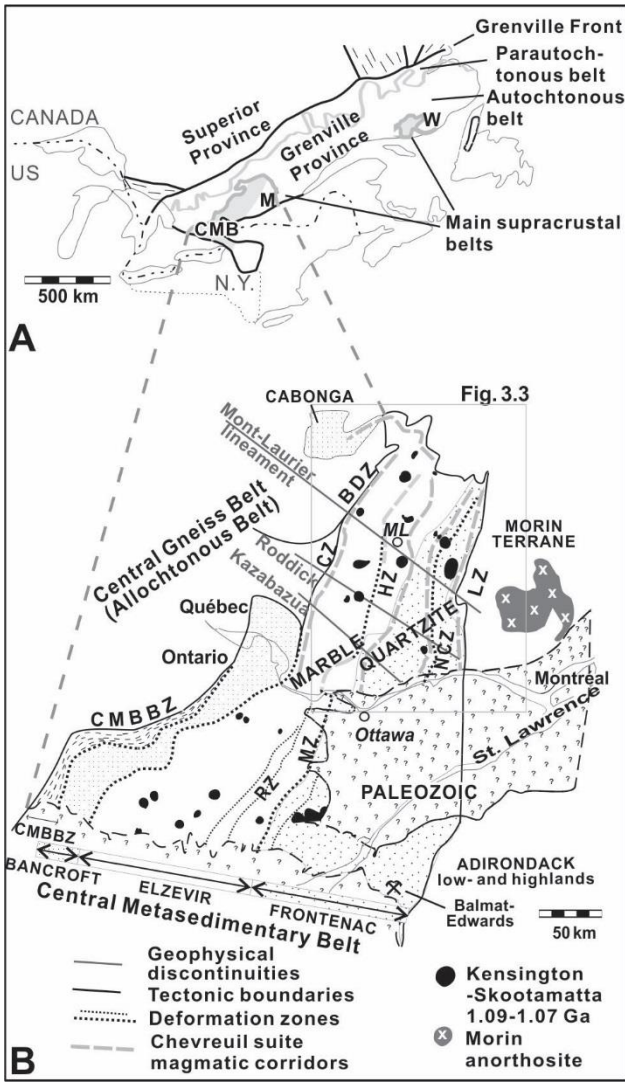

Figure 3.1. A. Subdivisions of the Grenville Province; modified from Rivers et al. (1989) including the Central Metasedimentary Belt (CMB), the Wakeham Group (W) and the Morin Terrane (M). **B.** Schematic subdivision of terranes and domains in the Central Metasedimentary Belt (modified from Corriveau 2013, Dufréchou et al. 2014 and reference therein). CMBBZ: Central Metasedimentary Belt Boundary Zone; BDZ, CZ, HZ, NCZ, LZ, M, and R: deformation zones of Baskatong-Désert, Cayamant, Heney, Nominingue-Chénéville, Labelle, Maberly and Robertson Lake.

3.1.2 1.40-1.30 Ga continental margin arc and opening of back-arc basins

From 1.4 to 1.3 Ga, rifting of the continental arc formed the Central Metasedimentary Belt and the Trans-Adirondack back-arc basins (McLelland et al. 1996, 2010; Chiarenzelli et al. 2011) in the western Grenville Province. These basins evolved southward into outboard arcs preserved in the Adirondack Highlands terrane and some Grenvillian inliers in the Appalachian orogen (McLelland et al. 2013). In the central Grenville Province, the Canyon Domain volcaniclastic rocks were deposited at 1.41 Ga; as per their inferred extension, the 1.44 Ga Montauban Group, they are hydrothermally altered (Dunning and Indares 2010). Both regions are intruded by 1.4-1.37 Ga intermediate plutons that show a continental arc signature (Sappin et al. 2009; Dunning and Indares 2010) as do the orthogneisses at the northern end of the Central Metasedimentary Belt to the west of the Montauban Group (Nantel and Pintson 2002a, b). South of the transverse NW-SE-trending Mont-Laurier lineament (Dufréchou et al. 2014), signature of orthogneisses from this age group changes to that of a juvenile volcanic-arc built over a thin Laurentian continental crust during an incipient rifting event (Blein et al. 2003). Within the Morin terrane, calc-alkaline granitic orthogneisses are potentially slightly younger (1.33 ± 0.03 Ga; Peck 2012). Intra-arc rifting of the Pinwarian continental arc during slab roll back could account for the distribution of 1.4-1.3 Ga rocks in the Grenville Province and the observation of remnants of ocean floor (back-arc) and active volcanic arcs (McEachern and van Breemen 1993; Hanmer et al. 2000; this work).

Dickin and McNutt (2007) interpreted the Central Metasedimentary Belt as a 1.3-1.2 Ga scissor-shape back-arc closing up northward, supracrustal rocks being deposited on blocks rifted from Laurentia. Starting rifting at 1.39 Ga would reconcile the northward variation in tectonic signature of the older, 1.4-1.3 Ga gneiss complex from island arc to the south and continental arc to the north. Considering that the Mont-Laurier lineament is interpreted as the geophysical expression of a lithospheric scale weakness initially developed in the Archaean basement of the Grenville Province (Dufréchou and Harris 2013), a change in lithosphere architecture along this discontinuity could have acted as a buttress for northward propagation of the rift, forcing scissor-shape back-arc rifting of the continental arc as early as 1.39 Ga.

3.1.3 Elzevirian and Shawinigan Orogenies

In the southern part of the Central Metasedimentary Belt, pre-orogenic arc magmatism took place between 1.29-1.26 Ga largely coevally with deposition of the Grenville Supergroup (e.g. unimodal 1284 Ma maximum depositional age derived likely from volcanic material within the Pyrites Complex in the Adirondack Lowlands; Chiarenzelli et al. 2015). Depositon of supracrustal rocks was followed by closure of marginal basins at ca. 1.25–1.22 Ga resulting in the Elzevirian Orogeny (see McLelland et al. 2013 and reference therein).

Arc collision in the south at 1.2 Ga led to 1.19 Ga granulite facies metamorphism in the northern part of the Central Metasedimentary Belt and in the Morin terrane (Corriveau and van Breemen 2000; Schneider et al. 2013) either marking the end of the Elzevirian orogeny of an early phase of the Shawinigan orogeny (Corriveau and van Breemen 2000; McLelland et al. 2013; Dufréchou et al. 2014). Peak metamorphism was followed by orogenic collapse in the CMB-Q (Dufréchou et al. 2014) whereas the main deformation phase in the Adirondack took place at ca. 1.18 Ga and is attributed to arc accretion (McLelland et al. 2013). In Québec, vertical and lateral emplacement of the Morin AMCG suite lead to strongly partitioned, intraplate bulk shortening, development of north-trending deformation zones, and extensive amphibolite-facies overprint in less competent part of the belt and along the deformation corridors at 1.17 Ga (Harris et al. 2001; Boggs and Corriveau 2004; Dufréchou et al. 2014). During initial contraction, mafic to felsic magmas rise along the deformation corridors internally to and along the Central Metasedimentary Belt (Corriveau and van Breemen 2000; Corriveau and Morin 2000; Dufréchou et al. 2014).

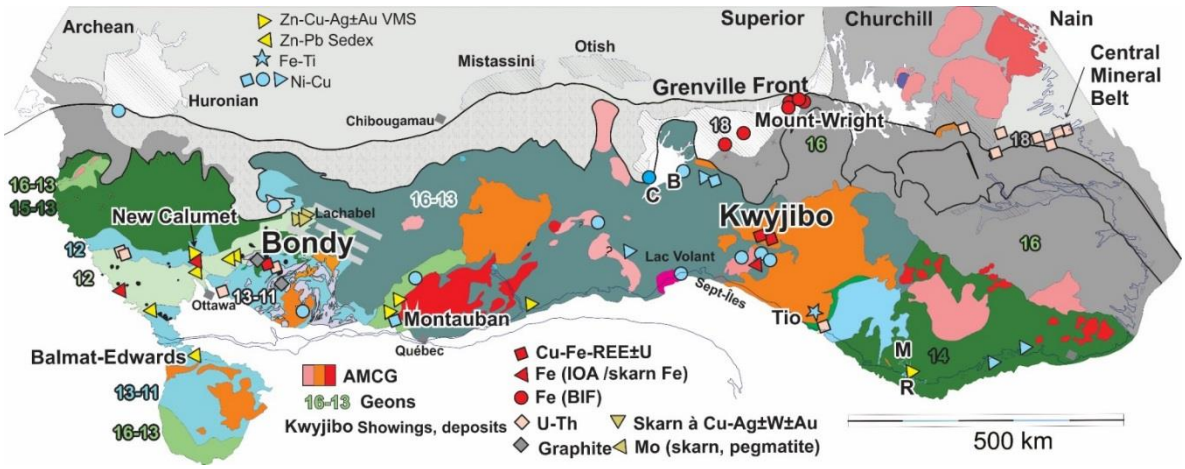

Figure 3.2. The Grenville Province in Canada and the U.S. (modified from Corriveau et al. 2007). Volcanic belts host the New Calumet and Montauban deposits and hydrothermal systems at Musquaro (M), La Romaine (R), Canyon domain (C) and Banded gneiss (B).

Dilation zones during lateral expansion of the AMCG suite led to emplacement of vertically layered mafic intrusions around one of the previously rifted fragment which acted a buttress, the Bondy gneiss complex. Onset of Morin AMCG suite emplacement is coeval with contraction at 1.165 Ga (Corriveau and van Breemen 2000; Corriveau and Morin 2000) but most of the suite postdates it (Emslie and Hunt 1990; Martignole et al. 2000; Peck et al. 2005).

Possible tectonic settings include slab roll back (Mosher et al. 2008), mild extension in a back-arc basin (Rivers 2008), lithospheric scale shear zones (Myers et al. 2008), and lithospheric delamination (McLelland et al. 2004; Morisset et al. 2009). The delamination related model is most consistent with the late- to postorogenic setting indicated by geochronology, the style of magma emplacement and the role of transverse structures in accounting for the successive tectonic event in the region (Dufréchou et al. 2014). In addition sheet-like intrusion not batholiths were emplaced within the lithospheric-scale shear zones active during the Shawinigan orogeny (Corriveau and Morin 2000).

3.1.4 Grenvillian Orogeny

The Grenvillian orogeny consists of the Ottawan (1.09–1.03 Ga) and the Rigolet (1.01–0.98 Ga) phases and is attributed to the collision of Amazonia with Laurentia. During the Ottawan orogeny, allochthons were thrust northwest toward, and over, the Archean and Paleoproterozoic foreland. The Central Metasedimentary Belt escaped reactivation during this orogenesis. Instead potassic-alkaline magmatism took place and is discussed in subsequent sections. Rivers (2008) interprets the belt as an orogenic lid down faulted against the high-grade terranes during orogenic collapse. Faulting would be reactivating existing faults since the Chevreuil intrusive suite stiches the Central Metasedimentary Belt to the Central Gneiss Belt to the west and to the north. Low-temperature mylonites and tectonic breccias are common along the western boundary of the Central Metasedimentary Belt (see Day 4 description of such mylonites) but have not been dated. They rework higher temperature mylonites based on the style of mylonitization of fragments within the low-temperature mylonites.

3.2 Geology of the northern half of the Central Metasedimentary Belt

In Quebec, the Central Metasedimentary Belt includes Mesoproterozoic supracrustal and intrusive rocks first metamorphosed to granulite-facies at 1.19 Ga with early orogenic collapse and final crystallization of leucosomes at 1.18 Ga. Subsequently, part of the belt was reactivated during the Shawinigan orogenesis and gneisses were retrograded locally to amphibolite facies between 1.17–1.16 Ga. These rocks structurally overlap the gneiss units that form the pre-Grenvillian margin of Laurentia (the allochthonous polycyclic belt/Central Gneiss Belt). They occur to the west of the Morin Terrane and its marble-rich supracrustal rocks and anorthosite-mangerite-charnockite-granite (AMCG) suite.

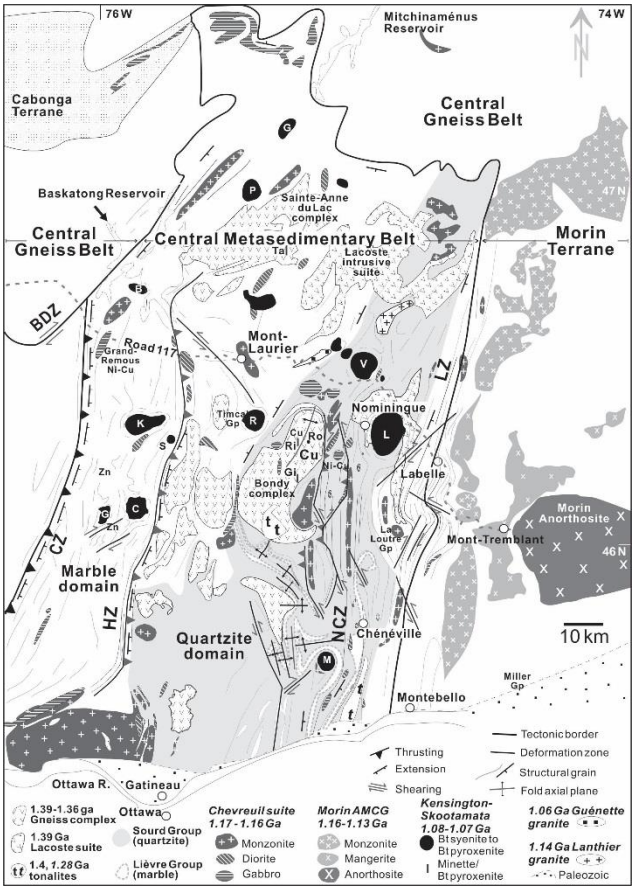

Figure 3.3. Location of gneiss complexes in the Central Metasedimentary Belt of Québec. Only the Bondy and Ste-Anne du Lac complexes have been subdivided. The others remain undifferentiated. These gneiss complexes are structurally overlain by the marble- and quartzite-rich lithotectonic domains (figure modified from Corriveau and van Breemen 2000; Corriveau and Morin 2000; new plutons of the Kensington-Skootamatta suite have been discovered and dated by Davis and Nantel 2016). CZ, HZ, NCZ,-LZ: deformation zones of Cayamant, Heney, Nominingue-Chénéville and Labelle respectively.

The Central Metasedimentary Belt is subdivided into a north-northeast-oriented, marble-rich domain to the west, bordered by a quartzite-rich domain to the east (Fig. 3.3). Granitic to tonalitic gneiss complexes form a series of domes structurally below the marble and quartzite assemblages. From oldest to youngest, the lithodemic units visited during Day 1 to Day 4 transects are:

1. Bondy gneiss complex (1.39-1.36 Ga),
2. Lacoste intrusive suite (1.40-1.36 Ga),
3. Lièvre group and Sourd group (1.28-1.25 Ga?),

4. Chevreuil intrusive suite (1.17-1.16 Ga),
5. Lanthier intrusive suite (1.14 Ga),
6. Kensington-Skootamatta K-alkaline suite (1.09-1.07 Ga),
7. Rolleau ultramafic intrusion, and
8. Guénette granitic suite (1.06 Ga; Fig. 3.4).

Figure 3.4. Guenette granite.

Geochronological and geological information on these suites (Fig. 3.3) can be found in Corriveau et al. (1990), Amelin et al. (1994), Friedman and Martignole (1995), van Breemen and Corriveau (1995), Hébert et al. (1996), Hébert and Nantel (1999), Corriveau and van Breemen (2000), Wodicka et al. (2004), Nantel (2008), Corriveau (2013) and Davis and Nantel (2016). Other lithodemic units occur in the northern part of the belt (e.g. Nantel and Pintson 2002b; Davis and Nantel 2016). One dioritic gneiss attributed to the Lacoste suite gave a Pinwarian age at 1450 Ma (Nantel 2008; Nantel et al. 2008). White granitic dykes coeval with, and predating or postdating Chevreuil mafic dykes are included in the Lanthier suite in this guidebook.

In addition to exposed basement rocks, the region has a widespread Quaternary sedimentary coverage associated with the various ice ages and the Champlain Sea. Boreal forest prevails in most of the Grenville Province and outcrops are generally poor except along lakes and rivers, along main roads, along dirt roads during and a few years after logging, and in the bush after forest fires. Overgrowth by bogs, lichens, trees mask within a few years former outcrops after logging or fires.

The Bondy gneiss complex is an elongate 15 km by 30 km northeast-oriented structural dome composed mainly of tonalitic to granitic gneisses and quartzofeldspathic gneisses metamorphosed to granulite facies. It shares the typical monotonous appearance of Grenvillian gneiss complexes that tend to remain undifferentiated during regional mapping (e.g. Wynne-Edwards et al. 1966). The complex hosts polymetallic Cu-dominant mineralization zones among an iron oxide and alkali-calcic alteration system that evolved to epithermal alteration and mineralization prior to being metamorphosed to granulite facies (Corriveau and van Breemen 2000; Corriveau 2013; Blein and Corriveau 2017).

In the quartzite domain, siliceous gneiss and quartzite prevail and occur with metapelite, biotite- or graphite-bearing quartzofeldspathic gneiss, pyrite-bearing paragneiss locally with tourmaline, marble, calc-silicate rock, and amphibolite. This assemblage forms the Sourd group and contains local graphite showings. The eastern edge of the domain comprises alaskitic and tonalitic gneiss and amphibolite interpreted to be part of the Lacoste intrusive suite. The structural grain trends north-northeast except in the central part where units of dolomitic and serpentine marble form folds with kilometre-scale amplitudes and east- or north-trending axial planes. These units extend northward and reach the interface between the marble and quartzite domains, forming the Lièvre group. On the basis of U-Pb dating of zircon inferred to be detrital, the metasedimentary units are estimated to date from between 1.28 and 1.25 Ga; however, the age of the Lacoste intrusive suite combined with field relationships indicate that some metasedimentary rocks are older than 1.36 Ga (Nantel and Pintson 2002a, b).

All the units of the marble and quartzite domains and of the gneiss complexes were metamorphosed and migmatized to upper amphibolite to granulite facies at between 1.2 and 1.18 Ga (Figs. 3.5, 3.6). Subsequently they were cut by five intrusive suites, three of which are of regional extent (Chevreuil intrusive suite, Kensington-Skootamatta potassic alkaline suite, and Guénette granitic suite).

Four large north-trending deformation zones occur in the Central Metasedimentary Belt in Quebec. The Cayamant deformation zone to the west separates the Central Metasedimentary Belt from the Central Gneiss Belt and the Labelle deformation zone to the east separates it from the Morin Terrane. The internal Heney and Nominingue-Chénéville deformation zones mark the eastern and western outcrop limits, respectively, of the gneiss complexes. These structures record amphibolite- facies deformation and correspond to listric seismic reflectors inclined to the east. Teledetection analysis and ground surveys highlight a network of conjugate northeast- and northwest-trending shear zones associated with the north-trending deformation zones (Rivard et al. 1999; Harris et al. 2001).

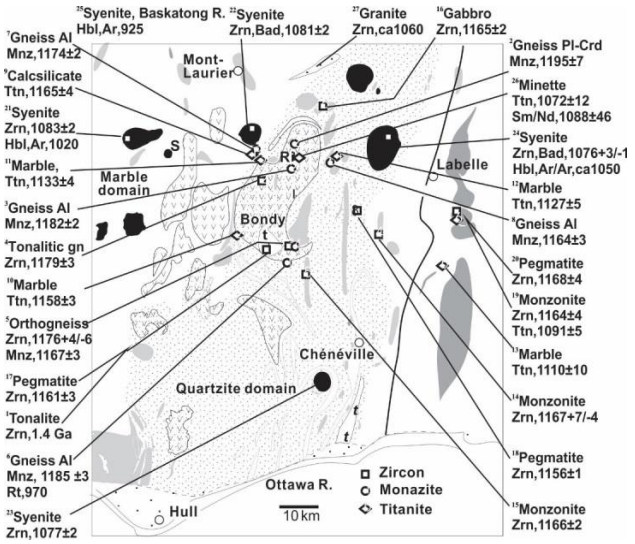

Figure 3.5. Summary of U-Pb ages in Ma (identification number refer to Table 9 in Corriveau (2013). Sources in Corriveau et al. (1990), Hanes et al. (1994), van Breemen and Corriveau (1995), Boggs (1996), Corriveau and van Breemen (2000), Wodicka et al. (2004), Corriveau (2013), van Breemen, Boggs and Corriveau unpublished data).

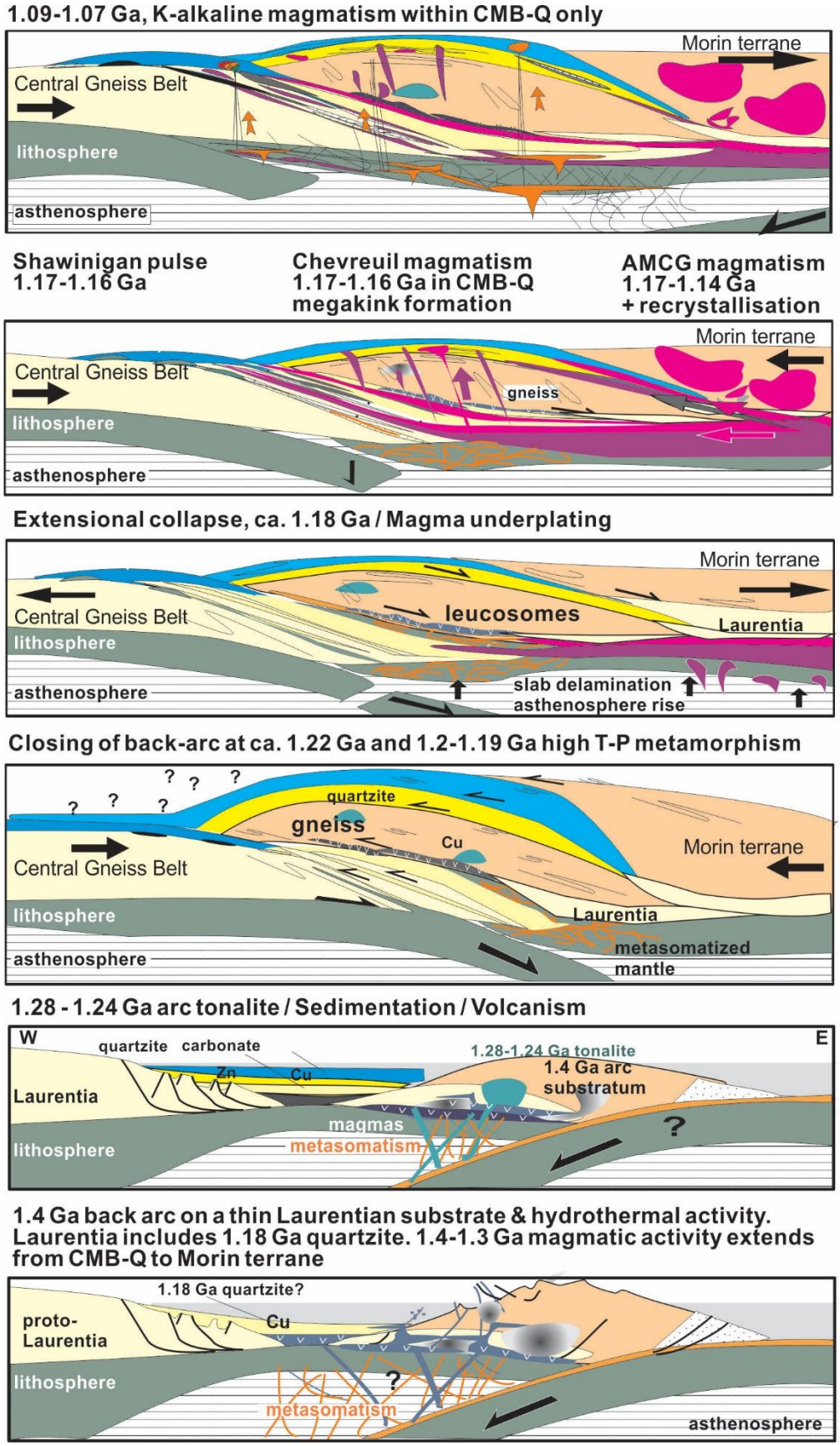

Figure 3.6. Cartoon of the evolution of the Central Metasedimentary Belt in Québec (modified from Corriveau and Morin 2000; Corriveau 2013).

Chapter 4: Miller graphite (Day 1 AM)*

The Miller graphite deposit is located 5 km to the north of Grenville in southern Quebec, approximately 75 km west of Montreal, and it is accessible from highway 50 and Scotch road (Fig. 4.1). The deposit is hosted in metasedimentary rocks of the Morin Terrane, approximately 20 km east of the Labelle deformation zone, which marks the western boundary of the Morin Terrane with the Central Metasedimentary Belt (Fig. 3.3).

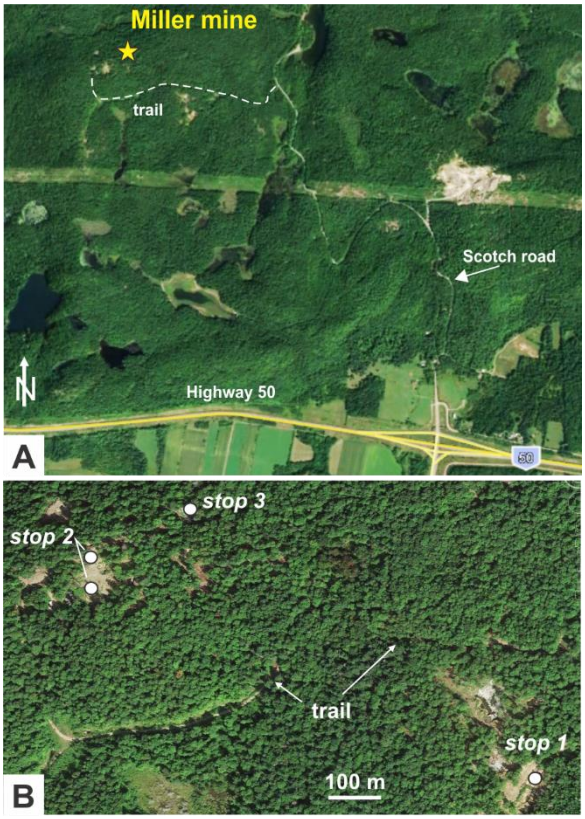

Figure 4.1. A. Map showing the access roads to the Miller deposit. The yellow star indicates the position of the Miller mine. **B.** location of the field stops 1.1.1-1.1.3. Image @2018 Google.

Graphite mining and first descriptions of graphite occurrences in the area surrounding the Miller deposit, by Sir Willian Logan, took place in the 19th century (Ells 1904; Spence 1920). Economic assessment of graphite resources was initiated in 2015 by Canada Carbon Inc. (100% ownership) and a recent evaluation estimates 79 200 t of graphite carbon (Cg %) open-pit resources (inferred & indicated) at a cut-off grade of 0.5 Cg % (2017, NI 43-101 Technical report of the mineral resource estimation of the Miller project). The Miller deposit includes high-crystallinity graphite occurring as veins and pods that are hosted in high-grade metamorphic rocks, and are thought to have precipitated from carbonic hydrothermal fluids. Preliminary field mapping, graphite $\delta^{13}C$ measurements and U-Pb dating of zircon were conducted on various lithologies of the Miller deposit and are presented herein to highlight the main characteristics of the deposit and help constrain processes leading to graphite concentration in high-grade metamorphic rocks such as the Morin Terrane.

4.1 The Morin Terrane

The Morin Terrane forms part of the allochthonous monocyclic belt of the Grenville Province (Rivers et al. 1989). It consists of granulite-facies orthogneisses, 1.33 Ga in age, and younger marble, paragneiss, quartzite and calc-silicate units typical of the Central Metasedimentary Belt (Martignole and Schrijver 1970; Rivers et al. 1989; Martignole and Corriveau 1991; Peck et al. 2005; Peck 2012). The gneisses are intruded by the Morin anorthosite massif and plutons of the 1165 to 1135 Ma Morin anorthosite-mangerite-charnockite-granite suite (AMCG; Emslie and Hunt 1990; Doig 1991; Friedman and Martignole 1995; Corriveau and van Breemen 2000).

The Morin terrane has undergone polyphase high-grade metamorphism prior to, and during and slightly subsequently to AMCG magmatism (Martignole and Corriveau 1991; Corriveau and van Breemen 2000; Peck et al. 2005). Bounding deformation corridors to the west (the coupled Nominingue-Chénéville and Labelle deformation zones) postdate early granulite-facies metamorphism and are largely coeval with 1.17-1.16 Ga Chevreuil sheet intrusions and onset of magma emplacement of the voluminous AMCG plutonic suite (Corriveau and van Breemen 2000; Dufréchou et al. 2014). Deformation was largely over by 1157 Ma (Corriveau and van Breemen 2000) with local reactivation at 1.07 Ga (Martignole and Friedman 1988). Each reactivation event is recorded either by monazite or titanite ages across the Central Metasedimentary Belt and Morin Terrane (Fig. 3.5; van Breemen, Boggs and Corriveau, unpublished data; Davis and Nantel 2016; Peck 2012).

4.2 Geology of the Miller deposit

Philpotts (1976) defined the main rock units and structural features exposed in the Grenville Township. Rocks underlying the Miller property consist of a 200 to 300 m thick marble horizon also comprising boudinaged quartzite, paragneiss and calc-silicate units that are surrounded by highly strained granitoid rocks and gneisses (Fig. 4.2). The surrounding gneisses are folded and consist of a variety of parageneses with garnet, biotite, plagioclase, sillimanite, and/or K-feldspar- (Fig. 4.3A-B). They show evidence of partial melting and locally mylonitization (Fig. 4.3B). Granitoid rocks are tightly folded and metamorphosed with a well-developed gneissic fabric (Fig. 4.3C). In such rocks, leucosomes are deformed and quartz defines a foliation. Regionally, such attributes are typical of gneisses

metamorphosed at 1.19 Ga at granulite facies and overprinted by amphibolite facies deformation at 1.17-1.16 Ga (see Corriveau 2013).

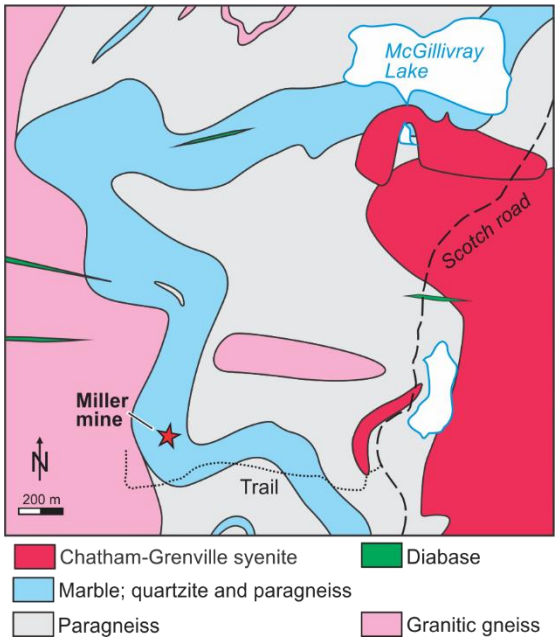

Figure 4.2. Geological map of the area surrounding the Miller deposit. The star indicates the location of the past-producing Miller mine pit. Modified from Philpotts (1976).

The Chatham-Grenville syenite forms large intrusive bodies exposed in a local quarry to the east of the Miller graphite deposit and metasedimentary rocks are cut by graphic-textured muscovite granite. Amphibolite is also present and diabase dykes belonging to the ~ 590 Ma Grenville dyke swarm (Kamo et al., 1995) are common. In addition, the Chatham-Grenville syenitic stock dated at 531.4±3.4 Ma (Ar-Ar plateau age on hornblende; McCausland et al. 2007) cuts the Grenville Province rocks as well as the diabase dykes, and is coeval with the formation of the Ottawa-Bonnechere aulacogen and its fault system (Philpotts 1976; McCausland et al. 2007).

The marble consists of granoblastic calcite and diopside with minor quartz, graphite and titanite. Many examples have compositional layering but it is generally medium to coarse-grained size and typical of Grenvillian marble that have been strongly deformed and subsequently recrystallized. Serpentine pseudomorphs after olivine, microcline and grossular were also documented (2017, NI 43-101 Technical Report of the Mineral Resource Estimation of the Miller Project).

The quartzite unit is granoblastic, contains diopside and is fine to medium grained, whereas the paragneiss layers are thin (< 10 cm) and biotite-rich. The calc-silicate rocks are mainly developed along or close to contacts of boudinaged quartzite and paragneiss within the marble unit, or along its contacts with the surrounding gneisses, and varies from a fine- to a coarse-grained (0.5-20 cm) facies (Fig. 4.3D-F). These rocks can be massive and devoid of foliation, or are strongly foliated with well-defined compositional banding (Fig. 4.3F-I). They also form large boudins and clasts in the marble unit as is typical of marble and calc-silicate units that have been strongly deformed (Fig. 4.3J-K). The coarse-grained calc-silicate facies, represented by skarn-type assemblages, consists of clinopyroxene (diopside and augite), plagioclase, quartz, wollastonite, titanite, graphite, zircon, grossular, and lacks calcite and dolomite (Fig. 4.3E-F). This coasrse-grained facies varies from massive and undeformed to locally strongly foliated and lineated. Vesuvianite is also locally present. Zircon, titanite and diopside are mutually intergrown and contain euhedral graphite inclusions. The distribution of the calc-silicate rocks is best explained by metasomatic replacement of the marble unit during high-grade metamorphism, with possible additional skarn formation in association with a contribution of magmatic fluids from AMCG suite magma emplacement.

Remobilization is common across the area as shown by the presence of carbonate veins that cut across calc-silicate breccias, themselves hosted among gneissic marble and calc-silicate assemblages where the gneissosity wraps around the overall packages of calc-silicate clasts (Fig. 4.3J).

4.3 Graphite occurrences

Graphite occurrences within the Miller deposit are variable in nature but mainly include homogeneously distributed disseminated 1-5 mm flakes of graphite (0.5 modal percent) in the marble, and fine to coarse (up to 3-4 cm) graphite disseminations, clusters, veins and pods in association with calc-silicate rocks. Stratabound replacement of the compositional layering and gneissosity by fine-grained graphite is locally well preserved and overlaps several layers (Fig. 4.3G-I). Some of these replacement fronts do not appear to have been significantly deformed subsequently. The graphite-bearing veins are highly strained to non-deformed and consist of massive, fine-grained to large crystalline graphite flakes. In some cases, veins cut the gneissosity (Fig. 4.3G). They show a similar mineralogy to pods, and either almost exclusively consist of graphite, or contain some proportion of euhedral wollastonite, and/or plagioclase crystals (Fig. 4.3L-O). The pods show evidence of structural control as some of them are well developed in the crests of folds (Fig. 4.3N). Pods and veins also occur in association with disseminated graphite and semi-massive graphite layers, usually concentrated along the contact zones between the quartzite and the marble, where fine to coarse-grained calc-silicate rocks are also developed (Fig. 4.3D-E and G-I). Massive graphite veins with sharp and straight contacts cut the ductile foliation in the gneisses, marble and calc-silicate rocks, do not contain wollastonite or plagioclase, and represent a very late hydrothermal or remobilization event (Fig. 4.3P).

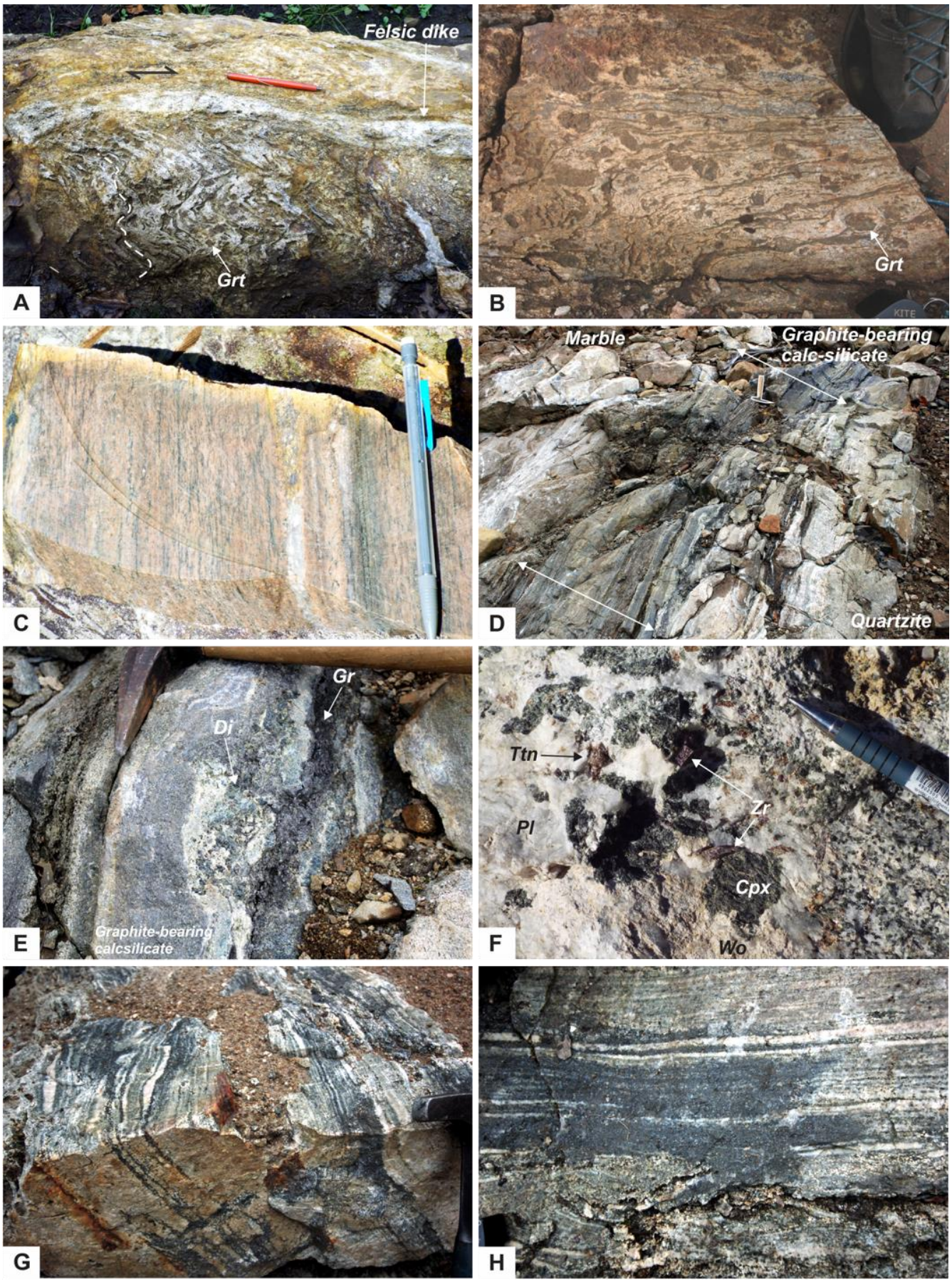
Felsic dike
Grt
A
Grt
B
C
Marble
Graphite-bearing
calc-silicate
Quartzite
D
Gr
Di
Graphite-bearing
calcsilicate
E
Ttn
Zr
Pl
Cpx
Wo
F
G
H

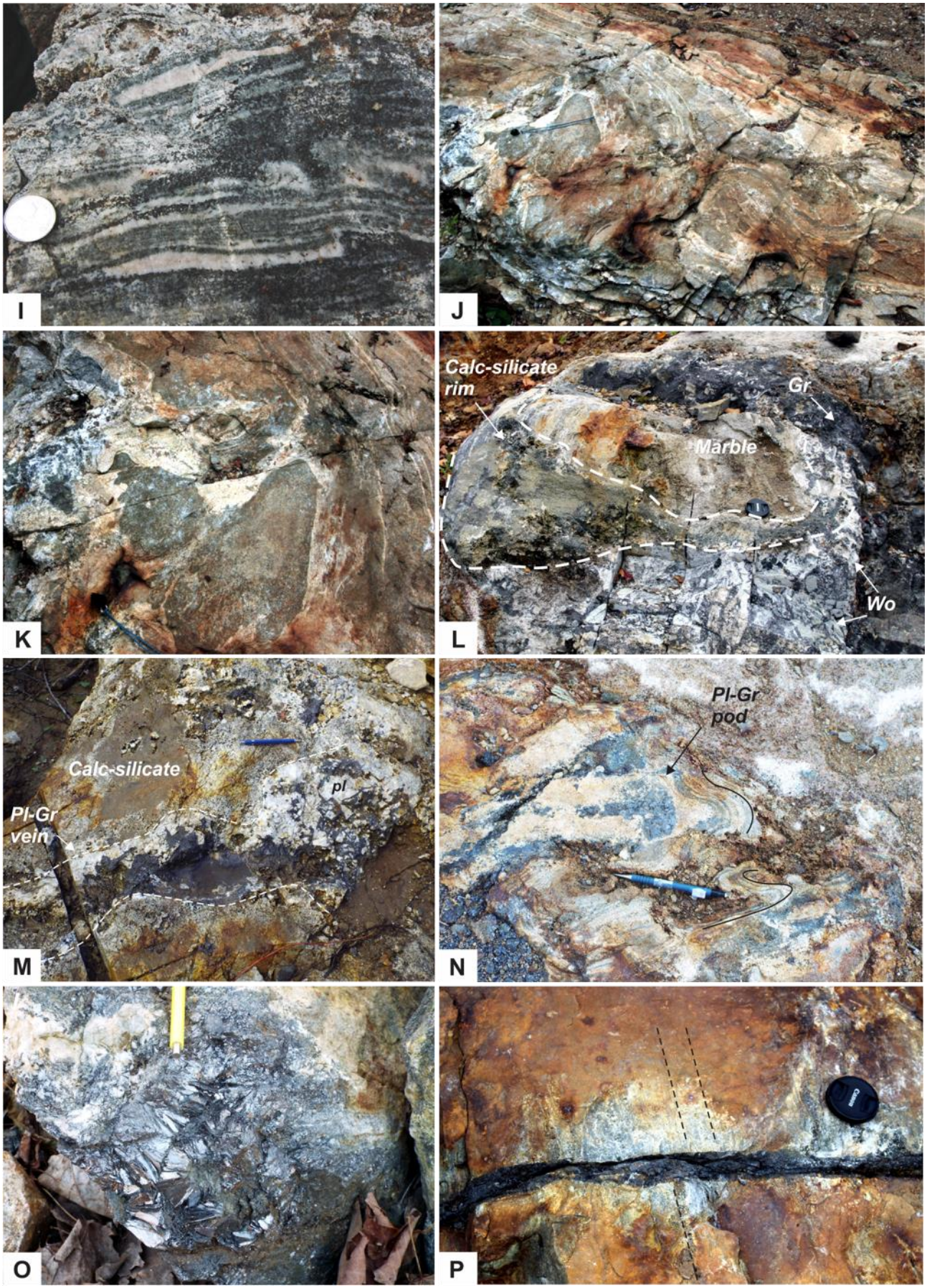
I
J
K
Calc-silicate rim
Gr
Marble
Wo
L
Calc-silicate
pl
Pl-Gr vein
M
Pl-Gr pod
N
O
P

Figure 4.3. Field photographs of graphite host rocks and occurrences. **A.** Folded gneissic layering (stippled line) in garnet (Grt)-bearing gneiss with dyke injection along deformation zone (black symbol) in axial plane of fold. **B.** Same locality as (A). **C.** Highly strained granitoid bounding the western contact of the main marble horizon on the Miller property. **D.** Graphite and calc-silicate rocks developed along contact between marble and quartzite. **E.** Calc-silicate rock hosting disseminated graphite and graphite layers. **F.** Coarse-grained plagioclase (Pl), titanite (Ttn), clinopyroxene (Cpx), wollastonite (Wo) and zircon (Zr) in calc-silicate rock. **G-I.** Banded calc-silicate rock with graphite replacing the skarn mineralogy. Note the presence of shallow-dipping graphite veins cutting the gneissossity. **J-K.** Boudinaged layers and clasts of calc-silicate rock. **L.** Graphite-wollastonite pod with marble enclave showing a calc-silicate rim. **M.** Graphite-plagioclase (Pl) vein in calc-silicate rock. **N.** Graphite-plagioclase pod in crest of folded calc-silicate rock. **O.** Crystalline graphite pod. **P.** Late graphite veins cutting the layering and the gneissosity in calc-silicate rocks (stippled lines).

4.4 Isotopic data

Carbon isotopic composition of graphite and U-Pb zircon geochronology were conducted on samples from the Miller deposit and yielded significant preliminary results. Graphite from the calc-silicate rocks and coarse-grained veins and pods, have $\delta^{13}C$ values that are negative (-11 to -1.5 ‰), but overlap with the range of $\delta^{13}C$ for calcite from Grenville terranes, and graphite from marble exposed on the Miller property (Fig. 4.4). The $\delta^{13}C$ values for graphite also overlap with vein graphite deposits hosted in amphibolite- and granulite- facies hosts in Sri Lanka and Montana (Luque et al. 2012).

One large zircon grain (1 x 2 cm) containing euhedral graphite inclusions was sampled from a coarse-grained calc-silicate rock. The sample was crushed and mounted for LA-ICP-MS analysis at the GEOTOP (Centre de recherche en géochimie et géodynamique) facilities in Montreal. Twenty spot analyses were conducted on ten zircon fragments, and yielded an age of 1143 ± 11 Ma interpreted as the age of zircon crystallization in the calc-silicate rock (Fig. 4.5). The coarse-grained and massive (isotropic) attributes of these rocks indicate that they formed after the pervasive 1.17-1.16 Ga deformation event that has been recorded by leucosomes and Chevreuil dykes.

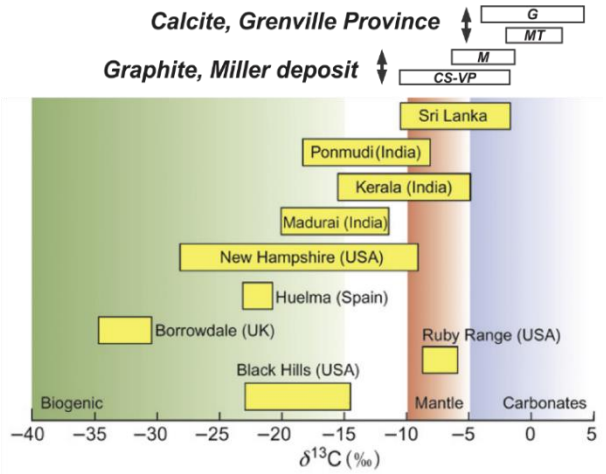

Figure 4.4. Ranges of carbon isotopic composition for fluid-deposited graphite occurrences. Ranges of $\delta^{13}C$ for main carbon sources: biogenic - green; red - mantle; blue - carbonates. MT - carbonates of the Morin terrane; G - carbonates from various Grenville terranes (Peck et al. 2005); Graphite from the Miller deposit: CS-VP – calc-silicate, veins and pods; M - marble. Modified from Luque et al. (2012). See Luque et al. (2012) for full references on ranges of $\delta^{13}C$ for graphite from various deposits.

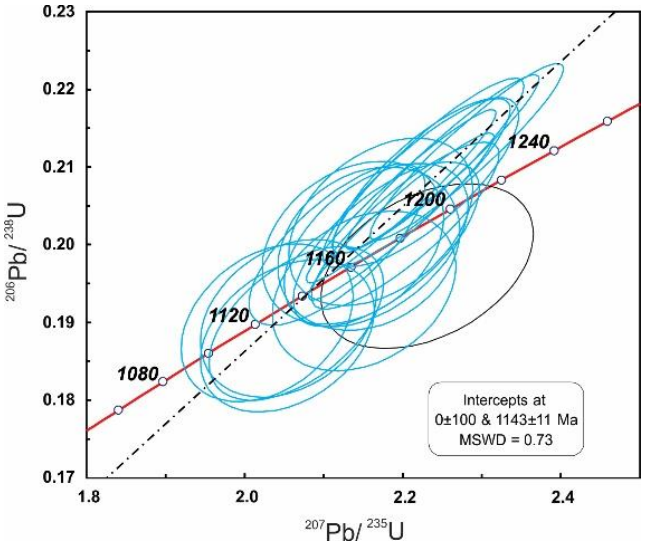

Figure 4.5. Concordia diagram for a one centimetre-size zircon crystal analysed by laser ablation ICP-MS.

4.5 Deposit model

The Miller graphite deposit is the result of a complex geologic and hydrothermal evolution linked to high-grade metamorphism and remobilization, as indicated by its spatial association with wollastonite-bearing veins and calc-silicate rocks. The nature of graphite occurrences, as well as their measured spread in $\delta^{13}C$ values also suggest that carbon may in part originate from decarbonatation of the marble unit, or mixing of more than one carbon source. The stratabound replacement of carbonate and calc-silicate rocks by graphite and the distribution of the replacement fronts across the gneissosity indicate that graphite precipitation postdates the gneissic foliation. Lack of field markers within currently available outcrop hampers interpretation as to whether this gneissosity represents the early, pre-AMCG suite, gneiss-forming event at ca. 1.19 Ga or the subsequent deformation coeval to AMCG emplacement suite (see Dufréchou et al. 2014).

Preliminary U-Pb zircon geochronology suggests that the high-grade metamorphism that gave way to decarbonation of the marbles to form graphite took place at *ca.* 1143 Ma within zircon-bearing calc-silicate rocks that escaped both the 1.19 Ga and the 1.17-1.16 Ga metamorphic events. This age is contemporaneous with the late stages of AMCG magmatism in the Morin terrane, emplacement of the anorthosite massif at 1.15 Ga, and renewed formation of skarn and endoskarn (Peck et al. 2005). In this setting, it is

however difficult to assess if calc-silicate rocks were also formed during high-grade metamorphism at 1.19 Ga, as recorded in the Central Metasedimentary Belt (which escaped to a large extent pervasive 1.17-1.16 Ga overprint) and which one are related to the emplacement of the AMCG suite.

Current working hypothesis is that graphite in the plagioclase- and wollastonite-bearing veins and pods precipitated either from the cooling of a C-H-O hydrothermal fluid, or from the mixing of CO_2- and CH_4-rich fluids as a result of graphite saturation. The principle of graphite saturation as a result of fluid mixing is best illustrated in the C-H-O system and elegantly synthesized by Simandl et al. (2015; see Fig. 4.6). In such a model, the carbonic fluids may be derived from devolatization of both the marble and the gneisses surrounding the Miller deposit, during the high-grade metamorphism of the metasedimentary rocks related to the emplacement of the AMCG suite within the Morin Terrane. Outcrop- and map-scale field relationships also indicate that folds and stratigraphic contacts may have played a major role in the mobilization and precipitation of coarse-grained graphite, since non-pervasively deformed graphite pods occur within fold hinges. In addition, graphite occurring as replacements of calc-silicate gneisses and as inclusions in zircon and diopside, indicates that graphite formed coevally or after the calc-silicate rocks at 1.43 Ga. The structurally-controlled graphite-plagioclase-wollastonite pods indicate that graphite was remobilized and precipitated from a hydrothermal fluid at high temperature. Graphite mineralization is overall paragenetically late, postdates 1.16 Ga deformation along the Nominingue-Chénéville and Labelle deformation zones, and was further remobilized in fractures as evidenced by the presence of late graphite veins. This study is preliminary and further mapping of field relationships and host rock characterization are necessary. We speculate that the presence of favourable units leading to skarnification and to the generation of carbonic fluids during magma emplacement and associated high-grade metamorphism, and of structural conduits and traps for fluids, are favourable features for the formation of graphite deposits in metasedimentary rocks of the Morin terrane.

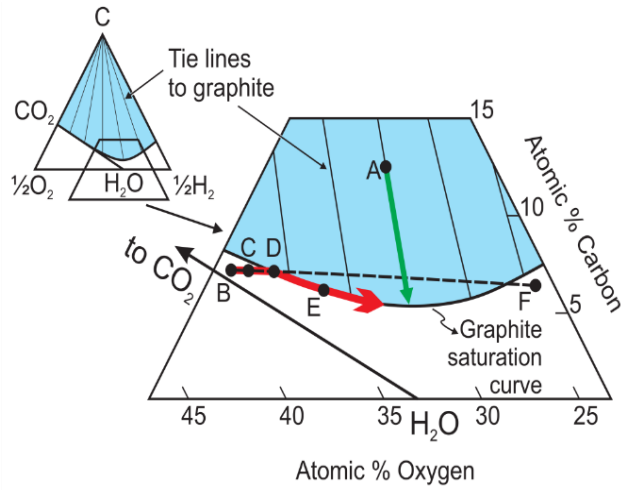

Figure 4.6. Ternary C-O-H diagram (600ºC - 3.5 kbar) showing precipitation of graphite from the fluid composition A (within the graphite stability field) and from mixing of fluids of composition B and F, both lying outside of the graphite stability field. Adapted from Simandl et al. (2015).

4.6 Field stop 1.1 for Day 1 AM

Stop 1.1.1 displays disseminated graphite in marble and graphite pods in calc-silicate rocks (Fig. 4.3N). Stop 1.1.2 exhibits highly strained contact between marble and coarse-grained wollastonite-diopside-titanite-zircon calc-silicate rocks with graphite veins (Fig. 4.3M), as well as graphite veins and pods (Fig. 4.3L and P). Stop 1.1.3 is on the site of the past-producing open-cut excavation of the Miller deposit.

Chapter 5: Chevreuil suite syntectonic magma emplacement in the Quartzite domain and Nominingue-Chénéville deformation corridor (Day 1 PM)

5.1 Chevreuil intrusive suite (1165±2 Ma)

The Chevreuil intrusive suite includes more than fifty homogeneous or composite sheet intrusions of porphyroid monzonite, heterogeneous diorite and gabbronorite, four vertically layered gabbronorite intrusions as well as a swarm of dykes (Corriveau 2013). The dykes and plutons of the Chevreuil intrusive suite can be traced from the Central Gneiss Belt to the Morin Terrane across the entire Central Metasedimentary Belt of Québec (Figs. 3.1, 5.1; Corriveau 2013). In the gneiss complex, intrusions are uncommon (one large sheet of gabbro) but dykes outcrop regularly. They are not deformed. U-Pb data support field relationships in terms of sequence of magma emplacement with plutonic phases first, between 1167 and 1164 Ma, followed by mafic and commingled mafic-felsic dykes (e.g. the 1161 Ma composite dyke within the Bondy gneiss complex) and then by pegmatite dykes (e.g. 1156 Ma pegmatite) (Corriveau and van Breemen 2000). Porphyritic monzonite, 1165 Ma in age, are also associated with the anorthosite mangerite charnockite granite (AMCG) suite of the Morin domain to the east (Corriveau and van Breemen 2000) and with a monzonite-gabbro suite of the Frontenac terrane in the Central Metasedimentary Belt to the south in Ontario (Davidson 1995a).

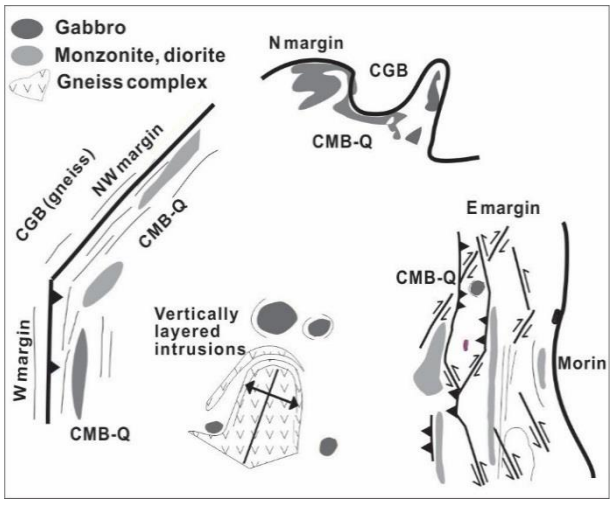

Figure 5.1. Synoptic view of the distribution of the Chevreuil intrusive suite showing sheet like intrusions along tectonic boundaries. Such style of emplacement along the fault zones along domain boundaries imply that the domain were adjacent to each others during emplacement. See discussion in Corriveau and van Breemen (2000) and Corriveau et al. (2007).

5.2 Sheet intrusions

The sheet intrusions of the Chevreuil intrusive suite are sub vertical and aligned along the tectonic margins of the Central Metasedimentary Belt in Québec and its extensive, north-south-oriented deformation zones (Cayamant, Heney, Nominingue-Chénéville, and Labelle). The sheet intrusions have a strong, planar, sub vertical fabric parallel to their general trends and defined by the preferred orientation of idiomorphic to hypidiomorphic feldspar crystals and microdiorite enclaves, and by magmatic layering defined by compositional, modal, or grain-size variations. Such fabrics have an igneous origin even though locally they give the rocks a gneissic appearance (Corriveau 2013). They result from magma flow driven by magmatic, sub magmatic, or solid state deformation with or without external stresses. In the Nominingue-Chénéville deformation zone, the structure and fabric of the sheets indicate emplacement by repeated injections of mafic and felsic magmas during regional east-west contraction. The microdiorite, monzonite, and pegmatite dykes associated with the Chevreuil intrusive suite were also emplaced syntectonically. Cross-cutting relationships and a U-Pb age indicate that this episode of emplacement was waning by 1157 ± 2 Ma. These intrusions, whose sub vertical aspect was acquired at the time of emplacement, differ significantly from mafic-silicic layered intrusions (MASLI), whose vertical structure results from transposition of layers that were horizontal at the time of or slightly after emplacement (Corriveau and Morin 2000; Saint-Germain and Corriveau 2003).

The distribution of the Chevreuil sheet intrusions along the belt's deformation zones and their primary intrusive, tabular, and concordant nature attest to the existence of tectonic margins along the belt before 1.17 Ga and to the current configuration of the various components of the belt at that time (Corriveau and van Breemen 2000). Similar age intrusions have recently been identified along the western margin of the Central Metasedimentary Belt in Ontario (Duquet and Easton 2017) in line with the tectonic model of Corriveau and van Breemen (2000) for pre-Shawinigan amalgamation of Central Metasedimentary Belt terranes to Laurentia. Chevreuil intrusions are coeval with the 1.165 to 1.35 Ga Morin AMCG suite farther east. This timing and the syntectonic nature of the Chevreuil intrusive suite show that the Morin AMCG suite was partly emplaced during a compressive orogenic pulse more than 40 Ma after peak metamorphism and therefore is not the product of anorogenic magmatism (see further discussion in Dufréchou et al. 2014).

The sheet intrusions of the Chevreuil intrusive suite and the host deformation zones correspond to east-dipping

listric seismic reflectors (Corriveau and Morin 2000). They are interpreted as magma conduits whose source is in felsic and mafic magma reservoirs located at the Moho under the Morin AMCG suite plutons. Magma ascent would have been triggered by deformation (Corriveau and Morin 2000; Dufréchou et al. 2014). These crustal-scale faults are partly enclosed in metasedimentary rocks. Channelling of magma along these faults facilitated the felsification of mafic magma during successive or simultaneous felsic and mafic magma injection, as well as the assimilation of metasedimentary rocks. Ultimately what is left of such assimilation are xenoliths largely monomineralic consisting of quartzite, skarn and coarse K-feldspar-rich component of pegmatite. In parallel close to zones of assimilation of marble, monzonites become enriched in clinopyroxene at the expense of the more typical hornblende and biotite paragenesis. These processes explain how the trains of gabbronorite and monzonite sheet intrusions formed along tectonic zones have precipitated magmatic Ni-Cu sulphides. For example, concentrations of magmatic sulphides reach 4.22% Cu and 0.75% Ni in the Grand-Remous pluton along the western margin of the belt; thus, tectonic margins and their roofs represent a first order target for magmatic Ni-Cu sulphide exploration in highly exhumed orogens (Corriveau 2013).

5.3 Stop descriptions for Day 1 PM

Day 1 in the afternoon focuses on the Chevreuil monzonite-gabbro suite (1.165 Ga) and the Sourd supracrustal sequence (ca. 1.3-1.2 Ga) in the Quartzite domain of the Central Metasedimentary Belt of Québec. Stop 1.1 starts by examining the supracrustal rocks of the Central Metasedimentary Belt and the adjacent Moring terrane and one of their numerous graphite prospect (Miller). Stops 1.2 to 1.4 contrast styles of magma emplacement along the Nominingue-Chénéville deformation zone and in the Quartzite domain. Stops 1.2 to 1.4 are within the Lac Chevreuil intrusion and stop 1.5 to the west in the Quartzite domain (Figs. 5.2, 5.3). The structure outlined by the mafic dykes and the intrusive sheets provide insights into the tectonic evolution of the belt. The intrusions and dykes also show typical attributes of syntectonic magma emplacement and of extensive country-rock assimilation. The stops are located in the Papineau Labelle Wildlife Reserve, NE of Ottawa-Hull and SW of Montréal.

Topics for discussion on magma emplacement for Day 1 and Day 3 include:

1. magmatic and tectonic foliations, and fabric development in plutonic rocks,
2. syntectonic magma emplacement,
3. role of crustal-scale ramp and dilation jogs as sites for magma transfer from mantle to crust, and
4. role of country-rock assimilation and magma comingling in the genesis of Ni-Cu magmatic ore.

These topics are addressed through the observation of sheet intrusions in Day 1 and if time permits the Kar-Ha-Kon layered intrusion in Day 3. They piggyback on ample case examples worldwide including those from the classic papers of Paterson et al. (1989), Pavlis (1996) and Irvine et al. (1998).

Directions: From Papineauville mid-way between Ottawa and Montréal along highway 50 take exit 205 (~45°39'50.3"N 75°01'05.8"W). Head North on Route 321 as far as Duhamel (from Duhamel you need to head to Accueil Gagnon, the point of entry to the Papineau Labelle Reserve if you have not paid your access fee beforehand.) From Duhamel turn left on Rue Principale (45.663973, -75.018290) and drive 2.0 km. Turn right onto Chemin du Tour du Lac and drive for 1.5 km. Turn right onto Chemin des Lacs and drive 10.1 km to park at the intersection with the Chemin du Lac Chevreuil and walk West for 0.5km for Stop 1.2 at 46.050041, -75.205346 (Stop R5 of "allies)" on the North side of the road.

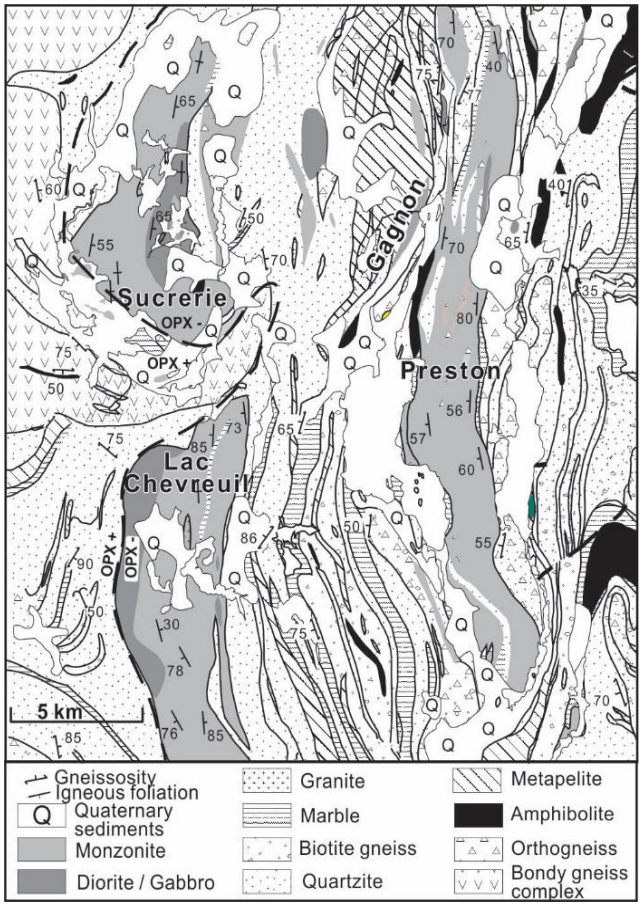

Figure 5.2. Sheet intrusions of the Chevreuil intrusive suite along the Nominingue-Chénéville deformation corridor (Corriveau and Madore 1994; Corriveau and van Breemen 2000; Corriveau 2013). Monzonite and diorite sheets present magmatic foliation parallel to the paragneissic host units and their gneissosity. Note the numerous paragneiss screens within the intrusive sheets.

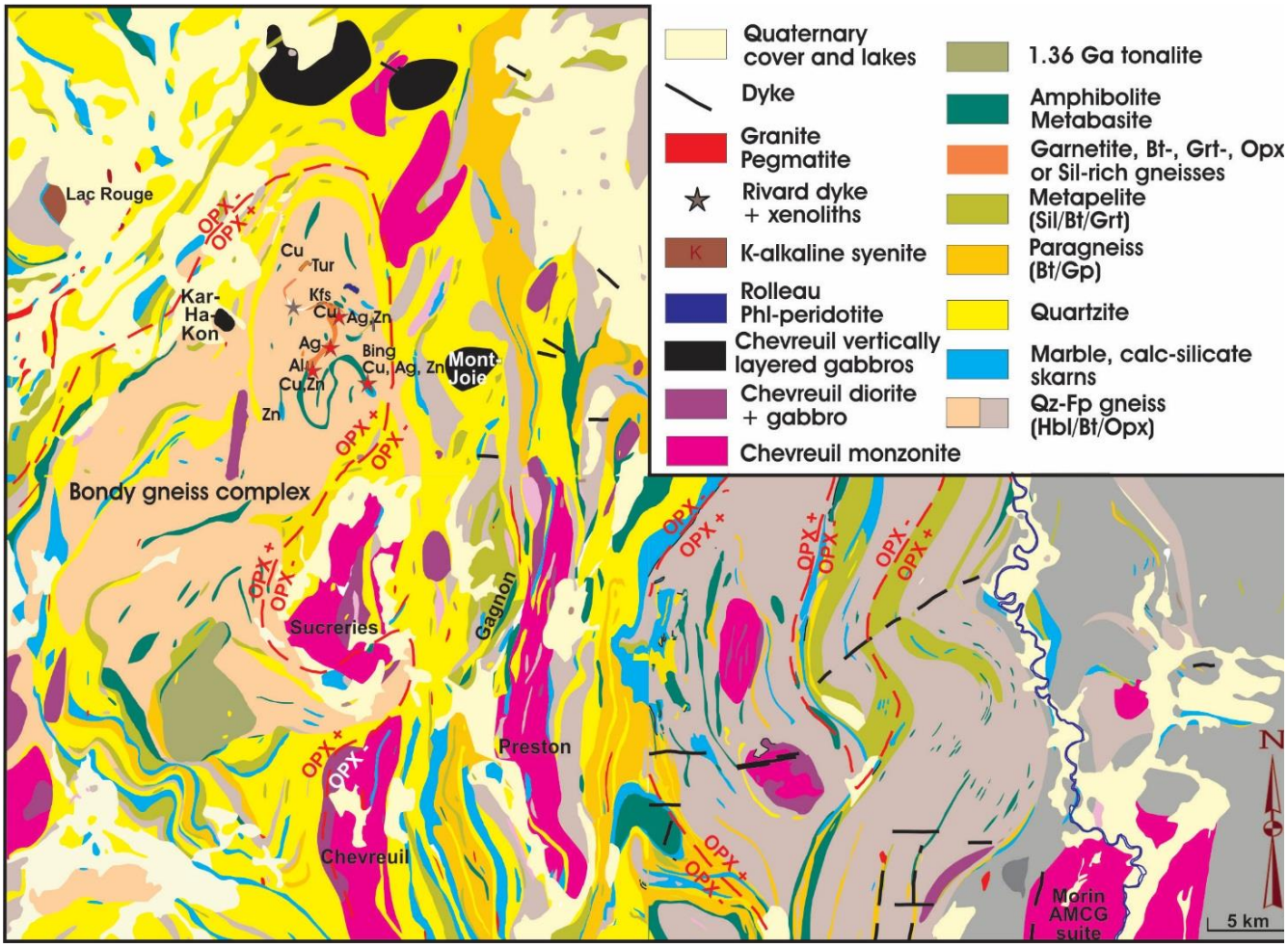

Figure 5.3. The four vertically layered mafic intrusion of the Chevreuil intrusive suite are distributed along the flank and the axis of the regional fold within which is nested the Bondy gneiss complex. Hence they postdate the regional-scale fold; their vertical nature is a consequence of their style of emplacement not tectonic transposition to verticality. Chevreuil intrusive suite sheets within high-strain zone such as the Gagnon sheets are pervasively recrystallized to amphibolite-facies. The former interpretation of the distribution of metamorphosed metasomatic lithofacies of the Bondy gneiss complex shown in this figure is revised in Chapter 7.

Stop 1.2
Sheet intrusion of monzonite among porphyroclastic gneisses of the Nominingue-Chénéville shear zone

The Lac Chevreuil pluton, after which we named the suite, consists largely of porphyroid monzonite (Fig. 5.4A, B). It was dated at 1165 million years (Corriveau and van Breemen 2000). The K-feldspar crystals are euhedral to subhedral and aligned along a flow foliation. Biotite is either aligned along this foliation or along subsolidus shears at an angle to the flow foliation. In contrast to the country-rock gneisses, the intrusion is not migmatized and is little recrystallized. Igneous and subsolidus foliations parallel the main fabric of the deformation corridor, the fabric of the host gneiss units, the contact of the intrusions and the many slivers of gneiss within the sheet intrusions (Fig. 5.2). This sheet intrusion is composite with both monzonite and diorite sheets.

At outcrop scale, enclaves and dykes of mafic (microdiorite) to intermediate composition are common and largely parallel to subparallel to the magmatic foliation (Fig. 5.4F). Cogenetic microdiorite enclaves tend to be lenticular (aspect ratio of 3:1 to 5:1) and fine grained; plagioclase phenocrysts and K-feldspar megacrysts are locally present. Other cogenetic mafic magmas form schlieren subparallel to the igneous foliation. Mafic component of the monzonite can vary greatly and locally the igneous foliation is deviated across sinistral NW-SE shear zones (Figs. 5.4C, 5.5). Many intermediate and mafic enclaves align crudely. Many intermediate or mafic schlieren and discontinuous sheets (centimetre to tens of centimetres in width) are also observed parallel to the igneous foliation defined by the orientation of the feldspar (Fig. 5.4D, E, G). This distribution of schlieren, enclaves and sheets is interpreted as a result of dyking along subsolidus fractures in the intrusions, and boudinage and enclave dispersion while magma flows along the sheet. In addition, crystal sorting is commonly observed leading to zones with abundant phenocrysts and zones nearly devoid of phenocrysts parallel

to the igneous foliation. Samples are available at the eastern extremity of the outcrop.

These magmatic corridors correspond to pronounced lineaments on satellite imagery. Corriveau and Rivard (1997) and Rivard et al. (1999) describe the structural make up and tectonic evolution of the deformation corridors based on the terrain fabric in Landsat imagery, specifically band 4 that was used to delineate many of the monzonite bodies. Fabrics oblique to the regional grain were recognized and structural analysis documented the role of anastomosing conjugate ductile shear zones and deformation corridors on magma emplacement and subsequent solid state deformation and recrystallization (Rivard et al. 1999; Corriveau and van Breemen 2000; Harris et al. 2001).

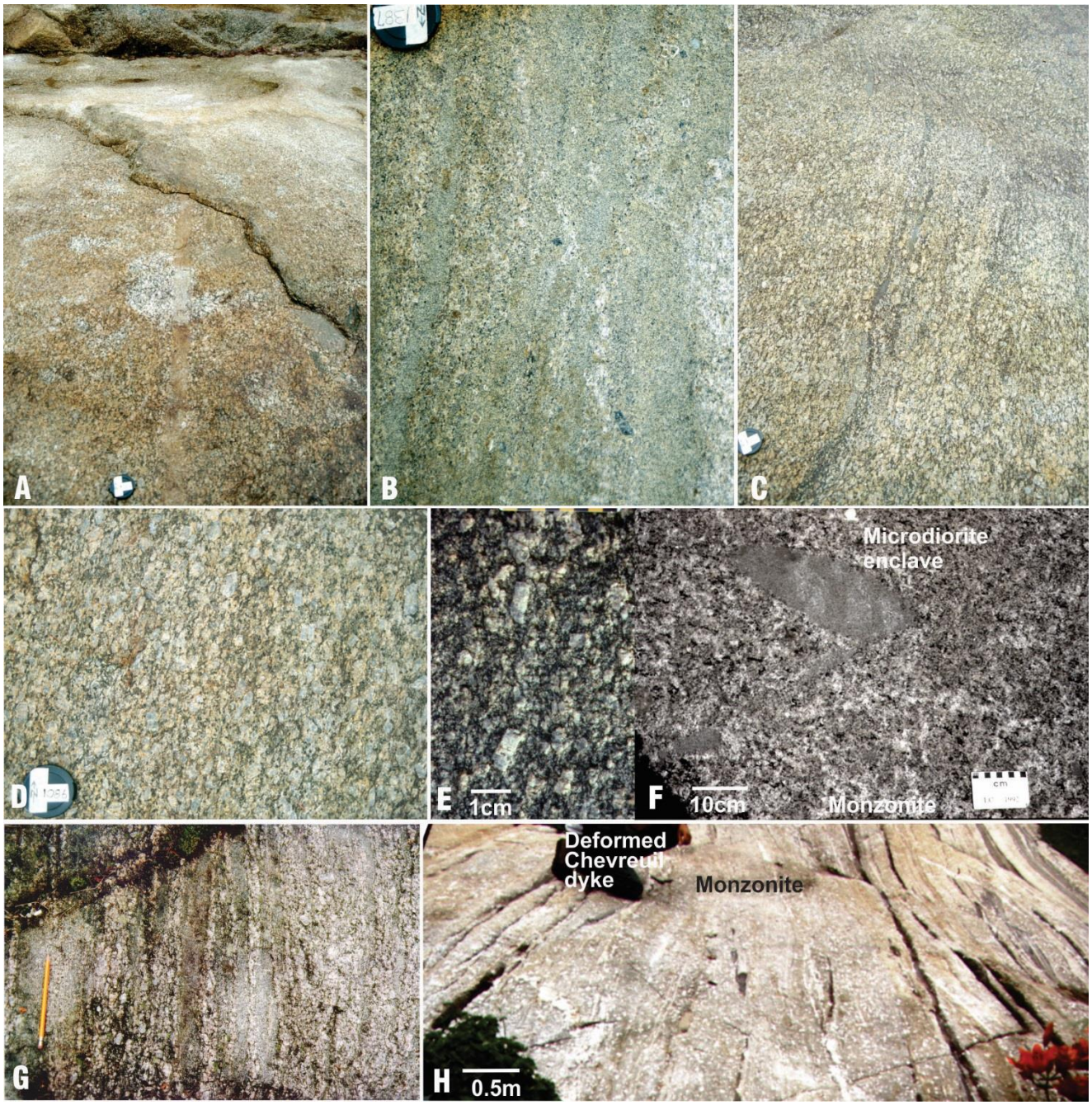

Figure 5.4. Porphyritic monzonite of the Chevreuil intrusive suite**. A.** Porphyritic monzonite of the Lac Chevreuil sheet intrusion cut by a fine-grained monzonite dyke with sharp rectilinear contacts. **B.** Fine-grained monzonite layers with diffuse non-rectilinear contacts that are parallel to the igneous foliation defined by the K-feldspar phenocrysts and a crude alignment of biotite. **C.** Mafic schlieren, N-trending igneous foliation and NW-trending sinistral shear within the Lac Chevreuil sheet intrusion. **D-E.** Close-up of the monzonite showing the igneous foliation defined by the crude alignment of feldspar crystals including the K-feldspar megacrysts. **F.** Cogenetic mafic enclaves. **G.** The igneous sheet intrusions also include zones with more abundant K-feldspar megacrysts. **H.** Deformed Chevreuil monzonite sheet intrusion and mafic dykes within the Nominingue-Chénéville deformation zone.

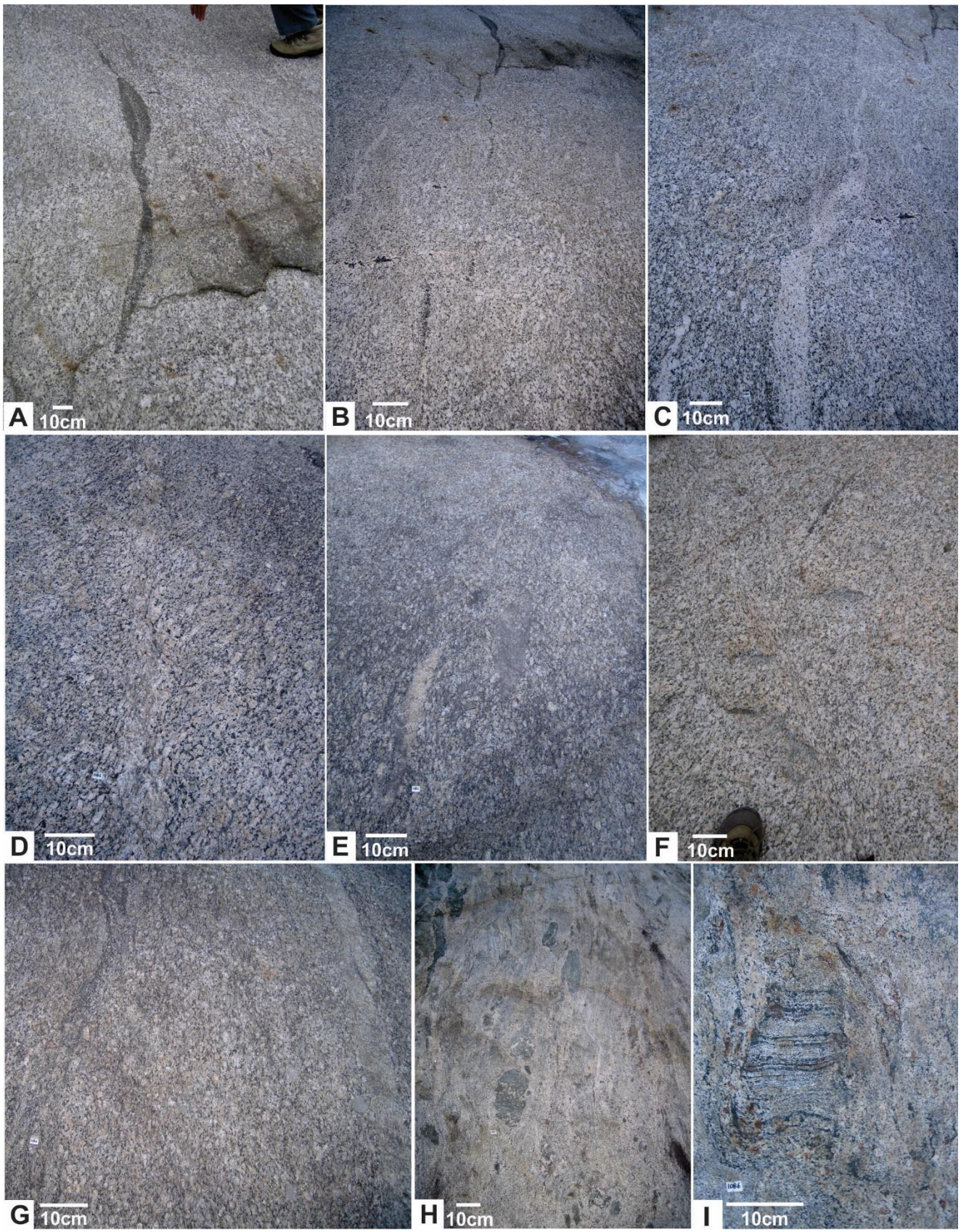

Figure 5.5. Sinistral and dextral shear within the Lac Chevreuil sheet intrusion. **A-G.** Syntectonic magma emplacement is parallel or discordant to the flow foliation of the monzonitic host. The preferred orientation of schlieren, K-feldspar megacrysts and enclaves define the igneous foliation. 1.165 Ga shearing is interpreted to have remobilized mineralization in the Bondy gneiss complex; styles of emplacement and deformation of Chevreuil suite are key regional markers. **H-I.** Intrusive sheets with skarn, paragneiss and cogenetic enclaves.

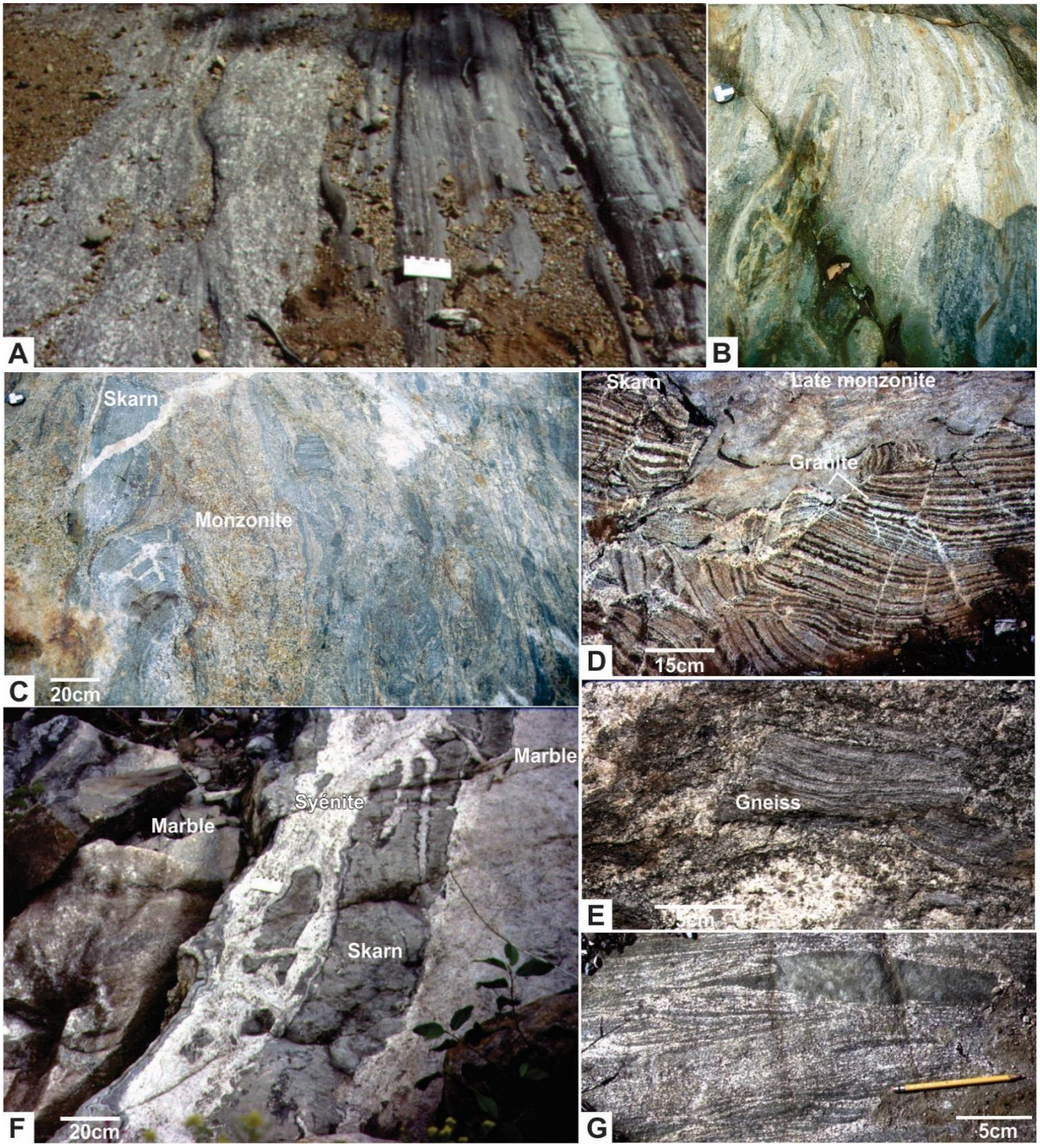

Figure 5.6. Magma emplacement of Chevreuil intrusive sheets along the contact of marble and quartzite units. **A.** Porphyritic monzonite parallel to gneissosity of host skarn. Igneous foliation is parallel to contact. **B.** Field record of assimilation of country rocks, magma flow, differentiation and mingling, and crystal segregation. **C.** Sheet intrusion within host skarn, flow foliation and zones of magma mixing. **D.** Layered skarn cut by later-stage monzonite and subsequently cut by granitic veins, some injected along skarn layering and contacts with monzonite. **E.** Examples of assimilated country rock among highly heterogeneous monzonite. **F.** Example of sheet emplacement of magma in marble away from Chevreuil suite rocks. Note that in this setting, marble is preserved as granitic dykes are volumetrically minor and do not carry sufficient heat and fluid to sustain extensive skarn development. Along the Lac Chevreuil intrusive suite, marble is regularly and pervasively transformed into skarn. **G.** Mafic magma was injected and deformed as more intermediate magma was emplaced.

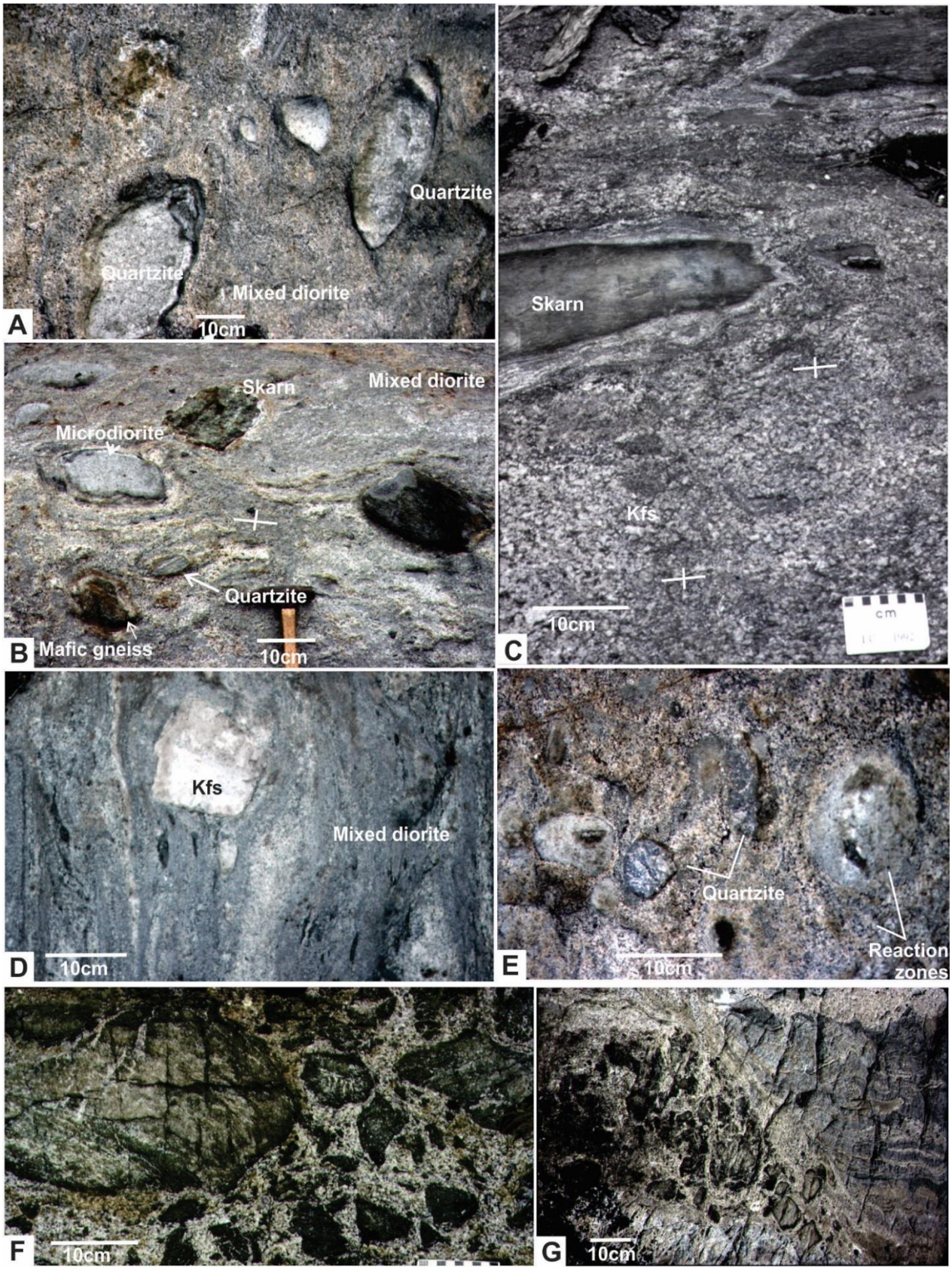

Figure 5.7. Zone of country rock assimilation between the monzonite and diorite sheets of the Lac Chevreuil intrusion. **A.** Mixed diorite with enclaves of quartzite. **B.** Microdiorite enclaves are elongated through magma flow and oriented parallel to the magmatic foliation of the hybrid diorite. **C.** Monzonite with enclaves of skarn. **D.** Fragment of a large K-feldspar most probably derived from a pink pegmatite. **E**. Diorite with enclaves of quartzite, gneiss, and microdiorite. **F-G.** Assimilation between the monzonite and diorite sheets.

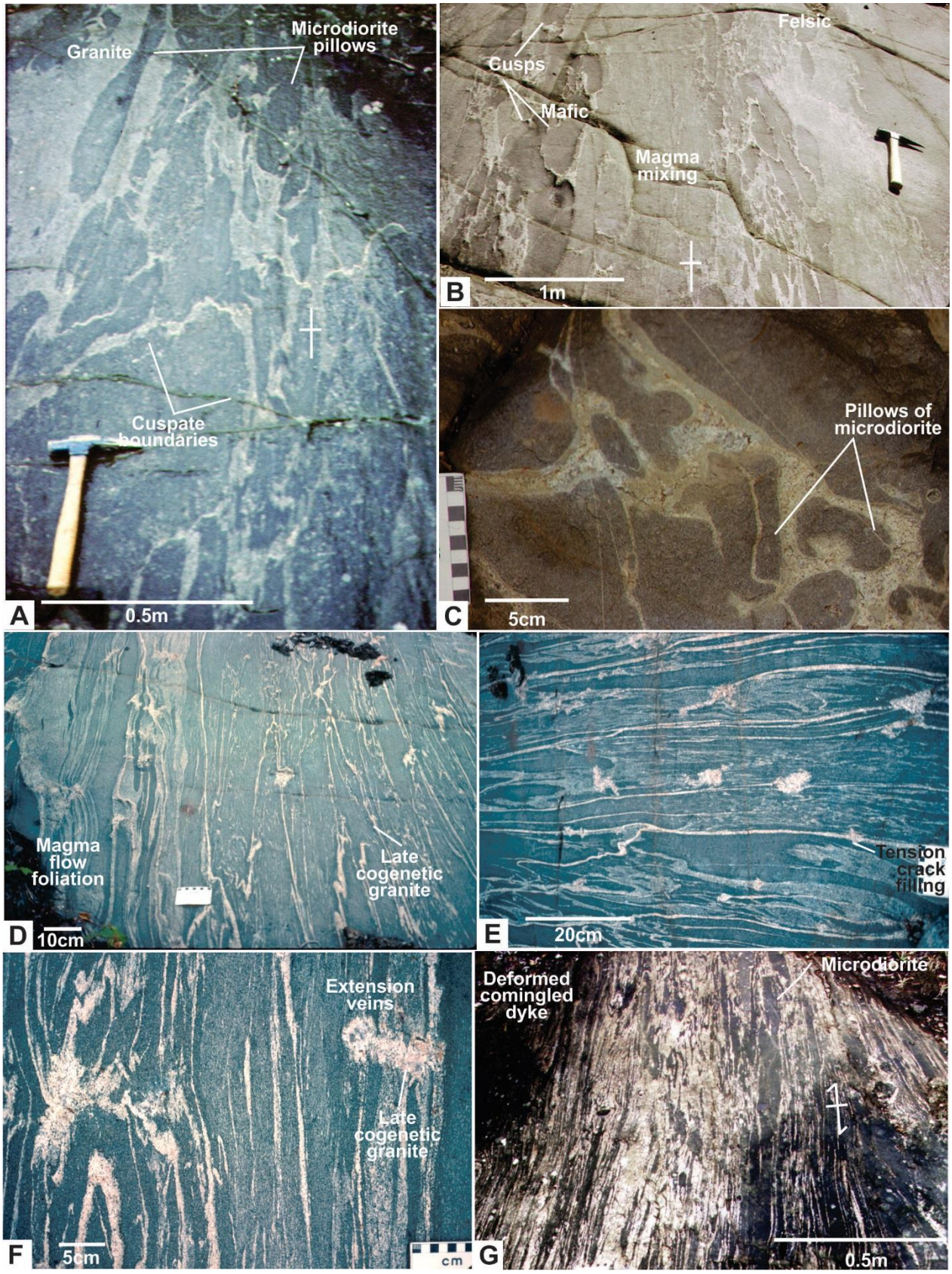

Figure 5.8. Dyke with magma mingling texture and flow foliation induced by syntectonic emplacement of coeval mafic and felsic magmas within an east-west contraction regime. Fractures following (partial?) solidification of the mafic-felsic dyke are filled by (largely coeval?) granitic magmas. **A.** Microdiorite pillows are elongated parallel to the wall rock during flow. **B**. Magma mixing in a mafic-felsic dyke. **C.** Detail of Figure 5.8B. **D-F.** Comingled layered dioritic dyke with pillows of varying shape ratios. **G.** Solid-state deformation of a comingled microdioritic dyke.

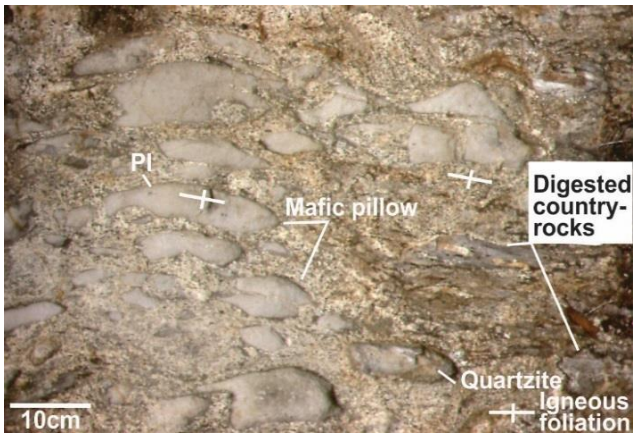

Figure 5.9. Mafic pillow and remains of digested country rocks in porphyritic monzonite. Mafic pillows and digested country rock xenoliths are elongated and aligned parallel to the igneous foliation of the monzonite, a consequence of magma emplacement.

Dextral ductile shear zones with a NNE orientation dominate in the north of the deformation corridor while sinistral shear zones with a SSE orientation are mostly present in the south. Where shear zones nearly parallel the regional foliation, the pitch of the mineral lineation increases indicating a reverse component. Boudinage and pinching and swelling of intrusion along the deformation zone are a consequence of displacement on conjugate shear zones and record regional N-S extension and E-W contraction. The monzonites predate this deformation and display parallel contacts and flow foliation structures without evidence of transposition of magmatic structures by subsequent events. The preservation of magmatic structures without transposition contrasts with later structures showing transposition due to conjugate shearing and evidence that late magmas were emplaced in conjugate shears. This change in structures demonstrates variations in the tectonic regime which Harris et al. (2001) interpret as indicating that the monzonites and layered intrusions were emplaced during a period of regional E-W extension. However in the late stages of this magmatism, the tectonic regime was one of compression for which deformation was focused along magmatic corridors such as the Nominingue-Chénéville zone. Evidence of this late deformation is often best preserved in the host gneisses at the border of plutons, the gneisses being more ductile. The shear zones, which can be traced regionally, die off in the vicinity of the plutons.

Stop 1.3
Wall-rock assimilation and repeated magma emplacement

Directions: Walk to the Chemin du Lac Chevreuil road at the far end of site R6 of the Vallies."Outcrops occur all along the road on the East side and in the bush nearby.

These outcrops display fracturing of the host rock during emplacement of magma, skarn formation, country rock assimilation, magma comingling, and repeated magma pulses (Figs. 5.6-5.9). They provide the best examples in the entire area, so PLEASE DO NOT DEFACE THE OUTCROP SURFACES BY TAKING SAMPLES!

At the start of the outcrop there is a net veined diorite dyke cut by seams of tourmaline, a common mineral in pegmatite veins and dykes associated with the 1165 Ma magmatism in the Nominingue-Chénéville deformation zone.

Following this, one can see a block of layered rock of uncertain nature and origin, "progressively" (from north to south) broken apart, incorporated, moved around, and digested by mafic and intermediate magmas that were cogenetic with monzonite (Fig. 5.6). Such dykes are common in the monzonite intrusions of the Chevreuil intrusive suite. To the South, on top of a knob, one can see a number of little pillows of fine-grained, grey microdiorite (looking like small whale backs) within a very heterogeneous monzonite. At the time of mafic magma emplacement, the monzonite was also in a magmatic state; the mafic magma formed elongate pillows in the felsic magma. This series of enclaves, not subsequently deformed in the solid state, most likely illustrates one of the first stages of formation of cognate microgranular enclaves in plutonic rocks. The monzonite is not porphyritic and encloses blocks of quartzite as well as many partly assimilated fragments with indistinct borders.

Stop 1.4
Sheet-like bodies of diorite and net-veined dykes

The outcrop on the South side of the road (46.049171, -75.203011) is on the western margin of a heterogeneous diorite sheet adjacent to the thicker monzonite sheet of stop 1.1. As per the other sheet intrusions it extends for several kilometres along the Nominingue-Chénéville deformation zone. In such composite intrusions diorite is most common whereas gabbros occur in sheet intrusions devoid of monzonite. Figure 5.10 illustrates one such gabbro with vertical foliation that is sharply cut by a Chevreuil dyke illustrating the change from vertical magma flow to vertical extension along subhorizontal fractures once crystallized.

The diorite is medium grained and contains numerous fragments varying from centimetre- to metre-scale in length and width. These fragments include diopsidite, and fine-grained igneous rocks. The boundaries of host-rock inclusions are difficult to pinpoint due to extensive assimilation of the xenoliths.

Proceed to the East; the outcrop on your right is also an heterogeneous diorite commonly with a composite net-veined texture. A metre-size enclave of ophitic gabbronorite occurs; the igneous foliation of the host diorite wraps around the enclave.

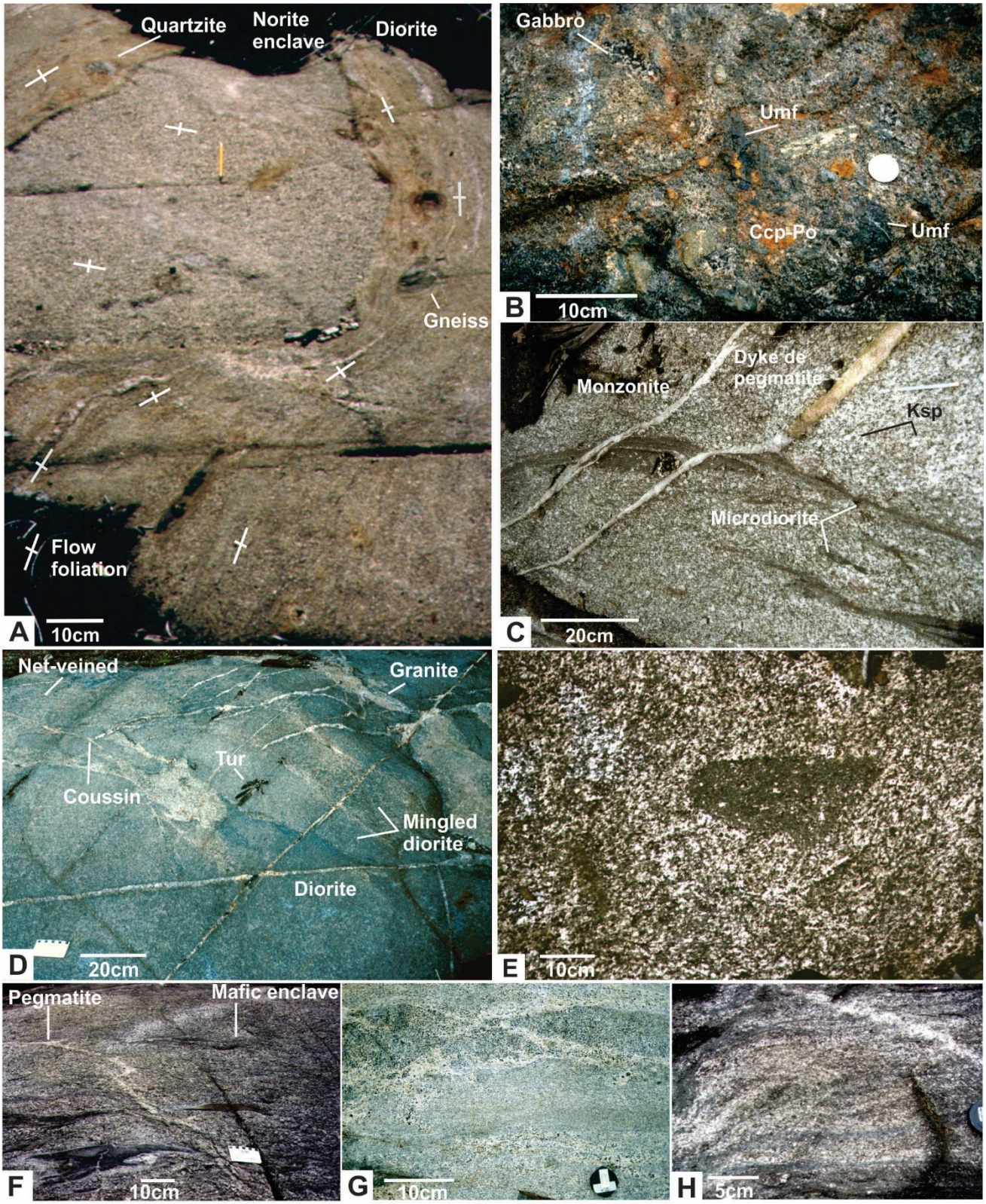

Figure 5.10. Mafic sheets of the Chevreuil intrusive suite. **A.** Lac Chevreuil diorite sheet with norite enclave. Flow foliation defined by plagioclase laths and seams of crystal segregation are present and flow around the enclave. **B.** Grand-Remous sheet with intrusive breccias and sulphide mineralization. **C.** Field record of magma flow, differentiation and mingling within the Lac Chevreuil diorite sheet. **D.** Deformed mafic dykes with minor boudinage along flow foliation. **E.** Cogenetic mafic enclave within monzodiorite of the Lac Chevreuil intrusion. **F.** Deformed mafic dykes and boudinage along flow foliation. **G.** Sheet emplacement of magma at outcrop scale. **H.** Mafic magma mingling and crystal segregation.

Figure 5.11 Gabbro sheet intrusion with vertical foliation and layering cut by a Chevreuil dyke with magma mingling textures.

Further east, composite net-veined dykes are abundant. Plagioclase phenocrysts among an aphanitic matrix are commonly aligned and define an igneous foliation parallel to that of the host monzonite and diorite. In contrast, along the margin with the country host quartzite, dykes and structures underwent subsolidus transposition and shear zones oblique to the foliation are observed. The monzonite becomes an augen gneiss. This deformation contrasts with the well-preserved magmatic foliation observed in the western section of these monzonite sheets and illustrates the late deformation focused along N-S corridors such as the Nominingue-Chénéville zone.

Stop 1.5
Quartzite and dykes of the Chevreuil and Lanthier intrusive suites

Drive 1.9 km further unto Chemin du Lac Chevreuil and turn left onto Route 3 for 400 m, then continue straight onto Papineau-Labelle Route 34 for 2.5 km (stop 1.5 at 46.053371, -75.265837).

After the stop, head west on Papineau-Labelle 34 and turn left onto Papineau-Labelle 4. Drive for 10.5 km and continue straight ahead onto Chemin de la Rivière du Sourd (do not turn right on Chemin du Lac Serpent/Papineau-Labelle 1) and drive for 16.6 km. Then turn right onto QC-309 N and drive for 73.3 km. Turn right onto Route Transcanadienne/QC-117 N to head for the Super 8 hotel.

The outcrops expose series of quartzite and paragneiss units cut by amphibolite dykes and subsequently folded together. The proportion of paragneiss to quartzite is typical of the Quartzite domain. The fold interference pattern within the quartzite reveals a pre-1.16 Ga polyphase deformation event which we attribute to the regional granulite-facies metamorphism at 1.2 Ga. Chevreuil (mafic) and Lanthier (granitic) dykes cut these folds. Chevreuil dykes form conjugate sets compatible with magma emplacement along conjugate shears under E-W extension. Lanthier and Chevreuil dykes are coeval at first (Fig. 5.11B) and folded with a vertical axial plane recording E-W compression. A non-deformed N-trending Lanthier granitic dyke has vertical igneous layering parallel to the dyke contacts. These dykes are key markers for the structural analyses of Harris et al. (2001) and Dufréchou et al. (2014). Contrast the style of deformation of these Chevreuil dykes with those along the deformation zone at the western margin of the Central Metasedimentary Belt (Figs. 5.11, 5.12). Note that the white granitic component of Chevreuil dykes across the belt resembles those of the Lanthier granitic suite (Figs. 5.12-5.17).

5.4 Deformation and metamorphism

5.4.1 Intrusive suites as tracers of Shawinigan and minor Grenvillian reactivation

Regional-scale markers are the 1.19 Ga gneisses, their 1.18 Ga anatectic leucosomes, and the dykes and intrusions of the 1.17 to 1.16 Ga Chevreuil intrusive suite, 1.08-1.07 Ga Kensington-Skootamatta potassic alkaline suite and the 1.06 Ga Guenette suite. The distribution of the Chevreuil intrusive suite extends across the entire belt and stiches the belt with adjacent Morin Terrane and Central Gneiss Belt. Style of magma emplacement and extent of deformation of the intrusive bodies and dykes of the Chevreuil intrusive suite constrain timing and sites of late stage reactivation.

In the gneiss complexes, Chevreuil dykes cut straight across gneisses and their leucosomes. Their common intricate magma comingling textures are diagnostic of the suite. Thus neither the dykes nor their host gneiss were deformed after 1.17 Ga. By behaving as rigid bodies during the Shawinigan reactivation at 1.16 Ga, the gneiss complexes escaped late stage penetrative deformation and recrystallization, retain peak regional metamorphic structures and mineral assemblages but were locally sheared along discrete fault zones (Harris et al. 2001; Dufréchou et al. 2011, 2014, 2015). The gneiss complexes preserve pervasively the high-pressure and high-temperature mineral assemblages and the fabrics of the early regional metamorphism. Peak conditions estimated by geothermobarometry are 950ºC and 10 kbar (at 33 km depth) (Boggs and Corriveau 2004). Uranium-lead ages of 1.20 to 1.19 Ga were obtained on zircon crystals from gneiss, and ages of 1.18 Ga ages were obtained from gneiss containing anatectic leucosomes (Corriveau and van Breemen 2000; Wodicka et al. 2004). Monazite ages are slightly younger at 1.18 and 1.17 Ga and record cooling through 750°C (Boggs et al. 1994; van Breemen and Corriveau 1995). The formation of the gneissic structure and the crystallization of the leucosomes are estimated to have occurred at 1.2 to 1.19 Ga and at 1.18 Ga, respectively. All fabrics are cut by Chevreuil dykes. Amphibolite facies prevails in the quartzite-rich domain including within the Nominingue-Chénéville deformation corridor but the early metamorphic record is still locally preserved (Boggs 1996; Boggs and Corriveau 2004).

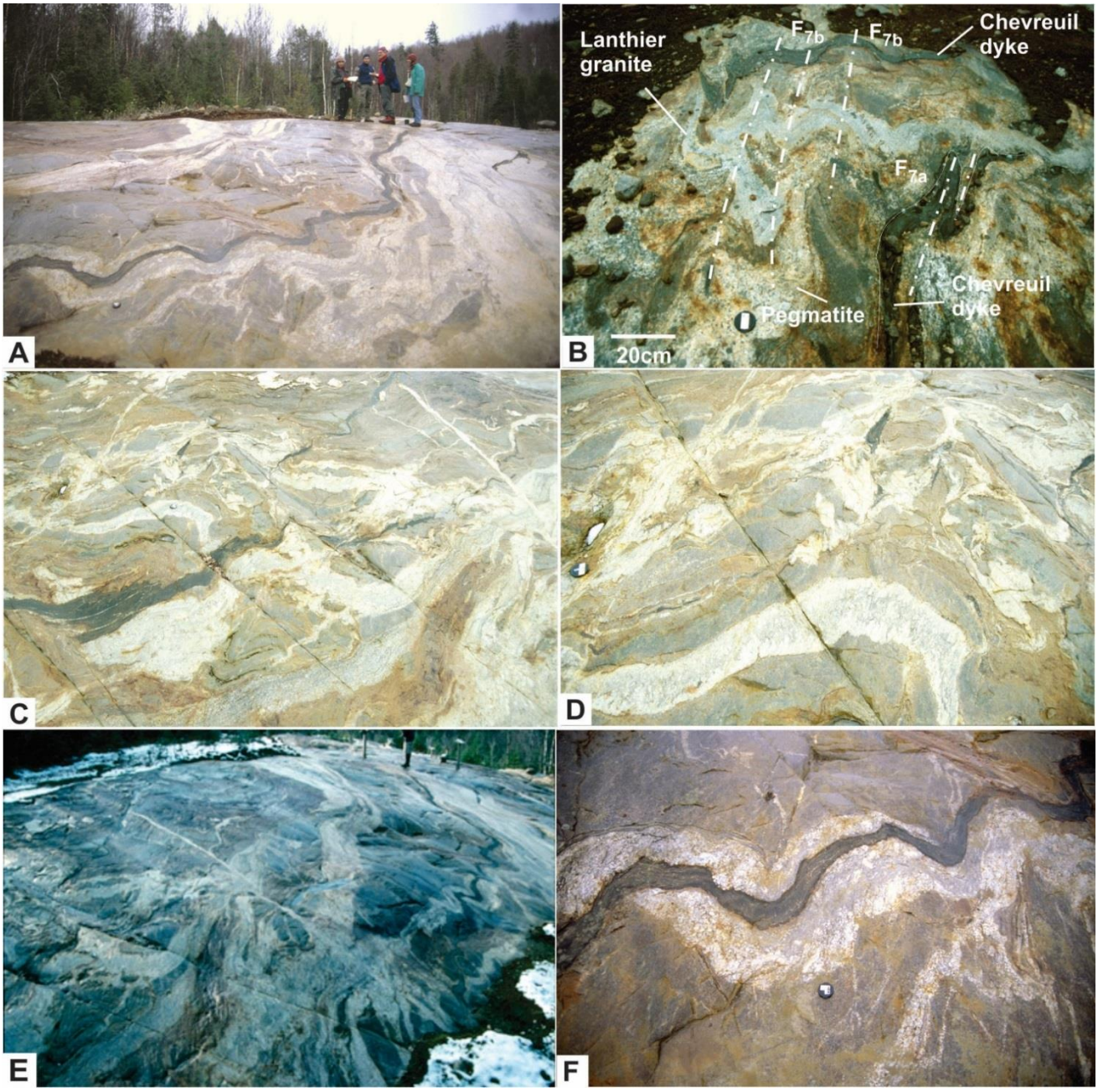

Figure 5.12. Mafic dyke of the Chevreuil intrusive suite cutting folded quartzite and their pegmatites and subsequently folded. **A.** Overview of the outcrop. **B.** Chevreuil intrusive suite mafic dykes cut by a Lanthier dyke which is itself cut by a Chevreuil dyke illustrating that these two suites are in part coeval. Both suites of dykes are folded. **C-F.** Chevreuil mafic dykes are emplaced within a set of conjugate shears and subsequently folded.

Figure 5.13. Mafic dykes of the Chevreuil intrusive suite in the Cayamant deformation zone are commonly folded.

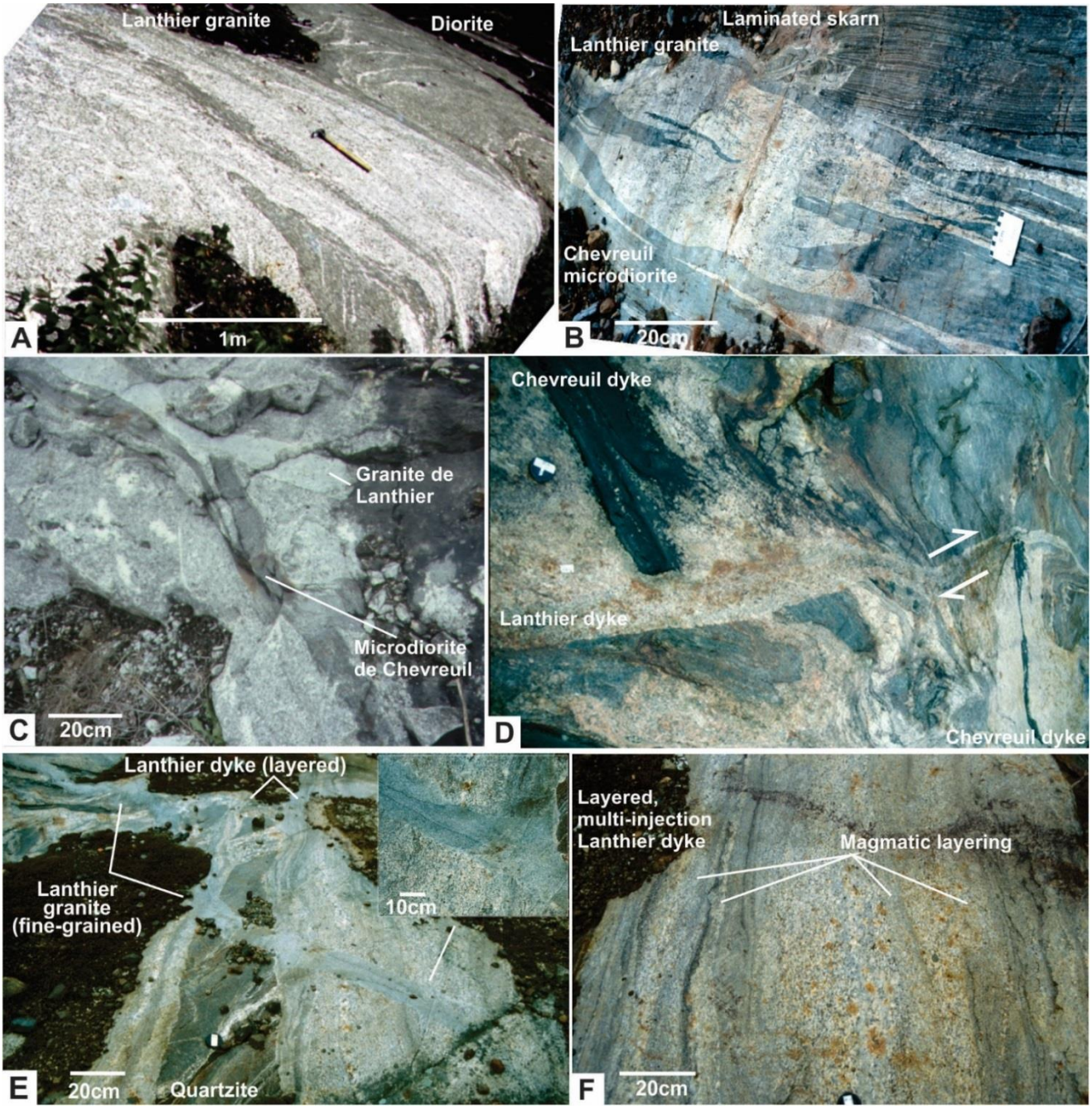

Figure 5.14. Granitic dykes of the Lanthier intrusive suite. **A.** Composite granitic dyke cutting Chevreuil suite diorite. **B.** Granitic veins mingled with microdiorite of the Chevreuil suite that cuts banded skarn. **C.** Close up of a Lanthier dyke cutting a mafic dyke of the Chevreuil suite. **D.** The late-stage granitic dykes are themselves emplaced in active sinistral fault zones that cut and brecciate a Chevreuil intrusive suite dyke. **E-F.** Composite granitic dyke with igneous layering cut by an homogeneous granitic dyke.

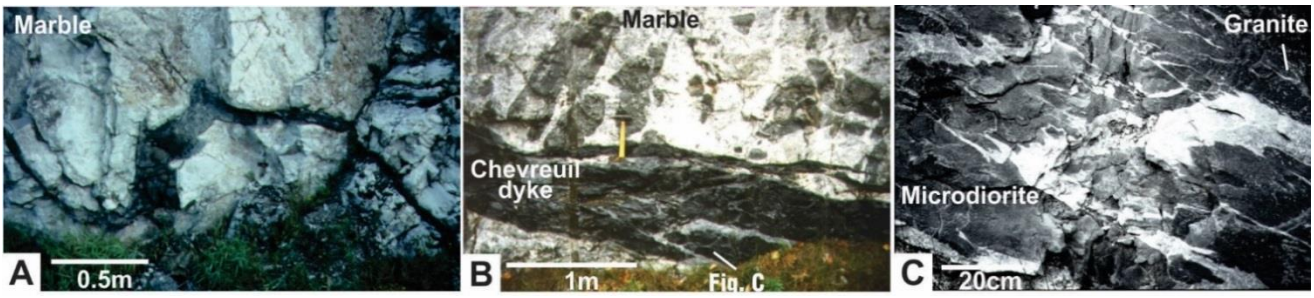

Figure 5.15. Mafic dykes of the Chevreuil intrusive suite in the western part of the Marble domain.

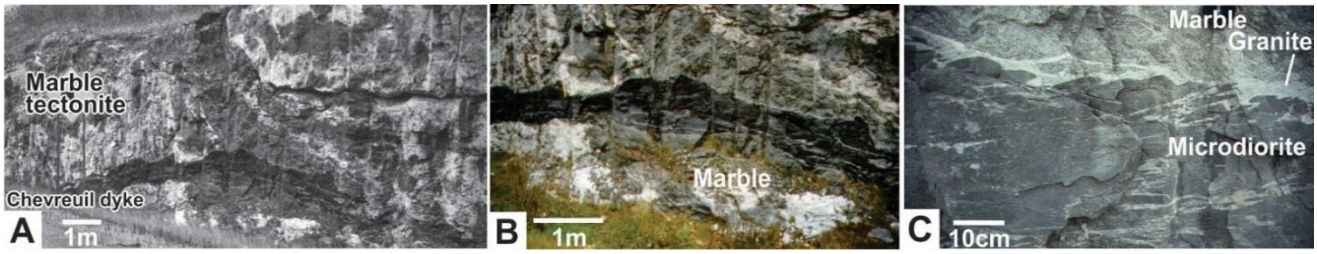

Figure 5.16. Mafic dykes of the Chevreuil intrusive suite in the eastern part of the Marble domain.

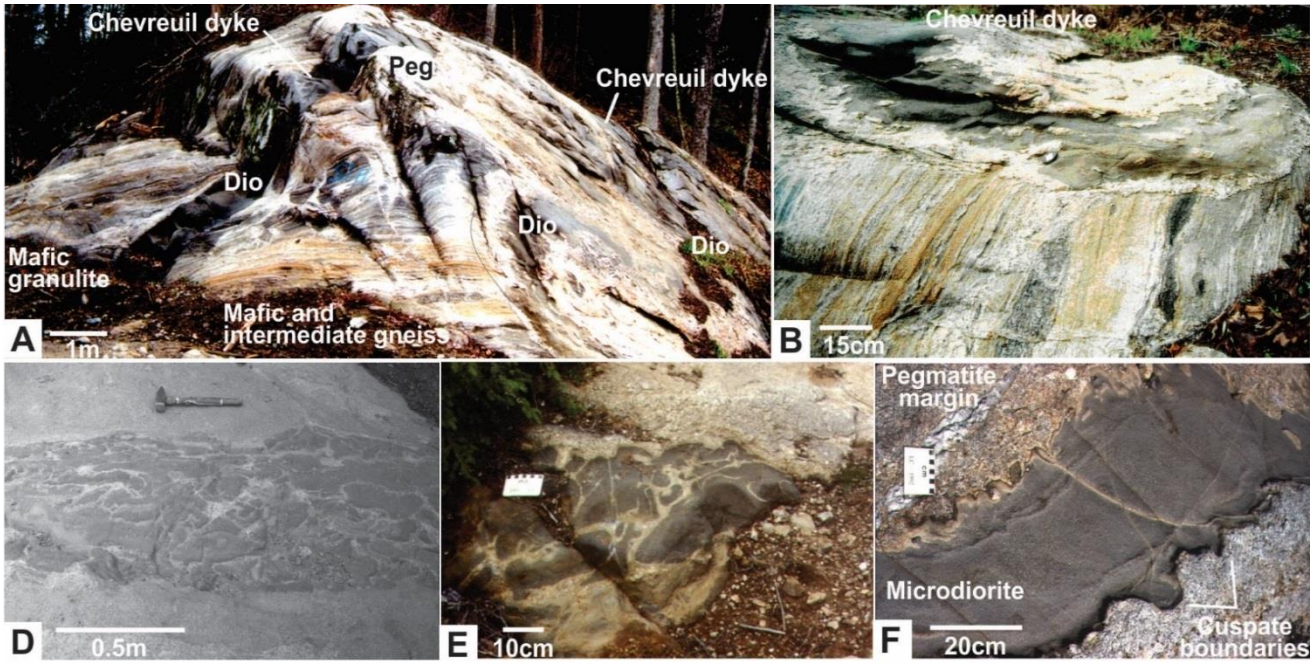

Figure 5.17. Mafic dykes of the Chevreuil intrusive suite in the Bondy gneiss complex. Note that the dykes are not folded.

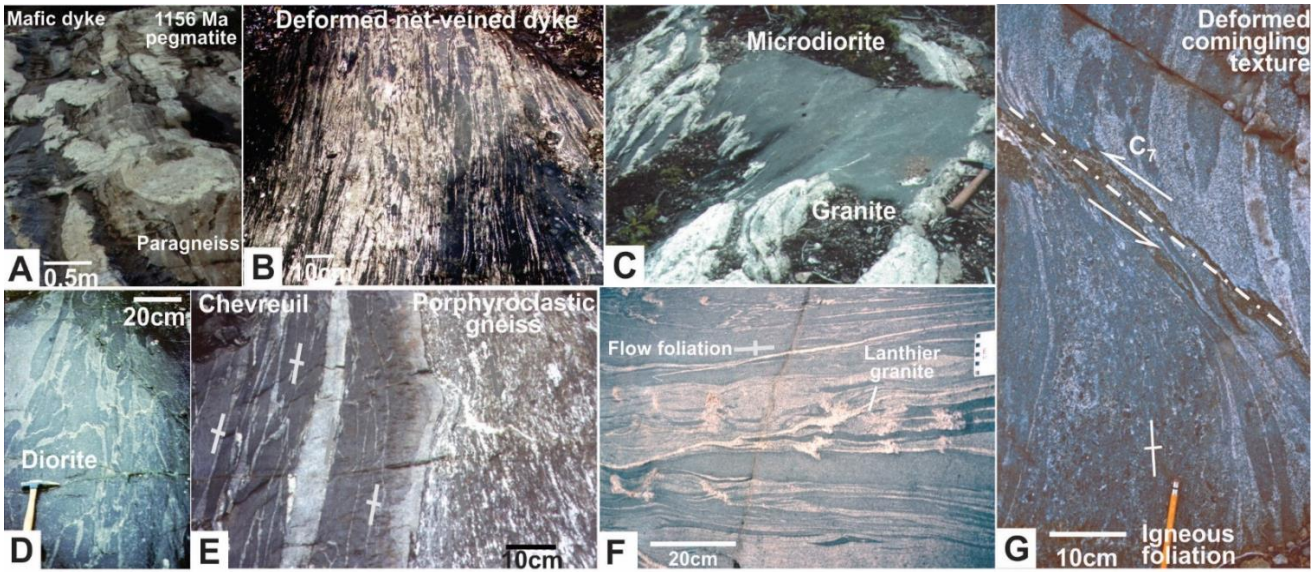

Figure 5.18. Mafic dykes of the Chevreuil intrusive suite in the Nomingue-Chénéville deformation zone.

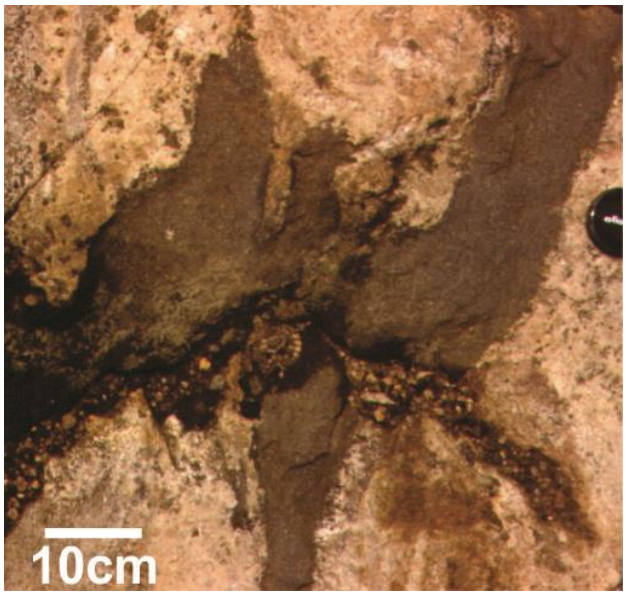

Figure 5.19. Folded Chevreuil dyke at amphibolite facies within the Labelle deformation zone.

The quartzite rich domain has rheological behaviour intermediate to that of the gneiss complex and marble domain and records successive orogenic events. In the Nominingue-Chénéville deformation zone, the mafic dykes were folded prior to 1156 Ma about axes parallel to the north-south deformation corridor, providing evidence of late stage reactivation of the ductile gneisses in the Quartzite domain (Fig. 5.18). In this corridor, the monzonite and diorite sheets largely retain their igneous texture.

In the Marble domain, Chevreuil dykes only undulate and retain their typical net veined texture. Gabbro and monzonite stocks are only slightly recrystallized.

In the Cayamant deformation zone, the marble-hosted mafic dykes of the Chevreuil intrusive suite have been deformed into west-verging folds and recrystallized to amphibolite facies (Fig. 5.19). They are not migmatized. The lack of migmatization contrasts with the host gneiss and indicates that the plutons postdate regional metamorphism even along the western boundary of the CMB-Q with the Central Gneiss Belt. Mafic dykes display west-verging isoclinal folds (whereas similar dykes within the CMB-Q are not deformed). Harris et al. (2001) interpret the deformation fabrics in the intrusive suite as evidence of thrusting and subsequent extension along the western margin of the belt. Conditions of the retrograde metamorphism are of 650ºC and 6 kbar over an area several kilometres wide (Indares and Martignole 1990). Thus, the marble domain was easily reworked because of the marble's high ductility and ubiquity. It contains structures and paragenetic assemblages from the last orogenic episodes to have affected the domain and its deformation zones, and little evidence of earlier episodes. The 1.08 Ga Kensington-Skootamatta suite plutons are not penetratively deformed or recrystallized (Corriveau and Gorton 1993). Their $^{40}Ar/^{39}Ar$ ages are at 950 Ma, 100 m.y. younger than in the rest of the CMB-Q (Hanes et al. 1994). Marbles are commonly mylonitized to very fine grained. The Cayamant deformation zones within the marble domain acted very ductilely and its marble sequences recrystallized easily. Early structures and assemblages were nearly totally erased during tectonic overprinting with only a few remnants of granulite facies preserved (Indares and Martignole 1984). Consequently, the marble rich domain records dominantly the "last gasps" of the Grenville orogeny to which it was subjected. The gneiss records retrograde metamorphic conditions of 750°C and 8 kbar (Indares and Martignole 1990) within the marble domain, and 650°C and 6 kbar (ibid; Kretz 1980, 1990; Perkins et al. 1982) along the strongly reactivated western margin of the belt.

Granulite-facies regional metamorphism and westward thrusting of the Central Metasedimentary Belt over the Central Gneiss Belt indicate that crustal thickening in the Central Metasedimentary Belt and in the gneiss units of the adjacent Morin Terrane took place before 1.2 Ga. There is a marked contrast in lithology between the marble and quartzite domains, although both domains are structurally above the gneiss complexes; the latter may therefore have served as basement for one or more marble and quartzite sedimentary basins. This interpretation is consistent with the model of an Andean- type Laurentian margin with a continental back arc proposed by Dickin and McNutt (2007) and McLelland et al. (2013).

5.4.2 Labelle deformation zone

The Labelle deformation zone (LZ) is a N-S striking, sub vertical shear zone separating the Central Metasedimentary Belt in Québec from the Morin Terrane. Based on oblique-reverse kinematic indicators observed in a shear zone to the east of the Labelle zone, Martignole and Friedman (1998) interpreted this zone to be a sinistral-thrust that accommodated northward transport of the Morin Terrane along with the dextral-thrust Taureau shear zone, which bounds the eastern flank of the terrane. This hypothesis has recently been questioned by Soucy-Laroche et al. (2015) who determined that the Taureau shear zone further east is a normal-sense shear zone active at ca. 1060 Ma. A second generation of down-dip lineation associated with normal-sense kinematic indicators indicate downtrow of the Morin Terrane, which is supported by the younger Ar/Ar hornblende cooling ages on the east side of the Labelle zone. Dufréchou et al. (2014) further documented that the “S” kink of the Labelle deformation zone coincided with a deep geophysical lineament interpreted as a Paleoproterozoic rift-related structure of the Archean basement that would have controlled the geometry of overlying structures during the Grenvillian orogeny. The tectonic evolution of the Labelle deformation zone is thus complex and requires further study, including modern petrochronological studies.

5.4.3 Ottawan imprints

Regional metamorphism was associated with 1.09-1.03 Ga Ottawan orogenesis in the southwestern Grenville Province, including in the Cabonga terrane and the Central Metasedimentary Belt in Ontario at 1.06 Ga. Rocks in the

Central Metasedimentary Belt in Québec were not metamorphosed during this orogenesis. Emplacement of the Guénette granite sheet at 1.06 Ga along the contact between the marble and quartzite domains is compatible with a structural control on magma emplacement and could reflect local fault reactivation. The presumed existence of northwest thrusts and the documented shears that postdate emplacement of the Rivard dyke suggest that the upper lithosphere sampled by the dyke occurs directly beneath the existing surface but that the deeper levels sampled may be farther to the east or southeast (Fig. 5.20).

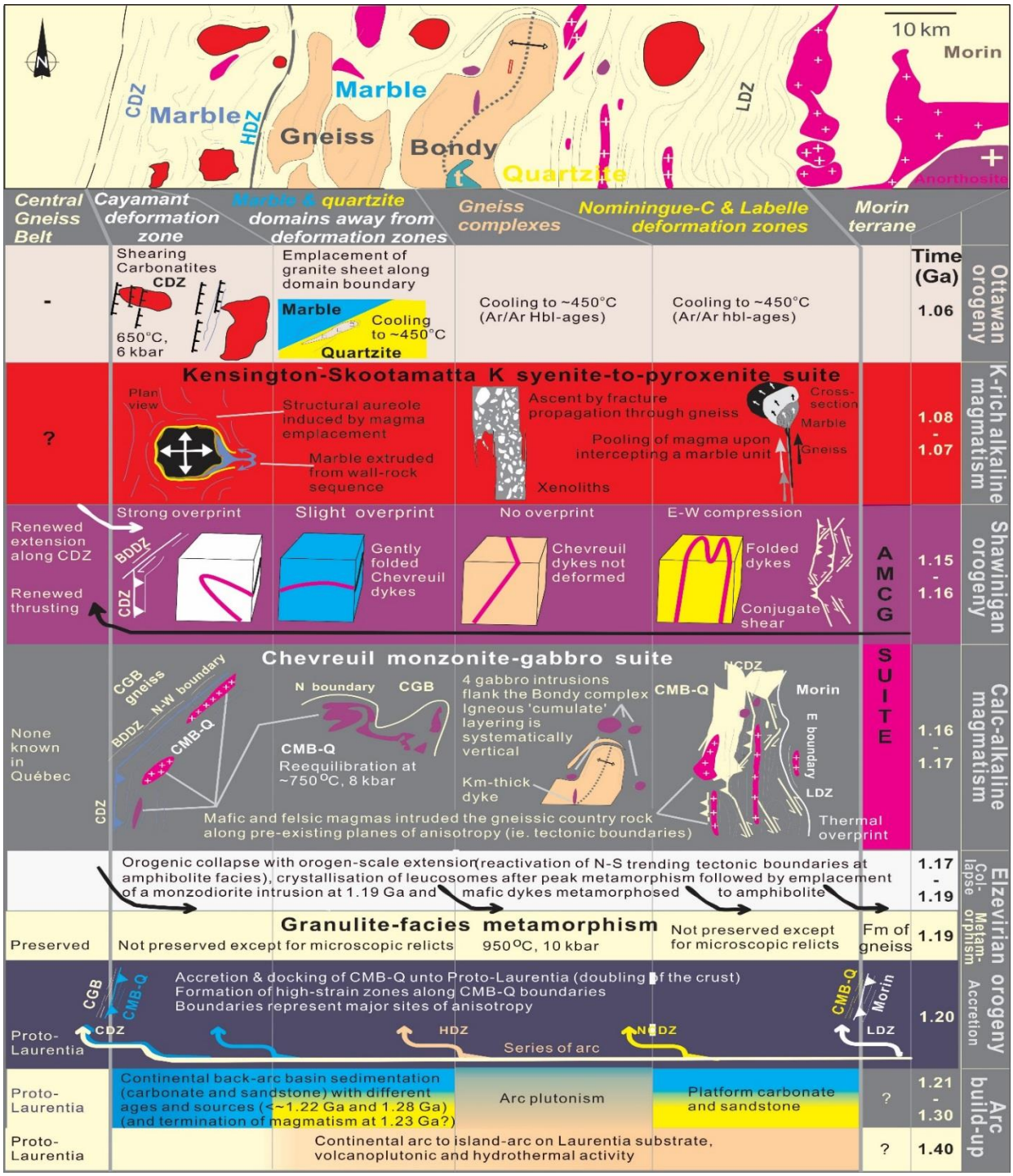

Figure 5.20. Synopsis of the tectonomagmatic evolution of the CMB-Q that led to a diachronous tectonometamorphic record of orogeneses across the belt (modified from Corriveau 2013 and Boggs and Corriveau 2004; additional information: this work; Schneider et al. 2013; Davis and Nantel 2016). Regional intrusive markers have similar parageneses, styles of magma emplacement and host gneisses (except at stop 4.2), suggesting that differential unroofing across the belt is minor (cf. Schneider et al. 2013 for a different interpretation).

Chapter 6: The Bondy gneiss complex, east sector (Day 2)

6.1 Topics for discussion

Topics for discussions for Day 2 and Day 3 on the Bondy gneiss complex (Fig. 6.1) are:

1. recognition of hydrothermal alteration zones at granulite facies,
2. field criteria for plutonic versus volcanogenic or sedimentary origin of felsic and mafic gneisses,
3. intensity of anatexis once common rocks have been hydrothermally altered prior to metamorphism (i.e. not enough Na or K for the rocks to melt),
4. enhanced degree of preservation of protolith textures where partial melting is low,
5. enhanced degree of deformation in biotite-rich metasomatic rocks,
6. interpreting the metasomatic imprint on host rocks beyond granulite facies metamorphism with a reasonable degree of confidence,
7. scale of melt migration, and
8. rheological control on preservation of structures and mineral parageneses associated with early orogenic events.

6.2 Overview

Field studies in the 30 km by 15 km Bondy gneiss complex have highlighted a series of Cu±Au mineral occurrences and prospects among an iron-oxide and alkali-calcic hydrothermal alteration system. The volcanic rocks have trace-element signatures of an island-arc and a back-arc built on thin continental substrate (Blein et al. 2003, 2004). The volcanic protoliths were dated between 1.39 and 1.36 Ga, metamorphic overgrowth record peak metamorphism at 1.2-1.19 Ga and leucosomes crystallized at 1.18 Ga (Corriveau and van Breemen 2000; Wodicka et al. 2004). Metamorphism of the hydrothermal system and its host rocks at granulite facies reached 950ºC and 10 kbar (Boggs and Corriveau 2004). In contrast to migmatites in the marble and quartzite domains, the leucosomes are largely non-deformed and the complex has largely escaped a regional-scale penetrative deformation at amphibolite facies between 1.17-1.16 Ga except for some local shear zones. The various phases of deformation observed throughout the complex have been described in detail in Harris et al. (2001). Post 1.18 Ga deformation can easily be recognized where pegmatitic veins or leucosomes are sheared.

The Bondy gneiss complex has been mapped at regional scale and described in detail in series of government publications (Corriveau and Jourdain 1993; Corriveau and Madore 1994; Corriveau et al. 1994, 1996a, b; Corriveau 2013). The field data are reported in the Québec SIGEOM database. If using this database, it is important to realize that there was no easy way to codify metamorphosed hydrothermal alteration zones in the Geofiche system of the Québec survey in the 90s and as such we used the codes for metapelites for sillimanite-bearing meta-alteration zones.

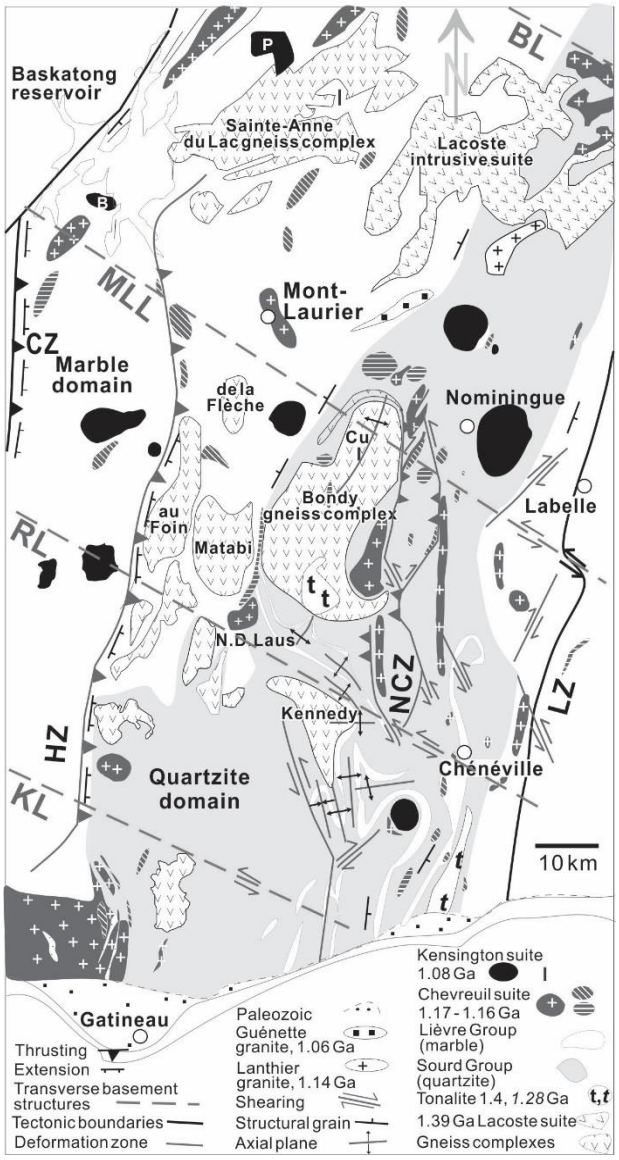

Figure. 6.1. Location of the Bondy gneiss complex with respect to major transverse basement discontinuities (modified from Corriveau 2013; Dufréchou et al. 2015).

During mapping, we found no paragneiss except for some local carbonate rocks whose origin was tested by W. Peck (unpublished data). Recently Blein and Corriveau (2017) use lithogeochemical discriminant diagrams to compare the composition of the metamorphosed hydrothermal alteration zones in the Bondy gneiss complex to a variety of deposit types and to the alteration facies of the systems in the Great Bear magmatic zone. They illustrate that the Bondy footprint is significantly similar to

those of IOCG deposits that evolve to epithermal caps. The discovery of this large-scale hydrothermal system illustrates that potentially economic mineralized zones can be found in the undifferentiated gneiss complexes of the Grenville Province. These are still often regarded as sterile.

6.3 Description and state of knowledge

The Bondy gneiss complex (Table 6.1; Figs. 6.2, 6.3, 6.4) comprises in its northern segment a series of felsic, intermediate and mafic amphibolites and metabasites gneisses with lithological layering and compositions compatible with a volcanic origin (basaltic, andesitic or rhyolitic lava and tuffs). Among these gneisses are extensive zones of garnet, biotite or orthopyroxene-rich gneiss, garnetites (some rich in quartz, biotite or magnetite, some with Fe or Cu sulphides), granoblastic tourmalinites among sillimanite-bearing gneisses, white plagioclase-dominant cordierite-orthopyroxene-bearing gneisses, series of aluminous gneisses with sillimanite-biotite-garnet, sillimanite-orthopyroxene-cordierite and cordierite-kornerupine-orthopyroxene assemblages, laminated K-feldspar rich gneisses, calc-silicate rocks, and diverse layered metabasites commonly with garnetites. These atypical rock types host a series of mineral showings (e.g. EM1, Lac Harvey, Bing; Fig. 6.4). They include magnetite and sulphides, either disseminated, as braided stringers or breccia. Magnetitite forms centimetre to decimetre-wide layers concordant with the gneissosity. They could represent deformed stockworks, breccia or veins. Siliceous, sodic, potassic, magnesian, aluminous and hyperaluminous gneisses (metasomatic rocks), carbonated (veins and alteration zones) and siliceous or magnetite rich units (veins, breccias, replacement zones) also occur. Their distribution is shown in Figure 6.2.

The metamorphosed metasomatic rocks occur as a series of discontinuous lenses concordant with the gneissosity at map scale. Some have distinctive geophysical signatures (Fig. 6.3). They have been grouped as a series of discontinuous lenses regionally folded some up to 10 km long and each of about 100 m to 200 m thick. Many metasomatic rocks are not included in Figure 6.2, including those of Day 2 stops, as they have yet to be mapped in detail and do not have a distinctive geophysical signature (Figs. 6.3, 6.4). Table 6.1 provides a synoptic description of the lithodemic units for the Bondy gneiss complex updated from Corriveau (2013).

Day 2 stops (Fig. 6.4) highlight the variety of potential metasomatic rock types, their cross-cutting relationships, the lack of mineral foliation parallel to compositional layering in gneisses where biotite is not abundant and the potentially primary layering in many localities. Beyond obvious leucosomes (Fig. 6.5), rock types that cut across compositional layering could be veins, breccias and replacement zones of the original metasomatic system.

Table 6.1. Lithodemic units of the Bondy gneiss complex modified from Corriveau (2013) and units in Québec Department of Energy and Natural Resources NTS 31J03 and 31J06 data in SIGEOM.

mPbdy$_{11}$	Monzonite, quartz monzonite and syenite; beige to white; fine to medium grained, granoblastic or with K-feldspar augens; heterogeneous; leucocratic; massive to foliated; with biotite, hornblende and/or clinopyroxene, magnetite and orthopyroxene; igneous in origin.
mPbdy$_{10}$	Metatonalite and quartz metadiorite; white; medium grained, granoblastic; leucocratic; homogeneous; massive, foliated or gneissic; migmatized; with biotite, clinopyroxene, hornblende, orthopyroxene and/or Fe-Ti oxides.
mPbdy$_{9}$	Marble and calc-silicate rocks: green to white; medium to coarse grained; massive, foliated or layered; with carbonate, clinopyroxene, phlogopite and/or titanite; include some skarns; sedimentary or hydrothermal in origin.
mPbdy$_{8}$	Plagioclase-dominant quartzofeldspathic gneiss: white; medium grained; foliated, layered and migmatite; with cordierite, kornerupine, orthopyroxene, phlogopite, plagioclase, tourmaline, quartz and accessory Fe-Ti oxides. Enclose stringers of tourmalinite, aluminous or sulphide-bearing gneisses; hydrothermal origin.
mPbdy$_{7}$	Aluminous gneisses; beige, grey or rusty brown; fine to medium grained; foliated, layered and migmatized; with biotite, chalcopyrite, cordierite, K-feldspar, oxides, plagioclase, orthopyroxene and/or sillimanite; with Fe or Cu sulphides locally; hydrothermal origin. Enclose biotite-rich garnetite.
mPbdy$_{6}$	Metagabbro and meta-anorthosite: white, grey and green; medium to coarse grained; leucocratic to melanocratic; granoblastic; massive to foliated; transposed magmatic layering; with clinopyroxene, garnet, hornblende and/or orthopyroxene and plagioclase.
mPbdy$_{5}$	Laminated to layered quartzofeldspathic gneisses: pink, locally rusty; leucocratic; cyclical asymmetric lamination, locally with relic graded bedding; locally migmatized; with biotite, K-feldspar, orthopyroxene, quartz and Fe sulphides; interpreted as K-feldspar-altered tuff or rhyolitic lava.
mPbdy$_{4}$	Layered amphibolite and metabasite: green to black; fine to medium grained; foliated, layered and migmatized; locally with a spotted texture; leucocratic to melanocratic; with biotite, clinopyroxene, garnet, hornblende, Fe-Ti oxides, plagioclase, sulphides and/or orthopyroxene; locally rich in magnetite. Enclose garnetite and hornblende gneiss locally.
mPbdy$_{3}$	Amphibolite; green; medium grained; mesocratic; granoblastic; massive, foliated or gneissic; migmatized; with biotite, clinopyroxene, garnet, hornblende and/or orthopyroxene and plagioclase. Enclose some hornblende gneiss locally.
mPbdy$_{2}$	Tourmalinite: black or brown; medium grained, granoblastic; massive to laminated; with quartz, tourmaline and trace of disseminated sulphides. Enclose some sillimanite-bearing gneisses and cut by kornerupine-quartz-plagioclase veins.
mPbdy$_{1}$	Granitic to tonalitic gneisses and undifferentiated quartzofeldspathic gneisses: beige to pink; fine to medium grained; granoblastic; foliated, layered and migmatized; leucocratic; with biotite, garnet, hornblende, orthopyroxene and/or Fe-Ti oxides. Enclose layers of amphibolite centimetres to tens of centimetres in width largely interpreted as transposed mafic dykes.

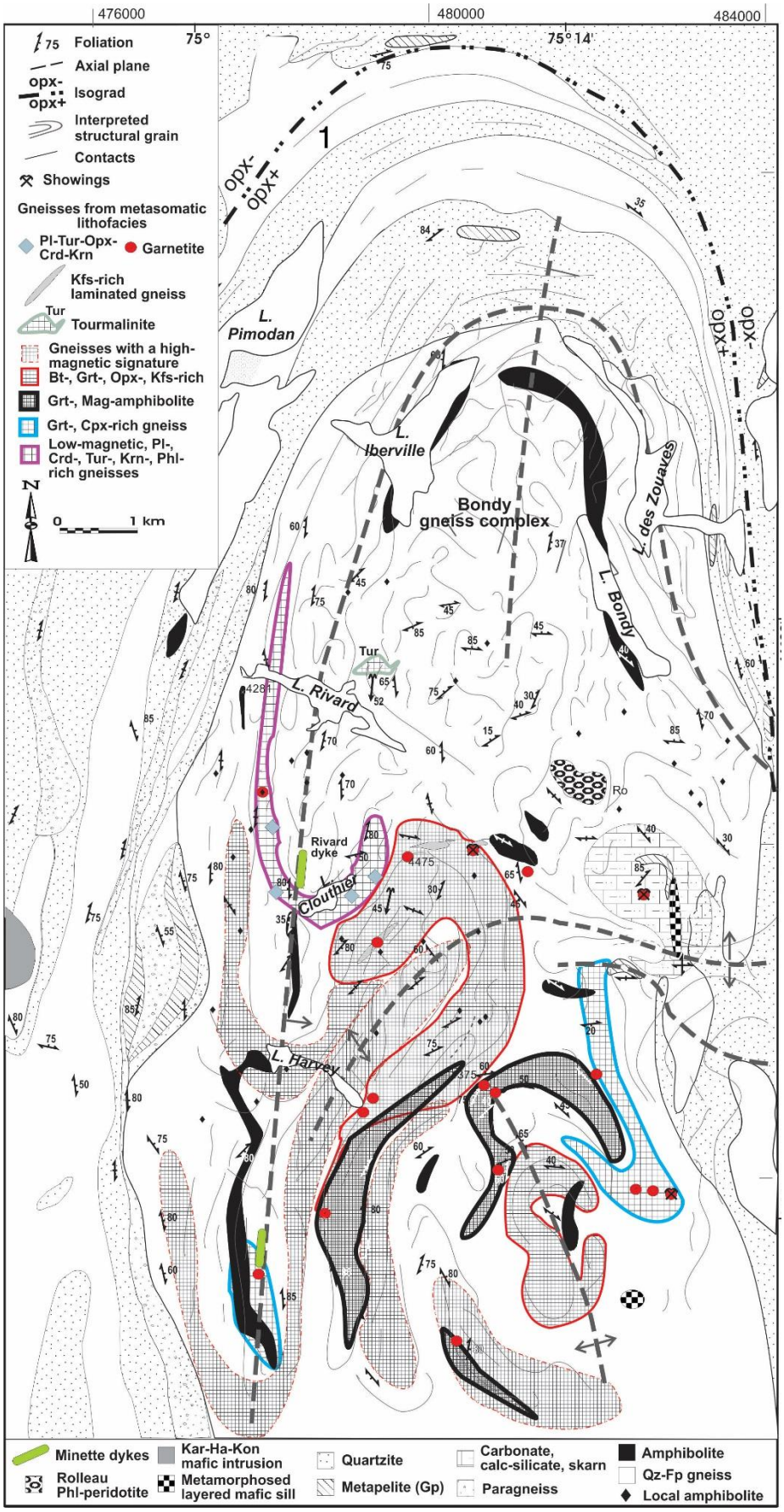

Figure 6.2. Current interpretation of the Bondy gneiss complex lithofacies. Extent of units combines mapping and aeromagnetic geophysical information. The eastern sector visited during Day 2 has yet to be mapped in detail. The western sector has been studied in detail in the 90s but new roads, hence new outcrops are available.

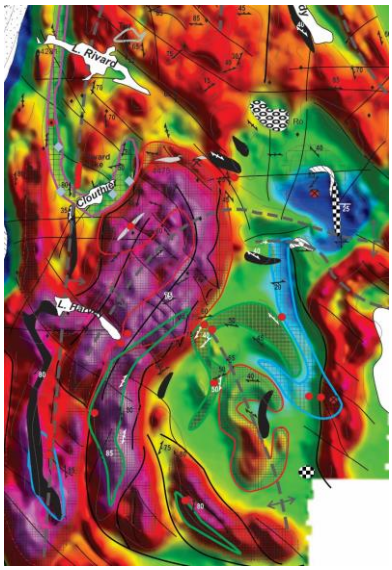

Figure 6.3. Geological map of Figure 6.2 reported on Figure 4 of Dufréchou et al. (2015).

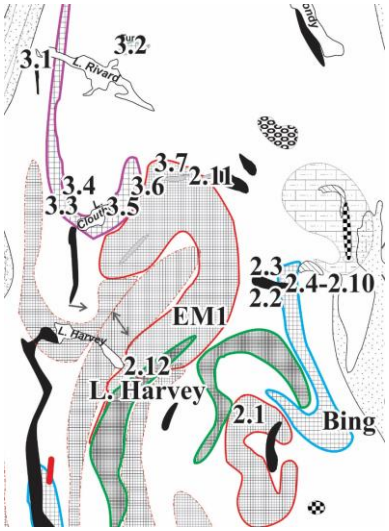

Figure 6.4. Location of Day 2 and Day 3 stops. Very little information is currently available to establish the extent of alteration facies and intrusive units that will be visited during Day 2.

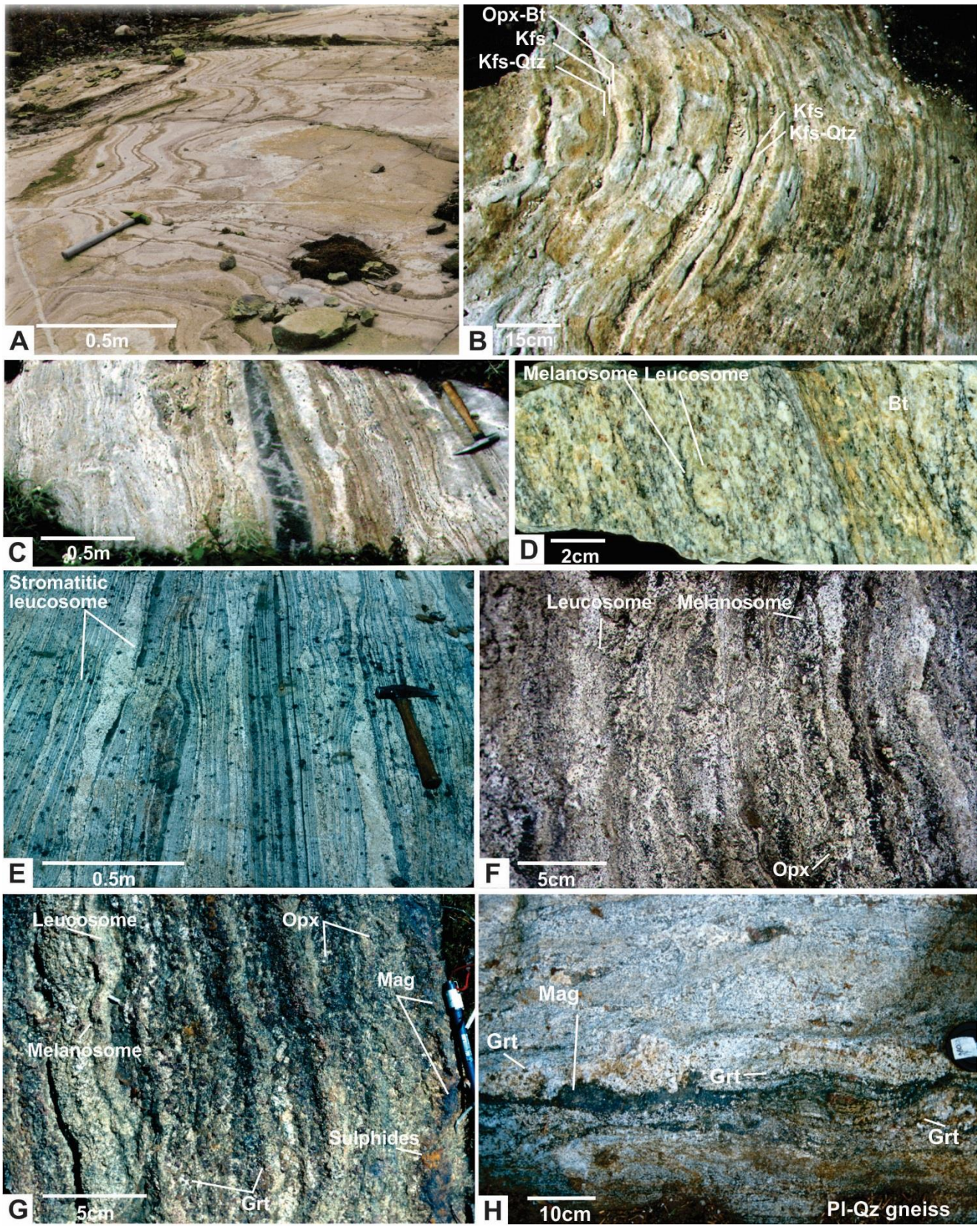

Figure 6.5. Variety of gneisses in the Bondy gneiss complex (Corriveau et al. 1997; Corriveau 2013). **A.** Granitic gneiss with mafic layers. **B.** Laminated K-feldspar quartzofeldspathic gneiss. **C.** Granitic gneiss with amphibolie layers. **D.** Felsic gneiss with garnet. **E.** Granitic gneiss with straight foliation. **F.** Biotite-K feldspar-magnetite-orthopyroxene-plagioclase-quartz migmatitic quartzofeldspathic gneiss. **G.** Biotite-K feldspar-magnetite-orthopyroxene-plagioclase-quartz migmatitic quartzofeldspathic gneiss. **H.** Anastomosed layers with magnetite and garnet in tonalitic gneiss.

At the end of the government project in 1998, this metamorphosed alteration system had been documented over an area of 9 by 6 km along an S-shape zone (Figs. 6.2, 6.3). A few mineral occurrences had been found with Cu contents reaching 8981 ppm; gold was anomalous (Corriveau and Jourdain 1993; Corriveau et al. 1994, 1997; Corriveau 2013). Geophysical anomalies were unveiled by the airborne magnetics, VLF and radiometric surveys of the Geological Survey of Canada (Hetu and Corriveau 1995) and were followed up by private sector with new geological and geophysical exploration programs (e.g. Richmond Minerals 2010). Strong positive aeromagnetic anomalies are associated with the alteration system and are distinctly higher than the pervasive magnetic highs associated with granulite-facies gneisses.

After the government project, new logging roads unearthed more outcrops of metamorphosed metasomatic rocks and mineral exploration has cleaned a few mineral showings across areas reaching 15 by 50 m. Day 2 will visit the Lac Harvey and Breccia trail showings. At Lac Harvey showing biotite-rich garnetite had been discovered by the Geological Survey of Canada and the importance of this outcrop as a mineral potential indicator noted. With these new discoveries of metamorphosed metasomatic rocks, the common presence of interference folding at outcrop to map scale, the presence of strong aeromagnetic anomalies where roads hence good outcrops have not been available, and the detailed fabric analysis of Harris et al. (2001) and Dufréchou et al. (2015) indicate that the internal architecture of the hydrothermal system is more complex than illustrated in Corriveau (2013). The latter was based on government mapping and geophysical data (Hetu and Corriveau 1995). The revised map in Figure 6.2 takes into account the new geophysical data of Dufréchou et al. (2015) but a lot remains to be done. No new maps were produced by private sector but a much better understanding of the extent of mineralization, variety of metal associations and the role of repeated faulting and shearing on mineralization was achieved.

6.4 Geochemical signatures

6.4.1 CCPI-AI-AAAI alteration signatures

The isochemical nature of high-grade metamorphism allows for chemical discrimination of metamorphosed hydrothermal ore deposits based on alteration indices and discriminant diagrams. As discussed in Chapter 2, premetamorphic fluid leaching and discharge associated with hydrothermal activities can lead, where intense, to severe element enrichment or depletion in host rocks. This is illustrated in Figure 6.6 for the Bondy gneiss complex where element contents of the variety of gneisses analysed are plotted with respect to their Ishikawa alteration index (Fig. 6.6). This index positively correlates with Per-aluminous Index, MgO and K_2O contents, and negatively correlates with CaO and Na_2O contents. Such significant element enrichments and depletions lead to unusual composition hence unusual modal mineralogy and in some cases atypical rock types. Field recognition of the resultant hydrothermal alteration zones can be done with a reasonable degree of confidence where parageneses, modal proportions, mineral colours and rock-type associations become significantly distinct from those of normal igneous and metasedimentary rocks (Bonnet and Corriveau 2007b; Corriveau 2013; Corriveau and Spry 2014 and references therein). Modelling do show however that many metasomatites once metamorphosed have nearly normal mineral assemblages and modes and resemble common rocks (see Chapter 2 and Trapy et al. 2015).

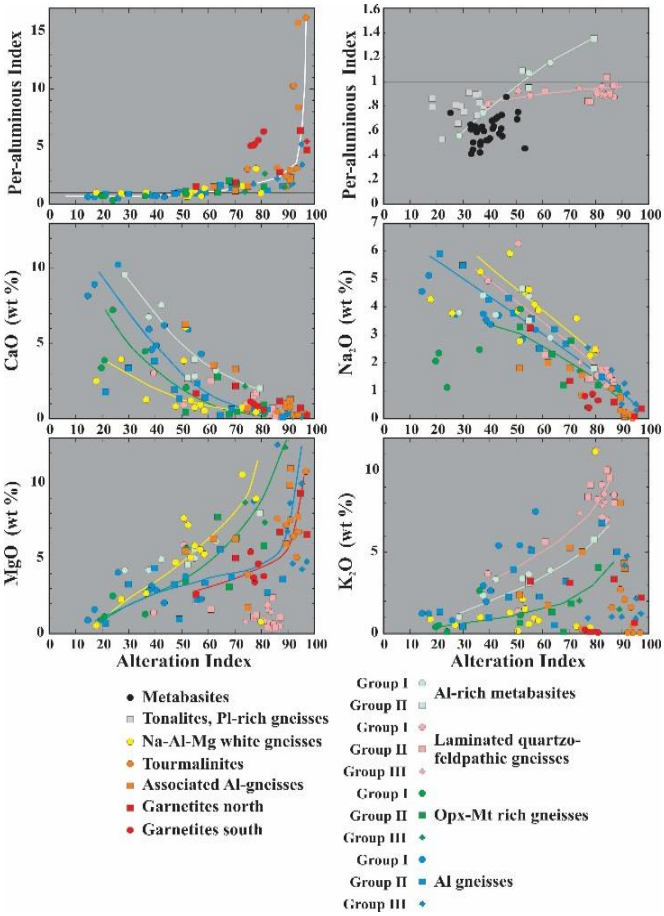

Figure 6.6. Harker diagrams.

The occurrence of hydrothermal alteration zones is also well illustrated in the alteration box plot of Large et al. (2001) which combines the Ishikawa alteration index (AI; based on K, Mg, Na and Ca contents; Ishikawa et al. 1976) and the chlorite-carbonate-pyrite index (CCPI; based on Fe, Mg, Na and K contents). The box plot is designed to discriminate least-altered rocks from hydrothermally or diagenetically altered rocks associated with volcanic massive sulphide deposits (Fig. 6.7). Samples plotting within the hydrothermally altered field (northeast part of the diagram) vary in composition as a function of the intensity of sericitization, chloritization, carbonate alteration and pyrite replacement of volcanic rocks. The diagenetic field (southwest half of the diagram) provides a mean to identify sea floor alteration and diagenesis of volcanic rocks.

Reporting geochemical data from known IOCG deposits and the Bondy gneiss complex indicates that this diagram is also very useful to interpret alteration trends in iron oxide alkali-calcic alteration systems and in metamorphosed hydrothermal systems for which identification of ore deposit model is particularly difficult.

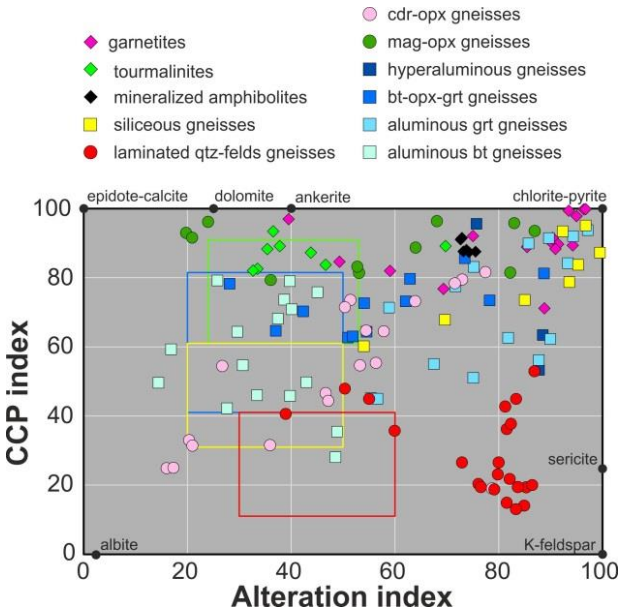

Figure 6.7. Alteration index versus CCP index diagram of Large et al. (2001) applied to metamorphosed metasomatic rocks of the Bondy hydrothermal system. Boxes are for basalt (green), andesite (blue), dacite (yellow) and rhyolite (red) composition.

Geochemical trends and potential alteration types derived from Figure 6.7 are the following:

1. Pink, laminated, K-feldspar-rich quartzofeldspathic gneisses display a first trend related to K alteration, and a second trend toward the chlorite pole related to chlorite-pyrite-bearing assemblages (Fig. 6.7).
2. Cordierite-orthopyroxene gneisses rich in plagioclase define a trend that extends from albitized protoliths toward intense chloritization (Fig. 6.7). Samples analysed are representative of the range between the most plagioclase-rich units to those where ferromagnesian minerals were most abundant either as disseminations or as discrete cluster or layers. The preferred interpretation for the enrichment in Mg and Si toward the chlorite pole is chloritization and silicification of HT Ca-Fe alteration zones and layers among albitites as observed in the Great Bear magmatic zone.
3. Magnetite-orthopyroxene gneisses are scattered along the chlorite-carbonate alteration trend of Large et al. (2001) that is characterized by high CCPI values (>80). Such alteration is an immediate footwall host to massive sulphide deposits both in mafic or felsic hosts however other deposit types may form such alteration types including IOCG deposits (Fig. 6.7).
4. Copper-mineralized amphibolites fall in a field between the chlorite-pyrite pole and the carbonates along which are scattered the variety of magnetite-orthopyroxene-bearing gneisses (Fig. 6.7). In addition, tourmalinites and associated siliceous-aluminous gneisses are characterized by a Mg trend related to chloritization (Fig. 6.7). Tourmalinites associated quartz-tourmalinite gneisses have enrichment in SiO_2 and Al_2O_3, suggesting advanced-argillic alteration and silicification.
5. Aluminous biotite and/or garnet-rich gneisses and orthopyroxene (Opx)-Bt-Grt gneisses defined two main distinct trends, a first trend related to potassic-ferroan alteration, and a second trend toward the chlorite pole (Fig. 6.7). Two samples define an incipient trend related to incipient potassic alteration.
6. In garnetites, we observe: 1) a mixing line between a calcic-ferroan alteration pole and a potassic-ferroan alteration pole, between garnetite with clinopyroxene and garnetite with biotite (Fig. 6.7); and 2) a group with high AI and CCPI values represented by garnetite with magnetite and garnetite with quartz (Fig. 6.7). This second trend suggests chloritization and/or silicification of earlier HT Ca-Fe and/or K-Fe alteration facies.

Seven principal hydrothermal alteration trends are evident from this diagram in the Bondy gneiss complex (Fig. 6.7):

1. sodic alteration in cordierite-orthopyroxene-plagioclase gneisses;
2. a HT Ca-Fe alteration in magnetite-orthopyroxene gneisses and some garnetites;
3. a potassic-ferroan in magnetite-rich, garnet-bearing gneisses and biotite garnetites;
4. a K feldspar alteration in laminated quartzofeldspathic gneisses;
5. chlorite alteration in siliceous gneisses associated with tourmalinites, cordierite-orthopyroxene gneisses, laminated quartzofeldspathic gneisses, aluminous gneisses and in some garnetites;
6. silicification in quartz-rich gneisses associated with tourmalinites, cordierite-orthopyroxene gneisses and in some garnetites; and
7. local advanced argillic alteration in hyper-aluminous sillimanite-rich gneisses.

Chloritization and silicification of earlier Na, K, Ca-Fe, K-Fe and sericitic alteration best account for observed trends.

Williams and Davidson (2004) developed a new alteration index (AAAI) to quantify strong SiO_2 enrichment and destruction of chlorite, carbonate and feldspar. In a box plot of AI versus the AAAI, samples from the sericitic zones plot in the upper right. Samples from the sericite-quartz and pyrophyllite-quartz-sericite zones have progressively lower AI values due to leaching and the formation of aluminosilicate minerals. In the inner zone of silicification and leaching, all elements used to calculate the AI are removed and it is no longer an effective index of alteration, whereas the AAAI values continue to increase to >95.

In Williams and Davidson (2004) discriminant plot, the addition of molar proportions of Na (pink), Ca (dark green), Fe (black), K (red), Mg (light green), and Si/8 (yellow)

further discriminates the main alteration facies as these cations are excellent proxies for their dominant mineral phases (Corriveau et al. 2010, 2016, 2017; Montreuil et al. 2013).

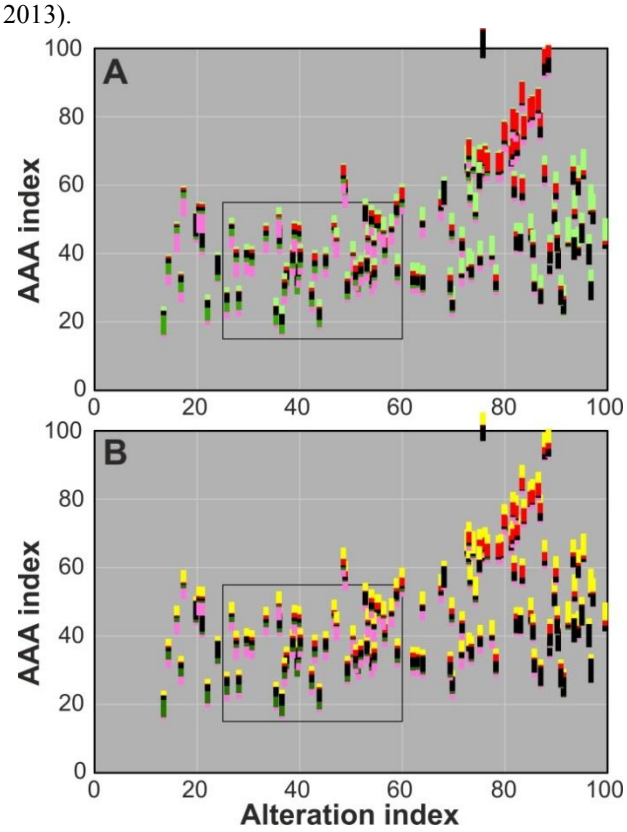

Figure 6.8. Alteration index versus AAA index diagram of Williams and Davidson (2004) applied to metamorphosed metasomatic rocks of the Bondy hydrothermal system. Bar codes reflect Na-Ca-Fe-K-Mg in (A) and Na-Ca-Fe-K-Si/8 in (B).

In Figure 6.8, Bondy gneiss complex samples define a clear trend to the upper right corner related to sericitic and/or potassic alteration. Few samples (hyper-aluminous sillimanite-rich gneisses) have AAAi higher than 90 related to advanced argillic alteration. In Figure 6.8 we clearly observed the development of chlorite alteration in samples with Alteration index values higher than 60, and with AAA index values lower than 65. This chlorite alteration occurs in siliceous gneisses, and in samples with Ca-Fe or K-Fe alteration.

6.4.2 IOCG discriminant diagram

In Figure 6.9, whole-rock composition of the Bondy gneiss complex samples interpreted to be metamorphosed hydrothermal alteration zones are plotted on the discriminant plot of alteration facies within IOCG and affiliated deposits. In Figure 6.10, the bar codes for these samples are plotted (data point at the base of the code bars are not shown in the diagram for clarity). The footprints of the Bondy gneiss complex is subsequently compared to that of volcanogenic massive sulphide deposits, IOCG and affiliated deposit and epithermal deposits (Figs. 6.11-6.15)

The molar proportions of the samples with Na (pink), Ca (dark green), Fe (black), K (red), Mg (light green), and Si/8 (yellow) further discriminate the main alteration facies as these cations are excellent proxies for their dominant mineral phases as discussed in Chapter 2 (Corriveau et al. 2010, 2016, 2017; Montreuil et al. 2013).

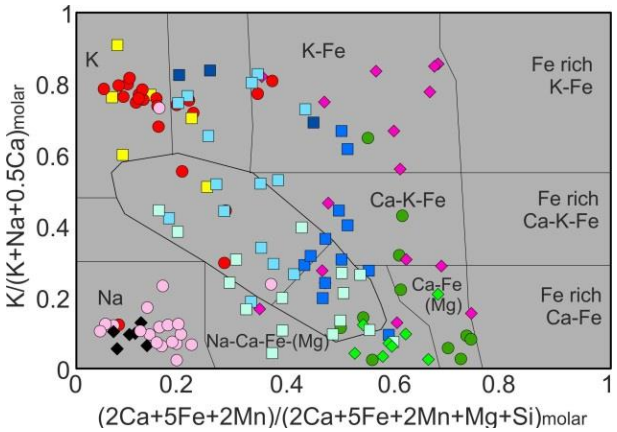

Figure 6.9. IOCG discriminant diagram of Montreuil et al. (2013) applied to Bondy metahydrothermal alteration zones.

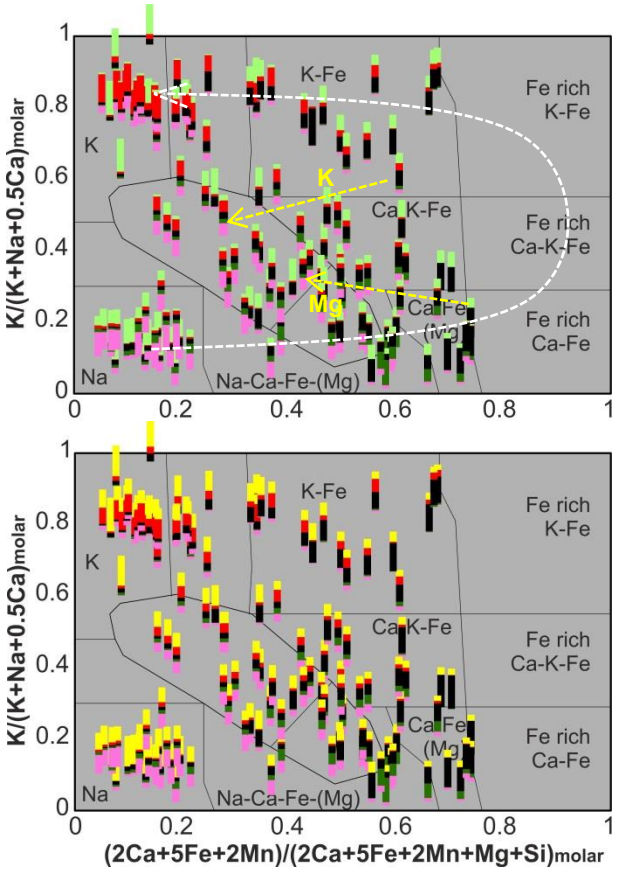

Figure 6.10. IOCG discriminant diagram of Montreuil et al. (2013) applied to Bondy gneiss complex meta-hydrothermal alteration zones. Signatures typical of prograde (white arrow) and retrograde (yellow arrows) paths are shown (see also Corriveau et al. 2017). Analyses can be found in Corriveau (2013). Bar codes reflect Na-Ca-Fe-K-Mg in (A) and Na-Ca-Fe-K-Si/8 in (B).

In Figures 6.9 and 6.10, Bondy metasomatites plot in the Na, HT Na-Ca-Fe, HT Ca-Fe, HT Ca-K-Fe, HT-LT K-Fe and K alteration fields; one or two cations dominate molar Na-Ca-Fe-K-Mg proportions. Plagioclase dominant gneisses with cordierite-orthopyroxene layers fall within the field of Na alteration with some Mg addition attributed to chloritization of original amphibole-bearing HT Na-Ca-Fe layers (Fig. 6.10A). Opx-rich aluminous gneisses and some amphibolites fall within HT Ca-Fe alteration. Magnetite-orthopyroxene gneisses outline Fe-rich alteration zones with the development of massive to well-layered magnetite-rich gneisses. Magnetite-rich, garnet-bearing gneisses and biotite garnetites fall within the K-Fe alteration field. Locally, K-feldspar prevails in laminated quartzofeldspathic gneisses that plot within the K alteration facies. These rocks fall on the prograde path of IOA-IOCG systems, though an Mg component typical of LT Ca-Mg K-Fe occurs throughout (Fig. 6.10B).

Some gneisses exhibit transitional alteration types dominated by two or three elements. These rocks record K alteration of HT Ca-Fe or HT Na-Ca-Fe metasomatites; retrograde overprints skew the signatures towards the field of least-altered rocks (Fig. 6.10). In Figure 6.10, some altered rocks display bar codes dominated by Mg and/or Si. These reflect intense chloritization and silicification of earlier Na, Ca-Fe, Ca-K-Fe, K-Fe and K metasomatites.The Bondy hydrothermal footprint is distinct from those of VMS deposits in that intense carbonatation, chloritization and silicification are not observed whereas Fe-dominant alteration is abundant (Fig. 6.11A, B).

In VMS deposits, altered rocks with Fe_2O_{3t} contents higher than 17.5 wt % are restricted to facies with AI values higher than 40, and CCPI values higher than 95 (Fig. 6.12A). In the Bondy hydrothermal system, high Fe_2O_3t contents are not restricted to facies with AI values higher than 40, and CCPI values higher than 95. Altered rocks with Fe_2O_{3t} contents higher than 17.5 wt % are characterized by CCPI values higher than 80, with no specific AI values (Fig. 6.12B). Therefore, in the Bondy hydrothermal system, iron enrichment in not restricted to sericite and/or chlorite alteration. Such high Fe_2O_{3t} contents have been observed in hematite-dominant IOCG footprint (Mantoverde district, Fig. 6.12C) or in the magnetite-dominant IOA-IOCG footprint (Great Bear magmatic zone, Fig. 6.12D).

Extensive albitites are not developed in VMS deposits though albitization is common. Most of the Bondy hydrothermal footprint is distinct from the ones of typical epithermal deposits (Fig. 6.13A, B) in that intense K and silicification is only restricted to part of the system. Moreover, intense advanced argillic alteration has not been observed until now in the Bondy hydrothermal system.

Comparison of Bondy data with the magnetite-dominant IOA-IOCG footprint of the Great Bear magmatic zone (Fig. 6.14a, b; Corriveau et al. 2017) illustrates that data from Bondy fall within most alteration facies characteristic of IOA-IOCG hydrothermal system, but are slightly off from the prograde metasomatic path of the Great Bear systems. At current levels of exposure, the Bondy gneiss complex lacks an IOA component (shown by lower Fe-enrichments), and show less Fe-rich K-Fe, Ca-K-Fe and Ca-Fe alteration facies than the Great Bear magmatic zone. The Bondy gneiss complex does display a pervasive and intense Mg footprint which is very typical of low-temperature alteration facies, such as chloritization and silicification, over Na, Ca-Fe and/or K-Fe metasomatites. Such intense Mg footprint has not been observed in the Great Bear magmatic zone.

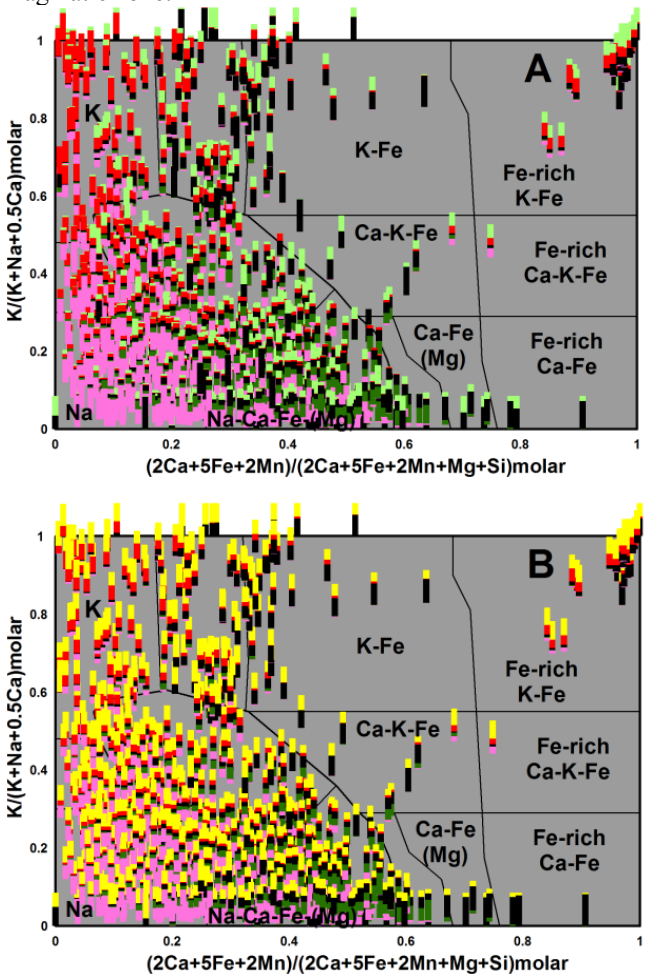

Figure 6.11. IOCG discriminant diagram of Montreuil et al. (2103) applied to VMS deposit chemical footprints, using data compiled by van Ruitenbeek et al. (2012). Same symbols as Figure 2.5.

Pervasive and intense Mg footprints are more common in hematite-dominated IOCG deposits such as in the Mantoverde district (Fig. 6.15) and are not common in magnetite-dominated IOCG settings such as the Great Bear magmatic zone. In the Mantoverde district, Si and Mg enrichments are superimposed over K-Fe and K alteration facies (Fig. 6.15). As observed in the Bondy hydrothermal system, the data of Mantoverde district are slightly off from the prograde metasomatic path of magnetite-dominated IOCG settings, such as the Great Bear systems (comparison of Figure 6.14 with Figure 6.15).

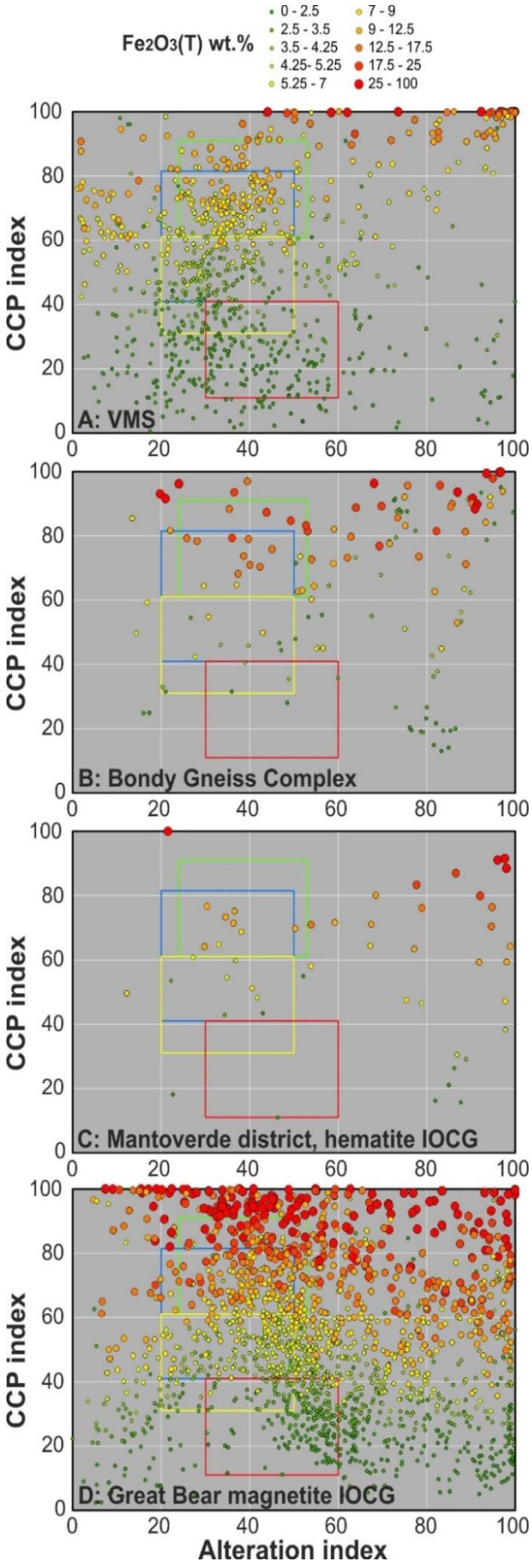

Figure 6.12. Alteration index versus CCP index diagram of Large et al. (2001) contrasting the Bondy gneiss complex signature with that of VMS and a variety of IOCG deposits and host systems. **A.** VMS deposit chemical footprints based on data from van Ruitenbeek et al. (2012). **B.** Bondy hydrothermal system based on data in Corriveau (2013). **C.** Mantoverde district Chile, hematite-group IOCG footprint based on data in Benavides et al. (2008). **D.** Great Bear magmatic zone IOA, magnetite-group IOCG and epithermal footprints based on data in Corriveau et al. (2015). Field of common igneous rocks as per Figure 6.7.

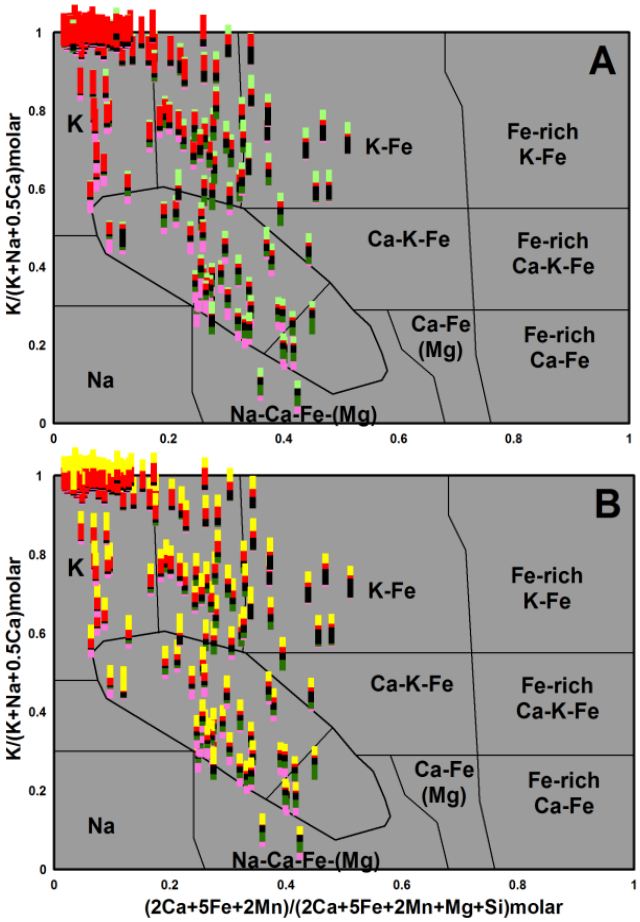

Figure 6.13. Plot of altered rocks within epithermal deposits and host systems based on data from Warren et al. (2007) on IOCG discriminant diagram of Montreuil et al. (2013). Same symbols as Figure 2.5.

Intense chlorite alteration without K-feldspar plots around a value of 0 for the K/(K+Na+0.5Ca) molar index and around a value of 0.5 for the (2Ca+5Fe+2Mn)/(2Ca+5Fe+2Mn+Mg+Si) molar index because of their Mg-rich composition devoid of Na and K. So, Fe-rich K-Fe, Ca-K-Fe and Ca-Fe alteration facies with latter chloritization are characterized by lower (2Ca+5Fe+2Mn)/(2Ca+5Fe+2Mn+Mg+Si) molar index, and plots are shifted to the left in Montreuil et al. (2013) discriminant plot (Figs. 6.10, 6.15).

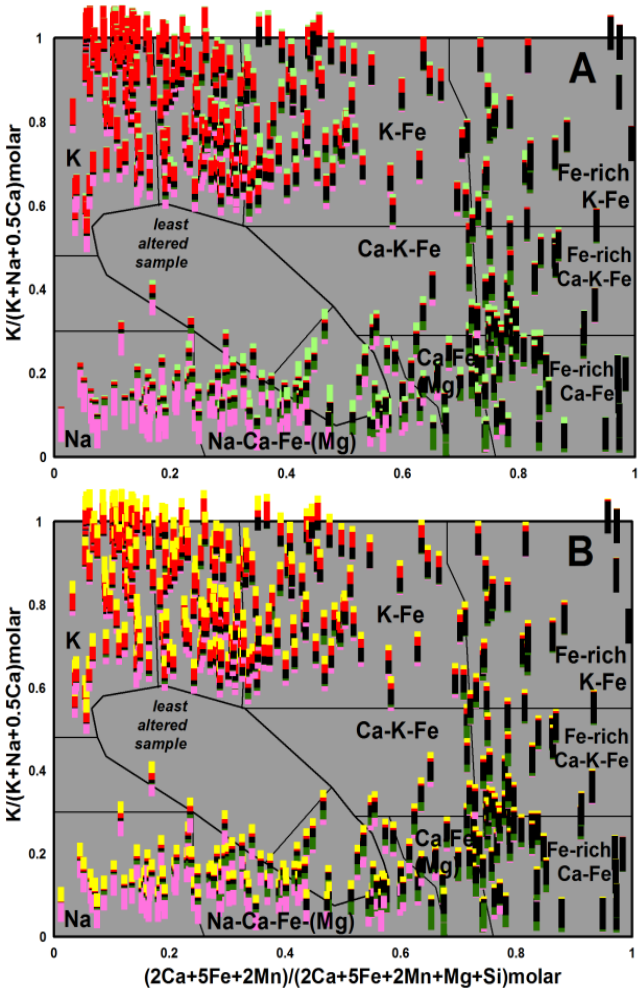

Figure 6.14. Plot of Great Bear magmatic zone IOA-IOCG-epithermal footprints based on samples with a single alteration type in Corriveau et al. (2015) dataset. Symbols as Figure 2.5.

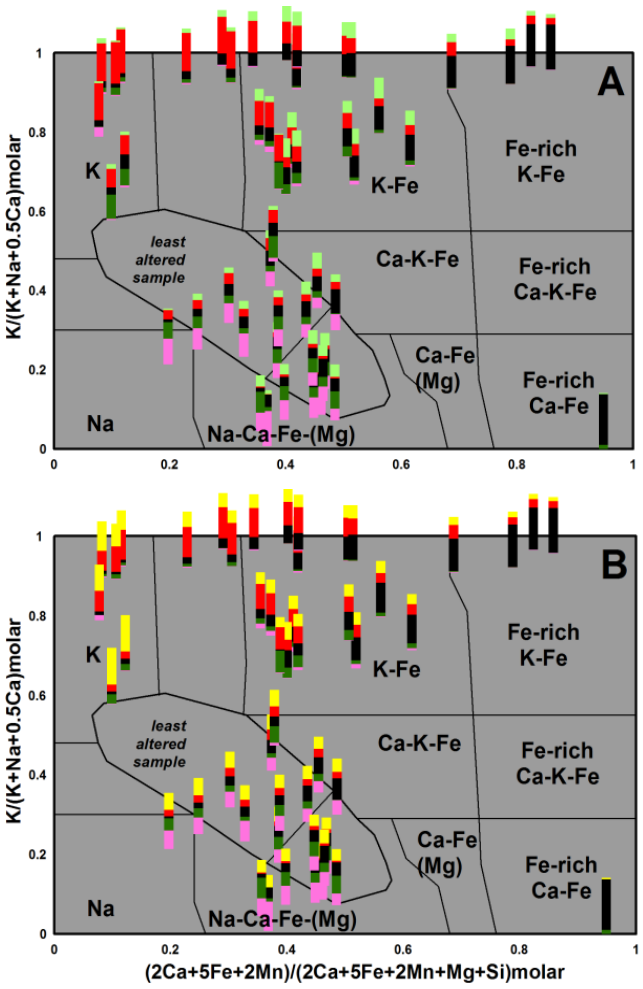

Figure 6.15. IOCG discriminant diagram of Montreuil et al. (2013) for the Mantoverde district, Chile using data from Benavides et al. (2008). Symbols as Figure 2.5.

6.4.3 REE mobility

In the Bondy hydrothermal system, the mobility of major elements recorded by the metamorphosed metasomatic rocks is associated with REE mobility. The REE patterns of laminated K-feldspar-rich quartzofeldspathic gneisses, biotite or garnet-rich gneisses, magnetite-orthopyroxene gneisses, cordierite-orthopyroxene gneisses, magnetite and quartz-rich garnetites, and tourmalinites are characterized by the progressive development of positively-sloped HREE. A few garnet-rich, Fe- or Mg-rich facies are characterized by chondrite-normalized REE profiles with negatively-sloped LREE ($[La/Sm]_n>1$), positively-sloped HREE ($[Tb/Yb]_n>1$), and strong negative Eu anomalies. Such profiles are defined as birdwing-shaped profiles (Baker and Hellingwerf 1986). In the complex, the rock types with birdwing-shaped REE profiles are commonly characterized by an unusual abundance of zircon. Although magmatic fractionation of accessory minerals (zircon, monazite, apatite etc.) can produce such profiles, it cannot explain the significant Zr enrichment of these rocks and the extreme fractionation Nb/Ta and Hf/Sm ratios.

Based on the extent of their REE fractionation, the REE profiles of the Bondy gneiss complex can be subdivided into five types.

Type I profile (high slope type) is characterized by high $(La/Sm)_n$ (2-4) and low $(Tb/Yb)_n$ ratios (1-2) (Fig. 6.16A). The Zr/Hf ratios associated with rocks with such profiles are fairly uniform (39-45), $(Zr/Sm)_n$ ratios vary from 1 to 2, and the Nb/Ta ratios between 17 and 25. Type II profile (slope type) is characterized by high $(La/Sm)_n$ (3-6) with flat HREE and $(Tb/Yb)_n$ ratios near 1 (0.9-1.5) (Fig. 6.16b). The Zr/Hf ratios of these rocks are also fairly uniform (39-47), their $(Zr/Sm)_n$ ratios vary from 1 to 4, and their Nb/Ta ratios between 17 and 50. Type III profile shows a light HREE enrichment with $(La/Sm)_n$ ratios between 1 and 2 and $(Tb/Yb)_n$ ratios lower than 1 (0.6-0.9) (Fig. 6.16c). These rocks have Nb/Ta ratios in the range of 20 to 30, Zr/Hf between 30 and 60, and $(Zr/Sm)_n$ between 1 and 13. Type IV profile (birdwing-shaped profile) is characterized by high $(La/Sm)_n$ (3-5), low $(Tb/Yb)_n$ ratios (0.5-0.8) and large negative Eu anomalies (Fig. 6.16D). These rocks have Nb/Ta ratios between 12 to 42, Zr/Hf between 27 and 40, and $(Zr/Sm)_n$ between 2 and 4. This profile mainly occurs in

plagioclase-dominant cordierite-orthopyroxene white gneisses and tourmalinites. Type V profile (V-shaped profile) is characterized by high $(La/Sm)_n$ (2-7) and very low $(Tb/Yb)_n$ ratios (0.2-0.8) (Fig. 6.16E). These rocks show Nb/Ta ratio of 20-45, Zr/Hf of 27-50 and $(Zr/Sm)_n$ of 2-20. Such signatures occur in magnetite-orthopyroxene rich gneisses, and in aluminous garnet-rich gneisses.

Besides some atypical igneous rocks, normal igneous and sedimentary rocks have negative or flat HREE slopes and highly variable LREE fractionation. Profiles of types I and II are similar to REE profiles of felsic volcanic rocks. In contrast, types III, IV and V profiles, with positive HREE slopes, suggest selective REE mobility related of rock interaction with hydrothermal fluids. Difference in bulk composition of the pre-alteration protoliths may or may not result in different metasomatic mineralogical assemblages depending of alteration intensity (cf. Rubin et al. 1993; Montreuil et al. 2013; Corriveau et al., 2016).

The tourmaline-rich unit hosted among phlogopite-sillimanite-bearing gneisses is a good candidate for a metamorphosed tourmaline alteration zone among argillic or sericitic altered units. The protoliths of tourmalinites are certainly tourmaline precipitation from exhalative F-brines also transporting aluminous clays colloids and dissolved silica or by percolation of these fluids in subsurface rocks.

Garnet-rich gneisses and garnetites are inferred to represent hydrothermally altered products of volcanic rocks, based on the gradational transition between quartzofeldspathic gneisses, aluminous gneisses, garnet-rich gneisses and garnetites. Magnetite-rich gneisses and garnetites fall within the Ca-Fe and K-Fe alteration fields (Fig. 6.9). The magnetite-rich gneisses and the garnetites are candidates for iron oxide-altered, magnetite-dominant and magnetite-phyllosilicate dominant HT Ca-Fe or HT K-Fe alteration types.

Hydrothermal activities can generate different REE profiles in the altered rocks and hydrothermal minerals, depending on the mineral phases (especially accessory minerals) of the protoliths and the minerals crystallized by the fluids (e.g. Montreuil et al. 2016b). In the Bondy gneiss complex, F-rich fluid and mineral phases enriched in LREE and HREE respectively must have been involved in the main hydrothermal alteration and REE fractionation process (Fu et al. 2003). Preferential removal of REE from the interstitial glass of the volcanic protoliths together with dissolution of plagioclase and subsequent external influx of HREE and HFSE can produce birdwing-shaped REE profiles. In turn, such profiles and/or unusual Nb/Ta, Zr/Sm ratios can be used as a sensitive marker of hydrothermally altered rocks in targeting mineral exploration.

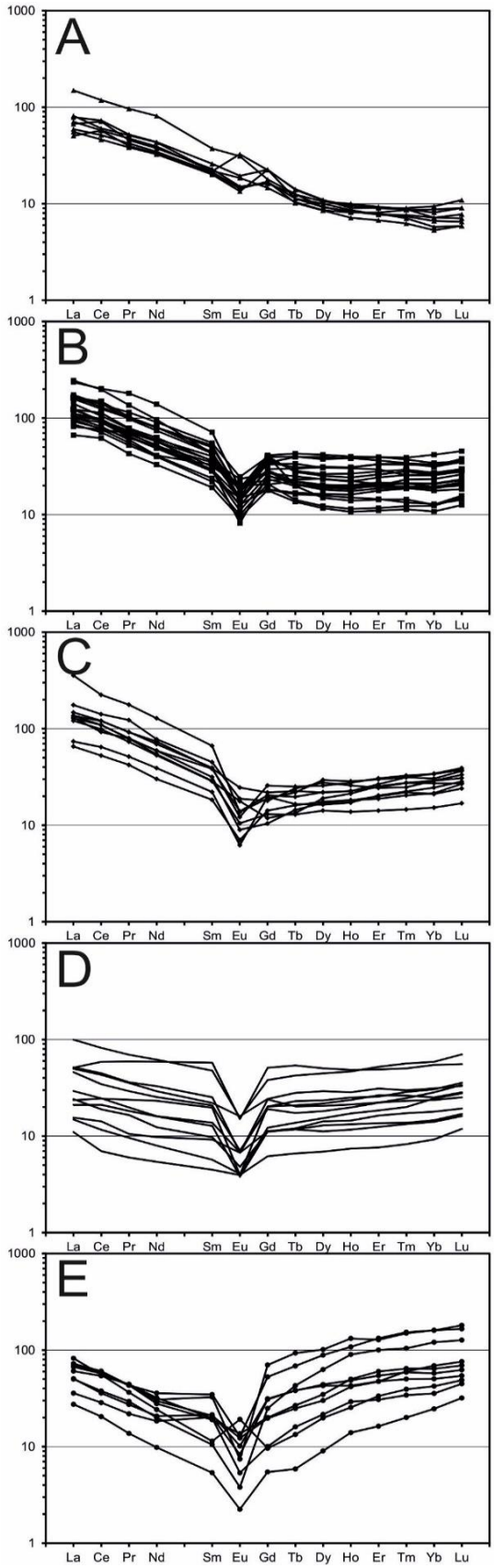

Figure 6.16. Chondrite normalized diagrams (normalizing values from Sun and McDonough 1989) for altered rocks of the Bondy hydrothermal system.

6.4.4 Summary

The metamorphosed hydrothermal footprint of the Bondy gneiss complex comprises (i) Na, (ii) HT Ca-Fe, (iii) HT K-Fe, (iv) LT K-Fe alteration facies, and finally (v) chloritization and silicification related to epithermal alteration. The chemical changes recorded by these facies have similarities to hematite-group IOCG deposits evolving towards epithermal caps.

Locally, hydrothermal activities mobilize REE altering original profiles and leading at the extreme to birdwing-shape REE patterns in the metasomatic rocks. In the complex, F-rich fluid and mineral phases enriched in LREEs and HREEs respectively must have been involved in the main hydrothermal alteration and REE fractionation process. Preferential removal of REEs from the interstitial glass of the volcanic protoliths together with dissolution of plagioclase and subsequent external influx of HREEs and HFSEs can produce birdwing-shaped REE profiles.

The birdwing shape REE profiles are particularly striking and common, Campbell et al. (1984) pointed out a strong positive correlation between the extent of element mobility and the size of ore deposits. If this correlation holds true than the Bondy gneiss complex could be particularly fertile considering the particularly well developed birdwing shape REE pattern in many of the gneisses (cf. Fu et al. 2003; Blein et al. 2004; this work).

6.5 Alteration mapping and footprint

6.5.1 Parageneses, mineral contents and major element composition

For the Bondy gneiss complex, finding cordierite-bronzite assemblages (stop 3.4) within an otherwise extremely white but non quartz-rich gneiss or calcite-rich marble triggered the additional mapping that led to the discovery of the alteration system and its mineralization. Such an assemblage is the granulitic equivalent of the cordierite-anthophyllite assemblage (i.e. magnesian chlorite schist) that can form through chloritization either in hydrothermal conduits across porous volcanic units associated with volcanic massive sulphide deposits (e.g. Figure 24b in Ohmoto 1996) or chloritic alteration at the low-temperature stage of iron oxide alkali-calcic alteration systems, a stage that follows or is coeval with alteration facies that form iron oxide copper-gold deposits (Corriveau et al. 2016; Montreuil et al. 2016a, b).

Other alteration zones were identified in the field by their abnormally high proportions of one or several of the following minerals (in alphabetical order): biotite (K), bronzite (Mg), chalcopyrite (Cu), clinopyroxene (Ca), cordierite (Al-Mg or Al-Fe), garnet (Al-Mg or Al- Fe), kornerupine (B), magnetite (Fe), orthopyroxene (Fe), plagioclase (Ca or Na), phlogopite (K-Mg), sillimanite (Al), and/or tourmaline (B) (Allard and Carpenter 1989; Bernier and MacLean 1993; Williamson et al. 2003; Corriveau 2013). Major elements data confirm the relative enrichments mapped by unusual minerals contents as shown in Figure 6.6 and data presented in Chapter 8.

6.5.2 Restites or metamorphosed metasomatites

The abundance of ferromagnesian and aluminous minerals can lead to rock components that resemble restites produced by partial melting of a normal metapelite followed by expulsion of the anatectic liquid (Bonnet and Corriveau 2007b). In the Bondy gneiss complex, leucosomes generated after the muscovite breakdown are commonly amoeboid, they have melanosome selvages that are distinct in distribution and assemblages from the more homogeneous mafic layers, leucosome parageneses are coherent from derivation from their host gneiss (kornerupine-bearing leucosomes in tourmalinites and tourmalinite-bearing gneisses, garnet cordierite-bearing leucosomes in biotite±sillimanite-bearing gneisses; orthopyroxene-bearing leucosomes in amphibolites and metabasites, etc.), and the compositional layering of the host gneisses remain fairly regular in thickness and style across outcrops and from one outcrop to the other without the development of layering parallel foliation as observed in Day 2 stops and in Figure 6.5. These attributes attest to the in situ origin of the leucosomes and to the low mobility of the liquids during anatexis. In this interpretation the abundant granitic veins are interpreted as externally derived. With this information and the rock assemblages, it was possible to avoid confusing metamorphosed metasomatic rocks with restites. This field technique has been successfully tested both in the Musquaro-La Romaine volcanic belt and the Bondy gneiss complex through geochronology (Wodicka et al. 2004; Bonnet et al. 2005; van Breemen and Corriveau 2005). At La Romaine, biotite-sillimanite-garnet gneisses were interpreted as metasomatic based on their varied mineral modes and could be traced to well-preserved lapillistones. Their zircon grains are igneous in morphology and identical to the volcanic host. In addition remnants of lapillistones were observed among the garnet-biotite-sillimanite gneisses. Similar textures were subsequently discovered in the Bondy gneiss complex, and interpreted similarly as those of the Musquaro-LaRomaine belt even though such biotite-rich rocks in the complex are more deformed.

Through field observation, it is possible to identify the extent of the segregation and remobilization of anatectic liquids and the nature of crystallization sites. You will note the in situ partial melts produced by low degree of melting, with leucosomes veins conformable with the gneissosity, the short migration distances of these melts (in the order of tens of centimetres), and thus the minimal remobilization during regional metamorphism. Sm-Nd isochron ages of mafic and intermediate gneisses of the Bondy gneiss complex are similar to U/Pb zircons ages obtained on intermediate and felsic magmatic rocks (Blein et al. 2003; Wodicka et al. 2004). These results confirm a minimal remobilization during regional metamorphism in the Bondy gneiss complex.

The complex forms a dome but it behaved as a solid body recording regional deformation during peak metamorphism (D1 phase of Vigneresse et al. 1996). This behaviour contrasts with the well-known granite-bearing migmatitic domes which lost cohesion during diatexites formation (such as in the D2 global uplift phase, ibid). In the Bondy complex, the leucosomes are commonly emplaced in shear zones and are interpreted as formed after 1.19 Ga and prior to 1.165 Ga deformation events. It is in this context that the Bondy gneiss complex is described in the next section.

6.6 Field strategies for exploration

The efficiency of mineral exploration in high-grade metamorphic terranes depends on the recognition of prospective systems, hence of the ability to apply mapping and exploration techniques to high-grade gneiss terranes outside of known deposits to find them, sample them appropriately and explore them efficiently (Bonnet and Corriveau 2007a, b). During field work, one can reconstruct mentally the chemistry of the rocks by documenting mineral parageneses and the mineral mode. It is also possible to use parageneses, modes, textures, structures and rock-type associations to make a diagnostic of potential protolith including usual sedimentary, volcanic and intrusive protolith as well as metasomatic protoliths and their potential premetasomatic usual sedimentary, volcanic and intrusive protoliths. In some cases, field interpretation of the presence of a metamorphosed hydrothermal system can be done with a reasonable degree of confidence. In other cases several alternatives remain, or the presence of a metamorphosed system cannot be diagnosed. To this effect key questions must be answered while mapping the outcrops visited in Day 2 (N.B., geochemical data is not available on these outcrops as they were uncovered by logging in the late 2000s after public geoscience research). To this effect we have left the figure captions largely blank so that you can make your own observation and descriptions. Question to answers are:

1. Which units have usual mineral parageneses, mineral mode and textures and can be mapped as typical ortho- or paragneiss?
2. Which units have atypical mineral parageneses, mineral mode and textures and can be mapped as metamorphosed hydrothermally altered (metasomatized) rocks with a reasonable degree of confidence?
3. Which units have fairly usual mineral parageneses, mineral mode and textures but nevertheless should be mapped as potential hydrothermally altered rocks and on what basis?
4. What are the various potential protoliths and what guide your working hypothesis?

Day 2 outcrops vector to Lac Harvey, EM1, Bing and Breccia Trail showings (see Richmond Minerals 2010).

6.7 Stop descriptions for Day 2

From the Super 8 in Mont Laurier (110 Boulevard Albiny Paquette, Mont-Laurier, QC J9L 1J1) head east on Route Transcanadienne/QC-117 S toward Avenue des Pins (1.0 km) (Fig. 6.17). Turn right onto Chemin Adolphe-Chapleau (5.6 km) and continue for 17.2 km onto the same road as it becomes Chemin de la Lièvre. (At 16.6 km you can see a beautiful double cover bridge on your right). Turn left onto Chemin de Ferme Rouge and drive for 3.8 km. Turn right onto Chemin Valiquette/QC-311 S for 1.8 km then left on Chemin du Lac Kar Ha Kon for 6.2 km. Turn left onto Route 3 and drive for 3.6 km. At a Y junction, stay on Road 3 (on your left). (Do not continue straight ahead on what looks like a much better road it is only a short cut for road 38.) Stay on Road 3 and drive another 7.2 km stay on your left to remain on Route 3. (Do not continue straight ahead at this sharp turn). Drive another 3.9 km and then turn left for Lake Michaud (Fig. 6.18). Drive 3.4 km and turn right for Lake Bing.

The road to Lake Ahern north of Route 3 leads to an extension of the hydrothermal system where zones of magnetite-bearing calc-silicate rocks are interlayered with various types of leucocratic to mesocratic gneiss (UTM: 477700m E, 5126450m N; outcrop 6023; Figure 12 in Corriveau 2013). Observed compositional layering may reflect an original volcanic stratification. Metamorphosed and deformed magnetite veins and potential magnetite breccias occur at this locality among garnet bearing gneisses (Fig. 6.19). A potassic alkaline dyke cuts typical leucocratic gneisses further to the north (Fig. 6.20). Though most gneisses resemble typical orthogneisses their composition fall either outside of the least-altered field or their barcodes point to alteration (Figs. 6.21, 6.22). Na-Ca-Fe and HT Ca-Fe alteration types prevail. Only one sample within the least-altered field has bar codes typical of igneous rocks. Others are best interpreted as Na-Ca-Fe alteration replaced by potassic alteration and by chloritized HT Ca-Fe alteration. These outcrops are completely overgrown. Visit must wait for the next cycle of logging or exploration to uncover these outcrops.

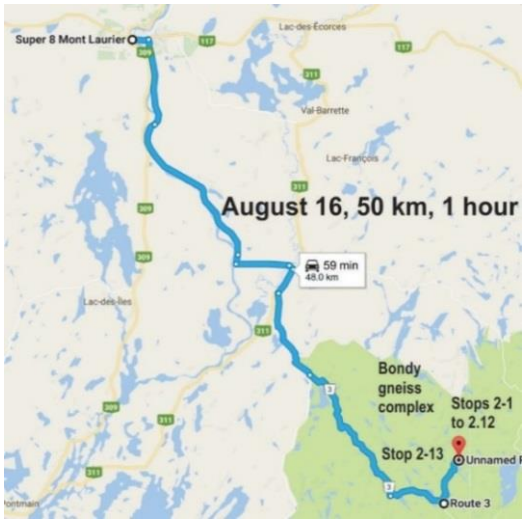

Figure 6.17. Day 2 route. Image @2018 Google.

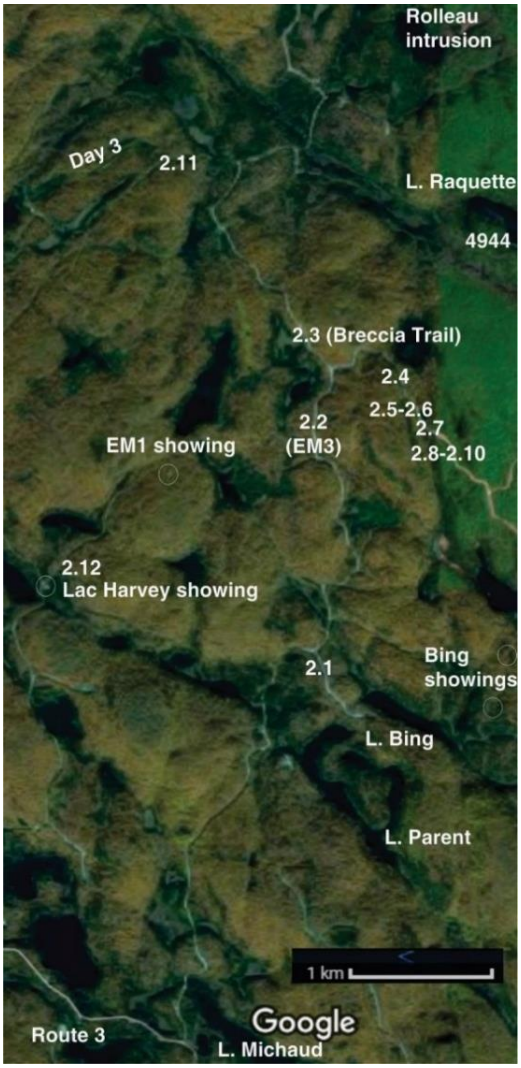

Figure 6.18. Stops location for Day 2 along the road for Lake Michaud, etc. Lake Ahern is to the west of the figure. Image @2018 Google.

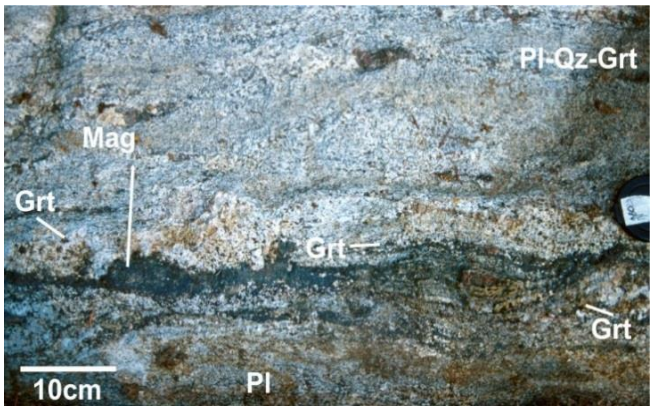

Figure 6.19. Magnetite and garnet veins sub concordant to a garnet-bearing leucosome that intrudes a plagioclase-quartz-garnet gneiss (CQA-6023; UTM zone 11: 477577mE, 5126674mN).

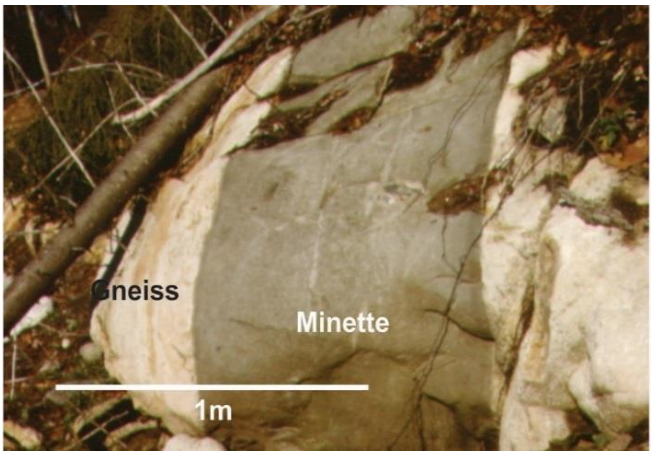

Figure 6.20. Minette dyke within leucocratic gneiss of the Bondy gneiss complex (CQA-6025; UTM zone 11: 477684mE, 5126760mN).

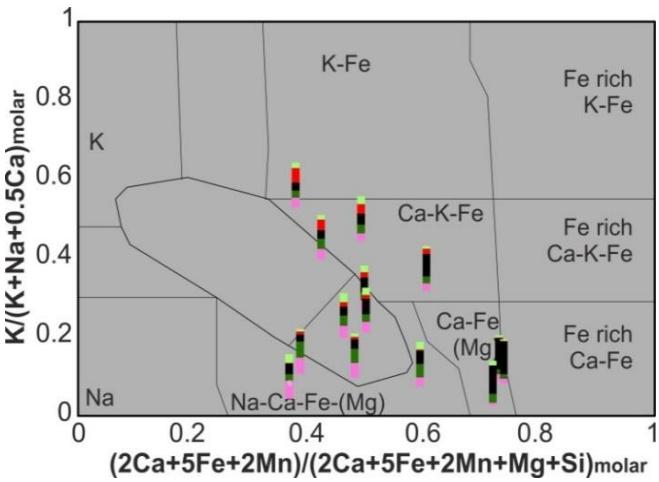

Figure 6.21. IOCG discriminant diagram with Na-Ca-Fe-K-Mg bar codes for samples from outcrops 6023 to 6026.

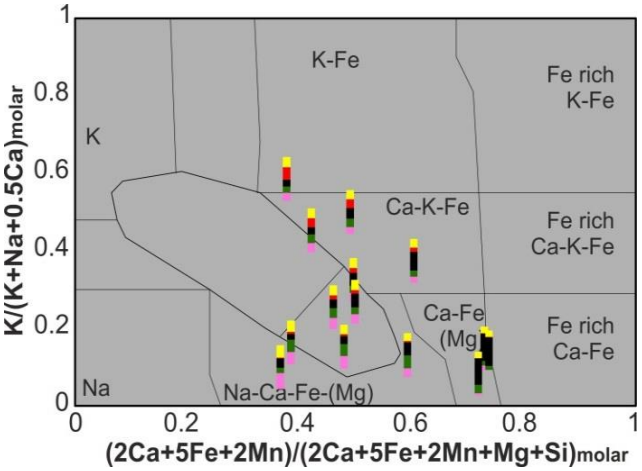

Figure 6.22. IOCG discriminant diagram with Na-Ca-Fe-K-(Si+Al)/10 bar codes for samples in Figure 2.5.

Stop 2.1
Lake Bing area

From Route 3, the side road to lakes Michaud, Parent, Bing, etc. follows the eastern edge of the Bondy gneiss complex (Fig. 6.18). Amphibolites and mafic granulites outcrop among a variety of quartzofeldspathic gneisses and based on their magnetic signatures they only form small discontinuous lenses (Fig. 6.3). The road leading northeast to Lake Bing crosses a layered intermediate to mafic gneiss. Beyond that are outcrops of garnet-bearing hornblende or clinopyroxene gneisses.

Government discovered a metre-scale layer of chalcopyrite-bearing garnetites intercalated with magnetite-bearing calc-silicate rocks and garnetiferous amphibolites and garnetite east of Bing Lake (8981 ppm Cu; UTM 483650mE, 5127230mN; Grt, outcrop 6054; Figure 12 and Table 3 in Corriveau 2013). This assemblage resembles outcrop 4944 south of Lake Raquette (Fig. 6.18) but there is no geophysical evidence for continuity of these units. These showings are not accessible by car but Day 2 stops provide an overview of such rocks among more leucocratic and less calcic gneisses.

Subsequent mineral exploration led to the discovery of the Bing showings (Richmond Minerals 2010) with vein and disseminated chalcopyrite, malachite, pyrite, and magnetite in a coarse-grained clinopyroxene-rich calc-silicate rock. Grab samples with up to 4% Cu and 21 g/t Ag, with an average of 3.2% Cu and 17 g/t Ag over an area exposed across 15 by 15 m (Fig. 6.23). Drill hole RB-05-08, on the Bing property, intersected 37.45 m grading 0.21% Cu with minor amounts of gold and silver.

Stop 2.1 is the newly cleared outcrop adjacent to outcrop 4341. It is on the western side of the new road toward the south shore of Lake Bing. It consists of leucocratic to mesocratic mafic granulites. Ghost of plagioclase are common and indicate that the precursor rocks was medium to coarse-grained. Garnet occurs sporadically among the metabasite where protoliths were least altered (Fig. 6.24). Most of this outcrop is considered as a 'normal' mafic granulite that was partially melted. Some components of the unit are more garnetiferous and we interpret them as a sign of hydrothermal alteration. The presence of garnet and clinopyroxene leucosomes implies minimum P-T conditions of 800ºC/10 kbar (Pattison 2003).

Figure 6.23. Bing showing calc-silicate rock with clinopyroxene, garnet and magnetite veined by chalcopyrite. Such veins are interpreted as remobilization of sulphides after peak metamorphism. Photo courtesy of Richmond Minerals from Antonoff et al. (2007).

A second outcrop along the road (north side) consists of crudely layered fine to medium-grained garnet-bearing quartzofeldspathic gneisses, mafic granulites with garnet-rich zones and garnetites (Fig. 6.25). Leucosomes are orthopyroxene or garnet bearing depending of host metabasite garnet content. A metamorphosed felsic dyke cut the gneissosity. Metamorphosed quartz veins are largely stratabound.

Garnetites are among the most easily recognisable rock types of a metamorphosed hydrothermal system. They are commonly interpreted as exhalites derived from a carbonate and chlorite precursor (e.g. coticule), and serves as guide to metamorphosed base-metal or gold deposits (Spry et al. 2000). Quartz-garnet gneisses also occur within igneous hosts (e.g. in metanorite, De La Blache igneous complex, Central Grenville Province), hence they are not exclusively sedimentary in origin but can also form through alteration of mafic protolith. In the present setting, the origin of the garnetite is interpreted as the metamorphic product of Al-enrichment due to a premetamorphic hydrothermal alteration.

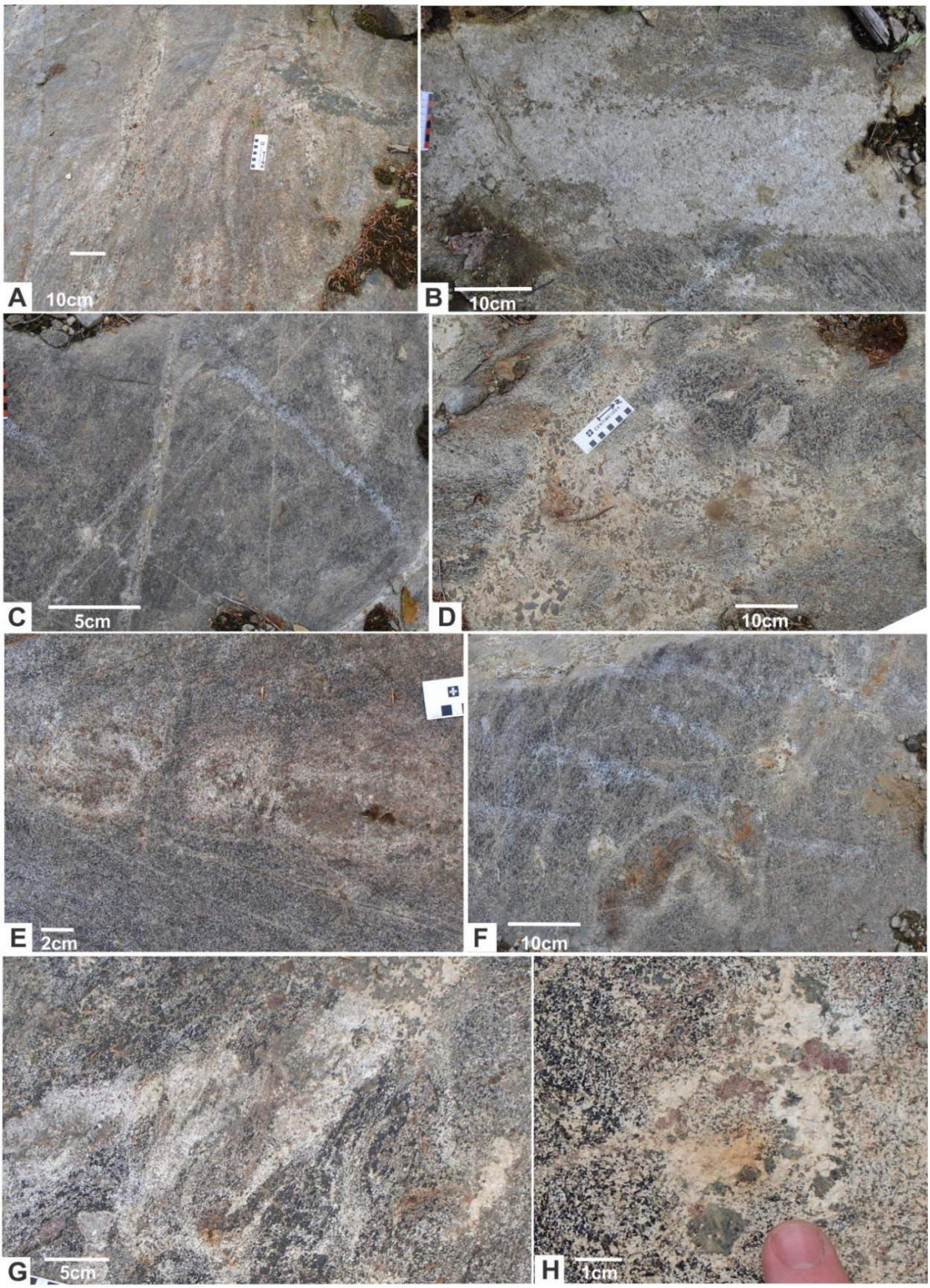

Figure 6.24. Stop 2.1. Outcrop 4341. Mafic granulites with gabbroic textures, heterogeneous zone with a coarser grain and local zones enriched in garnet. Zones richer in garnet have garnet-clinopyroxene leucosomes.

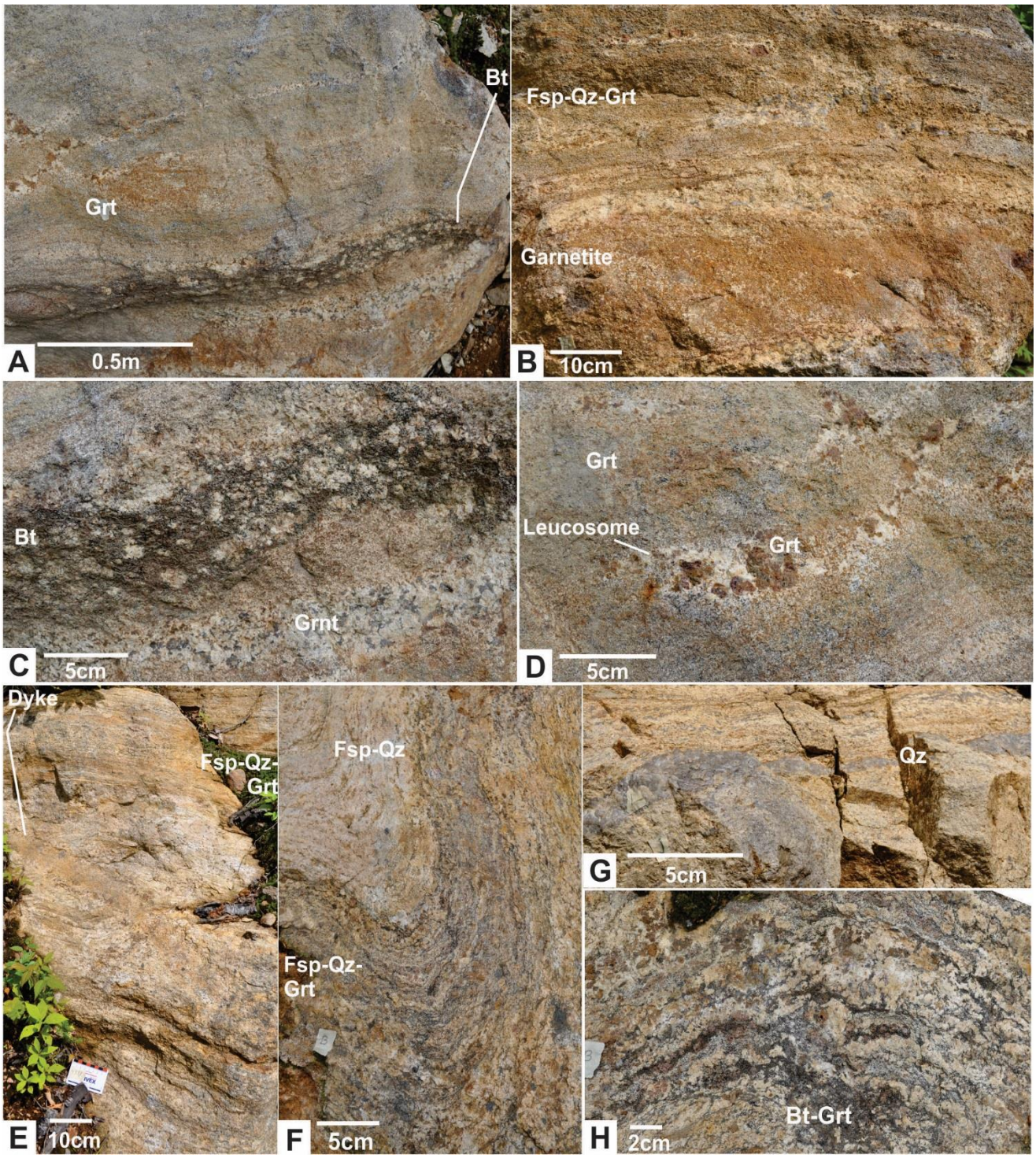

Figure 6.25. Mafic and felsic granulites with layers or zones rich in garnet or biotite east of outcrop 4341. **A.** Garnetite among mafic granulite with garnet-bearing leucosomes. Outside of garnet-rich zones the leucosomes bear orthopyroxene. **B.** Garnetite interlayered with garnet-bearing gneisses. **C.** Close-up of A. Biotite distribution mimics that of a former breccia. This layer is interpreted as a metamorphosed biotite-rich or iron oxide-sericite K-Fe breccia zone subconcordant to original layering of the protolith. **D.** Close-up of leucosomes in A. **E.** Metamorphosed felsic dyke cutting the layering of the gneisses. **F.** Garnet and biotite stringers among a zones of garnet-bearing gneiss. **G.** Metamorphosed quartz veins. **H.** Other biotite-garnet stringers.

Stop 2.2

Stop 2.2 (outcrop 1687; Figs. 6.28-6.34) consists of crudely layered fine to medium-grained garnet and locally clinopyroxene-bearing quartzofeldspathic gneisses. Green, diopside-dominant calc-silicate bands and pods and brown calc-silicate lenses and isolated pods with strong internal differential erosion (carbonate-bearing?) also occur (Figs. 6.26, 6.27, 6.33). Mineral assemblages are respectively Cpx-Grt±Mag and Cpx-Grt-Mag-Cb(?)-Sc(?) (Fig. 6.28). Where Cpx prevail, magnetite is absent. Quartz veins form halos along some of the calc-silicate lenses and also form a metre size breccia. Train of quartz-rich or garnet-rich lenses and pods parallel the compositional layering of the leucocratic gneisses others cut it (Fig. 6.34). The latter are interpreted as veins or breccia zones (Fig. 6.29). In most cases the ferromagnesian minerals have a distribution that is interpreted as premetamorphic however restitic material is locally observed in association with stromatitic leucosomes. Anastomosing zones of pink, K-feldspar-rich and garnet-bearing gneisses cut the compositional layering. Contacts are diffuse. Size and distribution of garnet grains are similar to those of the host gneisses and distinct from those of the leucosomes (which are coarser and of irregular distribution). These zones are interpreted as premetamorphic replacement zones of K alteration. These units are all folded and there is locally development of a weak axial-plane foliation defined by quartz, mafic clots, etc. Locally leucosomes are deformed; foliation is defined by quartz and local stringers of garnet (Fig. 6.30). Deformation that postdates the leucosomes postdates the Chevreuil intrusive suite. Down the hill, crucial characteristics are observed. A layered sequence that looks the same as the one uphill contains ~20-30% Grt spread evenly irrespective of the host composition (leucosome and mesosome). In migmatites, mesosomes are commonly composed of small garnet, whereas leucosomes are composed of large euhedral garnet (Figs. 6.31, 6.32). These observations suggest alteration of the protolith that favoured garnet growth in the altered rocks during granulite metamorphism.

Figure 6.26. Stop 2.2. Quartzofeldspathic gneisses with calc-silicate lenses.

Figure 6.27. Stop 2.2. Overview of outcrop.

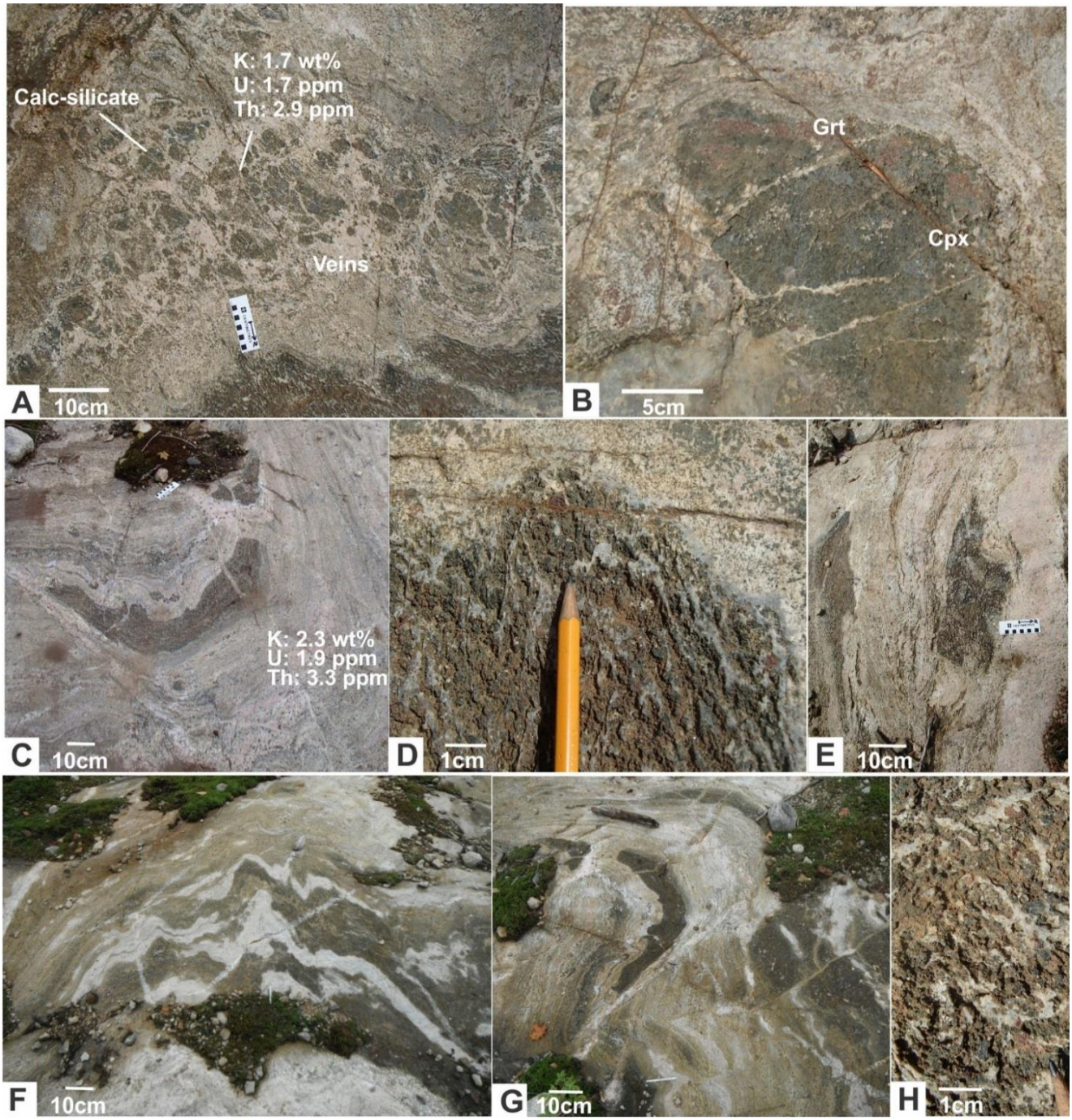

Figure 6.28. Stop 2.2. Calc-silicate rocks. **A.** Train of calc-silicate pods cutting across layering. **B.** Close-up of A showing that diopside dominates these zones. Garnet occurs very locally. **C-E.** Brown calc-silicate pods with diopside, brown carbonate and quartz. The quartz defines an axial planar foliation. **F-G.** Folding of calc-silicate layers and granitic veins. **H.** Zones bearing a brownish garnet.

Figure 6.29. Stop 2.2. Highly heterogeneous, layered and brecciated quartzofeldspathic gneisses.

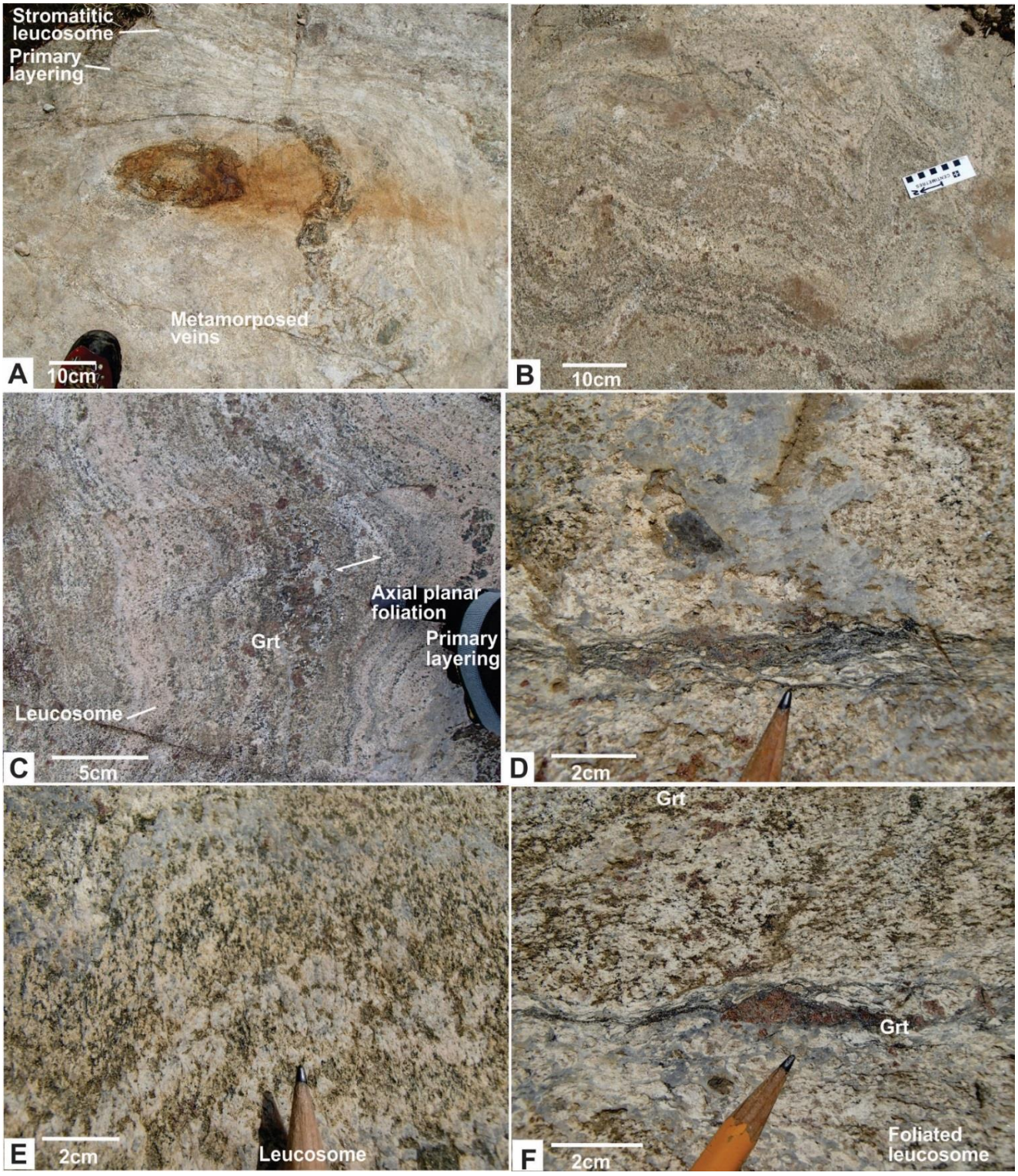

Figure 6.30. Stop 2.2. Quartzofeldspathic gneisses where K_2O range from 2 to 5 wt %. Contents of U and Th are low (< 2 ppm). **A.** Quartzofeldspathic gneisses. **B-C.** Garnet-bearing gneisses with irregular distribution of garnet along layering. **D.** Local shear cutting across a quartz-rich zone (vein?) spatially associated with granitic veins. **E.** Axial planar foliation. **F.** Local shearing in leucosomes with remobilization of garnet and magnetite along a stringer at an angle to shear plane.

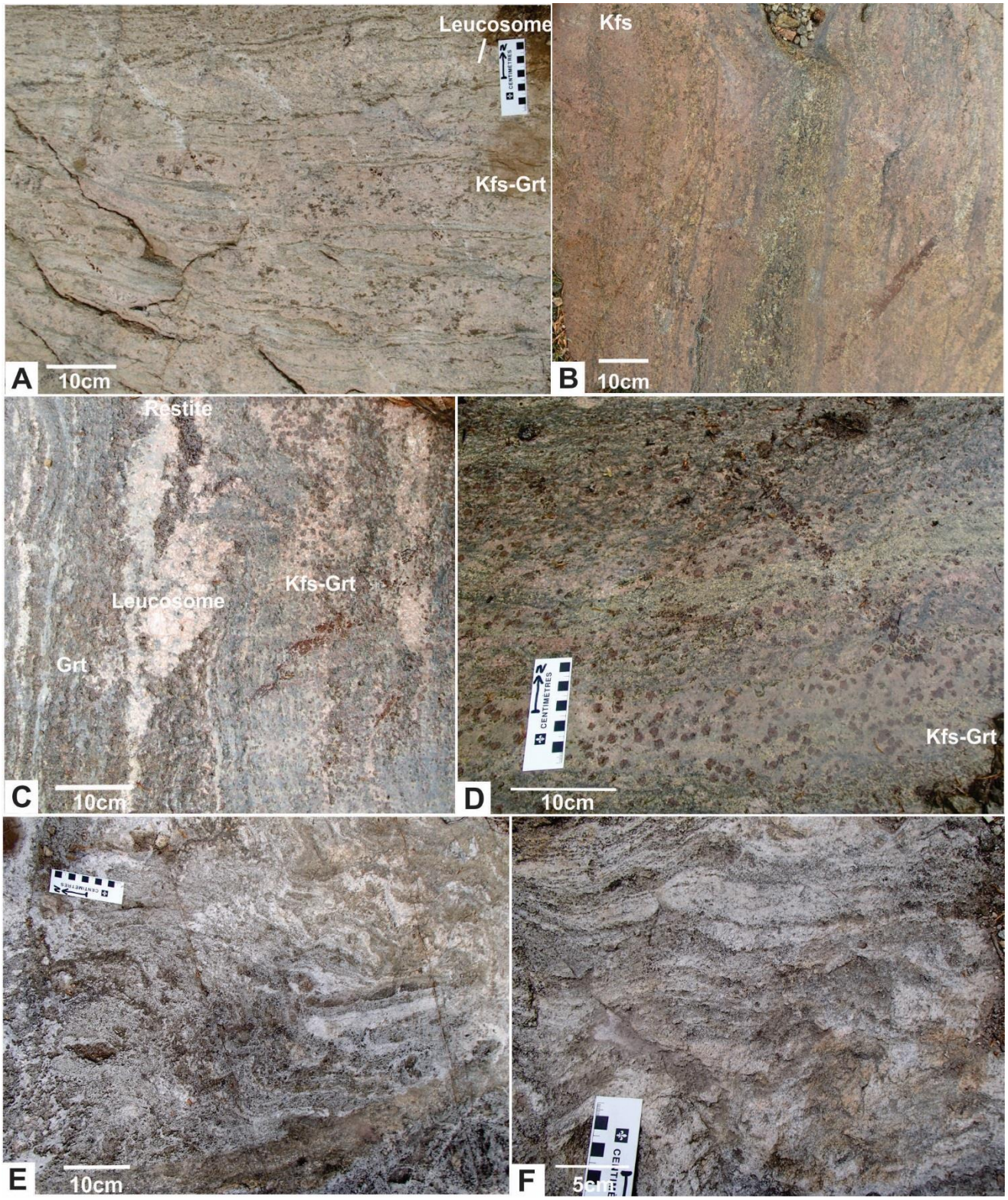

Figure 6.31. Stop 2.2. K-feldspar-rich quartzofeldspathic gneisses, and quartz or garnet-rich layers. **A.** Anastomosing zones of pink K-feldspar-rich, garnet-bearing quartzofeldspathic gneisses. The garnet shows an even distribution within the pink gneisses. **B.** Pink, K-feldspar-rich leucocratic gneisses. **C.** Garnet-bearing gneisses with irregular distribution of garnet along layering. **D.** Garnet are distributed evenly irrespective of layering. **E-F.** Quartz-rich gneisses.

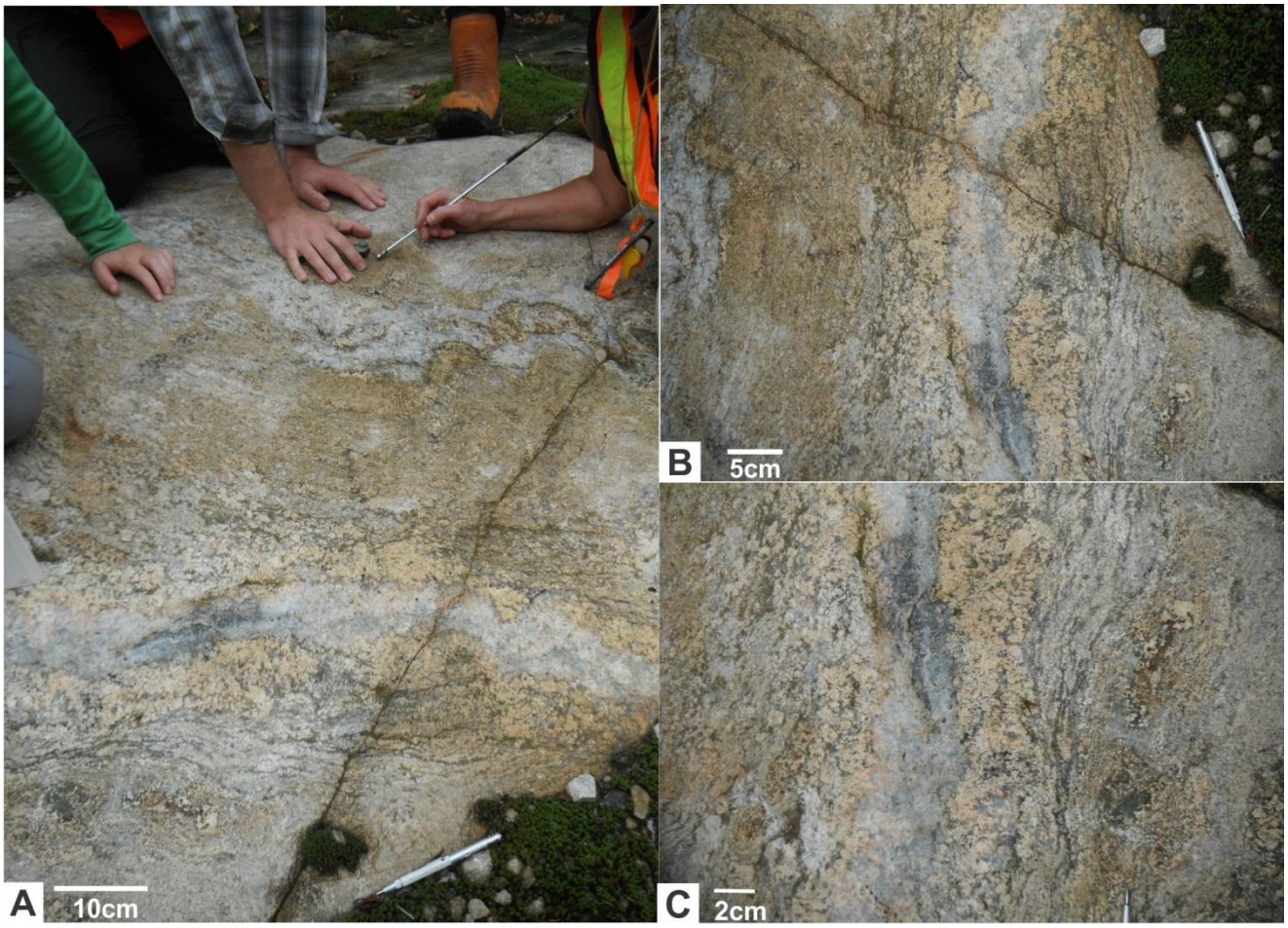

Figure 6.32. Stop 2.2. Granitic veins and quartz veins. **A-C.** Granitic veins, atypical by their irregular width and contacts cut across the gneissosity and are themselves cut by irregular quartz veins.

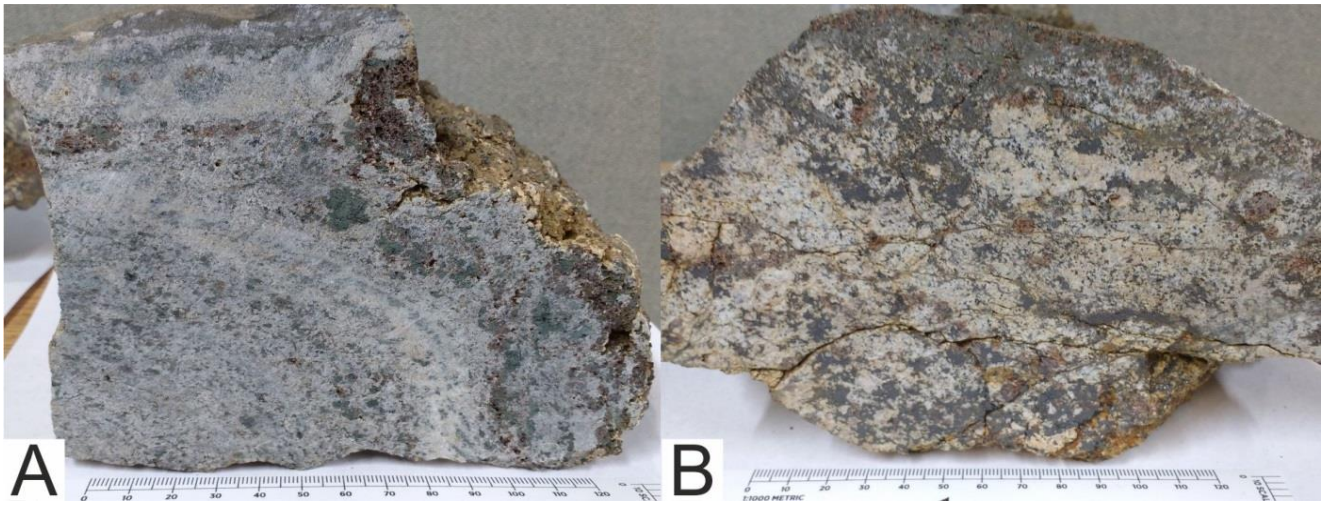

Figure 6.33. Stop 2.2. **A.** Calc-silicate lens. **B.** Quartzofeldspathic gneisses with garnet.

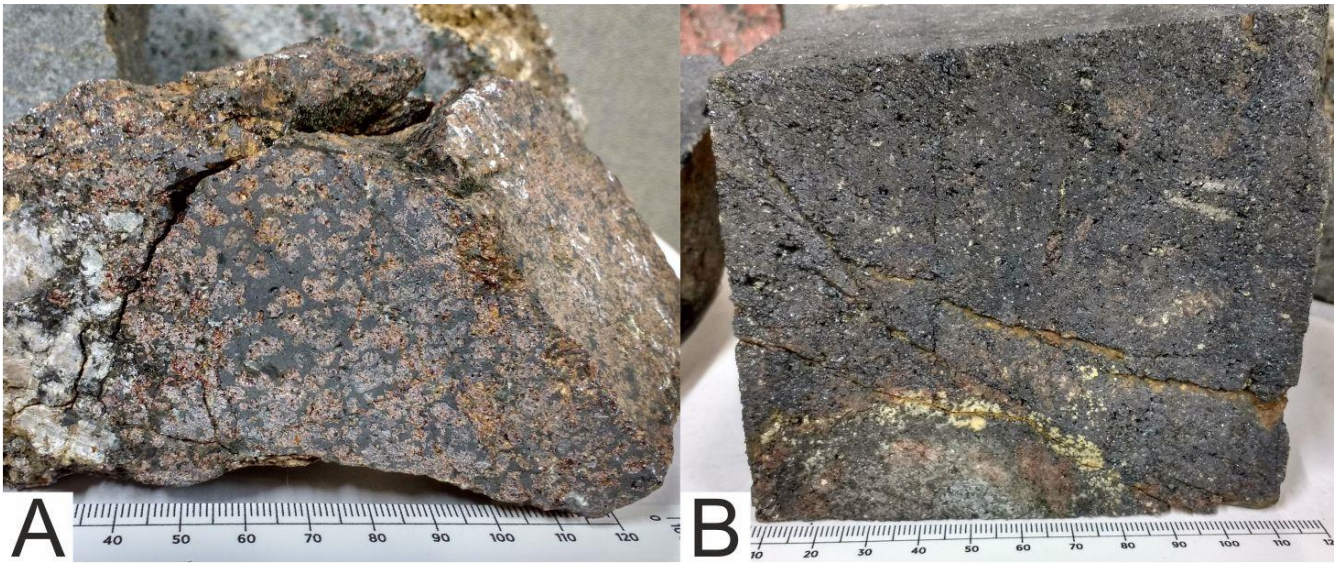

Figure 6.34. Stop 2.2. **A.** Sample of a lens of magnetite-rich garnetite. **B.** Sample from a magnetite lens with garnet, pyrite and apatite.

Quartzofeldspathic gneisses fall in the field of least-altered rocks (Figs. 6.35, 6.36). K-feldspar-rich quartzofeldspathic gneisses fall in the fields of least-altered rocks and potassic alteration (Figs. 6.35, 6.36). Finally, calc-silicate rocks fall in the field of Na-Ca-Fe alteration (Figs. 6.35, 6.36).

Stop 2.3
Breccia Trail

This outcrop is part of the series of outcrops of the Breccia Trail showings that share some similarities with the Lac Harvey showing in terms of rock types (e.g. garnetites, biotite-rich and magnetite-rich layers) and high airborne radiometric K anomalies (Figs. 6.37, 6.38). Grab samples of brecciated zones enriched in biotite and magnetite, with disseminated and vein pyrite and chalcopyrite have up to 0.4% Cu (Fig. 6.39). On the outcrop, gamma-ray measurements reach 7 wt % (Antonoff et al. 2007). Some magnetite-rich layers host apatite, biotite and pyrite and as such share affinities with IOA mineralization with potential for REE as discussed in Chapter 2 and Corriveau et al. (2016). As prognosticated from the paragenesis, magnetite concentrates are anomalous in REE (454 ppm; Antonoff et al. 2007). Areas rich in biotite are locally sheared and at the extreme are porphyroclastic. Garnetites are common and form diffuse to sharp layers adjacent to amphibolites, calc-silicate rocks or quartzofeldspathic gneisses (Fig. 6.40).

Most magnetite-rich layers fall in the field of Ca-Fe and Ca-K-Fe alteration facies (Figs. 6.41, 6.42). Only two samples fall in the field of Fe-rich K-Fe or Ca-K-Fe alteration facies.

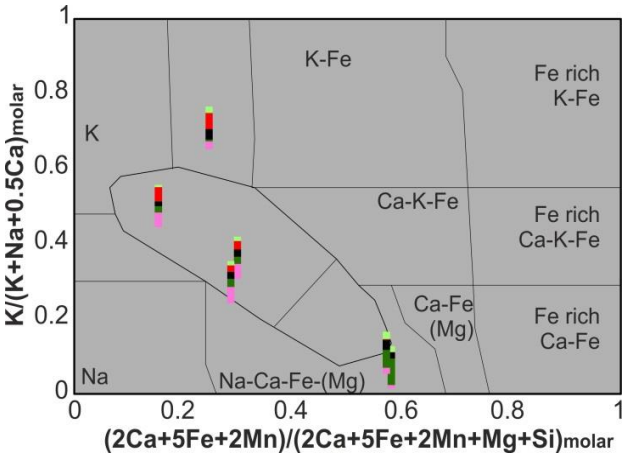

Figure 6.35. Composition of the Bondy gneiss complex quartzofeldspathic gneisses and calc-silicate rocks plotted on the AIOCG diagram of Montreuil et al. (2013). Colour coding of the Na-Ca-K-Fe-Mg bar codes in Figure 2.5. Laminated quartzofeldspathic gneisses fall within the K alteration facies.

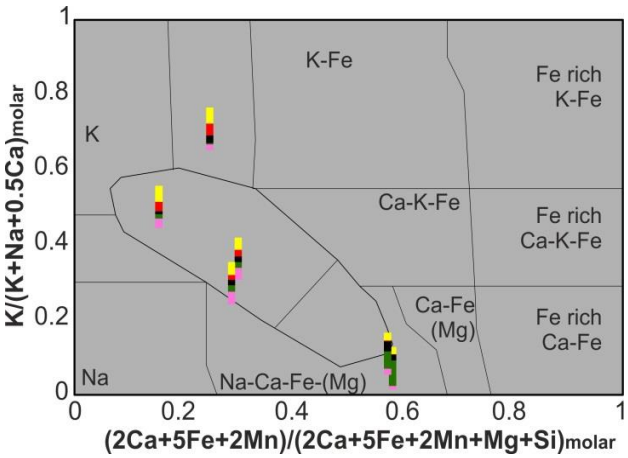

Figure 6.36. Same samples as in Figure 6.35 with Na-Ca-Fe-K-(Si+Al)/10.

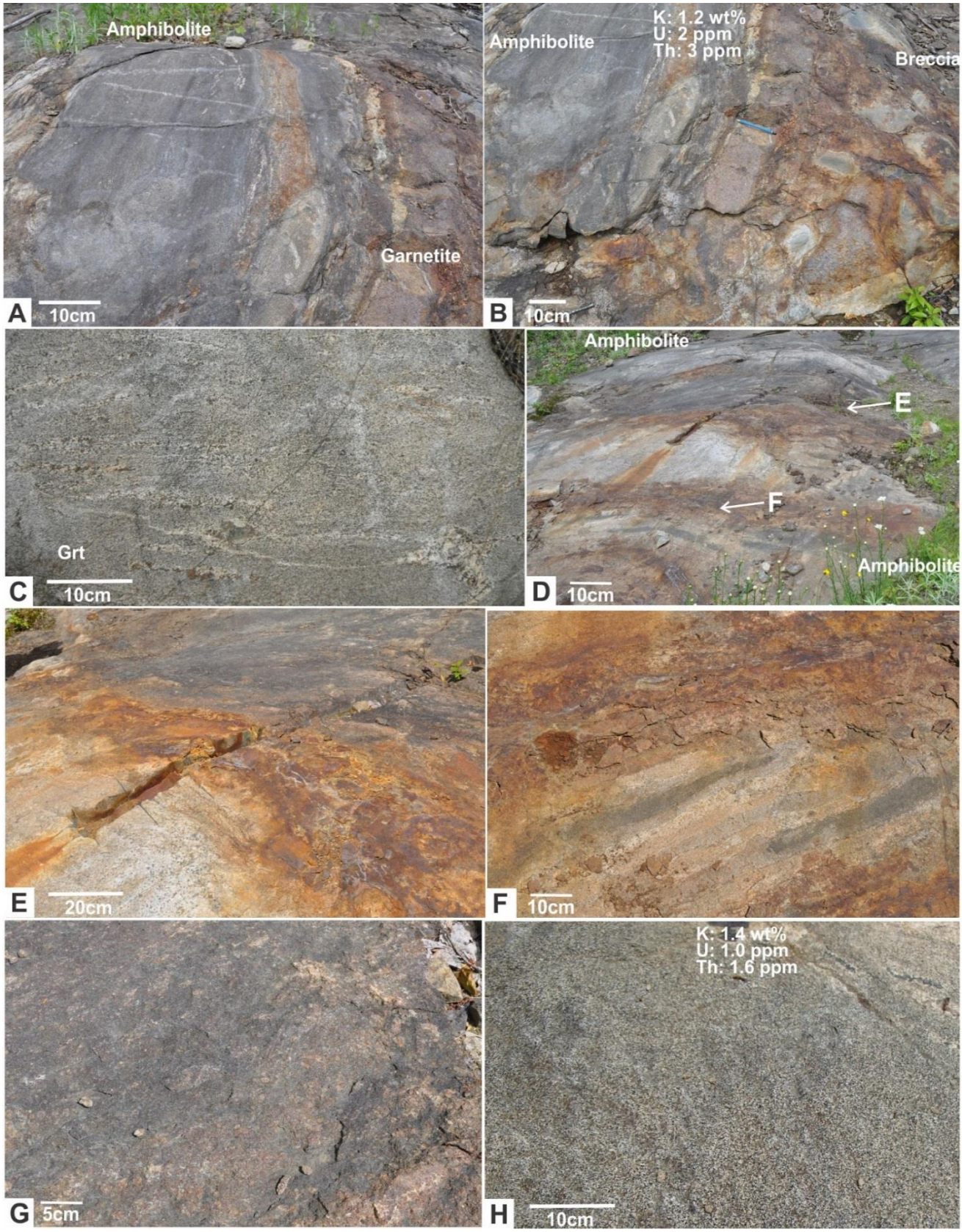

Figure 6.37. Stop 2.3. Amphibolites, garnetites and layered quartzofeldspathic gneisses with locally rusty zones. Note the brecciated zone in B.

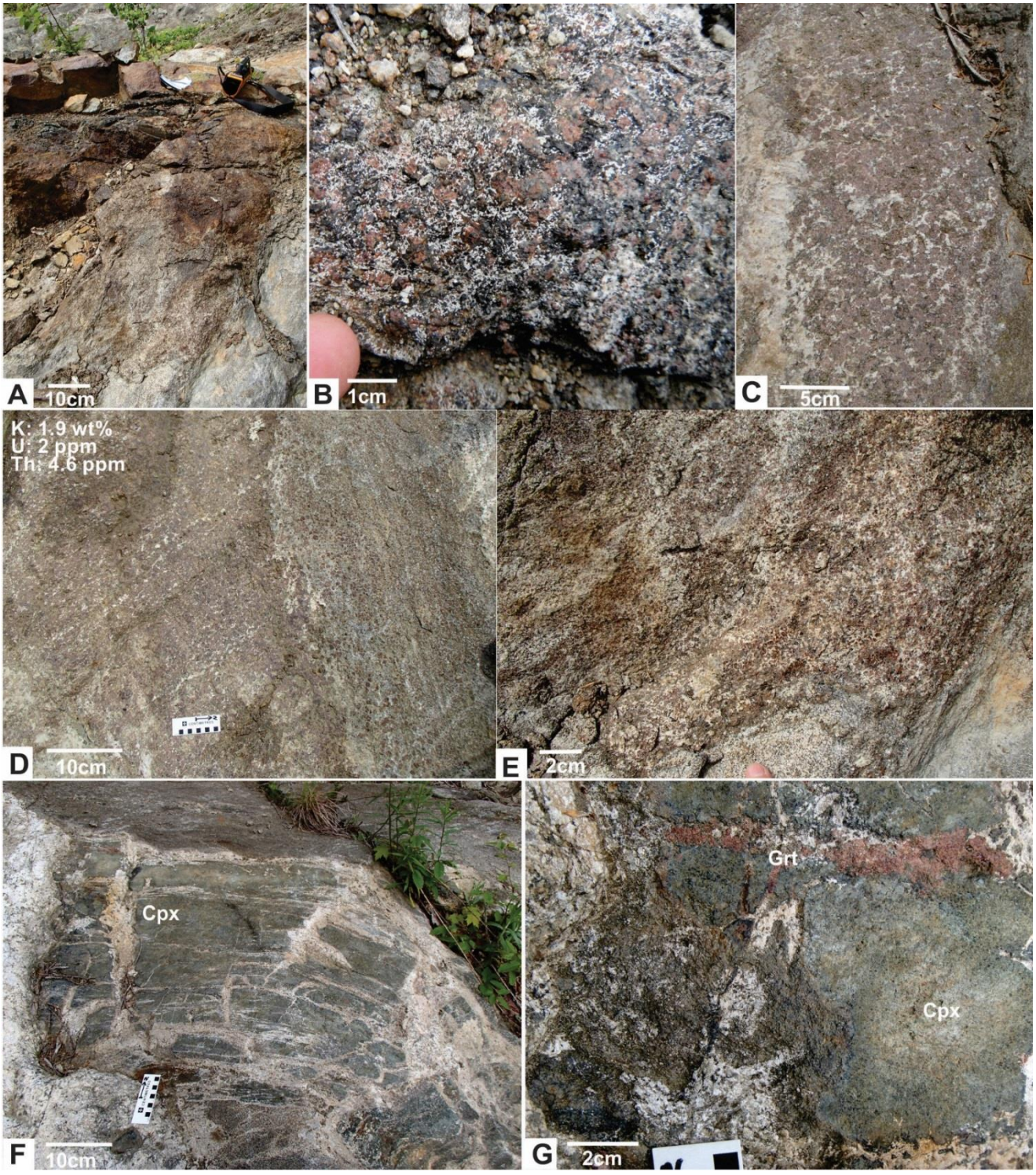

Figure 6.38. Stop 2.3. Garnetites, garnet-rich gneisses and calc-silicate zones typical of metamorphosed hydrothermal alteration zones (see Bonnet and Corriveau, 2007b; Corriveau 2013; Corriveau and Spry 2014).

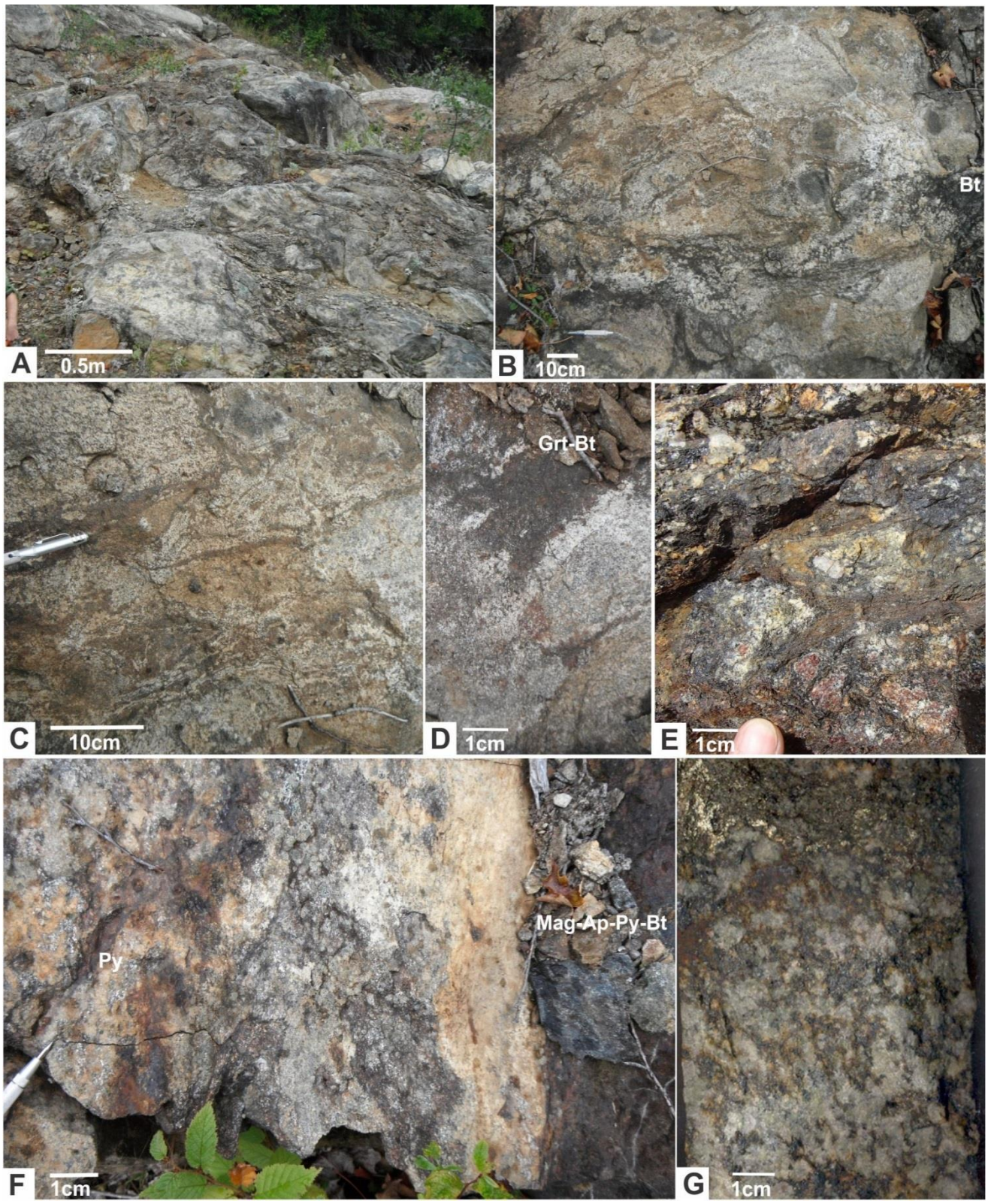

Figure 6.39. Stop 2.3. Brecciated zones with biotite-rich zones, sulphide-bearing quartzofeldspathic gneisses (pyrite visible on outcrop, chalcopyrite reported by Antonoff et al. 2007) with magnetite rich stringers and magnetitite layers with apatite, pyrite and biotite. **G.** Photo courtesy of Richmond Minerals from Antonoff et al. (2007).

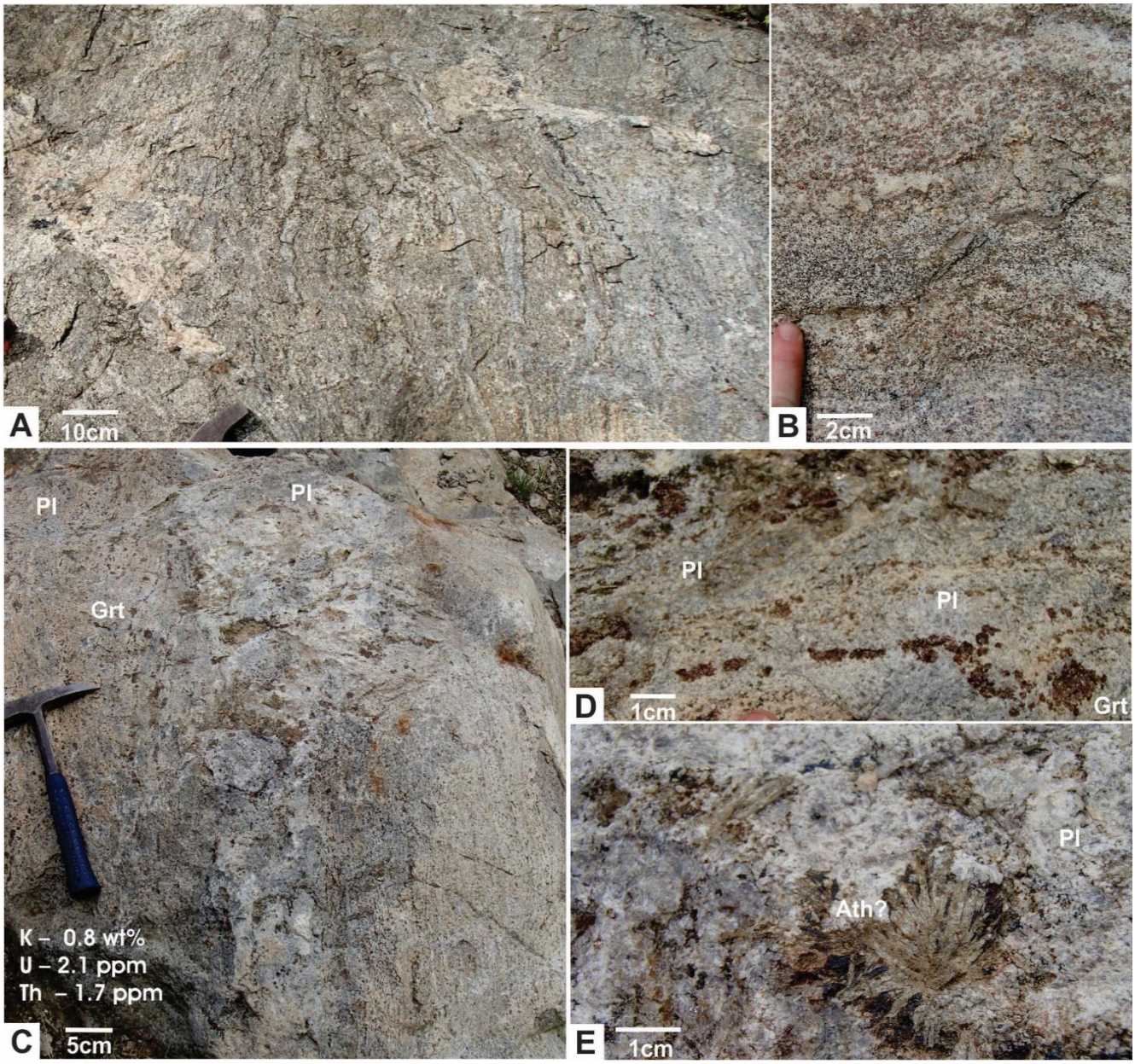

Figure 6.40. Stop 2.3. Plagioclase-rich gneisses locally with stringers or layers rich or richer in garnet. The train of elongate rectangular shape of garnet with plagioclase haloes is not a trait of common metamorphic rocks but magnetite-bearing veins with albite haloes do occur in IOAA systems and once metamorpshosed could lead to the observed features. Plagioclase veins cut also host rock compositional layering and stringers, attribute that would be compatible with a metamorphosed veins as well.

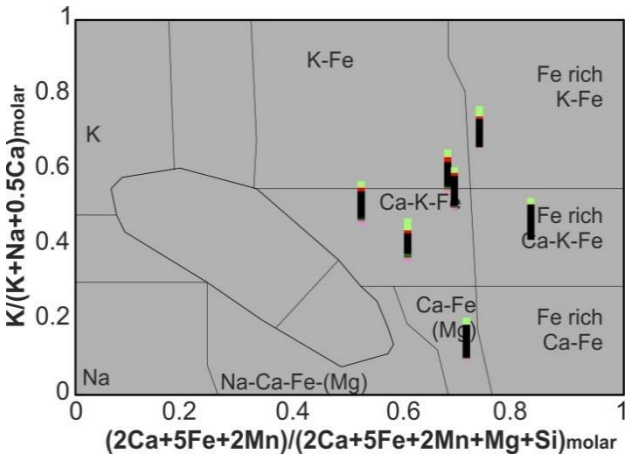

Figure 6.41. Composition of the Bondy gneiss complex magnetite-rich layers plotted on the AIOCG diagram of Montreuil et al. (2013). Colour coding of the Na-Ca-K-Fe-Mg bar codes in Figure 2.5. Magnetite-rich layers fall within the Ca-Fe, Ca-K-Fe and Fe-rich Ca-K-Fe alteration facies.

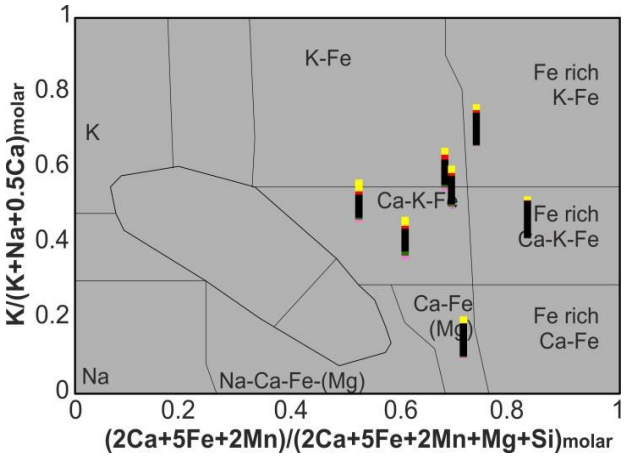

Figure 6.42. Same samples as in Figure 6.41 with Na-Ca-Fe-K-(Si+Al)/10 bar codes where(Si+Al)/10 is in yellow; other colour codes as per Figure 2.5.

Stop 2.4
Lake Parent Cpx-bearing grey gneisses

This outcrop display massive to layered clinopyroxene-plagioclase dominant gneisses with or without garnet (Figs. 6.43, 6.44). Variegated and diffuse zones rich in plagioclase cut these gneisses and resemble zones of metamorphosed albitization. Both rock types are cut by trains of calc-silicate boudins interpreted as former veins. K-feldspar-dominant coarse-grained veins with a syenitic composition cut all units and show some 'stratabound' incursion along the gneissosity (Fig. 6.43). Such a feature is typical of potassic alteration in IOAA systems. The pink 'syenitic' veins are commonly spatially associated with the diopsidite (Figs. 6.43G, 6.44) and folded upright in the core of the outcrop-scale fold. It appears to be synshearing on the flank.

The dominant clinopyroxene-bearing intermediate gneisses have about 2 wt. K_2O and are poor in U and Th (<2.6 ppm). The K-feldspar veins have 5 wt % K_2O are poor in U (1 ppm) and are slightly higher in Th (reaching 4.5 ppm). They are commonly associated with irregular haloes of biotite. This can be interpreted as potassic alteration of an intermediate rocks leading to the crystallization of biotite instead of K-feldspar along the haloes once metamorphosed.

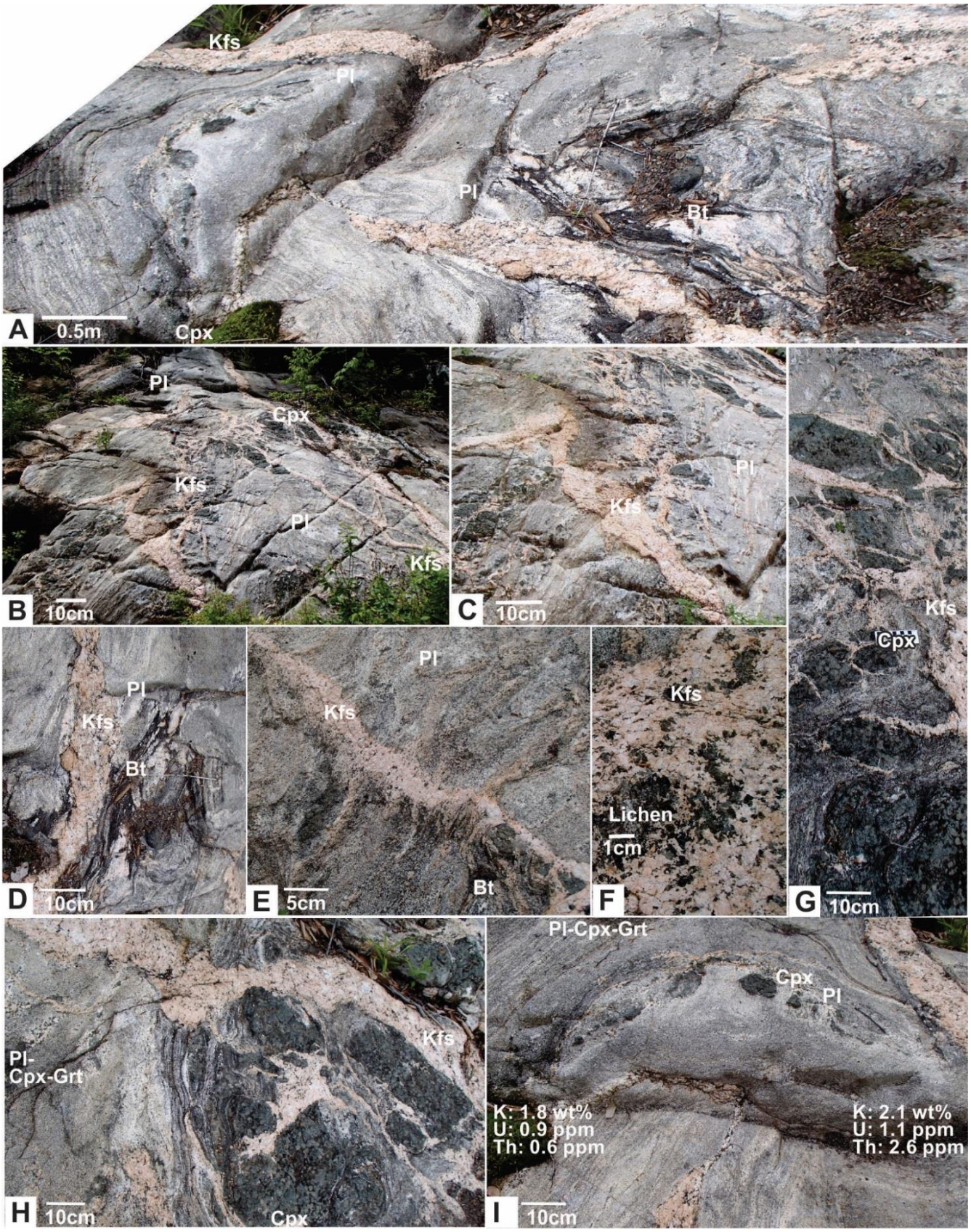

Figure 6.43. Stop 2.4. Massive to layered clinopyroxene-plagioclase dominant gneisses (with ou without garnet) with K-feldspar-dominant coarse-grained veins of syenitic composition.

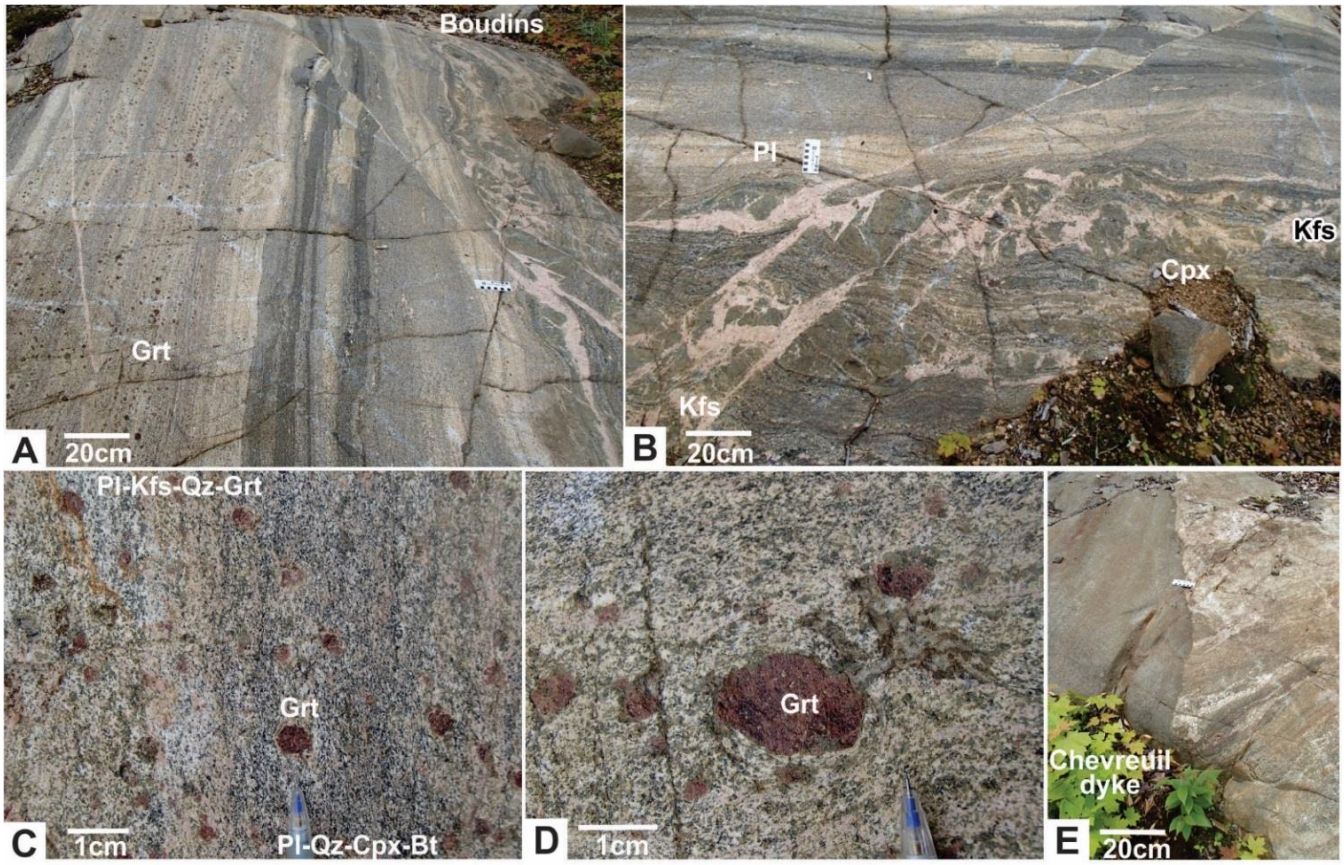

Figure 6.44. Stop 2.4. Massive to layered clinopyroxene-plagioclase dominant gneisses with garnet.

Units of amphibolites also occur and some are interlayered with garnet-bearing intermediate to leucocratic gneisses. Within the amphibolite gneiss there are several lenses of more mafic composition interpreted as cogenetic enclaves (Figs. 6.45, 6.46). Amphibolites units can be fairly massive, compositionally layered (Fig. 6.46) or severely deformed and foliated.

Figure 6.45. Stop 2.4. Foliated amphibolite with deformed mafic enclaves and layers of calc-silicate rocks.

Figure 6.46. Stop 2.4.

Again at this outcrop, a crucial question is to determine if the layering is primary or not. There does not seem to be any foliation folded at the hinge of the upright folds. The folds are thus interpreted as F1 and the foliation on the limbs of map-scale folds as S1. In a relationship similar to stop 2.2, part of a layered sequence contains pervasive garnet, whereas the other does not. This is compatible with modification of protolith composition by premetamorphic metasomatism.

Stop 2.5
Lake Parent

This outcrop consists of clinopyroxene-amphibole-K-feldspar gneisses with and without garnet. The gneiss fabric is cut sharply by clinopyroxene-bearing mafic dykes locally with cogenetic mafic enclaves (Figs. 6.47, 6.48).

Both variety of intermediate gneisses (with and without garnet porphyroblasts) have 3.4 wt % K_2O, are low in U (<2.5 ppm) and have Th that reach 10 ppm. The two mafic dykes are rectilinear and not pervasively deformed nor folded. They appear recrystallized and locally sheared. Age is uncertain. They have 3.3 wt % K_2O, 2 ppm U and 7.5 ppm Th. They may belong to the Kensington-Skootamatta suite and be shoshonitic or potassic alkaline dykes.

Figure 6.47. Stop 2.5. Rectilinear mafic dykes.

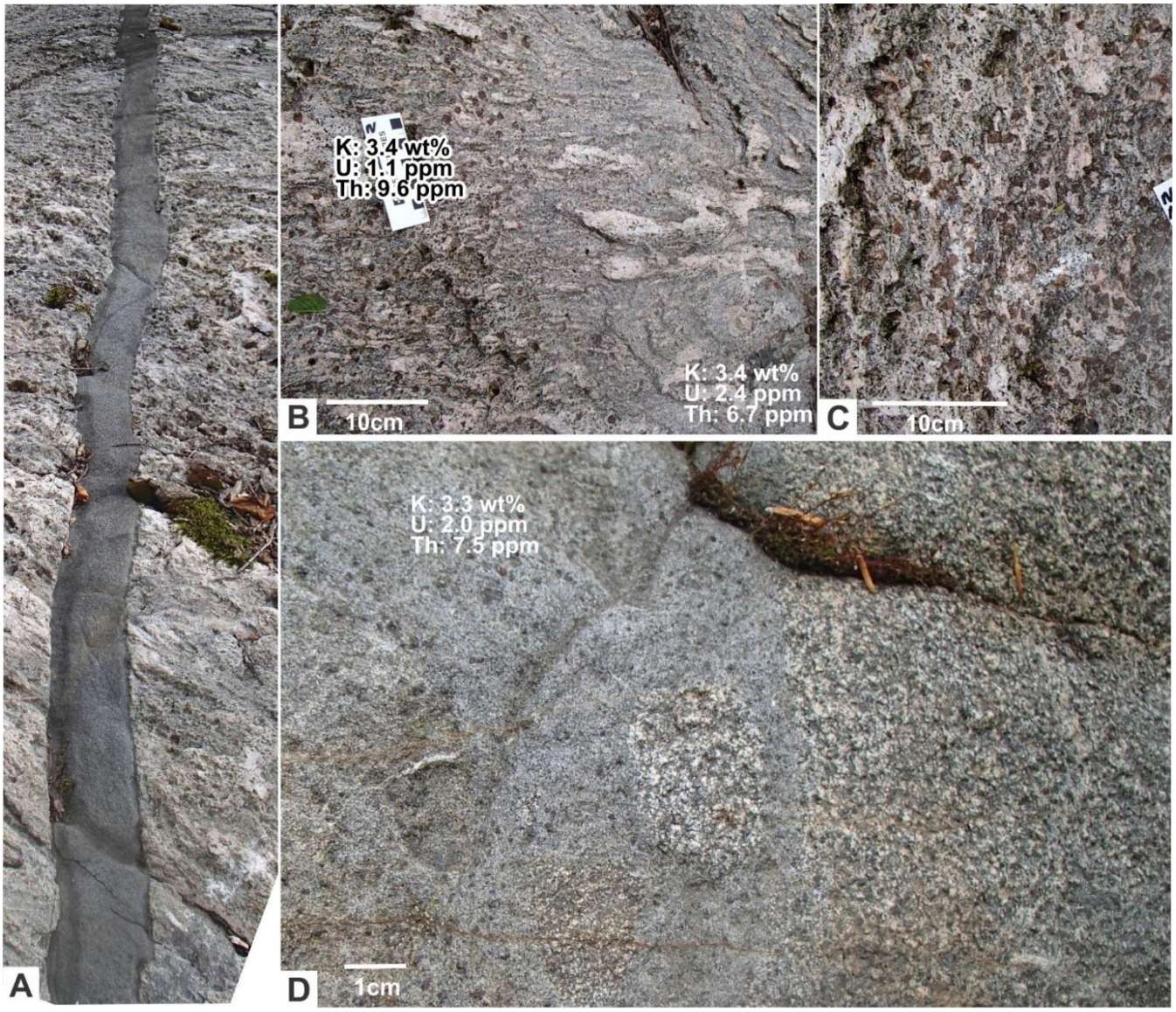

Figure 6.48. Stop 2.5.

Stop 2.6
Lake Parent

Stop 2.6 provides an overview of common mafic to felsic orthogneisses metamorphosed to granulite facies. A unit of amphibolite is either massive though recrystallized or is pervasively deformed and foliated. The massive variety preserves fossil plagioclase phenocrysts among a highly heterogeneous matrix (Fig. 6.49). The phenocrysts are defined by square-shaped mosaics of granoblastic plagioclase. Their original sizes were of a few millimetres. The ghost plagioclase phenocrysts are crudely aligned and define an igneous foliation that is at a right angle to the metamorphic foliation. Irregular patches of medium to coarse-grained gabbros occur within the porphyritic metagabbro. These gabbroic zones are very heterogeneous with mafic clots of clino- and orthopyroxene among ghost plagioclase laths defining an intergranular texture. The host porphyritic gabbro is more leucocratic along these enclaves and preserves the textures of the plagioclase microlites.

In addition to the coarse-grained gabbro enclaves, the porphyritic gabbro displays zones that are rich in amphibole and garnet. Here the garnet displays retrograde metamorphic haloes of plagioclase. Very mafic, clinopyroxene-dominant veinlets are also observed and merge with leucogabbro zones which may have been veins originally. Some amphibolites are devoid of phenocrysts ghosts and may have been massive originally.

The intermediate to felsic orthogneisses display remnants of coarser feldspar crystals within a former medium-grained matrix. The mafic minerals are largely orthopyroxene and the rock has 1.2 wt % K_2O, 1 ppm U and 4 ppm Th. The rocks are all pervasively recrystallized and granoblastic and may contain mafic enclaves with varied textures and mineral assemblages. These gneisses are intercalated with layered amphibolites of uncertain origin (volcanic, volcaniclastic, plutonic?). Plagioclase-dominant zones resemble recrystallized anorthosite. They seem to cut across the intermediate gneisses and in this setting one should not exclude the possibility of an albitite.

A lot more work needs to be done on these outcrops.

Figure 6.49. Stop 2.6. Close-up of Figure 6.44 showing fossil plagioclase laths and phenocrysts.

Notes

Stop 2.7
Lake Parent intrusive breccia

A spectacular 10 m wide intrusive breccia with mafic and anorthositic xenoliths occurs within a mangeritic unit (Figs. 6.50, 6.51). The mafic enclaves are fine grained. A Chevreuil dyke cut the intrusive breccia.

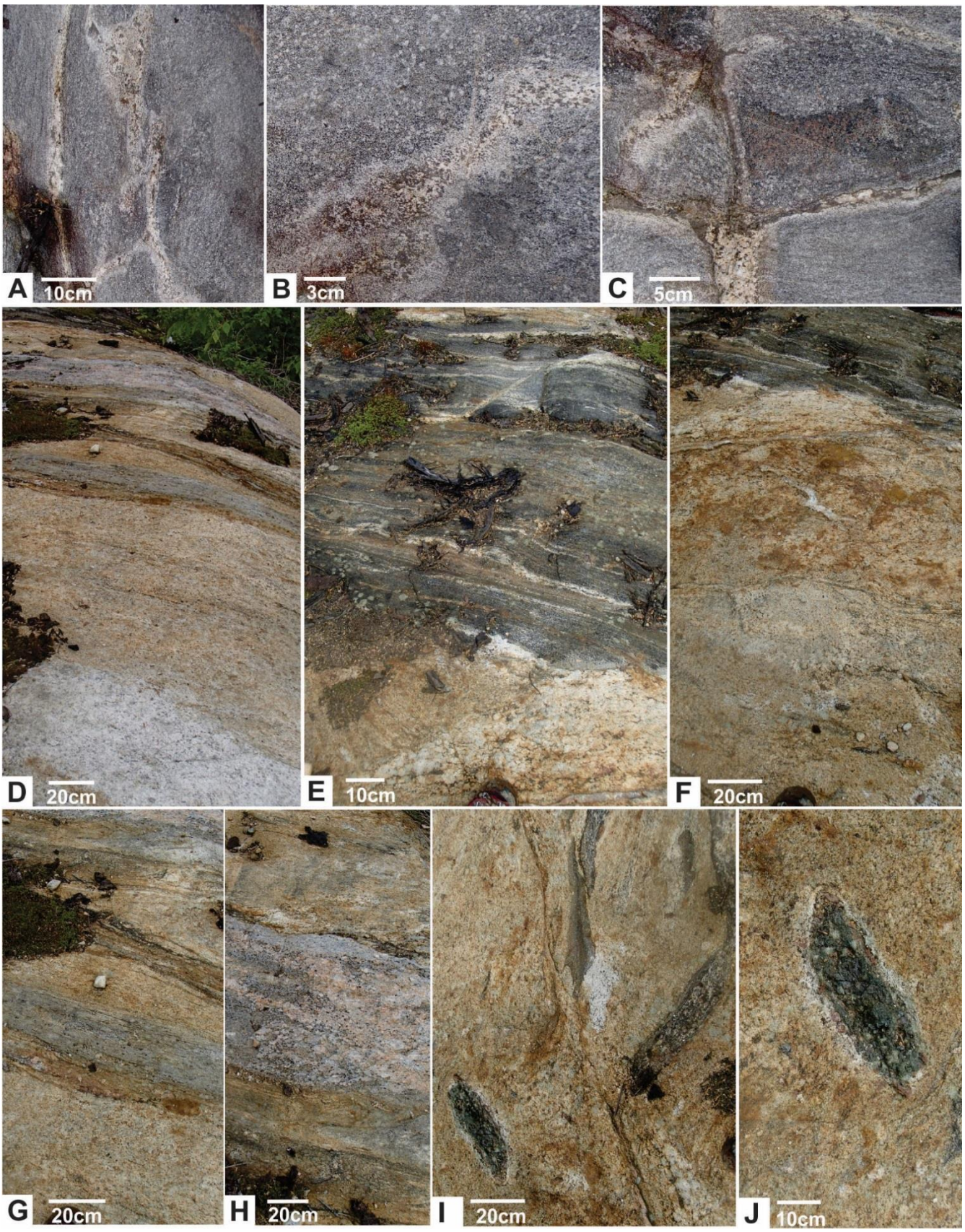

Figure 6.50. Stop 2.6.

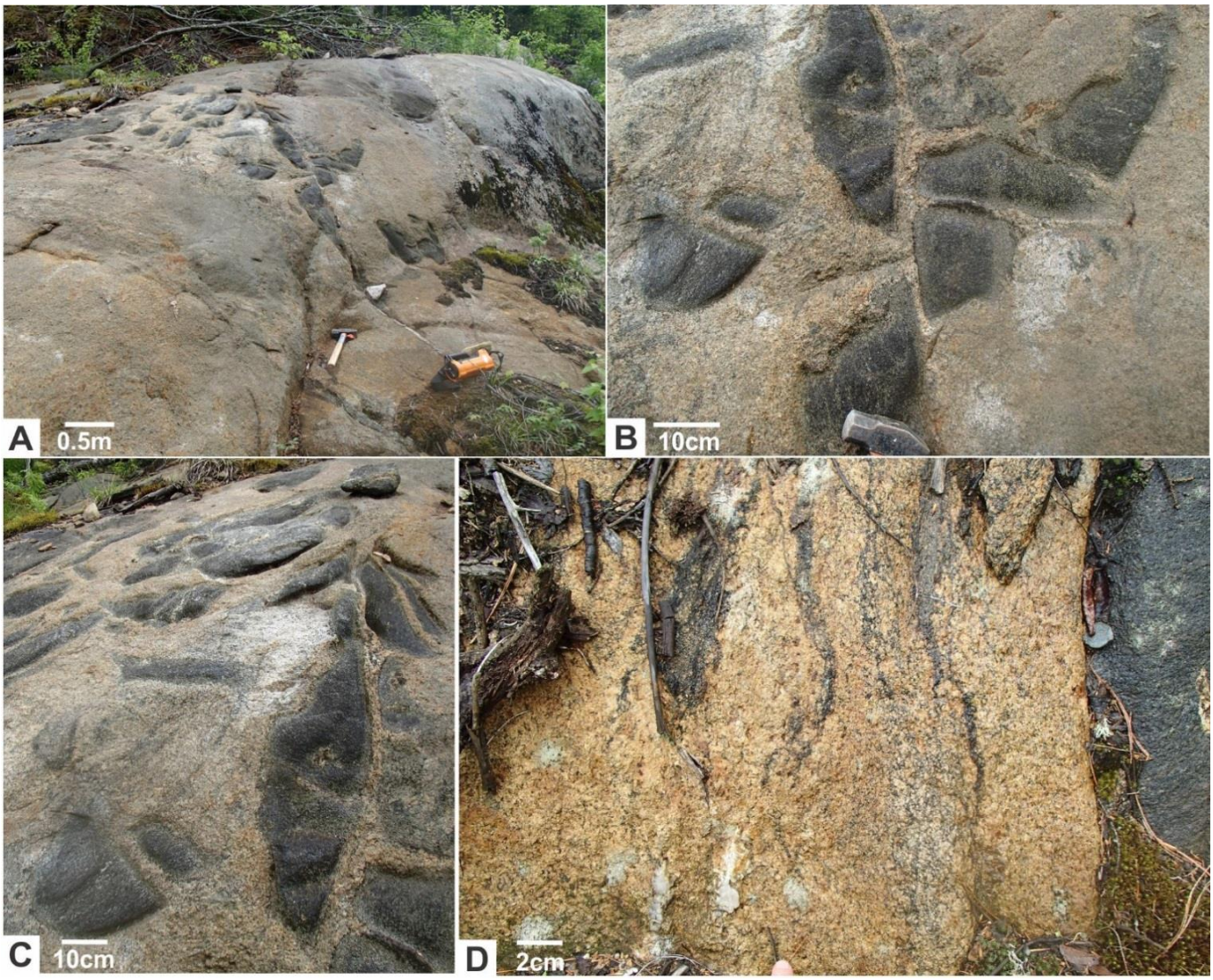

Figure 6.51. Stop 2.7. Intrusive breccia. Fragments of amphibolites have orthopyroxene-bearing reactions rims with host mangerite.

Stop 2.8
Lake Parent K-feldspar-rich gneisses

Layered and heterogeneous K-feldspar-rich garnet-bearing gneisses are cut by a mafic dyke that is folded (Fig. 6.52). The gneiss has 4.1 wt % K_2O, 1.7 ppm U and 13 ppm Th based on gamma-ray spectrometer measurements of outcrop. The mafic dyke has 1.3 wt % K_2O, 1 ppm U and 2 ppm Th. The distribution of garnet porphyroblasts is commonly fairly homogeneous across compositional layering as if it represents an attributes that is superimposed across original layering. Locally, some layers have abundant garnets. The distribution of garnet may illustrate the distribution of alteration along (i.e. stratabound alteration) or across layering (more pervasive alteration) as is typical in IOAA systems. The premetamorphic composition of the alteration that favours the crystallization of metamorphic garnet varies but may correspond to sericitization prior to metamorphism. This unit was not studied during the GSC project. Working hypothesis is that it may represent a metamorphosed phyllic, K- or a K-Fe alteration facies.

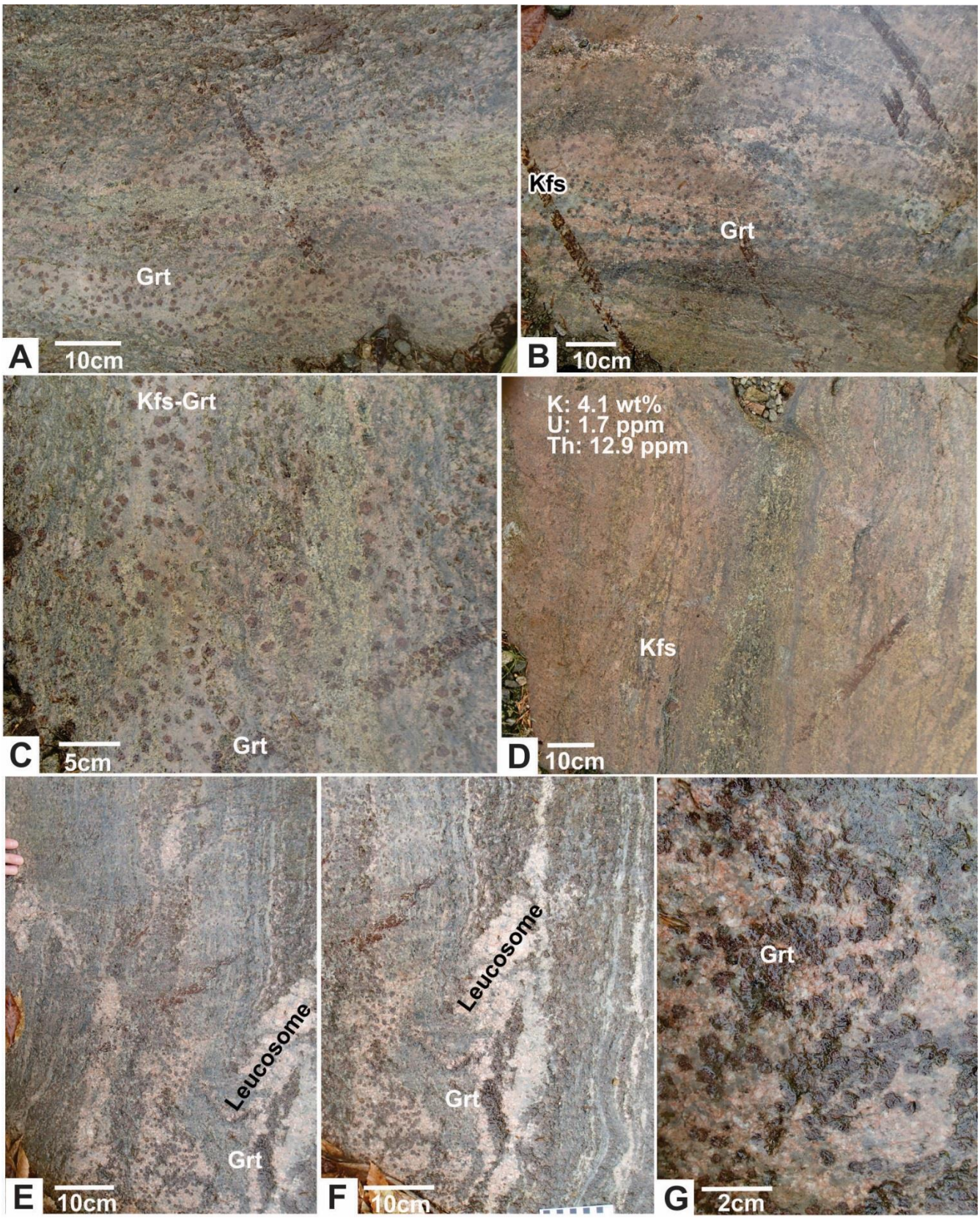

Figure 6.52. Stop 2.8. Layered K-feldspar-rich gneisses with garnet distribution across or along compositional layering. Note that the distribution of high ot higher garnet contents is largely not spatially associated with the leucosomes and is interpreted as resulting from premetamorphic hydrothermal alteration. Local zones of high garnet modes within leucosomes are however best interpreted as local restites.

Stop 2.9
Lake Parent comingled dykes

Comingled mafic dykes can be observed at this outcrop (482087 E, 5130030 mN; Fig. 6.53).

Figure 6.53. Stop 2.9. Comingled mafic-felsic dyke.

Stop 2.10
Marble breccia and orthogneisses

A spectacular 10 m wide intrusive breccia with mafic and anorthositic xenoliths occur within a mangeritic unit (Figs. 6.54, 6.55, 6.56). The mafic enclaves are fine grained. A Chevreuil dyke cuts the intrusive breccia.

Figure 6.54. Stop 2.10. Orthogneisses and marble tectonite.

Figure 6.55. Stop 2.10. Marble tectonite with medium grained and granoblastic calcite. Calcite is a power law material and recrystallizes and coarsens very easily (Carter and Tsenn 1987).

Figure 6.56. Stop 2.10. Boudinaged calc-silicate unit.

Stop 2.11
Outcrop 1659
Garnetite unit (argillic alteration) and associated orthopyroxene-biotite gneiss (sericitic alteration) and layered amphibolite (interpreted as metavolcanic rocks)

In the heart of synform is an aluminous and ferrous lithofacies (outcrop 1659) which contains a variety of quartzofeldspathic gneisses with orthopyroxene, biotite, magnetite and locally chalcopyrite (Fig. 6.57). The gneisses range from leucocratic to mesocratic and are compositionally layered. Magnetite-bearing garnetite with chalcopyrite and pyrite also occur (6540 ppm Cu, Table 3 in Corriveau 2013).

The garnetite with magnetite occurs as decimetre-thick layers with garnet (20-50%), magnetite (5-15%), biotite or orthopyroxene (up to 30%), K-feldspar (5-10%), and plagioclase (5-10%). In this outcrop they are mineralized in chalcopyrite (1 to 2%). The garnet grains have Mn content from 0.2 to 1.7% (Boggs and Corriveau 2004), markedly lower than Mn-rich garnet in exhalites. Chemical signature includes high $Fe_2O_3^t$ (28 to 40%) and MgO contents (6.5 to 10.8%), low Al_2O_3 contents (10 to 14%), birdwing-shaped REE profiles and high Zr content. Gold is anomalous reaching 277 ppb.

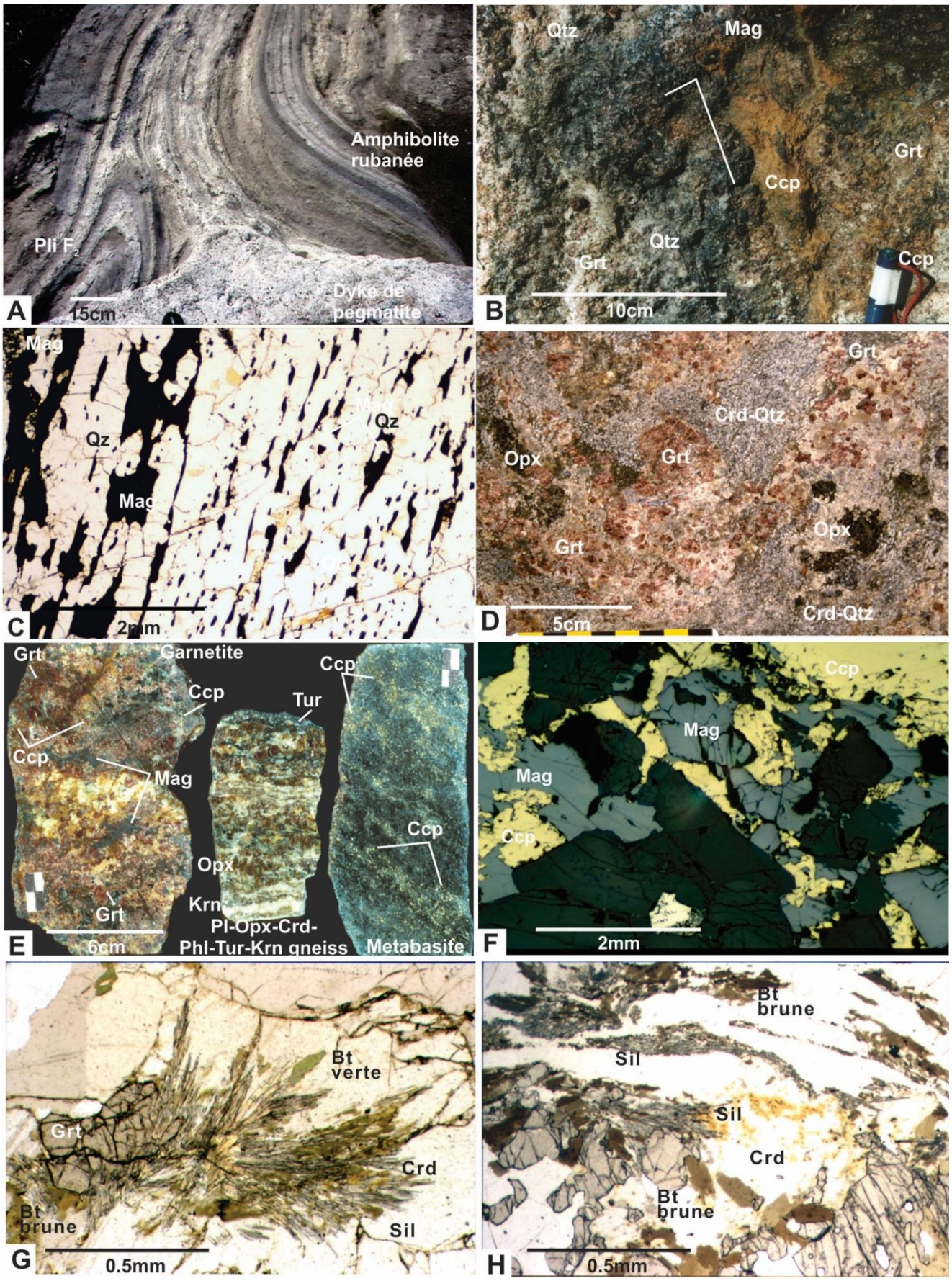

Figure 6.57. Stop 2.11. Outcrop 1659. Chalcopyrite bearing amphibolites and garnetites. Detailed figure caption on following page.

Figure 6.57. Stop 2.11. Outcrop 1659. Chalcopyrite bearing amphibolites and garnetites.
A. Layered metabasite with a possible volcanic layering. These metabasites are nearby Cu showings. **B.** Cu showing in a magnetite-quartz garbetite. **C.** Photomicrograph (transmitted light-plane polarized) of magnetite-quartz layer interpreted as a magnetite breccia transposed in the foliation (CQA-1659; UTM : 480513mE, 5132001mN). **D.** Garnetite with cordierite-quartz layers. **E.** Hand-specimen photograph of the garnetite with clinopyroxene and magnetite (CQA-1659), of white cordierite-orthopyroxene gneiss with orthopyroxene-rich layers (CQA-1654, stop 3.4), kornérupine and tourmaline, and cupriferous magnetite-rich metabasite associated with clinopyroxene-magnetite-rich garnetite (CQA-1659; UTM : 480513mE, 5132001mN). In the garnetite, red xenomorphe garnet is scattered and has a modal concentration around 20%. The matrix contains sulphides and magnetite. **F.** Photomicrograph (reflected light-plane polarized) of cupriferousmetabasite with chalcopyrite, clinopyroxène and magnetite (CQA-1659; UTM : 480513mE, 5132001mN). **G.** Photomicrograph (transmitted light-plane polarized) of retromorphosed cordierite in green biotite and sillimanite (CQA-1659-2; UTM : 480513mE, 5132001mN). **H.** Photomicrograph (transmitted light-plane polarized) of brown biotite with sillimanite parallel to the metamorphic foliation (CQA-1659H; UTM : 480513mE, 5132001mN)

The garnetite hosts a 30x10 cm lens of chalcopyrite-rich metabasite (5 to 7%) and is associated with layered magnetite-rich metabasite, felsic laminated gneiss, garnet-cordierite, garnet-orthopyroxene or orthopyroxene-biotite gneisses locally with abundant magnetite and some sulphides.

Some units of layered amphibolites are mineralized in chalcopyrite (5073 ppm Cu, Table 3 in Corriveau 2013) and are locally rich in magnetite (up to 20%) and bear spinel. Siliceous and ferriferous levels are also observed and consist of quartz ribbons associated with magnetite, spinel, orthopyroxene and zircon. A massive magnetite layer, 2 cm in width, is associated with the quartz-rich gneiss.

Cordierite-garnet-hypersthene gneisses, rich in zircon crystals of inframillimetre size, bears locally some kornerupine. Plagioclase-quartz gneiss with antiperthitic spinel-oligoclase, magnetite granitic gneiss and laminated K-feldspar-dominant quartzofeldspathic gneiss also occur.

Layered amphibolites, locally sulphides-rich, fall in the field of Na-Ca-Fe alteration, orthopyroxene-biotite gneisses in the field of Ca-K-Fe and K-Fe alteration facies, and garnetites in the field of Ca-Fe and Ca-K-Fe alteration facies (Figs. 6.58, 6.59).

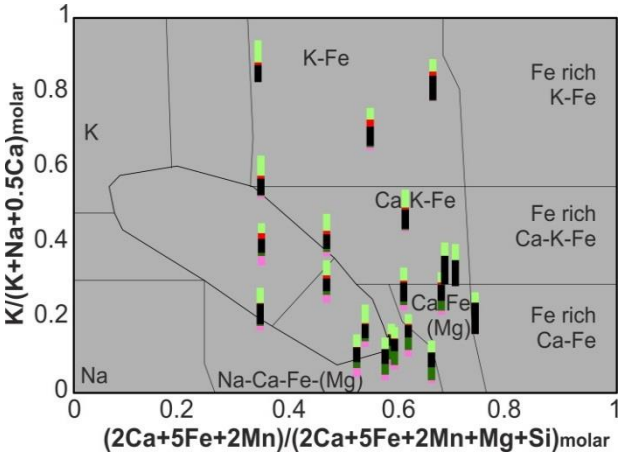

Figure 6.58. Composition of the Bondy gneiss complex rocks from outcrop 1659 plotted on the AIOCG diagram of Montreuil et al. (2013). Colour coding of the Na-Ca-K-Fe-Mg bar codes in Figure 2.5.

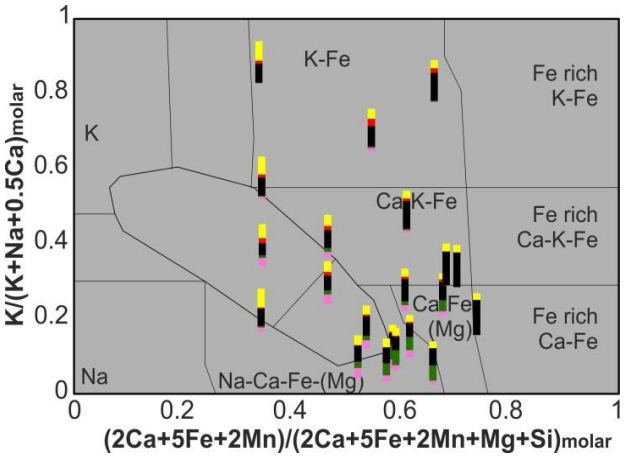

Figure 6.59. Same samples as in Figure 6.56 with Na-Ca-Fe-K-(Si+Al)/10.

Stop 2.12
Lac Harvey showing

The Lac Harvey showing (outcrop CQA-2401, UTM: 479373mE, 5128942mN) consists of a variety of garnet, magnetite or biotite-rich gneisses including biotite- and magnetite-bearing garnetites comprising about 30 to 50% millimetre-size subhedral garnet in a biotite-rich matrix (Figs. 6.60-6.62). The modal concentration of magnetite is 1 to 2%. Garnet is red, subhedral to anhedral and centimetre in size. Other garnet-rich gneisses consist of subhedral to anhedral orthopyroxene (5-9 mm) and pink to red garnet (15% modal concentration; 1-3 cm) set among biotite, quartz and plagioclase. Layered biotite-garnet-K feldspar-plagioclase-quartz gneisses have pale pink poeciloblastic garnet in the core of some leucosomes. The latter are massive, coarse-grained and surrounded by a biotite rich melanosome. Note that this outcrop was cleaned after the GSC project. Additional research is needed to assess the varied composition of the rocks and their implications in terms of mineral exploration.

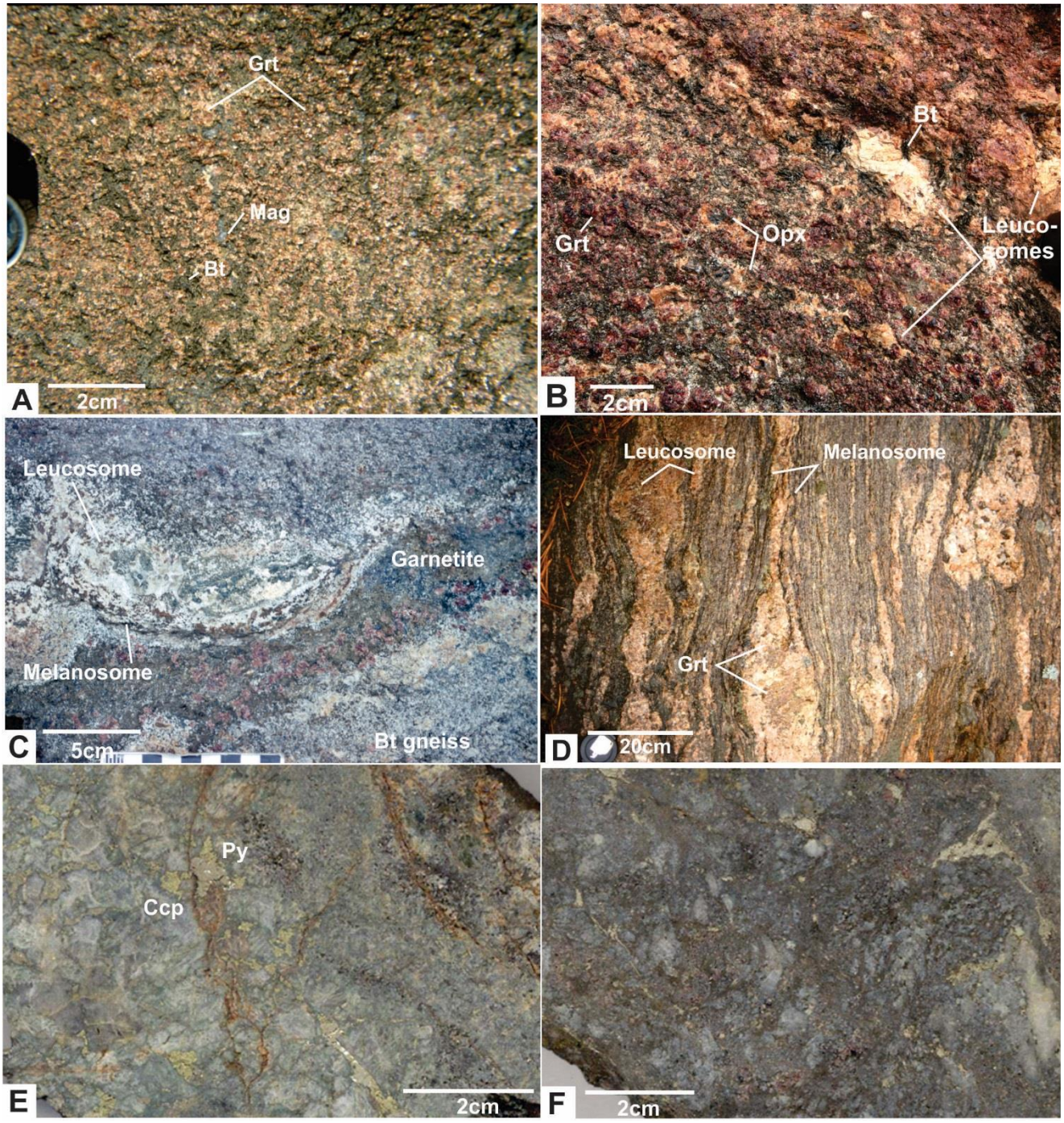

Figure 6.60. Lac Harvey showing. **A.** Biotite-magnetite-rich garnetite with 30% of millimetre automorph garnet in a biotite-rich matrix. **B.** Coticule with garnet, quartz, orthopyroxene and plagioclase. The orthopyroxene forms euhedral to subhedral millimetre-scale (5-9 mm) crystals. These crystals occur among quartz and plagioclase. Red to pink garnets form anhedral centimetre-scale (1-3 cm) crystals, locally associated with quartz. Garnet and orthopyroxene occur among a fine-grained matrix composed of biotite, quartz and plagioclase. **C.** Layered aluminous gneiss with a garnetite layer and a non-foliated massive leucosome with a marginal biotite-rich melanosome. **D.** Aluminous gneiss with a biotite-garnet-K-feldspar-plagioclase-quartz assemblage. **E-F.** Hand-specimen of biotite-magnetite-rich garnetite mineralized in pyrite and chalcopyrite.

Figure 6.61 (next page). Lac Harvey showing. **A.** Overview of the outcrop with anastomosing rusty garnet-bearing quartzofeldspathic gneisses interpreted as hydrothermally altered units. **B.** Amphibolite and biotite-orthopyroxene, quartzofeldspathic and garnet-rich quarzofeldspathic gneisses with stromatolitic leucosomes and granitic veins. **C-F.** Note the heterogeneity of rock composition within and across layers with garnet or biotite-rich layers. Magnetite contents vary across layers and can locally be abundant. **G-H.** Metamorphosed amphibolite dyke crosscutting the gneissosity and the leucosomes but displaying reaction rims with the gneisses.

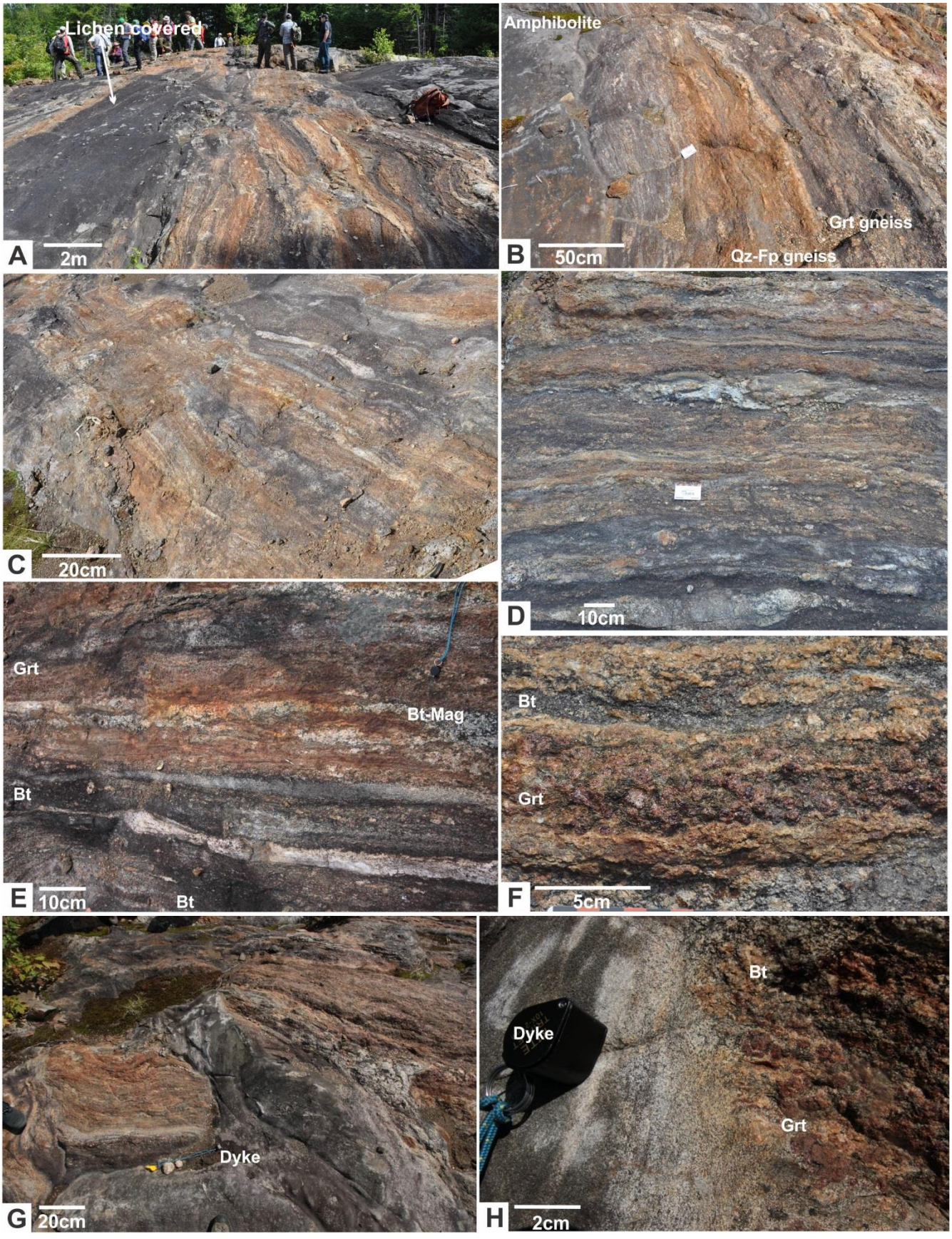
Lichen covered
A
2m
Amphibolite
Grt gneiss
B
50cm
Qz-Fp gneiss
C
20cm
D
10cm
Grt
Bt-Mag
Bt
E
10cm
Bt
Bt
Grt
F
5cm
Dyke
G
20cm
Bt
Dyke
Grt
H
2cm

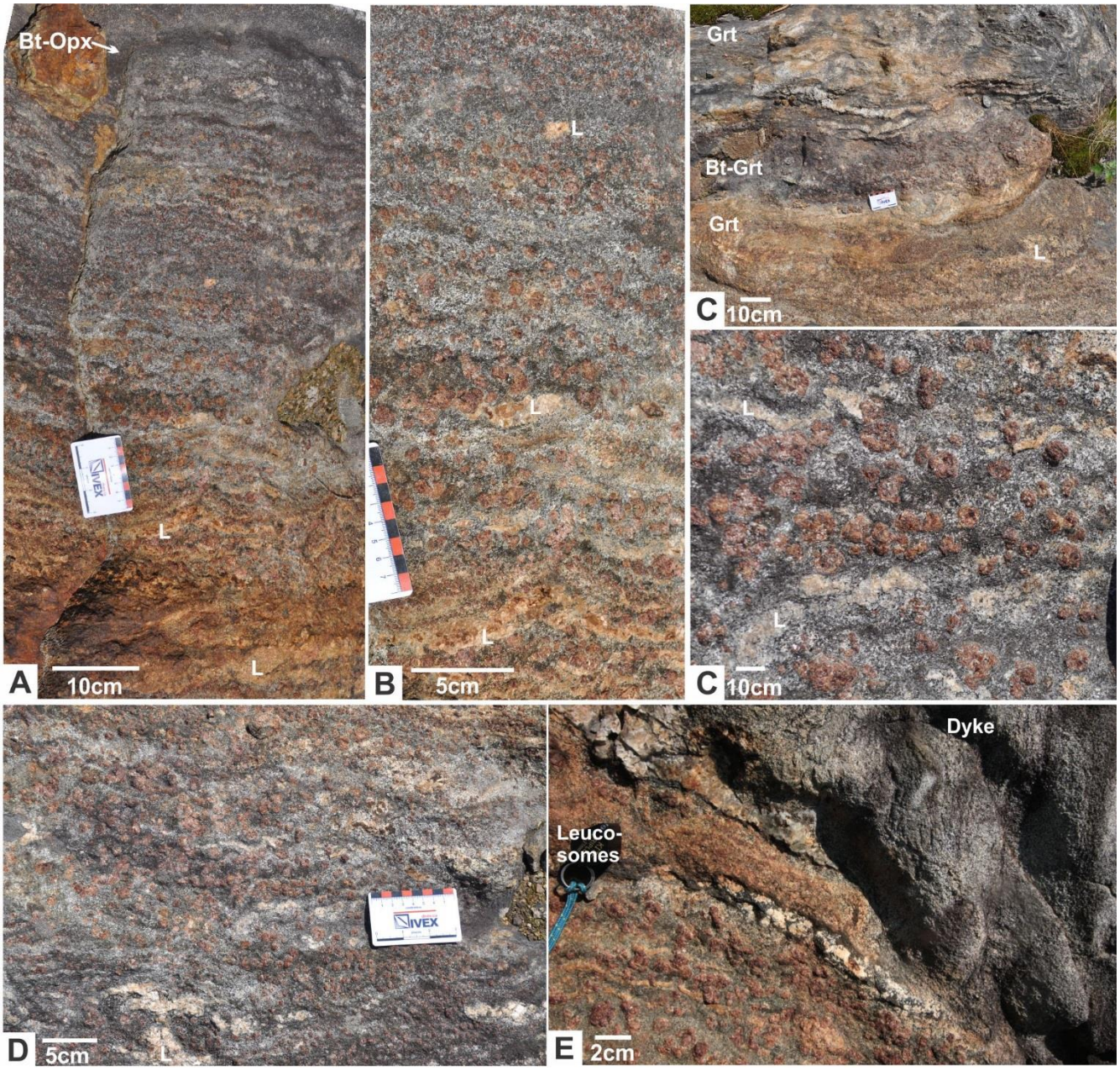

Figure 6.62. Lac Harvey showing. **A.-D.** Biotite, magnetite and orthopyroxene-bearing garnet-rich gneisses and local garnetites with orthopyroxene-bearing discontinuous leucosomes. **E.** Amphibolite dyke cutting across biotite-bearing leucosomes and garnet-rich gneisses. Note the sharp contact between the amphibolite dyke and the gneissosity. This dyke could be part of the same generation of dykes as the one of stop 3.1.

Chapter 7: Kar-Ha-Kon vertically layered intrusion (Day 2)

Directions. Back onto Road 3, turn left. To your left before Lac Tigy is a trail/road in a clearing going to site R24 of the geological rallies. This site provides a cross-section of the Kar-Ha-Kon mafic layered intrusion. The road was overgrown in 2017. In contrast road conditions to visit the Montjoie vertically layered intrusion were better (see stops 12 to 15 in Corriveau and Rivard 1997).

7.1 Vertically layered gabbroic intrusions

The four sub circular gabbronorite intrusions of the Mont-Laurier area (e.g. Kar-Ha-Kon and Montjoie intrusions, Day 2) systematically present sub vertical gabbroic to anorthositic layering and magmatic foliation as well as vertical magmatic erosion planes and channels (Corriveau and Jourdain 1992; Corriveau et al. 1994, 1996b; Corriveau and van Breemen 2000; Corriveau 2013). The magmatic foliation, defined by plagioclase laths, is pronounced, vertical, parallel or locally oblique to layering and crudely concentric as is the layering at the scale of the intrusion. The layers are cut by peneconcordant ultramafic sills and veins, and are locally brecciated and cut by gabbro (Fig. 7.1). All layered intrusions have vertical internal igneous fabrics, regardless of their structural position along the flanks and hinge of the early regional-scale antiform that has folded the Bondy gneiss complex. (Figs. 7.2, 7.3) We interpret this regularity as an evidence of the primary vertical nature of the layering. Such layering occurs within Mesozoic Monteregian stocks that intruded the St. Lawrence Lowlands and for which tectonic transposition of a conventional layered intrusion can be discounted entirely (Corriveau et al. 1989). Accordingly, the internal magmatic structures of the layered intrusions of the Chevreuil intrusive suite are interpreted as the product of the flow and crystallization of mafic magma along the walls of sub vertical cylindrical conduits, with occasional disturbances caused by new injections of mafic magmas. Faulting of layers was observed in the Kar-Ha-Kon intrusion.

The ultramafic rocks in the layered intrusions have local Ni-Cu sulphide mineralization. Since magma emplacement followed the vertical layering (Fig. 7.3), it likely came from the base of the intrusion. By adapting the conventional model of gravitational deposition of magmatic sulphides, the presence of these ultramafic rocks could indicate a potential for magmatic sulphides at depth. A gravimetric survey through one of the layered intrusions indicates that it extends to a depth of less than 3 km with some parts only a few hundred metres deep. Some of these mafic bodies are cut by pegmatite dykes. Whereas the gabbros are not recrystallized or pervasively deformed, the pegmatites are locally porphyroblastic mylonites and ultramylonites, illustrating strain partitioning in rigid bodies (Fig. 7.4). The emplacement of these bodies during an orogenic event and the subvertical layering that formed as magmas were crystallizing along the walls of the conduits bring a different perspective on crystallization processes than that provided by classic layered intrusions (e.g. Irvine 1980).

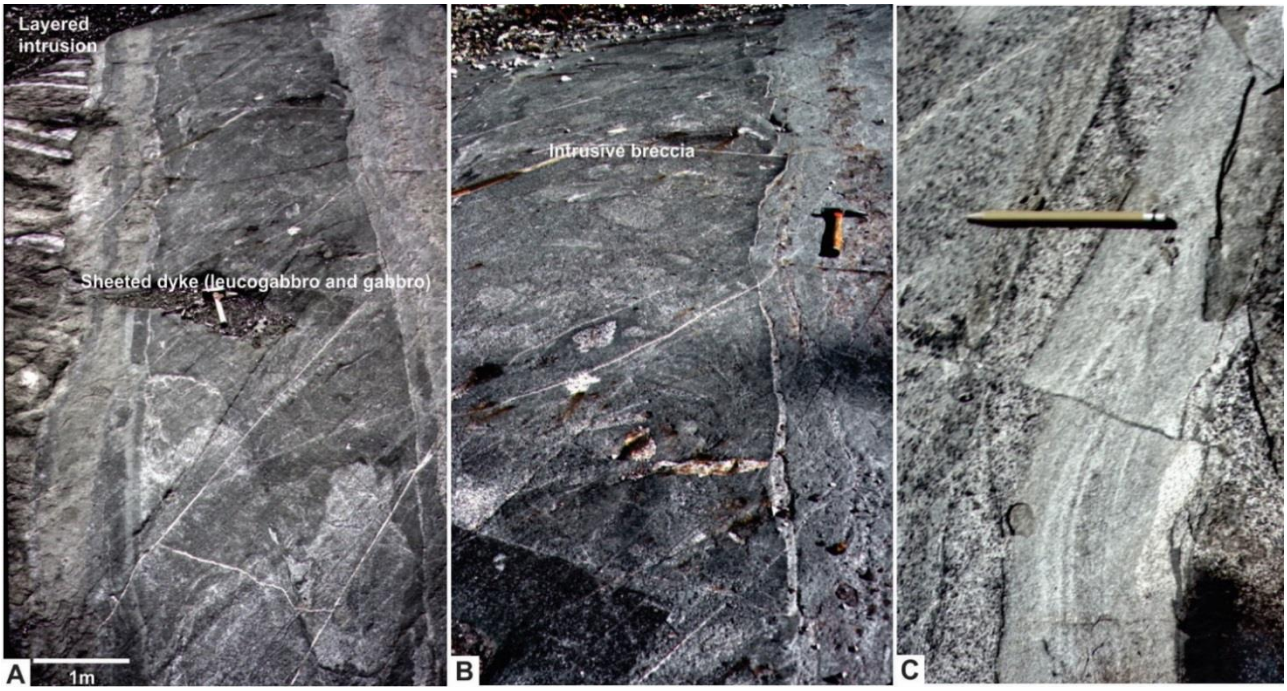

Figure 7.1. Sheeted gabbro dykes and intrusive breccias in the Kar-Ha-Kon intrusion. **A.** Composite dyke of gabbro juxtaposing an intrusive sheet and a breccia in the layered intrusion. **B.** Detail of the gabbro dyke of Figure 7.1A. The foliation, the layering and the schlieren are magmatic not metamorphic. **C.** Detail of the gabbro dyke of Figure 7.1A. The isoclinal fold is magmatic not solid-state.

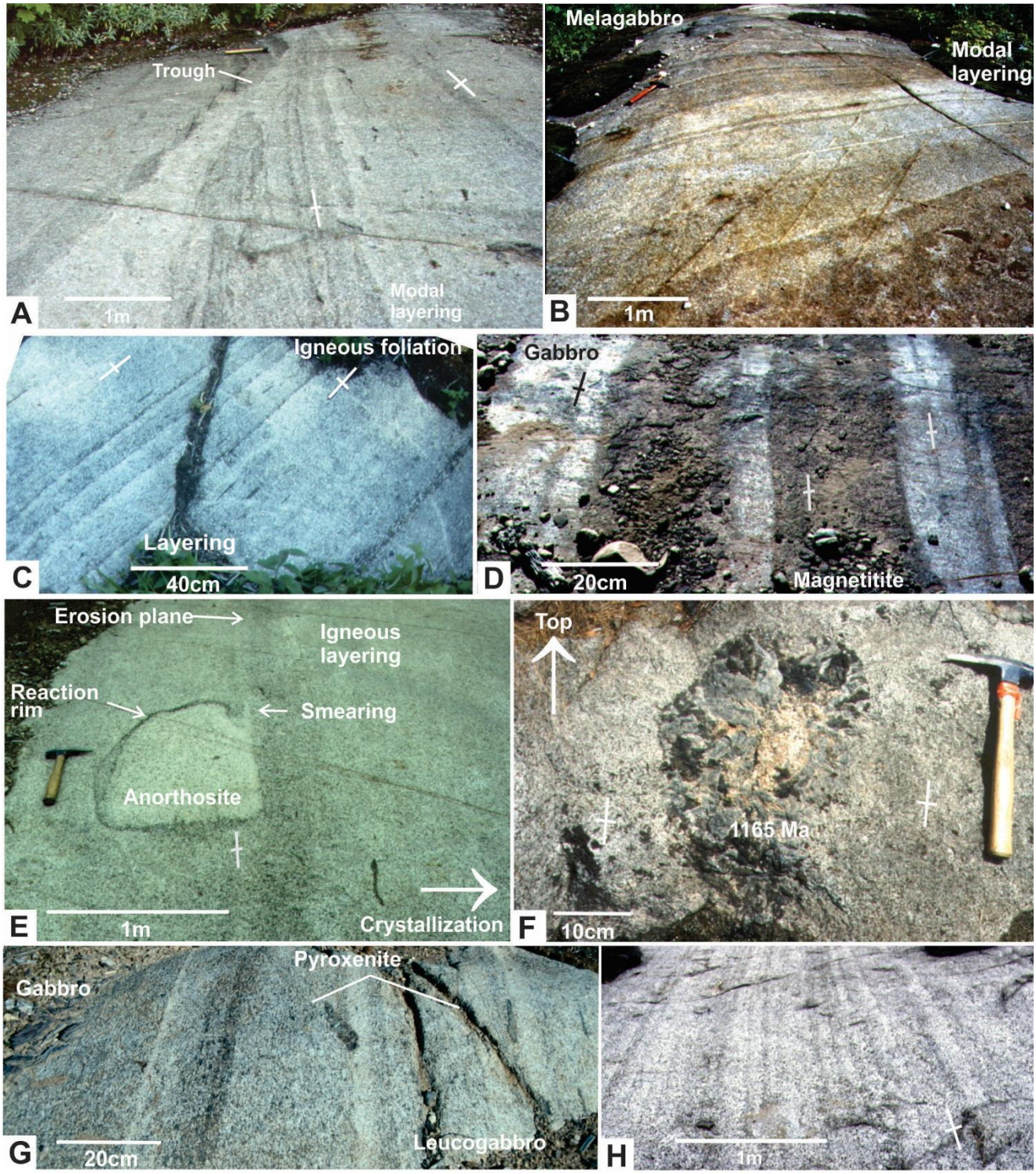

Figure 7.2. Layering in the series of layered gabbro stocks flanking the Bondy gneiss dome is consistently vertical. Thickness of layering varies, and an erosional trough and fallen blocks with reaction rims locally occur (see Irvine et al. 1998 for similar features in other layered intrusions). **A.** Vertical rhythmic layering in the Kar-Ha-Kon intrusion. The intrusion is characterized by magnetite-rich layers. **B.** Vertical structures in the Kar-Ha-Kon intrusion are outlined by the preferred orientation of plagioclase laths and of compositional layering. **C.** Rhythmic subvertical layering in the Montjoie intrusion. **D.** Compositional vertical layering of alternating gabbro and magnetitite. **E.** Anorthositic block with reaction rim and a smeared contact that bears evidence of subvertical magmatic currents and entrainement of crystal mushes. **F.** Vertically elongate pocket of pegmatitic gabbronorite in the Lacordaire intrusion with more felsic material at the top bearing zircons. Zircons have been dated to 1165 Ma ± 2 Ma (Corriveau and van Breemen, 2000). Such pockets record upward ascent of lighter magmas-fluids and can be used as pointing toward surface in line with the interpretation that the vertical orientation of the layering is primary. **G.** Vertical magmatic layering in the Lac du Rang pluton. **H.** Vertical layering in the Monteregian Mesozoic Mont Saint-Grégoire intrusion illustrating primary vertical layering.

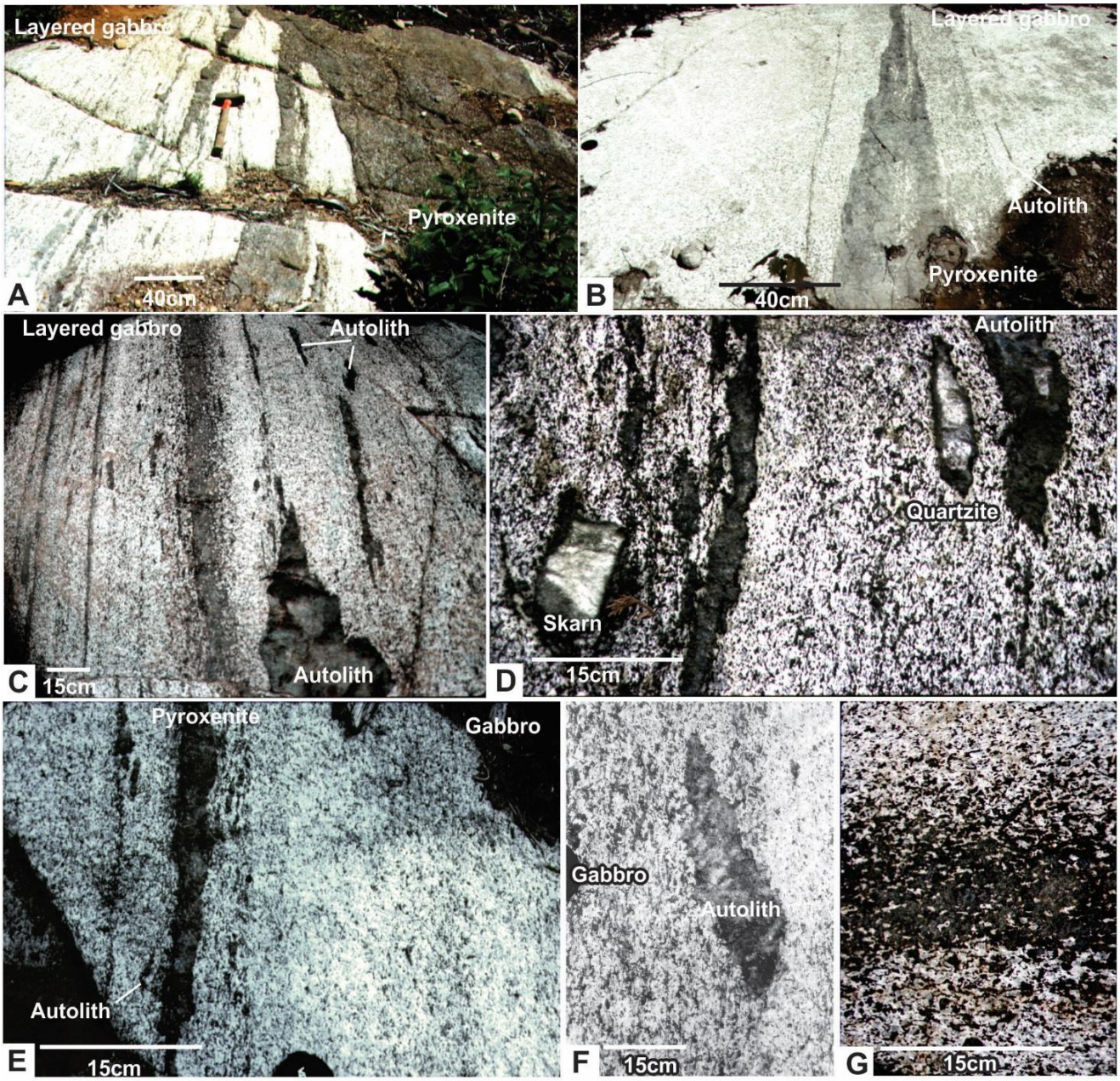

Figure 7.3. Vertically layered gabbro intrusion with cogenetic mafic enclaves and skarn and quartzite xenoliths cut by ultramafic rocks. **A.** Layered gabbro cut by a pyroxenite dyke with apophysis. The gabbro has a planar structure defined by the orientation of the plagioclase laths. **B.** Ultramafic intrusive sheet within the vertically layered gabbro. **C.** Layered gabbro with ultramafic autoliths. **D.** Layered gabbro with ultramafic autoliths and xenoliths of quartzite and pyroxene-rich calc-silicate rocks. The angular and elongate xenoliths are oriented parallel to the magmatic foliation and are surrounded by a massive clinopyroxene reaction ring. **E.** Pyroxenite autolith oblique to magmatic foliation. **F.** Detail of C showing a pyroxenite autolith oblique to magmatic foliation. **G.** Detail of the modal layering in a melanocratic gabbroic layer of C.

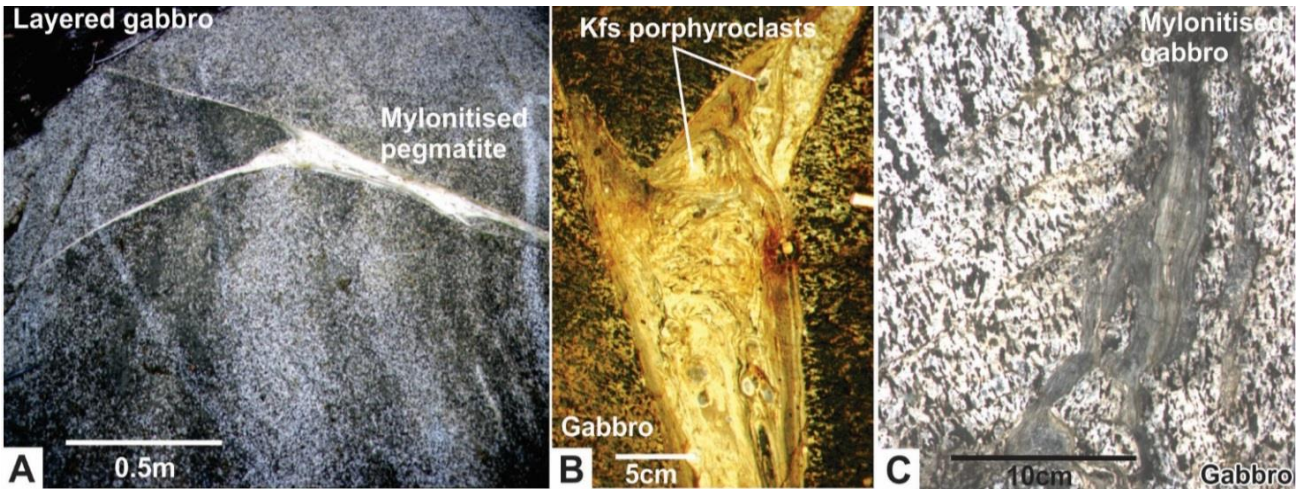

Figure 7.4. Strain partitioning in the vertically layered mafic intrusion. **A.**, **B.** Pegmatite within non deformed gabbros can be pervasively mylonitized. **C.** Mylonitization of the gabbro is rare but occurs locally.

Chapter 8: Bondy gneiss complex, west sector (Day 3)

Directions: Along road 3 East of the lac Kar-Ha-Kon, turn North at the intersection for lakes Toncamp, Légende, Sardines, Coindrelle. Reset your odometer to 0. A second intersection with a sign is located further north on road 3. If you missed the first turn, turn left at this intersection and continue with the listed mileage (0.2 km difference). About 1 km North, stay to the right at the junction with the second road for lacs Toncamp, Sardine and Coindrelle. You will pass Lac Provost creek then a swamp then at about 2.5 km keep left at the junction to Lac Toncamp.

Point of interest: West of the Bondy complex, around Lac Légende (outcrops 4450 to 4455) and 400 m East of Lac Toncamp (outcrop 4458), you will come across some biotite-graphite gneiss (outcrops 4450, 4452) and garnet-graphite-sillimanite gneiss with layers of biotite-quartzite which also locally contain garnet or graphite (outcrops 4451, 4454, 4458). *Continue on the road and keep right at the junction for Lac Coindrelle. At 6.5 km you will find stop 2.1.*

8.1 Stop descriptions for Day 3

Stop 3.1
Quartzite (overgrown)

Quartzite intercalated with quartzofeldspathic gneiss and cut by an amphibolite dyke outcrop in the vicinity of the Bondy gneiss complex. The amphibolite dyke is recrystallized and both the dyke and its metamorphic foliation are folded (Fig. 8.1).

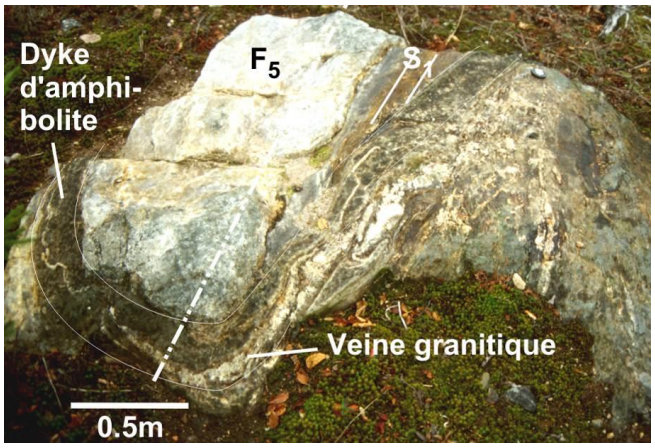

Figure 8.1. Quartzite and other paragneisses of the Quartzite domain cut by an amphibolite dyke metamorphosed and folded.

Stop 3.2
Tourmalinite and kornerupine-bearing veins among aluminous gneisses

The tourmalinite forms a very discrete, thick and homogeneous unit that appears stratabound with respect to adjacent aluminous gneisses. These rocks are very magnesian and either potassic (aluminous gneisses) or sodic (tourmalinites) as illustrated in the AIOCG diagram of Figures 8.2, 8.3 and 8.4. The unit consists of fine grained, granoblastic tourmaline among quartz and plagioclase (Fig. 8.3). Veins of plagioclase-quartz-kornerupine (elongate green crystals) cut the tourmalinites and are locally derived through the breakdown of the tourmalinite assemblages (Boggs and Corriveau 2004). No cross-cutting veins of tourmaline have been observed in the gneisses of the Bondy gneiss complex except for some tourmaline stringers that are locally folded in Stop 3.3.

Two origins are possible for the tourmalinites. They are exhalative or represent a concordant hydrothermal alteration front within albitites or albitized rocks. If exhalative, and in the absence of sedimentary basins in the complex, tourmaline would have precipitated in a submarine volcanogenic hydrothermal environment or slightly below surface among argillaceous units. Once metamorphosed, such tourmalinites have a tourmaline-quartz assemblage and a well laminated or layered structure (Figs. 8.5, 8.6) as described in Slack et al. (1993). In contrast to laminated tourmalinites, the tourmaline alteration of albitites observed in the Great Bear magmatic zone (Fig. 8.3) does not lead to extensive veining but most commonly to heterogeneous, massive zones of replacement with local irregular and poorly formed veins. Such a superposition of tourmaline alteration on albitites would explain the sodic-iron-magnesium association of some of the tourmalinites analysed in the Bondy gneiss complex. We favour this interpretation especially that such zones in the Great Bear were also commonly K-feldspar altered subsequent to tourmaline precipitation.

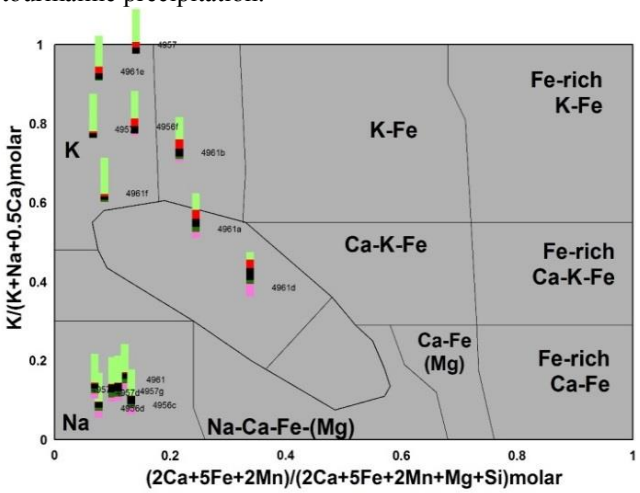

Figure 8.2. Composition of the Bondy gneiss complex tourmalinites and associated aluminous gneisses plotted on the AIOCG diagram of Montreuil et al. (2013). Colour coding of the Na-Ca-K-Fe-Mg bar codes in Figure 2.5. The tourmalinites fall within the sodic alteration facies. The aluminous gneisses fall within the K alteration field typical of K-felsite and phyllic alteration facies.

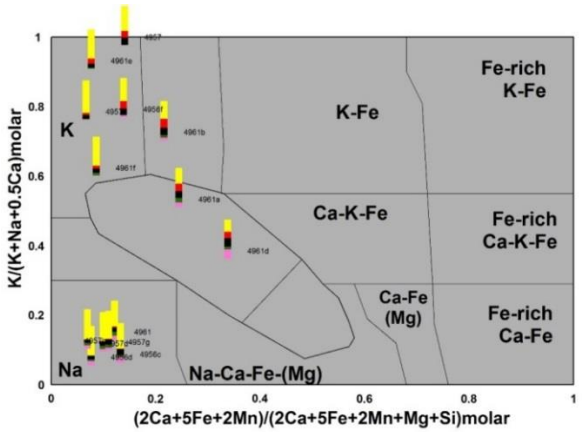

Figure 8.3. Same samples as in Figure 8.2 with Na-Ca-Fe-K-(Si+Al)/10 bar codes.

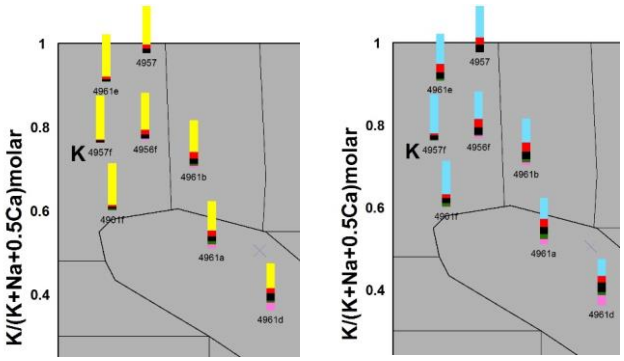

Figure 8.4. Bar codes of Figure 8.3 Al gneisses with Si (yellow in left diagram) and Al (blue in right diagram) instead of (Si+Al)/10. Note that Si and Al proportions are nearly the same.

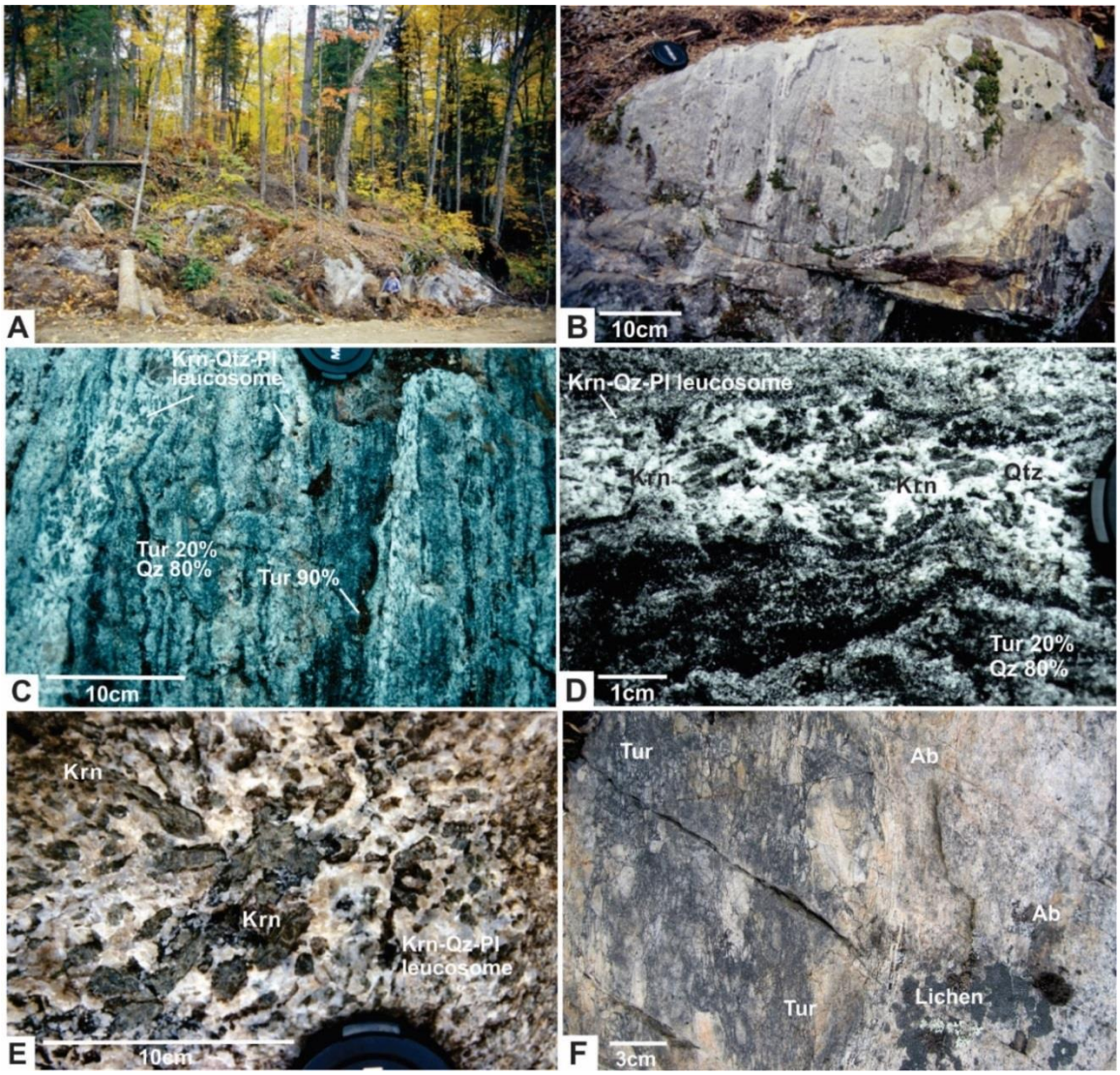

Figure 8.5. Tourmalinites from the Bondy gneiss complex and tourmaline alteration in albitites from the Great Bear magmatic zone. **A-B.** Stop 3.2, tourmalinite with veins of plagioclase-quartz and kornerupine. Contrast the heterogeneous character of the tourmalinites with the laminations of metamorphosed sedimentary tourmalinites depicted in Figure 8.6 and discussed in Slack et al. (1993). **C.** Veins of kornerupine crosscutting tourmalinites. **D.** Medium-grained tourmalinite mainly consists of quartz and black tourmaline (modal concentration of 15 to 20 %). Centimetre melanocratic layers contain about 70-80% of tourmaline. **E.** Detail of kornerupine-plagioclase-quartz vein. The kornerupine crystals can reach a length of about 10 cm.

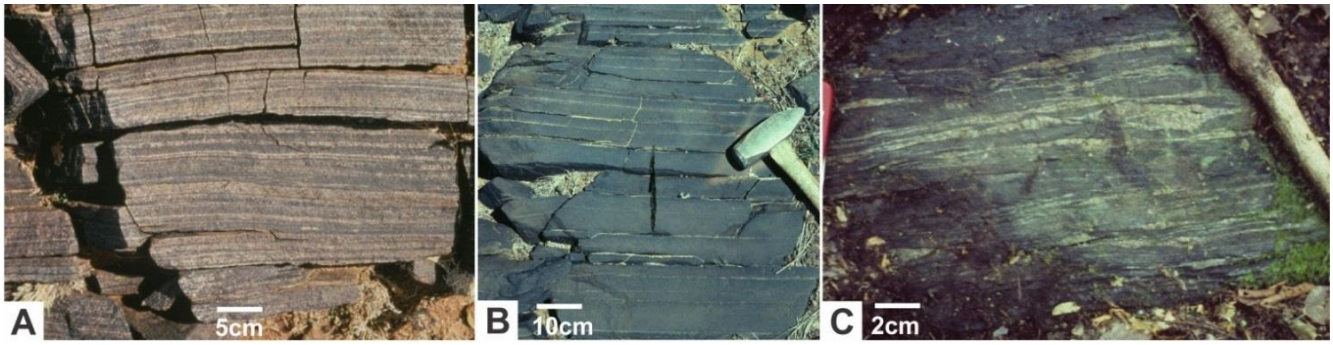

Figure 8.6. Tourmalinites from the Broken Hill deposit described in Slack et al. (1993). Photos courtesy of John Slack.

Stop 3.3
Layered garnet-amphibolite (overgrown)

This layered amphibolite marks the western limit of the Bondy gneiss complex. It is representative of most amphibolite units in the northern part of the complex. It is composed of centimetre- to decimetre-scale layers of mesocratic to melanocratic garnet amphibolite along with plagioclase-hornblende-garnet-quartz gneiss (4281, Fig. 8.7). None of the layers is anorthositic unlike, and thus differing from, layered sills found elsewhere in the area. This gneiss-amphibolite assemblage may have been derived from volcanic accumulations. Note that the granite veins show a west-facing polarity which may correspond to the tops of original gneissic layering during migmatization. A reconstruction of the paleo-structure based on this way-up criteria puts the gneissosity as subhorizontal at the time of veins emplacement.

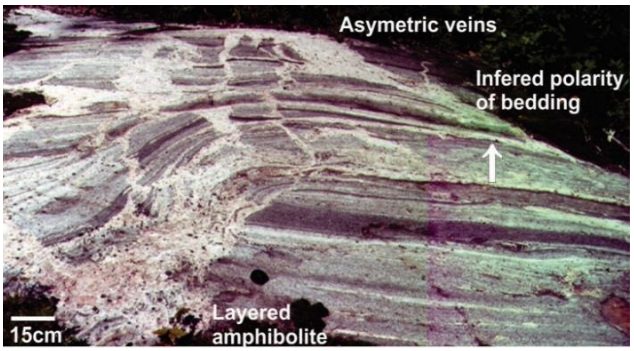

Figure 8.7. Layered amphibolite interpreted as a potential volcanic sequence. Pegmatite structures serve as proxies for interpreting original way-up of layering.

Stop 3.4
White plagioclase-cordierite-orthopyroxene gneiss

The magnesian lithofacies is a white, quartz-bearing, plagioclase-dominant gneiss with cm-thick horizons containing magnesian orthopyroxene (honey colour), magnesian cordierite (blue), magnesian kornerupine (pale green and resembling apatite), magnesian tourmaline (black) and zircon (only observed in thin section). Accessory minerals are magnetite, pyrite, pyrrhotite and chalcopyrite (traces). The abundance of plagioclase, the magnesian composition of the rock (pale colour ferromagnesian minerals), and the very high metamorphic grade give this unit its very unusual white colour. The outcrop is in fact as white as marble and could easily have been overlooked during mapping as marble is very common in the Mont-Laurier area (Fig. 8.8). Kornerupine is common in the leucosomes and attest to their in situ nature.

In Figure 8.8 we illustrate the strong resemblance of this outcrop with Great Bear examples.

Figure 8.8. White, layered, plagioclase-dominant gneiss in the Bondy gneiss complex and potential analogues in the Great Bear magmatic zone.
A. White, layered, plagioclase-dominant gneiss interlayered with centimetre to tens of centimetre-thick mesocratic layers of orthopyroxene-cordierite-phlogopite-tourmaline-kornerupine gneiss. Locally one can observe millimetre-scale stringers of dark fine-grained tourmalinites. Veins of kornerupine and cordierite bearing leucosomes also occur (CQA-1654; UTM 478406mE, 5131980mN). **B.** Stringers of tourmalinites. This fabric was originally considered an evidence of F_1 folding and the tourmaline formed as a meta-exhalite S_0 layer. Such features have been observed in tourmaline replacement zones and associated veinlet in the Great Bear magmatic zone as illustrated in Figure 8.8F. There the fold-type structure is primary and part of the replacement zone of Figure 8.5F casting doubts on original interpretation for the Bondy gneiss complex and providing an alternative origin more compatible with the plagioclase-rich nature of the host gneisses. **C.** Close up of mesocratic layers in A where the mesocratic layers consists of orthopyroxene, cordierite, plagioclase and quartz. **D.** Orthopyroxene and cordierite form clots with plagioclase and quartz which are bordered by tourmalinite seams mm in size and parallel to the gneissosity. **E.** Leucosomes with orthopyroxene and phlogopite cutting across the gneissosity. **F.** Non-deformed vein of tourmaline among extensive tourmalinization zone of albitites in the Southern Breccia corridor in the Great Bear magmatic zone. **G.** Stratabound albitization of metasiltstone cut by fine-grained amphibole-dominant alteration zone also largely stratabound in nature south of the NICO deposit. **H.** Parallel veins and breccias filled with amphibole among albitites in the De Vries area of the Great Bear magmatic zone.

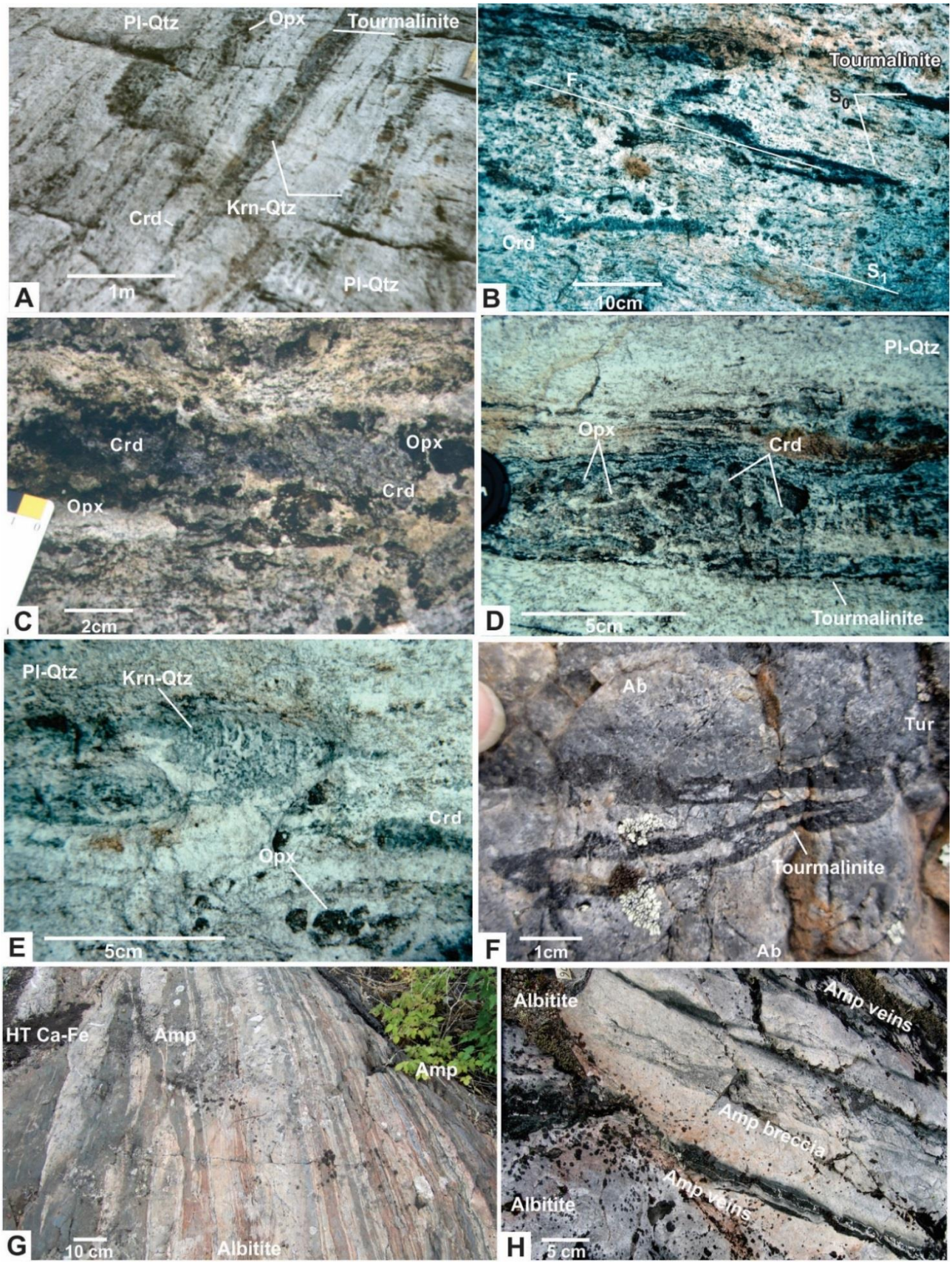

Figure 8.8. Metamorphosed and non-metamorphosed albitites. **A-E.** Bondy gneiss complex examples. **F-H.** Great Beat magmatic zone examples. Detailed figure caption on previous page.

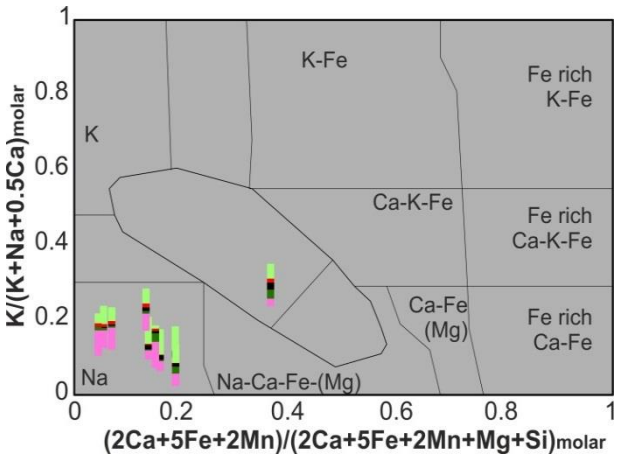

Figure 8.9. Composition of the Bondy gneiss complex white plagioclase-cordierite-orthopyroxene gneisses plotted on the AIOCG diagram of Montreuil et al. (2013). Colour coding of the Na-Ca-K-Fe-Mg bar codes in Figure 2.5. White plagioclase-cordierite-orthopyroxene gneisses fall within the sodic alteration facies and the high Mg content may result from chloritization.

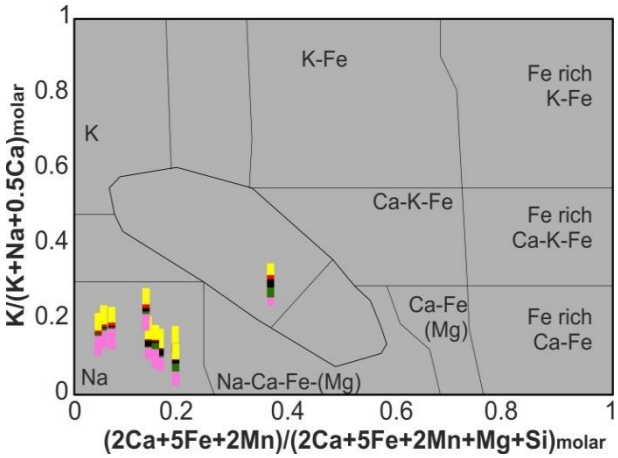

Figure 8.10. Same samples as in Figure 8.9 with Na-Ca-Fe-K-(Si+Al)/10.

The gneiss has a mineral assemblage comparable to cordierite-orthoamphibole gneiss (Schreurs and Westra 1985; Guiraud et al. 1996) and chloritic alteration zones (Trägårdh 1991) found in alteration pipes associated with VMS deposits. However, the prevalence of plagioclase and the highly sodic composition are in conflict with such an interpretation. Mass-balance calculations record a loss in Ca and gain in Na, Mg, K and Si with respect to the adjacent non-altered rhyolitic protolith, compatible with K-feldspar destruction, sericitization and chloritization (Blein et al. 2004). Such chloritization zones occur at the expense of stratabound HT Ca-Fe alteration among albitized host rocks in the IOAA systems of the Great Bear magmatic zone. White plagioclase-cordierite-orthopyroxene gneisses fall in the field of sodic alteration with high Mg proportion suggesting a superimposed chloritization (Figs. 8.9, 8.10).

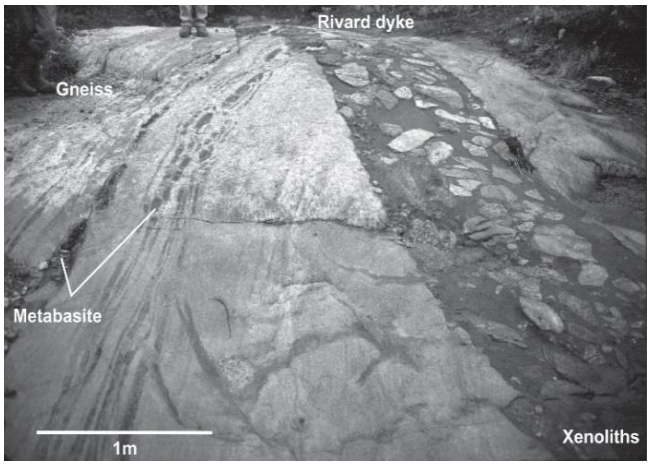

Figure 8.11. The Rivard dyke cutting across the layering of a typical outcrop of granulite-facies quartzofeldspathic gneiss in the Bondy gneiss complex.

Stop 3.5
Typical quartzofeldspathic gneiss of the Bondy gneiss complex

A brief look at the gneiss hosting the Rivard dyke to put into perspective the atypical nature of the suite of gneissic rocks forming the hydrothermal system (Fig. 8.11). Note the crude compositional layering define by slight changes in ferromagnesian content, the presence of amphibolite layers which are more typical of amphibolite dykes than primary layering in volcaniclastic rocks. The rock is interpreted as an orthogneiss of uncertain origin. We will come back to observe the Rivard dyke subsequently.

Stops 3.6 and 3.7
Fe-Al lithofacies (argillic alteration of a lapilli-stone)

A variety of Fe-Al lithofacies depleted in Ca prevails in this series of outcrops (4474, 4475; Figs. 8.12, 8.13). They comprise sillimanite-garnet-biotite gneisses, layers rich in garnet, cordierite or biotite and magnetite, a white plagioclase-rich gneiss with hypersthene, cordierite, and kornerupine, laminae of tourmalinite and some rusty gneiss with sillimanite. Zircon is ubiquitous in thin sections. Sulphides are common. Such aluminous gneisses occur at the Prieska ore body in South Africa (Theart et al. 1989; Sheepers and Cornell 1990). The abundance of the ferromagnesian and aluminous minerals in this series of gneisses result in hydrothermally derived metamorphic rocks that resemble and thus can be misinterpreted for pelitic restites.

These Fe-Al lithofacies fall in the fields of Ca-Fe, Ca-K-Fe and K-Fe alteration facies within the AIOCG discriminant diagram and their bar codes are typical of such facies (Figs. 8.14, 8.15). Few samples fall in the least-altered field and their bar codes are typical of high-temperature Ca-Fe alteration facies metasomatites that have been subsequently chloritized (Figs. 8.14, 8.15).

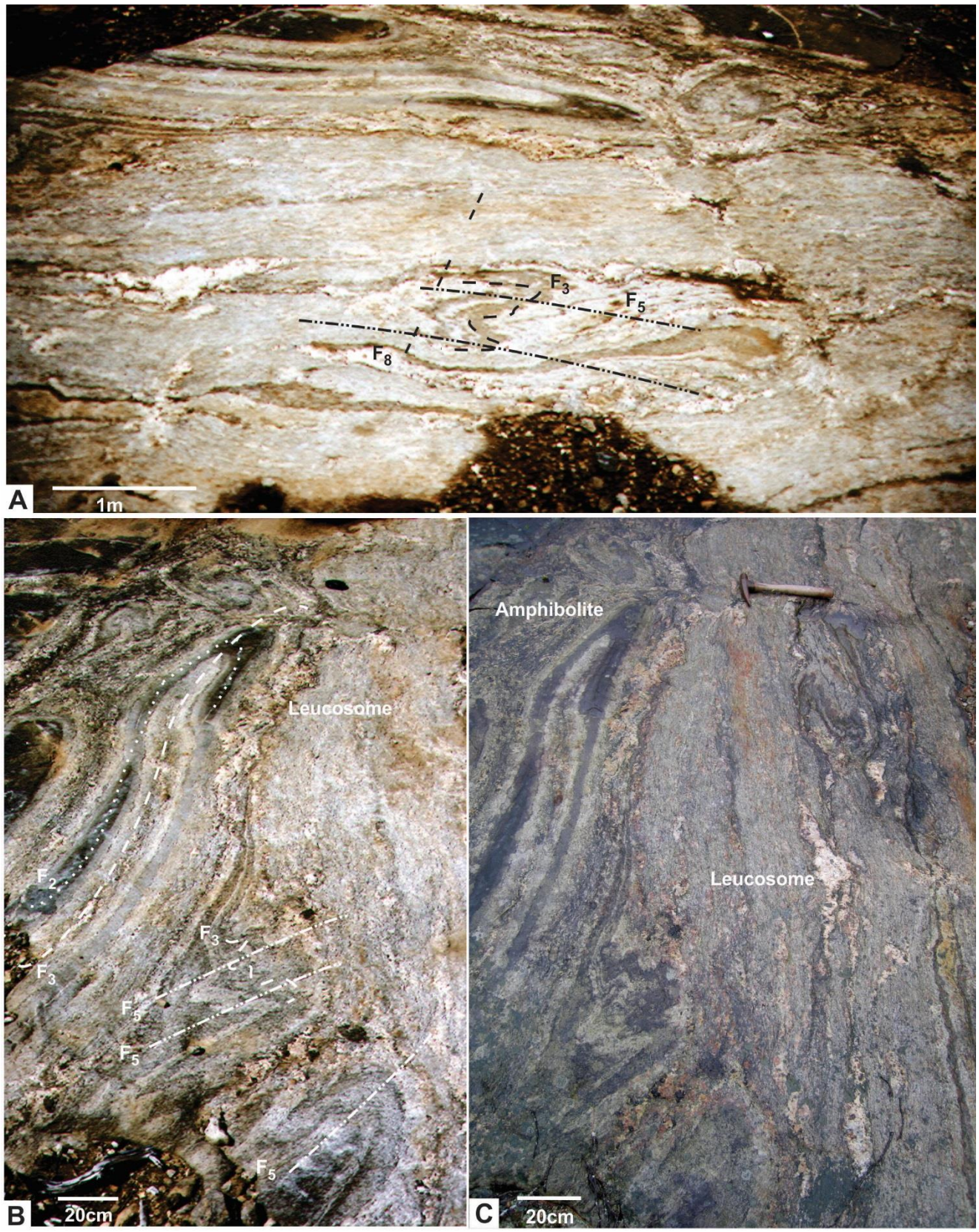

Figure 8.12. Stops 3.6. Outcrop 4474. See Harris et al. (2001) and Dufréchou et al. (2015) for a detailed structural analysis of this and other outcrops of the Bondy gneiss complex.

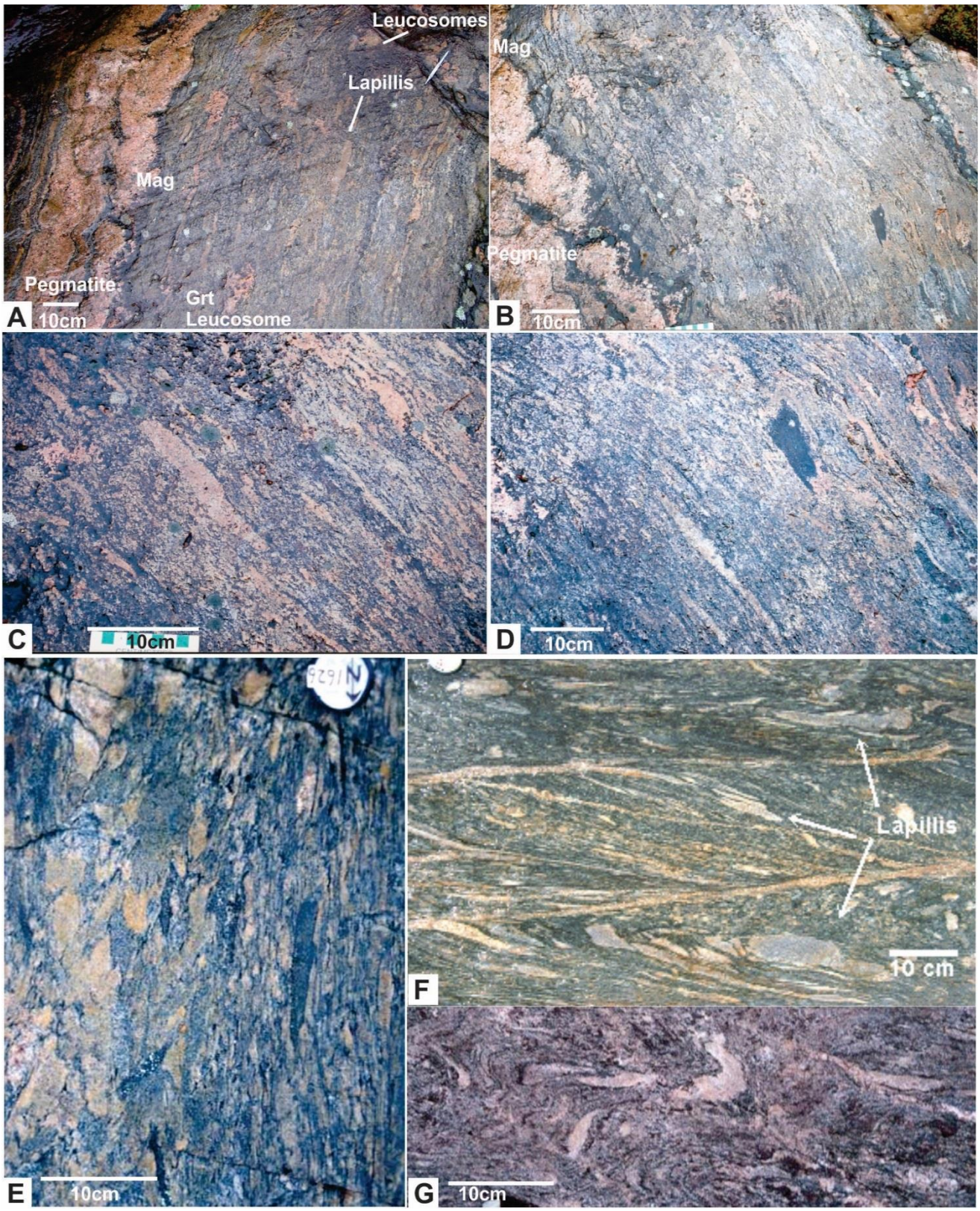

Figure 8.13. Stop 3.7. Outcrop 4475. **A-D.** Bondy gneiss complex. Photo courtesy of Michael Downes. **E-G.** Lapillistone at granulite facies from the La Romaine supracrustal belt, eastern Grenville Province. Lapillistone in E are least altered. Lapillistones in F and G are argillic altered, sheared and invaded by local leucosome veins.

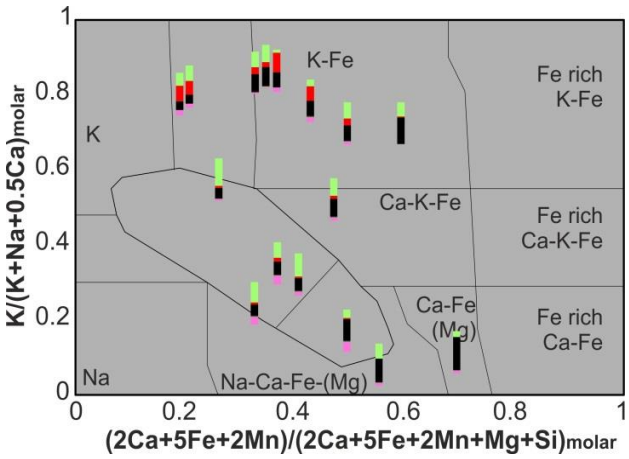

Figure 8.14. Composition of the Bondy gneiss complex Fe-Al lithofacies plotted on the AIOCG diagram of Montreuil et al. (2013). Colour coding of the Na-Ca-K-Fe-Mg bar codes in Figure 2.5. Fe-Al lithofacies fall within the potassic alteration facies. Note that chloritization of high-temperature Ca-Fe alteration facies typically displace whole-rcok composition towards and fall within the least-altered field. The significant Mg component of the bar codes is a diagnostic feature of such overprints and helps discriminate overprinted alteration facies and least-altered common rocks.

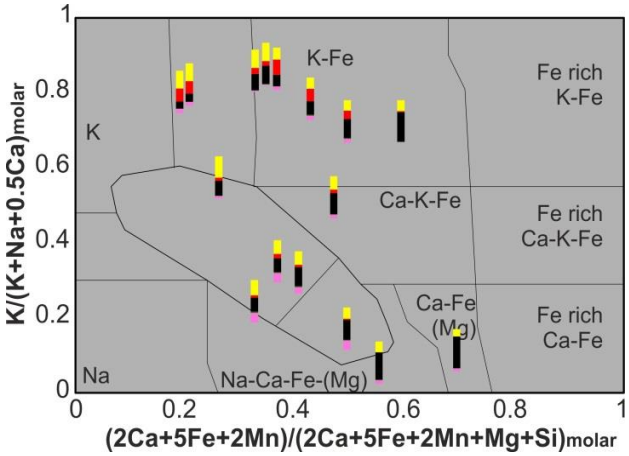

Figure 8.15. Same samples as in Figure 8.14 with Na-Ca-Fe-K-(Si+Al)/10 bar codes. Note that the incremental decrease in Si+Al component is typical of rocks incrementally altered in iron oxides.

The amoeboid character of the leucosomes in the aluminous gneisses and their assemblages, systematically coherent with those of the leucosomes, are criteria that attest to an in situ derivation and to a low mobility of the melt at the time of the anatexis (e.g. Sawyer 1999). This observation provides strong evidence that the unusual mode of aluminous phase is not simply due to partial melting. Systematically using these criteria and the coherency of the rock units' package with those typical of metamorphosed hydrothermal alteration systems and their meta-exhalites permitted to avoid confusing these units with restites. The complex forms a dome but it behaved as a solid body recording regional deformation during peak metamorphism (Vigneresse et al. 1996). This behaviour contrasts with granite-bearing migmatitic domes that loose cohesion during diatexites formation (ibid).

Geochemical comparison with the composition of the North American Shale composite of Gromet et al. (1984) supports a hydrothermal nature for the aluminous gneisses and the field-inferred relative enrichments in major elements (Blein and Corriveau 2017). In Figures 8.16 and 8.17, North American Shale composite of Gromet et al. (1984) fall in the field of least-altered rocks, and K-Fe alteration field.

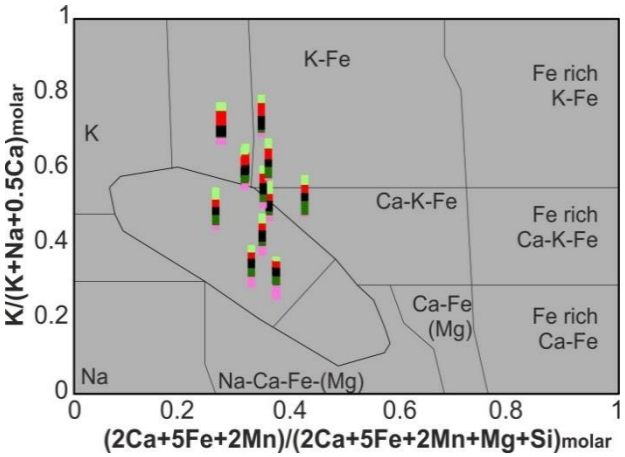

Figure 8.16. IOCG discriminant diagram with Na-Ca-Fe-K-Mg bar codes for samples from the North American shale composite of Gromet et al. (1984).

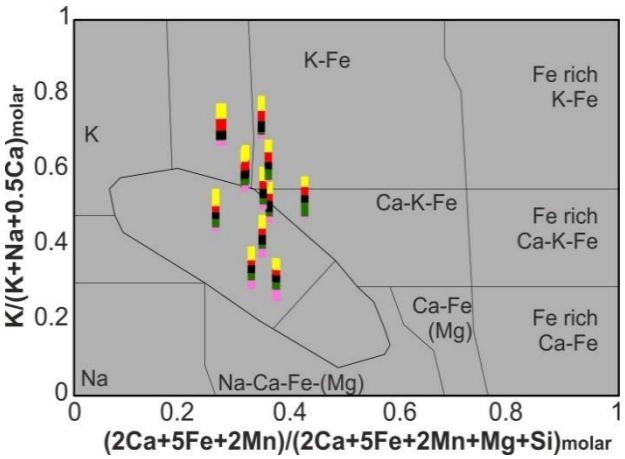

Figure 8.17. IOCG discriminant diagram with Na-Ca-Fe-K-(Si+Al)/10 bar codes for samples in Figure 8.16.

The discovery of lapilli texture within the aluminous gneiss provides strong evidence that the gneisses were in part originally volcanic and altered prior to metamorphism (Fig. 8.13). The fragments (<10 x 2 cm) are very fine to fine grained, felsic to mafic and have wispy contacts typical of lapillis. Next to this outcrop, at stop 3.7, is a laminated, K-feldspar-dominant gneiss interpreted as a pervasively K-feldspar-altered rhyolitic tuff.

Biotite-sillimanite rich units have high gold content (644 ppb) while the orthopyroxene-biotite rich gneisses have systematically about 50 ppb gold (Corriveau 2013). Though Cu can reach 0.85 % at stop 16, Zn and Mn are very low in

gahnite and garnet (Boggs and Corriveau 2004).

The outcrops record several phases of deformation. The gneiss fabrics and anatectic leucosomes preserve respectively peak pressure and peak temperature mineral assemblages estimated by geothermobarometry to 950ºC and 10 kbar (33 km depth) (Boggs and Corriveau 2004). U-Pb ages of 1.20 to 1.19 Ga were obtained on zircon grains from gneisses, while a gneiss laden with anatectic leucosomes yielded a 1.18 Ga age. Moreover, grains of monazite interpreted as metamorphic give ages between 1.18 to 1.17 Ga (Corriveau and van Breemen 2000; Wodicka et al. 2004). The formation of the gneissosity and the crystallization of the leucosomes are thus estimated at 1.2-1.19 and 1.18 Ga respectively. D_1 fabrics record maximum crustal thickening. They were folded isoclinally (phases F_2 and F_3) then cut by the leucosomes, which record the maximum temperature reached (Harris et al. 2001).

Stop 3.8
Laminated K-feldspar-rich quartzofeldspathic gneiss, a metamorphosed K-feldspar-altered rhyolitic tuff)

Laminated quartzofeldspathic gneisses are characterized by leucocratic, cyclic, asymmetric, centimetre-scale compositional layers locally repeated in a very systematic order starting with (Fig. 8.18):

1. a coarse-grained K-feldspar-rich layer;
2. a medium-grained granitic layer with K-feldspar and quartz; and
3. a biotite-rich layer with K-feldspar, quartz and orthopyroxene.

The contact between K-feldspar-rich and biotite-rich layers is abrupt. In contrast to layers in straight gneiss, these layers have a cyclic and graded grain size, sharp contacts, and no porphyroclasts. The cyclic and asymmetric nature of the layering is inferred to be primary, rather than an artifact of deformation or segregation during partial melting. The layering has been transposed but not created by metamorphism and associated deformation. The lack of quartz-rich units among the laminated quartzofeldspathic gneiss, combined with the nature and the texture of the layering, are best reconciled with a rhyolitic tuff protolith (e.g. Figure 5c in Rogers 2001).

Most laminated K-feldspar rich quartzofeldspathic gneisses fall in the field of potassic alteration (Figs. 8.19, 8.20). One sample within the least-altered field has bar codes typical of igneous rocks.

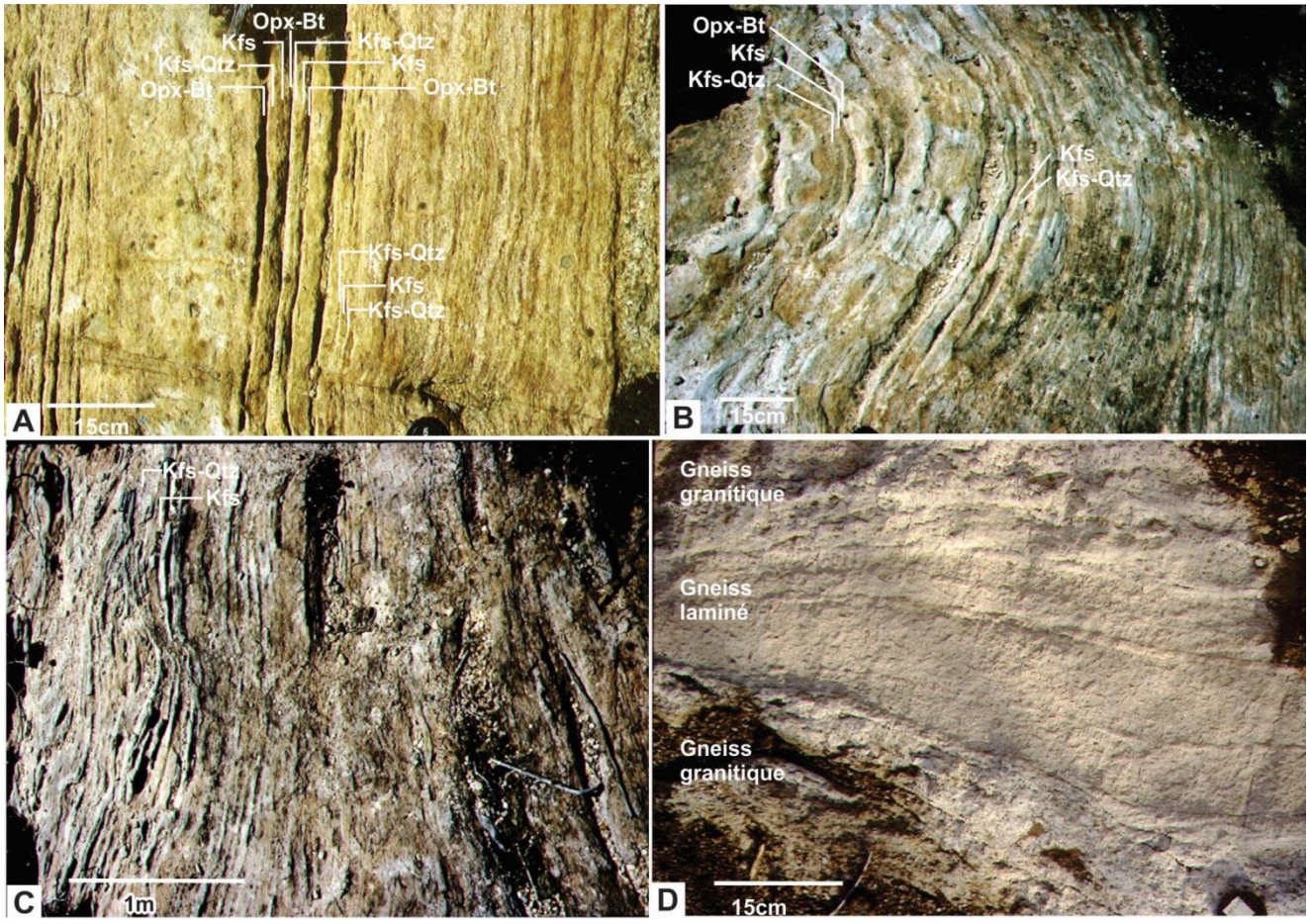

Figure 8.18. Laminated, K-Feldspar dominant quartzofeldspathic gneisses. **A.** Fine- to medium-grained laminated quartzofeldspathic gneiss with centimetre layers. This unit outcrops over a few tens of metres and gradually changes to more typical migmatized quartzofeldspathic gneisses. B. Open fold in laminated quartzofeldspathic gneisses. **C.** Laminae are continuous over several metres. **D.**

Laminated gneiss intercalated with granitic gneiss.

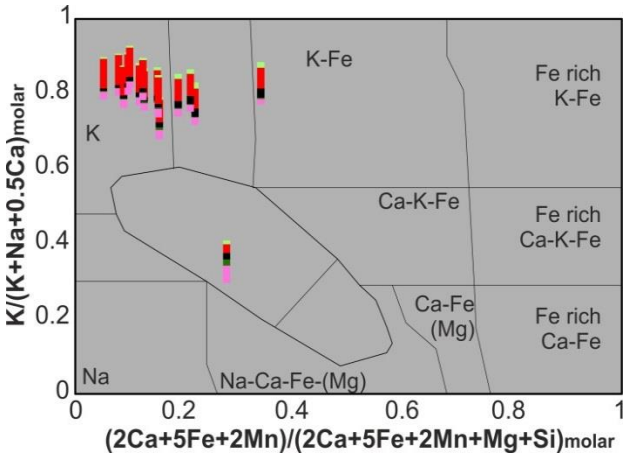

Figure 8.19. Composition of the Bondy gneiss complex laminated K-feldspar quartzofeldspathic gneisses plotted on the AIOCG diagram of Montreuil et al. (2013). Colour coding of the Na-Ca-K-Fe-Mg bar codes in Figure 2.5. Laminated quartzofeldspathic gneisses fall within the potassic alteration facies.

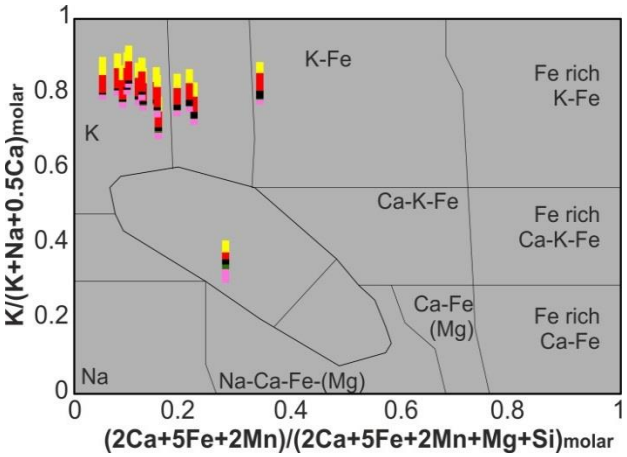

Figure 8.20. Same samples as in Figure 8.19 with Na-Ca-Fe-K-(Si+Al)/10 bar codes.

Chapter 9: The Rivard dyke (Day 3)

9.1 Rivard dyke and xenoliths

The Rivard minette dyke contains thousands of mantle (?) to lower crustal xenoliths. It was emplaced at 1072 Ma in the Bondy gneiss complex, almost 100 m.y. after regional metamorphism. It is exposed for more than 200m, has a fairly regular width of 1.7m, trends N-S and is steeply dipping (Fig. 9.1). A second minette dyke containing a few xenoliths, the Girard dyke, outcrops 8 km due south of the Rivard dyke and is also within the gneiss complex. Another minette dyke occurs along a similar trend to the north and has been dated at 1080 Ma (Nantel 2008). This area also contains several K-alkaline stocks, one of which has been dated at 1072 Ma (Nantel 2008). The minette dykes likely belong to a regional extensional north-south fracture system.

9.1.1 Rock type and mineralogy

The Rivard dyke comprises at least six injections of ultrapotassic minette lamprophyre with clinopyroxene and biotite phenocrysts in a matrix of clinopyroxene, biotite, alkali feldspar, plagioclase, amphibole, apatite, titanite, sulphides, carbonates and quartz. Xenocrysts include clinopyroxene, K-feldspar, garnet, orthopyroxene, titanite, quartz and zircon. The xenoliths consist of dunite, wehrlite, websterite, clinopyroxenite, mafic granulite, gabbro, metabasite, calc-silicate rock, granite, gneiss and quartzite (Figs. 9.2, 9.3, 9.4). The mafic granulite and ultramafic xenoliths are exotic with respect to the rocks of the CMB-Q. The intermediate to felsic xenoliths reflect the regional geology (Corriveau et al. 1994, 1996a, b; Corriveau and Morin 2000; Corriveau 2013).

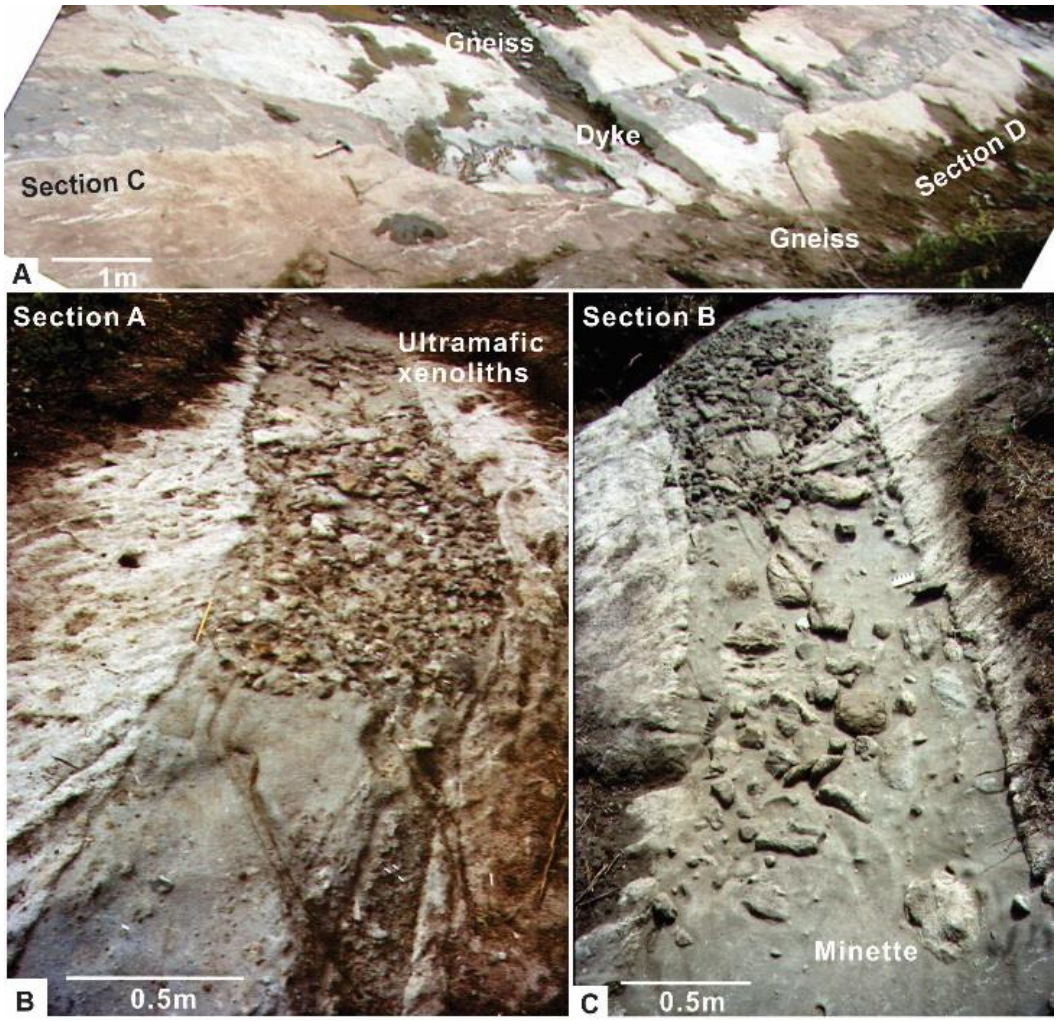

Figure 9.1. The Rivard dyke and its various sections. **A.** Sections C and D. In these sections, the dyke intersects the tonalitic gneiss of the Bondy gneiss complex at a low angle with respect to the gneissosity. Its contacts are sharp and generally rectilinear. **B.** Section A in which there is a strong accumulation of xenoliths over a few metres. These xenoliths are small and rounded and have a mafic and ultramafic composition. Their accumulation suggests that there was local congestion in the dyke. **C.** Section A at its northwestern extremity. Style of magma emplacement and xenolith formation can be find in Morin and Corriveau (1996).

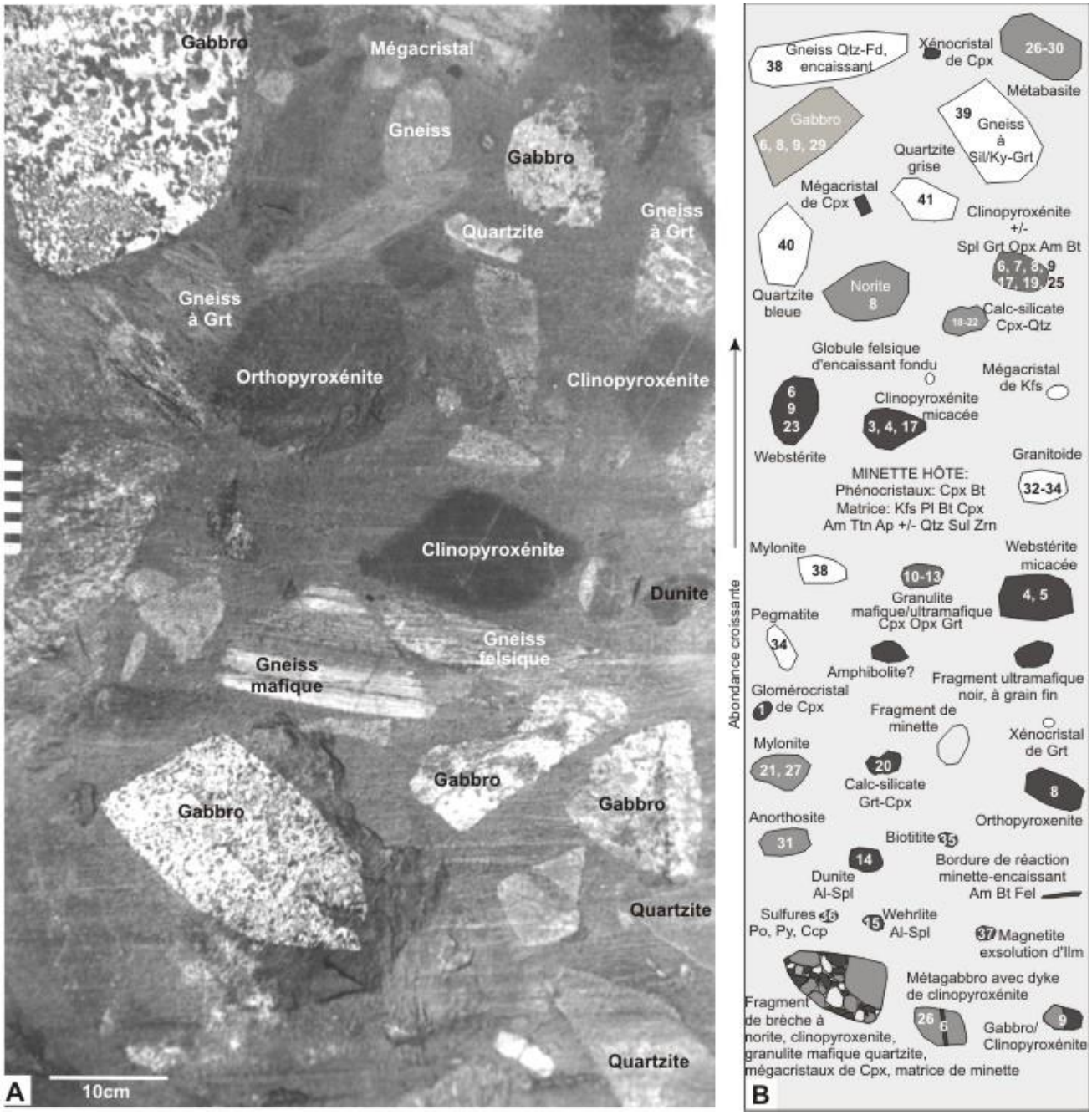

Figure 9.2. Morphology and typology of the various groups of xenoliths. All fragment types are described in Morin (1998). **A.** Section C rich in gabbroic xenoliths. Density of xenoliths is high (50 to 500 xenoliths per square metres) but clasts remain largely surrounded by minette magmas. One zone is clast supported along a bend in the dyke in section A. **B.** The xenoliths have been subdivided into 41 types by Corriveau and Morin (2000) from data in Morin (1998). Figure from Corriveau (2013).

9.1.2 Composition

The lamprophyre is ultrapotassic (K_2O/Na_2O in wt %: 2.2; 5 wt % K_2O; 50 wt % SiO_2; 6 to 9 wt % MgO) and enriched in large-ion-lithophile elements and light-rare-earth elements (3000 ppm Ba; 95 ppm Ce; 1700 ppm Sr; La/Yb: 20). These magmas belong to the Kensington-Skootamatta K-alkaline and shoshonitic suite emplaced between 1090 and 1076 Ma in the Central Metasedimentary Belt of Quebec and Ontario.

9.1.3 Age and composition of xenoliths

The xenoliths of garnet-, Al-spinel- and phlogopite-bearing clinopyroxenites and websterites (Mg# 56-92, Cr: up to 3400 ppm; Al_2O_3: 3-18 wt %), and xenoliths of mafic granulites have ca. 1.9 Ga Nd and Pb model ages (Amelin et al. 1994). Garnet-clinopyroxene Sm-Nd and Pb-Pb ages cluster around 1.08 Ga, indicating that the xenoliths have equilibrated until their extraction by the host lamprophyre (Amelin et al. 1994). Dunite and wehrlite (metamorphic

textures, Mg# 87, and olivine with Fo 90-94) xenoliths have unusually low Ni (ca. 40 ppm) and Cr (ca. 125 ppm) and their spinel is aluminous (Morin et al. 2005).

9.1.4 Depth of origin

These xenoliths record maximum P-T conditions of ca. 25 kbar and 1050°C. Initial εNd and $^{206}Pb/^{204}Pb$ for clinopyroxene are coeval with those of the potassic plutons, but initial $^{87}Sr/^{86}Sr$ ratios are distinctly higher. This apparent absence of xenoliths from the source, the maximum pressure of equilibration of the xenoliths at mantle depth, and the clinopyroxene-phlogopite cumulus xenoliths, interpreted as cognate with the host lamprophyre (Morin et al. 2005), suggest that magma did not ascend directly to the surface from its source, but instead ponded in the upper mantle. Thus, the pressures recorded provide only a minimum depth of origin (75 km) for this type of magma.

Figure 9.3. Morphology and types of xenoliths.

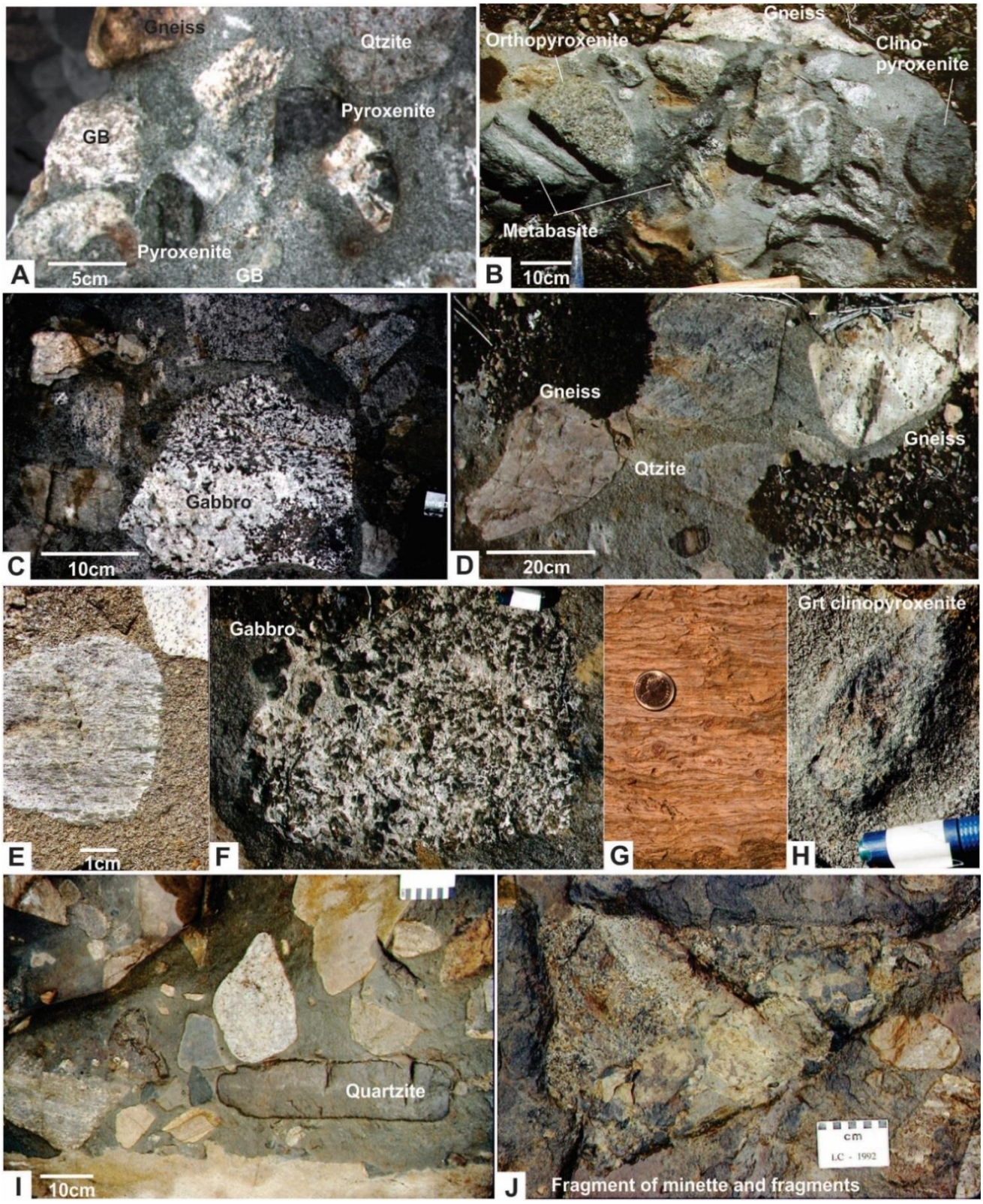

Figure 9.4. Range of xenolith types within the Rivard intrusive breccia. **A.** Variety of coarse-grained gabbro (GB). **B.** Second outcrop discovered during regional surveys in 1992. **C.** Xenolith of gabbro. **D.** First discovered outcrop. The abundance of quartzite in the dyke suggests that supracrustal levels likely originating from a platform form a component of the lithosphere under the Central Metasedimentary Belt. **E.** Metagabbro with a pronounced tectonic foliation. **F.** Gabbro with large plagioclase grains now completely recrystallized without tectonic transposition. **G.** Felsic mylonite xenolith with garnet porphyroclasts. **H.** Xenolith of garnet clinopyroxenite. **I.** Angular xenoliths of varied composition. **J.** Fragment of minette containing xenoliths of anorthosite, norite, clinopyroxenite, mafic granulite, quartzite, metabasite, and megacrystals of clinopyroxene.

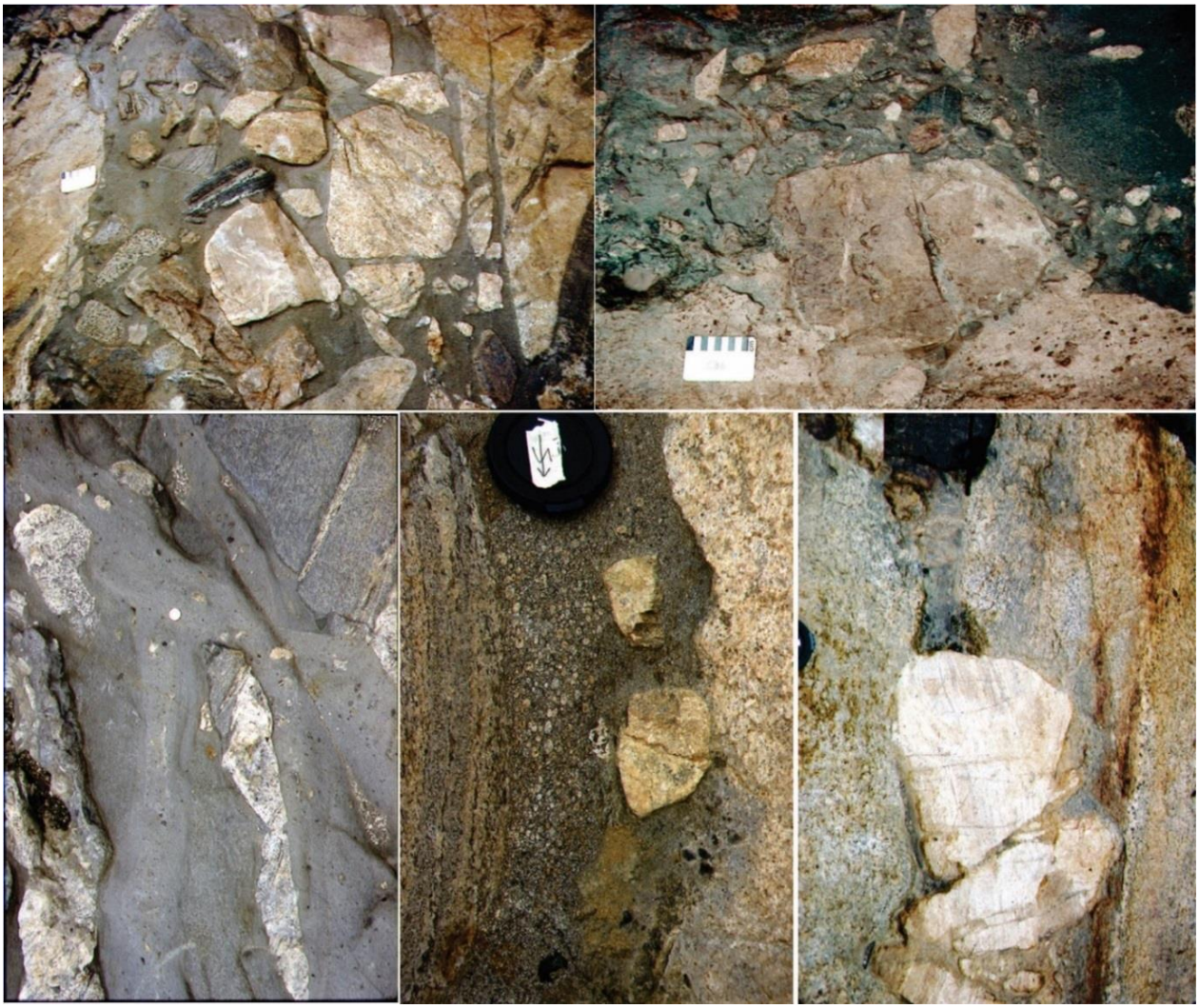

Figure 9.5. Style of magma emplacement, xenolith transport and imbrication.

9.1.5 Ascent mechanism of minette-type lamprophyre

Insights on fragmentation processes during dyke propagation at deep crustal levels and mechanism of xenolith transport in minette magmas are preserved in the Rivard intrusive breccia (Morin and Corriveau 1996). Field evidence, such as dyke parallel apophyses and wall rock fragments broken free to various extents, indicate that the xenolith formed through:

1. early fracturing of wall rock by inelastic deformation at high confining pressure during dyke propagation; and
2. intrusion of magma in fractures with progressive detachment of fragments from the walls (Fig. 9.5; Morin and Corriveau 1996).

The high variety of xenolith types suggests that fragmentation operated on an extensive section of the lithosphere.

The deep setting of the dyke combined with pre heating of the country-rock by early injection of magma and continuous delamination led to partial melting of the walls, formation of pseudobreccias, as well as mechanical removal of early formed chilled margins. Rapid ascent of the magma is suggested by the presence of large dense fragments and the brittle to ductile deformation at the margins of some xenoliths implying strong impact. A minimum ascent velocity of 50 cm/s is estimated from the settling rate of a 40 cm pyroxenitic xenolith. The minette magma had a low viscosity of ca. 4x101 Pa.s, but the high xenolith content increased the effective viscosity of the liquid solid mixture to ca. 103 Pa.s during emplacement. This favoured laminar flow of the magma as well as xenolith suspension. The magma ability to fragment and incorporate xenoliths was so efficient that it led to solidification at mid-crustal levels. Structural studies on coeval plutons indicate that marble units at these depths can also stop and trap this type of magma and inhibit it from reaching surface (Corriveau and Leblanc 1995; Corriveau et al. 1998). Stagnation in the upper mantle, long crustal residence time, intense fracturing and fragmentation recorded by the Rivard dyke provide a case example of impediments to minette extrusion (Corriveau et al. 1996b; Corriveau and Morin 2000).

Chapter 10: Transect across the Central Metasedimentary Belt and the Morin Terrane (Day 4)

10.1 Stop descriptions Day 4 AM

Stop 4.1
Marble tectonic breccia

Stop within the town of Mont-Laurier along highway 117 (46°33'00.9"N 75°31'01.8"W; 46.550239, -75.517174). Park at the parking lot at 2597 Chemin de la Lièvre N and cross the road South to a marble tectonic breccia at the East side of the entrance to the hospital. Marble tectonites are common in the CMB of Québec. The marble displays coarse grain sizes, a commonly continuous compositional layering and laminations and discontinuous, commonly chaotic trains of enclaves (Davidson 1995b; Fig. 10.1A, B). These tectonites differ from and may include zones of lower temperature marble mylonites as observed to the South of Grand Remous and within the Bancroft terrane of the Central Metasedimentary Belt of Ontario (Van der Pluijm 1991). Contorted string of calc-silicate rocks can be common and enclave of mylonitized gneiss preserved attesting of the high strain undergone by host rocks prior to the pervasive recrystallization of marble to coarse grains.

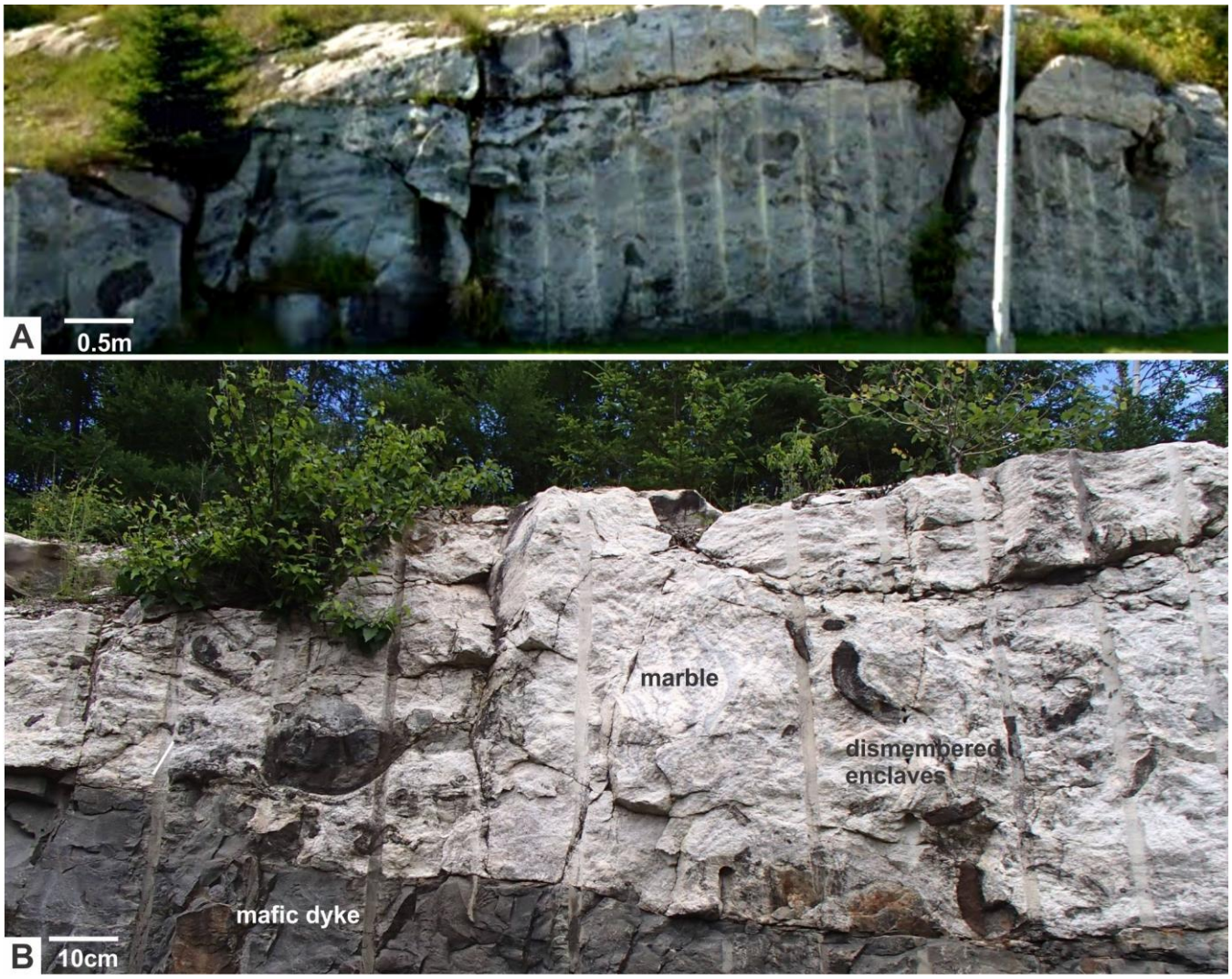

Figure 10.1. Marble tectonic breccia typical of the CMB. **A.** Stop 4.1. Dismembered mafic dyke forming a train of mafic enclaves with irregular to locally cuspate boundaries and convolute shapes. The enclaves differ markedly from xenoliths of layered calc-silicate rocks within the marble breccia that are shown in greater detail in Figure 10.2. Photo from Google Street view, 2012, accessed February 2018. **B.** Dismembered amphibolite dykes forming trains of enclaves within marble tectonites. These series of enclaves from early mafic dyke sets and their marble host are cut sharply by a mafic dyke of the Chevreuil suite. This outcrop occurs to the southeast of stop 4.2 within the marble domain.

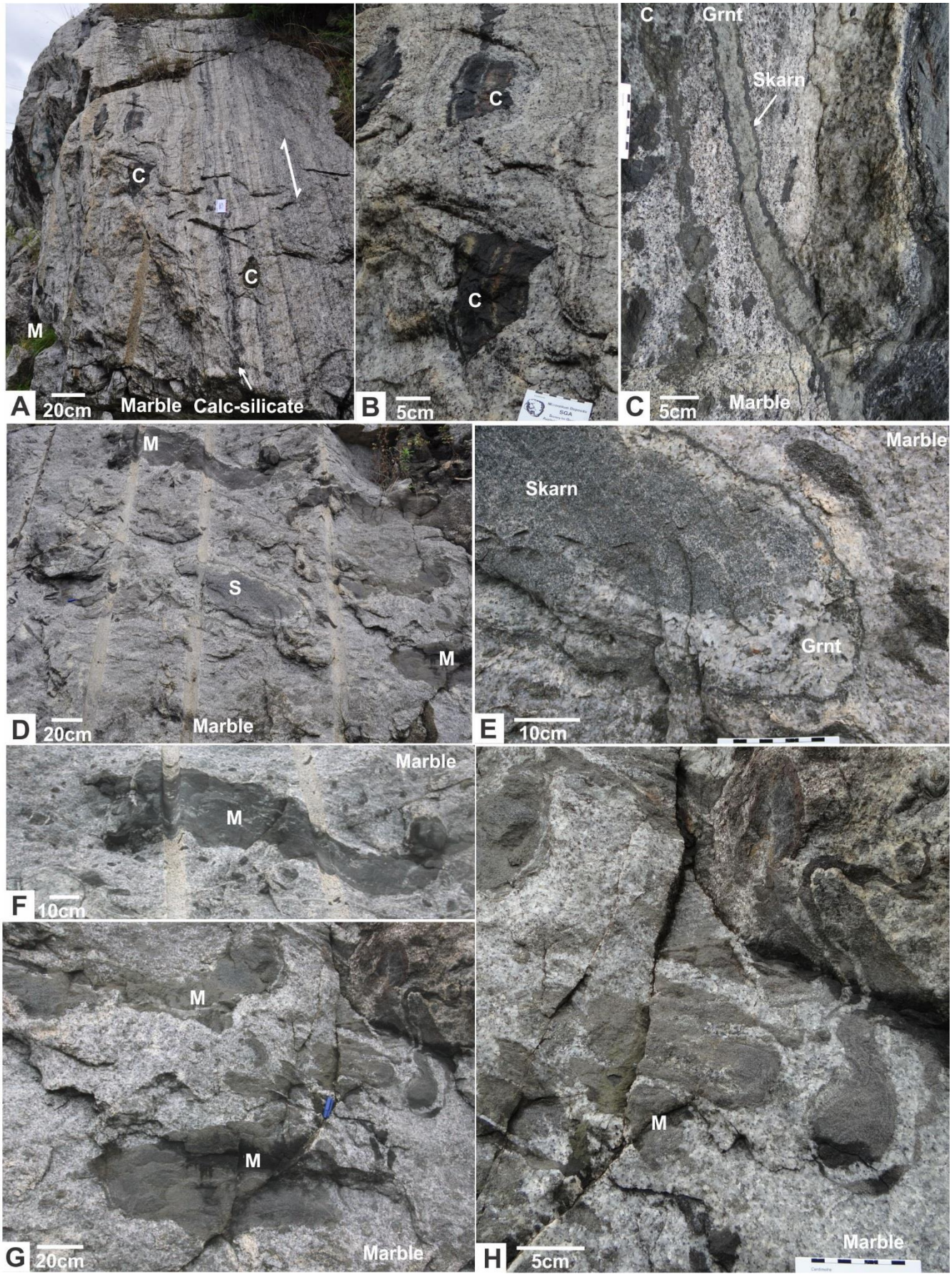
A
20cm
Marble
Calc-silicate
C
C
M
B
5cm
C
C
C
Grnt
Skarn
C
5cm
Marble
D
20cm
Marble
M
S
M
E
10cm
Marble
Skarn
Grnt
F
10cm
Marble
M
G
20cm
Marble
M
M
H
5cm
Marble
M

Figure 10.2. Stop 4.1. Marble tectonic breccia. **A.** Dismembered calc-silicate layers where large fragments are sparsely distributed along layering with warping of marble flow layering around fragments. Fine laminations within the marble are defined by 1) calc-silicate layers that are irregular in thickness with many calc-silicate clots and boudins (see layer at the tip of arrow for calc-silicate) and 2) different abundance of calc-silicate minerals (to the right of the arrow). **B.** Close-up of calc-silicate boudins with layering that suggest derivation form a sedimentary protolith. **C.** Granitic dyke with exoskarn along contact with marble. **D-E.** Enclave of skarns interpreted as a boudins of mafic and felsic magmas having reacted with marble to form skarns. **F-H.** Mafic enclaves with irregular to locally cuspate boundaries and convolute shapes.

: solid-state foliation; M: mafic enclave interpreted as emplaced in a magmatic state; S: skarn; C: enclaves of calc-silicate rocks most likely derived from the metamorphism of siliceous carbonate rocks and subsequently boudinaged (see Jiang 2010 for examples of deformed calc-silicate layers within a more ductile host).

Stop 4.1 presents a fairly chaotic outcrop pattern with numerous dismembered boudins of calc-silicate rocks and amphibolites (Fig. 10.1A). Marble displays a strong gneissosity that wraps around some of the xenoliths and not others (Figs. 10.1, 10.2). Laminations and layering consist of boudins and trains of calc-silicate rocks and minerals, largely diopsidite and diopside respectively. Granitic dykes with exo-skarns along its margins cut the marble tectonites and foliation (Fig. 10.2A, B). These dykes may belong to the granitic dyke swarm displayed at stop 10.2, which we provisionally included in the Lanthier suite as we did for the white granitic dykes at stop 1.5. The enclave at Figure 10.2E (also marked by S in Figure 10.2D) includes a mafic and a felsic (granitic) component. The mafic component is replaced by a skarn paragenesis. The granitic margin contains clinopyroxene and the margin of the entire enclave consists in an exo-skarn. The coupled mafic and felsic component may represent magmatic commingling with the availability of silica fostering the replacement of this magmatic enclave while others have not been megascopically replaced by skarn paragenesis.

A very distinct set of enclaves is observed at this outcrop: amphibolite enclaves with local cuspate boundaries with its host marble and swirly, convolute structures. They are best interpreted as resulting from magma flow within a very ductile medium that, itself, behaved like a more viscous magma as would felsic magmas. Some convolute enclaves and irregular margins of enclaves within deformed hosts are observed in metasedimentary rocks (cf. Davidson 1995b; Jiang 2010) however not at the extent that this outcrop records, which is much more similar to magma mingling structures. The brecciated structural pattern observed at this outcrop thus likely results from a high viscosity contrast between soft marble and much stronger calc-silicate and amphibolite and soft marble and similarly viscous crystallizing mafic magmas.

Stop 4.2
Tectono-magmatic evolution of the CMB-Q

This stop provides an overview of the tectono-magmatic evolution of the CMB in Québec and its interpretation is based on the regional geology and the regional tectono-magmatic markers described in detail in Corriveau (2013). Since the publication of this bulletin of the Geological Survey of Canada, new age data have been released by Davis and Nantel (2016) for the northern part of the CMB.

The outcrop is about 70 m west of the bridge at Grand Remous on the North side of Highway 117 (location 46°37'13.8"N 75°55'07.4"W; 46.620499, -75.918707). Rocks consist of garnet and biotite paragneisses and calc-silicate rocks including trains of granitic material, feldspar crystals, porphyroclastic leucosomes and pegmatitic intrusions, some of which dismembered to give the rock an apparently pervasive porphyroclastic texture. An amphibolite-facies gneissosity is pervasive and the trains of granitic material align within this foliation. A boudin enclosed within the S_2 foliated gneisses record the earlier S1 foliation so does the folded compositional layering and stromatitic leucosomes of Figure 10.2A, C. The gneissic host rocks are cut sharply by several dykes belonging to the 1.17-1.14 Ga Lanthier granitic suite, the 1.17 Ga Chevreuil intrusive suite and the 1.06 Ga Guénette granite suite (Figs. 10.3-10.7).

The gneissic structure of this outcrop markedly differs from that of other deformation corridors in the CMB-Q. Across the belt, regional markers of rocks non deformed after peak metamorphism have non foliated stromatitic leucosomes. Markers of post-peak metamorphism and pre-Chevreuil suite deformation consists of foliated, boudinaged and locally porphyroclastic stromatitic leucosomes and white pegmatite veins (Corriveau 2013). Regionally the stromatitic leucosomes formed between 1.19 and 1.18 Ga whereas the white pegmatites are most likely 1.18 Ga in age (Corriveau and van Breemen 2000; Corriveau 2013; Wodicka et al. 2004). Based on regional geology, we interpret the gneisses at this outcrop to have been metamorphosed to high-grade (likely granulite facies) at 1.19-1.20 Ga. Further to the South, relics of granulite facies parageneses and pressure-temperature conditions are preserved (Indares 1982; Indares and Martignole 1984). In their papers, these authors also described the amphibolite-facies retrogression of gneisses from granulite to amphibolite facies in line with regional field observations and petrological studies across the CMB-Q (e.g. Indares and Martignole 1990; Boggs, 1996; Boggs and Corriveau 2004).

Though at first glance the rock may look highly porphyroclastic, clear evidence of porphyroclasts does not prevail within the trails of granitic material. Figure10.2F displays evidence of recrystallized tails of the feldspathic fragments. In Figure 10.2E, the trains of feldspathic and granitic material display attributes of remnants of leucosomes left in their host after significant melt extraction (see Bons et al. 2008). Evidence for this include the lobate or diffuse margins of the leucosomes. Figure 10.2G is

especially telling as the quartz within the leucosome is not deformed. All pink leucosomes are undeformed, implying melt-present deformation. Nice subhedral crystals of K-feldspar typical of well crystallized leucosomes and coarse-grained granitic veins are illustrated in bottom-right of Figure 10.2D and in Figure 10.2G. On this basis, most of the strain shown along S_2 was likely acquired while melt was present and the granitic leucosomes and veins partly crystallized. Partial melting may thus have led to emplacement of stromatitic leucosomes along the S_2 gneissosity. Renewed deformation while melt was crystallizing, strongly deformed the granitic material which now largely consist of trains of granitic and feldspathic material and local porphyroclasts. These trains and the biotite defines the gneissosity S_2. Retrogression at amphibolite facies and the pervasiveness of the S_2 foliation is likely due to the ability of the water exsolved from the granitic leucosomes to react with former paragneisses to form the pervasive biotite-garnet assemblages. In the process, the parageneses of the former gneisses were pervasively retrograded to amphibolite facies. Mafic magma emplacement coevally with deformation of host paragenisses at amphibolite facies is recorded in the earlier stop (4.1). Such post-peak metamorphism and pre Chevreuil suite mafic dykes swarms metamorphosed at amphibolite facies are recognized across the CMB-Q but their ages have not been established yet.

White pegmatite veins were emplaced along the S2 gneissosity. They are deformed, commonly are tapered but not commonly boudinaged and locally internally foliated in a solid state though most internal fabrics results from magmatic compositional heterogeneities. These white pegmatites are interpreted to be 1.18 Ga in ages. They are most common within marbles and are commonly uraniferous (Lapointe 1995; Cuney and Kish 2004).

White granitic dykes cut sharply the gneissosity S2. The dykes have straight contact, are emplaced parallel to S2 or cut it and are interpreted to be coeval with the granitic dykes observed at Stop 1.5. We correlate such dykes with the Lanthier suite of Hébert and Nantel (1999) based on their granitic composition, and crosscutting relationships with their hosts and with the other suite of dykes. These white granitic dykes slightly predate, are coeval with and slightly postdate the Chevreuil suite and its mafic and commingled mafic-felsic dykes. The white granitic component of Chevreuil dykes resemble megascopically Lanthier dyke material. To our knowledge, no chemical analysis is available for the granitic component of the Chevreuil dyke nor of the white granitic dykes to see if they all belong to a single suite.

Chevreuil suite dykes regularly display syntectonic magma emplacement attributes within deformation corridors but are non-deformed within the Bondy gneiss complex as discussed in more depth at Chapter 5. At this stop, the Chevreuil dyke locally resembles a banded gneiss with felsic and mafic bands but as the dyke is followed longitudinally, magma-mingling textures can be seen to incrementally vary from

1. non-deformed (within extension jogs), to
2. slightly deformed with mafic pillow being slightly elongate with no megascopic internal foliation, to
3. moderately deformed with a pervasive solid state foliation defined by mafic clots within the mafic component and tightening of the granitic components (vein like aspect resulting from mingling with abundant mafic magmas) that results in apparent fold structures, and to
4. very locally highly deformed gneisses.

The Chevreuil dyke is replaced locally by metasomatic amphibole and plagioclase that display a coarse-grained texture (with internal recrystallization) and a patchy anatomosing distribution that recrystallize both the felsic anad mafic components of the dyke are destroy host textures (Fig. 10.7D-F). The Lanthier dykes parallel to gneissosity are fine grained, homogeneous and straight as are those within the conjugate set that cut gneissosity. These dykes differ from the white pegmatites in being not boudinage and in having sharp straight contacts with the paragneisses. The Guénette dyke is homogeneous, isotropic and equigranular. It cuts sharply both Lanthier and Chevreuil dykes.

As stated in our introductory statement for this stop, this very well exposed outcrop provides an exceptional wrap-up of the evolution of the CMB-Q. As illustrated in Corriveau and van Breemen (2000), Corriveau (2013) and Fig. 5.20, the western boundary of the CMB-Q has been subjected to granulite facies metamorphicms at 1.19 Ga based on field relationships of well dated metamorphic and intrusive markers across the belt and a microscopic and pressure-temperature record. Age of sedimentation remains poorly constrained but recent work suggests that maximal sedimentation age of some quartzites are younger than 1217 Ma and 1280 Ma with source rocks being in the younger sequence largely the gneiss complexes of the CMB-Q such as the Lacoste magmatic suite and the gneisses of the Bondy gneiss complex. These 1.45-1.35 Ga rocks (Wodicka et al. 2004; Davis and Nantel 2016) formed horsts within a continental back-arc basin that transects the margin of Laurentia (see chapter 5; Dickin and McNutt 2007; McLelland et al. 2013). The potentially older sedimentary sequence has a dominant 1.8 Ga source (Davis and Nantel 2016).

Chevreuil sheet intrusions emplaced along the main fabric of the deformation corridor along the western boundary of the CMB-Q are cut at right angle by Chevreuil dykes. As observed to the South, the Chevreuil dyke at stop 4.2 also cut the gneissosity along the deformation corridor at Grand Remous but relationships between Lanthier and Chevreuil dykes and structural information implied by conjugate emplacement of Lanthier dyke and synemplacement deformation of Chevreuil dyke need to be studied in more details. The Guénette granite dyke at stop 4.2 is highly typical of other dykes of this suite and represents the most westerly example we know of.

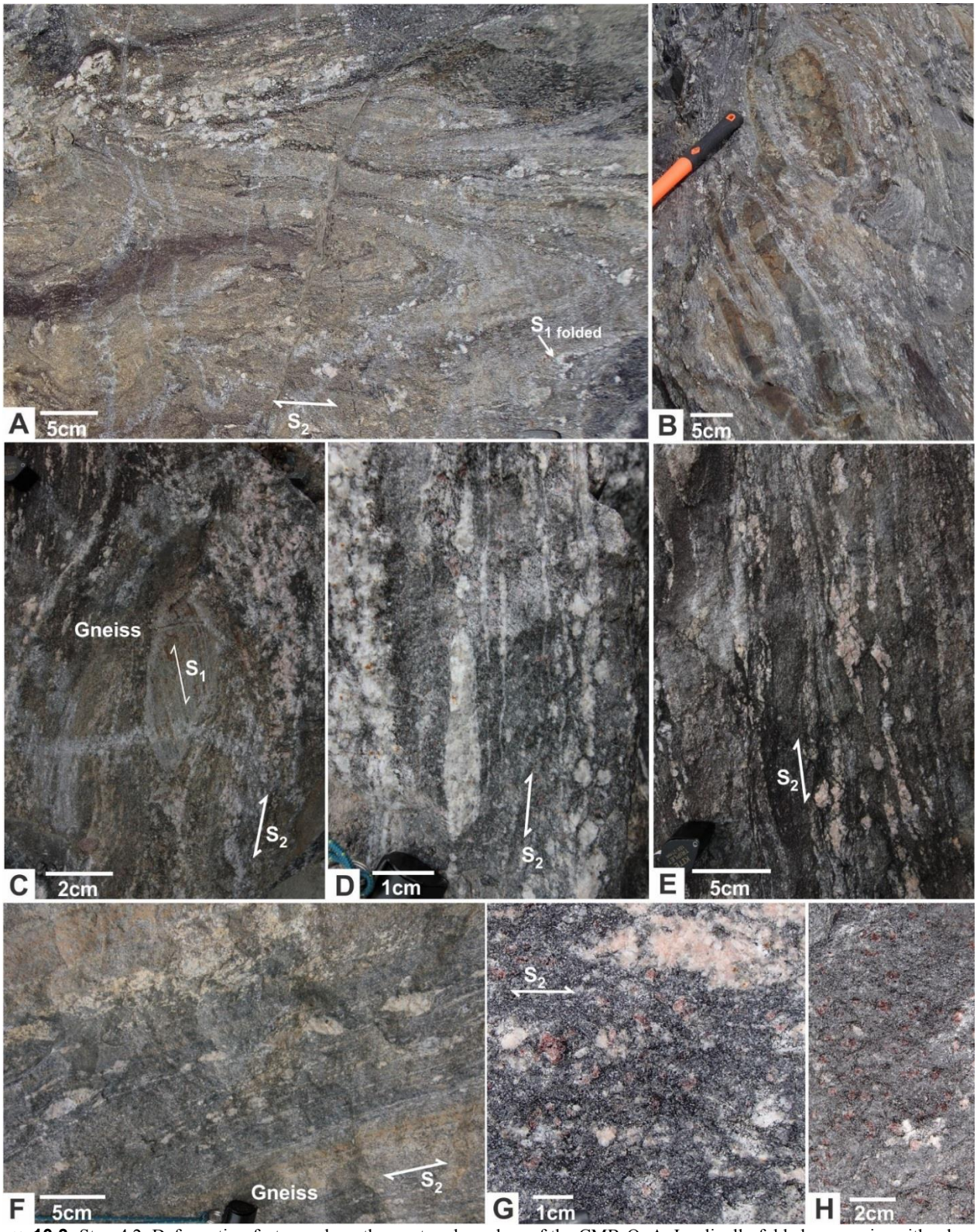

Figure 10.3. Stop 4.2. Deformation features along the western boundary of the CMB-Q. **A.** Isoclinally folded paragneiss with a layering interpreted to represent a primary compositional bedding transposed along the S_1 gneissosity. Axial plane foliation defined by biotite is parallel to the gneissosity S_2, which represents the main fabric across the outcrop. Trains of porphyroclasts follow the trace of axial planar foliation along S_2 whereas the least-deformed leucosomes are preserved within fold noses. They may preserve a record of folded S_1. **B.** Dismembered calc-silicate layers transposed parallel to S_2 within semi-pelitic, garnet-biotite paragneiss. Trains of porphyroclasts are interpreted as dismembered and deformed stromatitic leucosomes along S_2. **C.** Boudin of a gneiss preserving the S_1 foliation, and wraped around by S_2. **D-F.** Trains of white granitic porphyroclasts within garnet-biotite paragneiss. **G-H.** Close-up of garnet-biotite paragneiss and porphyroclastic leucosomes. ⟷: solid-state foliation S_1 and S_2.

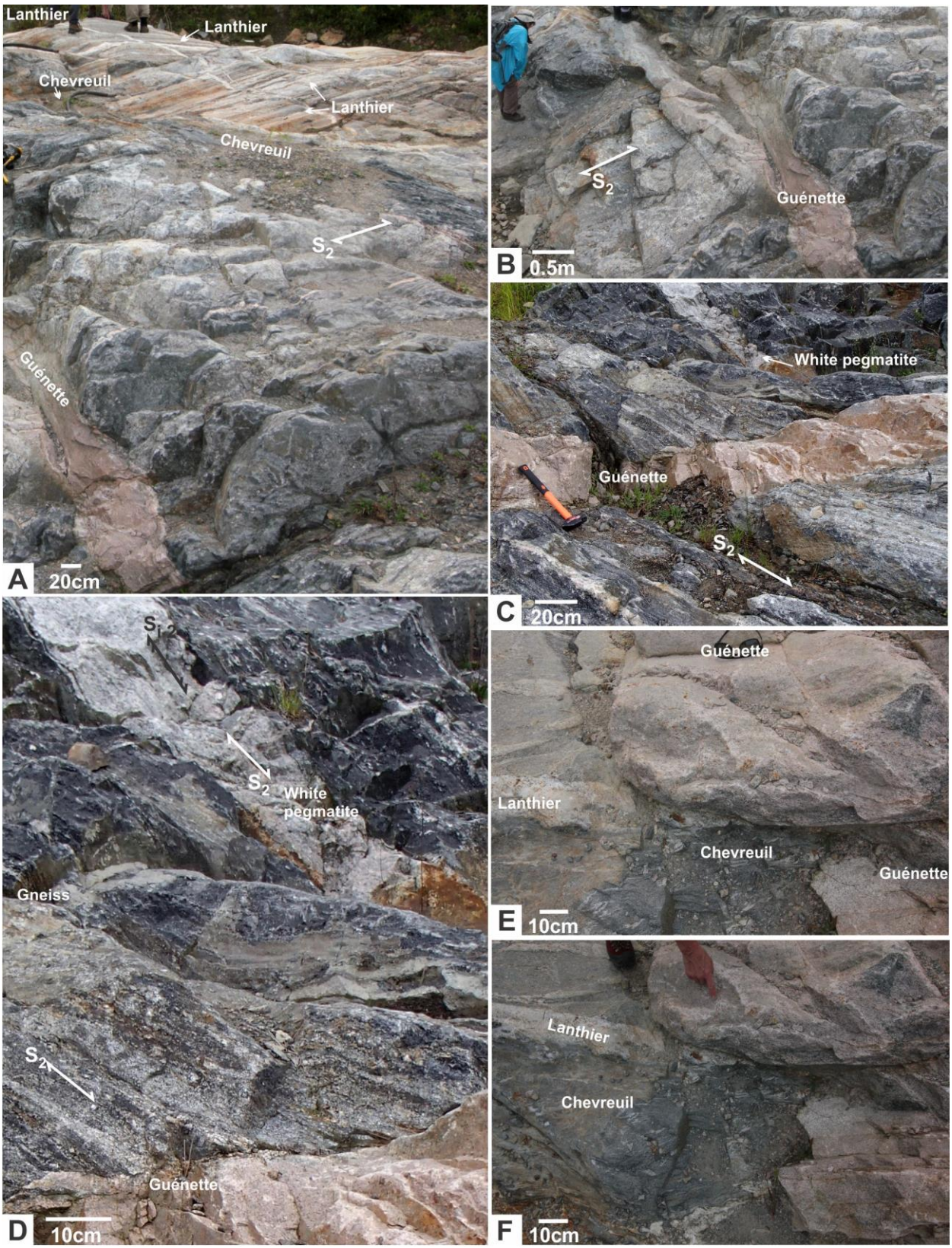

Figure 10.4. Relative crosscutting relationships between the 1.17-1.14 Ga Lanthier granitic suite, the 1.17 Ga Chevreuil intrusive suite and the 1.06 Ga Guénette granite suite with the host paragneiss. **A.** A Guénette dyke, a Chevreuil dyke and a set of Lanthier dykes cut across gneisses and trains of porphyroclasts. The Lanthier dykes form a conjugate set. **B.** Close-up of 'A' with more leucocratic gneisses among the garnet-biotite paragneisses. **C-D.** Deformed white pegmatite dykes with tapered zones and igneous S_{12} and solid-state S_2 foliation parallel to the gneissosity S_2. Variations in composition defined the igneous foliation within the dyke. **E-F.** Guénette dyke cutting across Chevreuil and Lanthier dykes. ⟶: solid-state foliation; ⟶: Igneous foliation within white pegmatite.

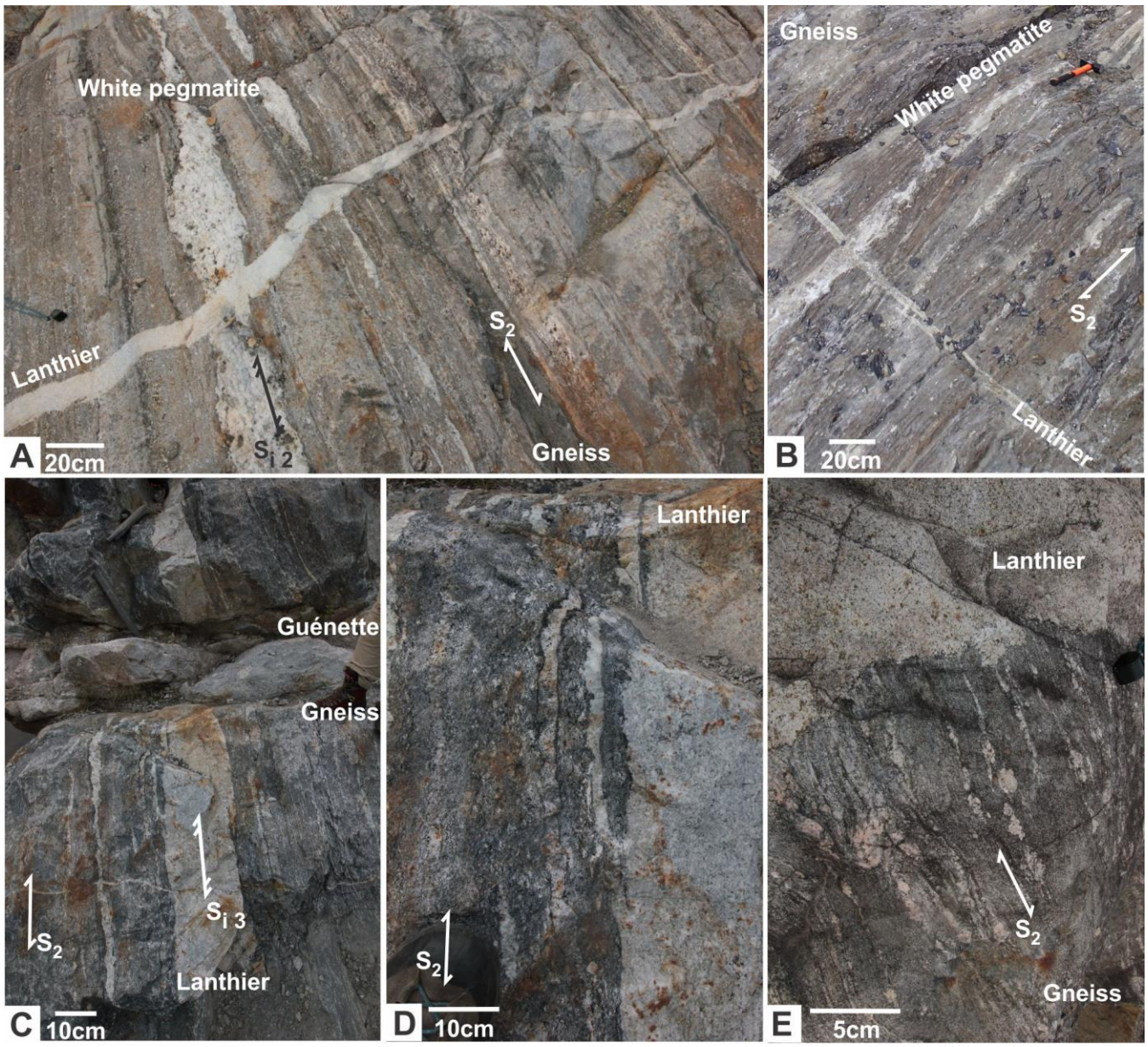

Figure 10.5. Space-time relationships between Lanthier dykes and host paragneisses. **A-B.** Lanthier dykes with sharp, fairly straight contacts cut deformed white pegmatite dykes and the porphyroclastic paragneisses. Note that dyke thickness in A increases sharply across a synmagmatic fault and that apophyses form locally. **C-D.** White Lanthier dyke emplaced parallel to gneissosity S_2 with apophysis cutting sharply across S_2. Note that the thickness of the dyke is fairly constant and contacts are straight. **E.** Close up of a Lanthier dyke cutting porphyroclastic paragneisses. ⟶: solid-state foliation; ⟶: Igneous foliation within white pegmatite and Lanthier dyke emplaced parallel to S_2.

Figure 10.6 (next page). Syntectonic emplacement of Chevreuil dyke after the development of the gneissosity S_2 highlighting renewed but partitioned deformation at 1.17 Ga (Corriveau and van Breemen 2000). **A-B.** Chevreuil dyke cuts the S_2 foliation of the paragneisses and is cut by a Guénette dyke. The Chevreuil dyke is composite with granitic and mafic magmas displaying internal commingled textures. In contrast, dyke margins are largely granitic with irregular internal contacts with the mafic and commingled component of the dyke. **C-G.** Internal commingled structure of the Chevreuil dyke and external granitic component. Note that in C, the dyke segment has been significantly deformed parallel to the dyke contact and original flow foliation. In D, folded veins are in fact the commingled granitic component between elongate mafic pillows. Further elongation of pillows and solid-state deformation has thinned the mafic pillows. Note that the thickness of the Chevreuil dyke in F greatly varies, increasing in an extensional jog with little commingling and sharply decreasing along strike with the commingled components forming elongate pillows. In D and G commingled granitic vein components are zoned with a pink coarser grain core and a white mantle. The mafic pillows have elongate shapes and cuspate boundaries well preserved in these segments of the dyke where solid-state deformation is minor. In D and E a similar zonation is observed along dyke contacts. ⟶: solid-state foliation in the gneiss (gneissosity S_2); ⟶: Igneous foliation, a solid-state fabric has significantly thinned the elongated mafic pillows defining the igneous foliation in A and C.

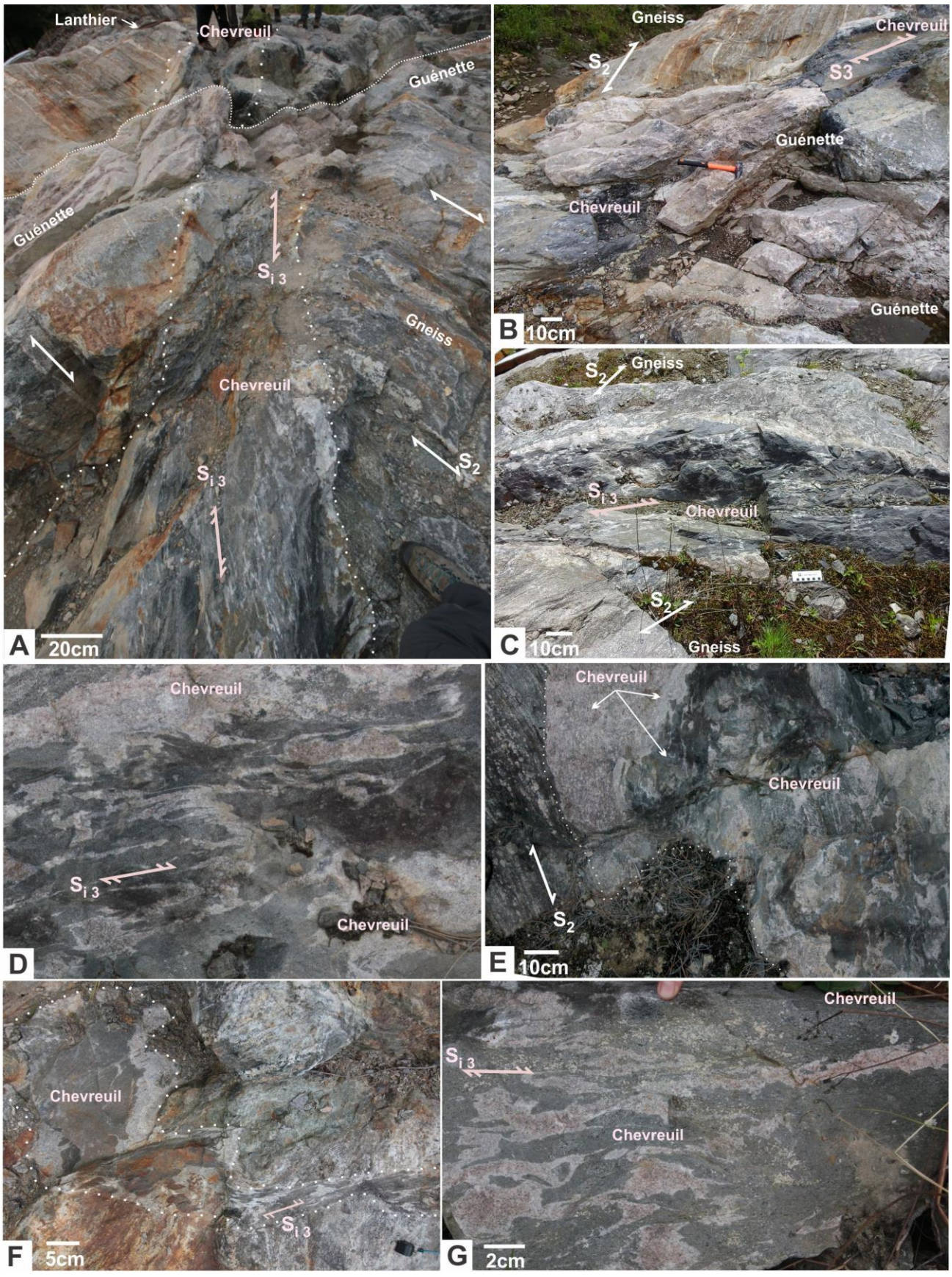
Lanthier
Chevreuil
Guénette
Guénette
$S_{i\,3}$
Gneiss
Chevreuil
S_2
$S_{i\,3}$
A 20cm
Gneiss
S_2
Chevreuil
S3
Guénette
Chevreuil
Guénette
B 10cm
S_2
Gneiss
$S_{i\,3}$
Chevreuil
S_2
Gneiss
C 10cm
Chevreuil
$S_{i\,3}$
Chevreuil
D
Chevreuil
Chevreuil
S_2
E 10cm
Chevreuil
$S_{i\,3}$
F 5cm
Chevreuil
$S_{i\,3}$
Chevreuil
G 2cm

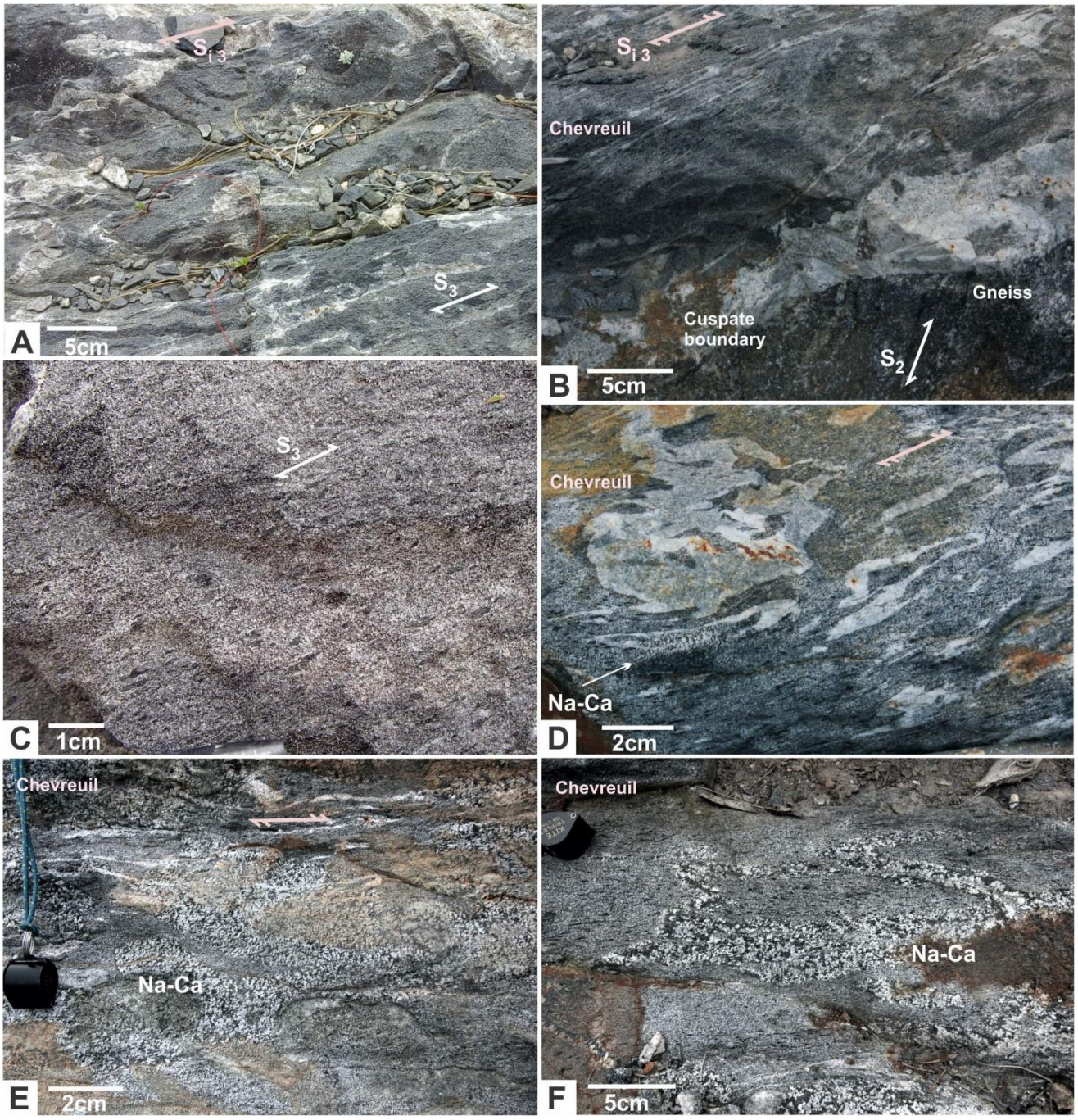

Figure 10.7. Solid-state deformation and metasomatism of a Chevreuil dyke. **A-D.** Solid-state deformation defined by the preferred orientation of mafic clots within the mafic component as shown in the close-up photo of C, whereas the flow foliation is best preserved by the commingled granitic vein components as shown in A and D. Solid-state elongation of pillows and increased transposition of granitic veins along the internal S3 foliation in D. **D-F.** Both the granitic and mafic components and magmatic and solid-state foliation fabrics are cut by anastomosing zones of homogeneous and isotropic metasomatic plagioclase and amphibole. Symbols as in Figure 10.6.

Stop 4.3
Lacoste gneiss

The stop is to the east of exit 162, highway 117 on Du Pont street. Park in the small stretch of road to the northwest. The most interesting outcrop is on the southeast side of Du Pont Street. The 1.40-1.36 Ga Lacoste gneiss was formed coevally with the volcanic rocks and tonalitic intrusions of the Bondy gneiss complex. The outcrop mainly consists of granitic and other felsic gneisses, interlayered with amphibolite layers. In contrast to the Labelle shear zone, the foliation is shallowly-dipping and the lineation is well developed. A mafic dyke with clinopyroxene phenocrysts overgrown by hornblende cuts across the foliation at a shallow angle (Fig. 10.8A). It displays textural attributes of the Chevreuil intrusive suite and as observed across the entire Central Metasedimentary Belt most of the strain was acquired before 1.17-1.16 Ga. Notice also the sulphide-rich late fault surfaces (Fig. 10.8B).

Stop 4.4
Labelle deformation zone

The Labelle deformation zone separates the CMB from the Morin Terrane (Fig. 10.9). It is a sub vertical zone of high strain ~5-10 km with complex kinematics probably involving an early sinistral shearing at granulite grade followed by normal shearing. This new outcrop on the east side of exit 142 on HW117 exposes highly deformed orthogneisses (Fig. 10.9A), metapelitic gneisses (Fig. 10.9B) and a marble breccia layers (Fig. 10.9F). Metapelite contains leucosome with large (0.5-1.5 cm) euhedral to subhedral garnet interpreted as peritectic crystals formed during biotite dehydration melting (Fig. 10.9B). This leucosome also contains sulphides (Fig. 10.4D). Near this leucosome, a calcite-rich vein cuts the foliation. Such veins are common in the Grenville Province. All rock types are highly deformed into straight gneiss (Fig. 10.9A), but lineation is not well-developed. The earliest lineation is down dip and formed locally by recrystallized garnet. In faces parallel to this lineation (and perpendicular to the foliation) normal-sense (Morin Terrane down) kinematic indicators can be observed locally (Fig. 10.9C). A sub horizontal lineation is observed locally (Fig. 10.9E), and seems to be younger than the down dip lineation. These observations contrast with the sinistral shearing at granulite grade overprinted by normal-sense shearing documented previously for the Labelle deformation zone (Martignole and Corriveau 1991; Zhao et al. 1997).

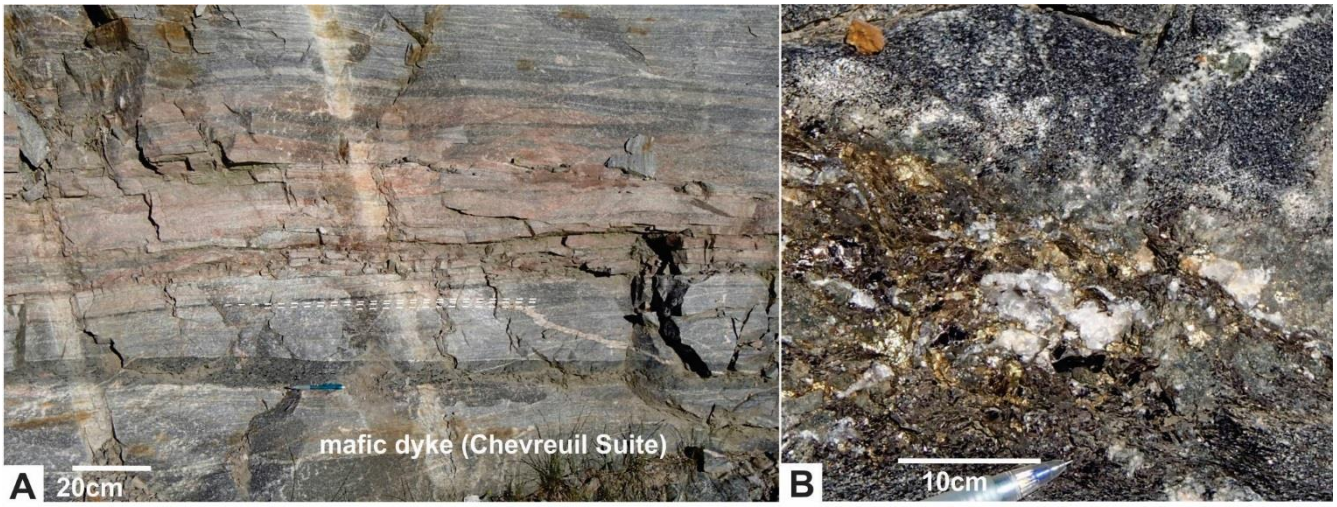

Figure 10.8. Rocks outside the Labelle deformation zone. **A.** Stop 4.4. Lacoste gneiss. The foliation (white stippled lines) is cut by a mafic dyke typical of the 1.17-1.16 Ga Chevreuil intrusive suite. **B.** Close-up of late-stage sulphides.

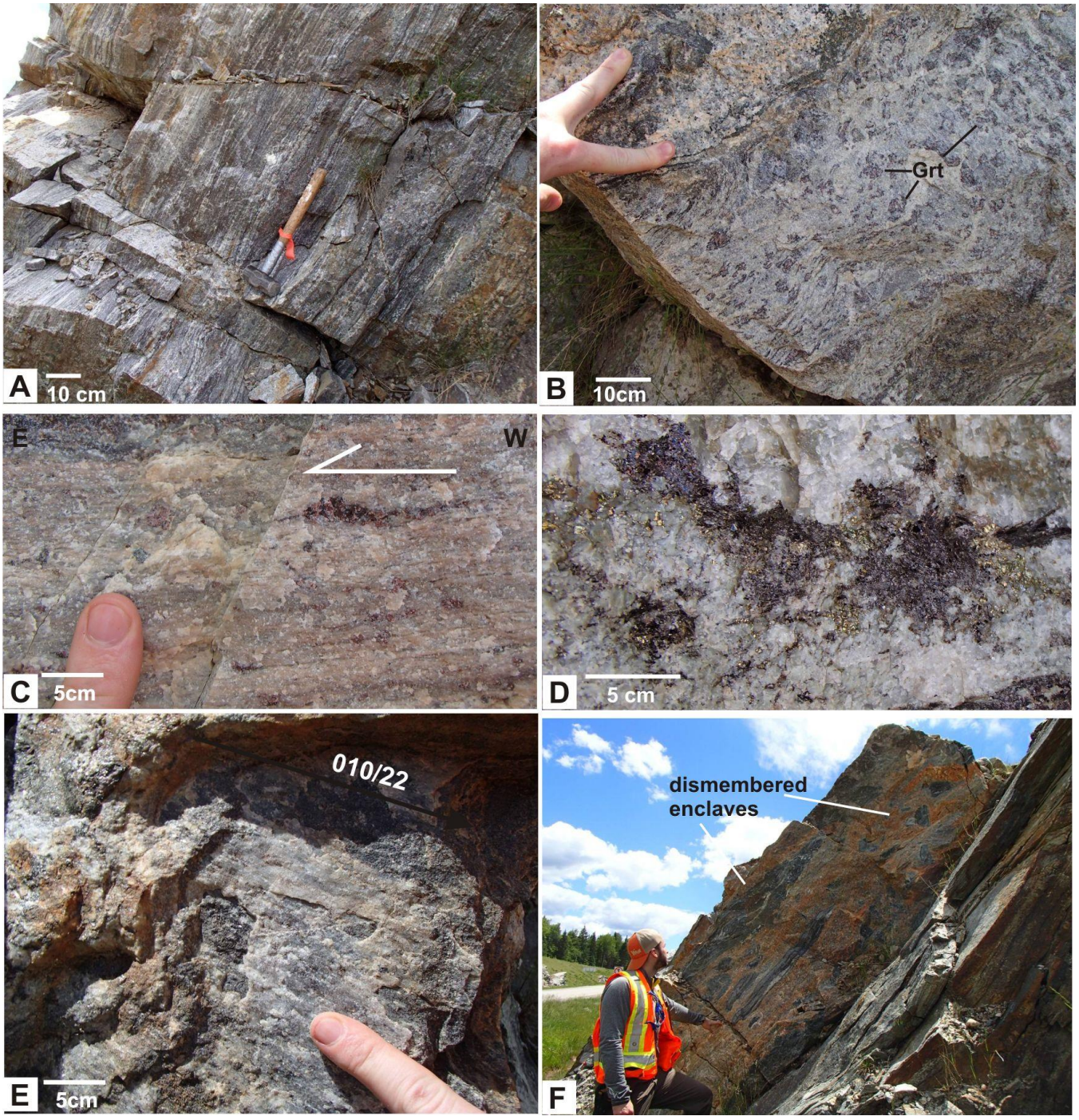

Figure 10.9. Stop 4.4. Labelle deformation zone. **A.** Subvertical straight gneiss. **B.** A garnet-bearing leucosome in a metapelitic gneiss. **C.** Sigma-type kinematic indicator formed by recrystallized garnet. The sense of shear is normal or Morin Terrane down. **D.** Leucosome in B is rich in sulphides. **E.** Second generation of lineation is sub horizontal. **F.** Marble tectonic breccia. See text for details.

Stop 4.5
Morin anorthosite

Garnet-clinopyroxene anorthosite of the 1.15 Ga Morin anorthosite (Fig. 10.10). Garnet forms coronae around clinopyroxene. Igneous textures are largely preserved except within localized shear zones.

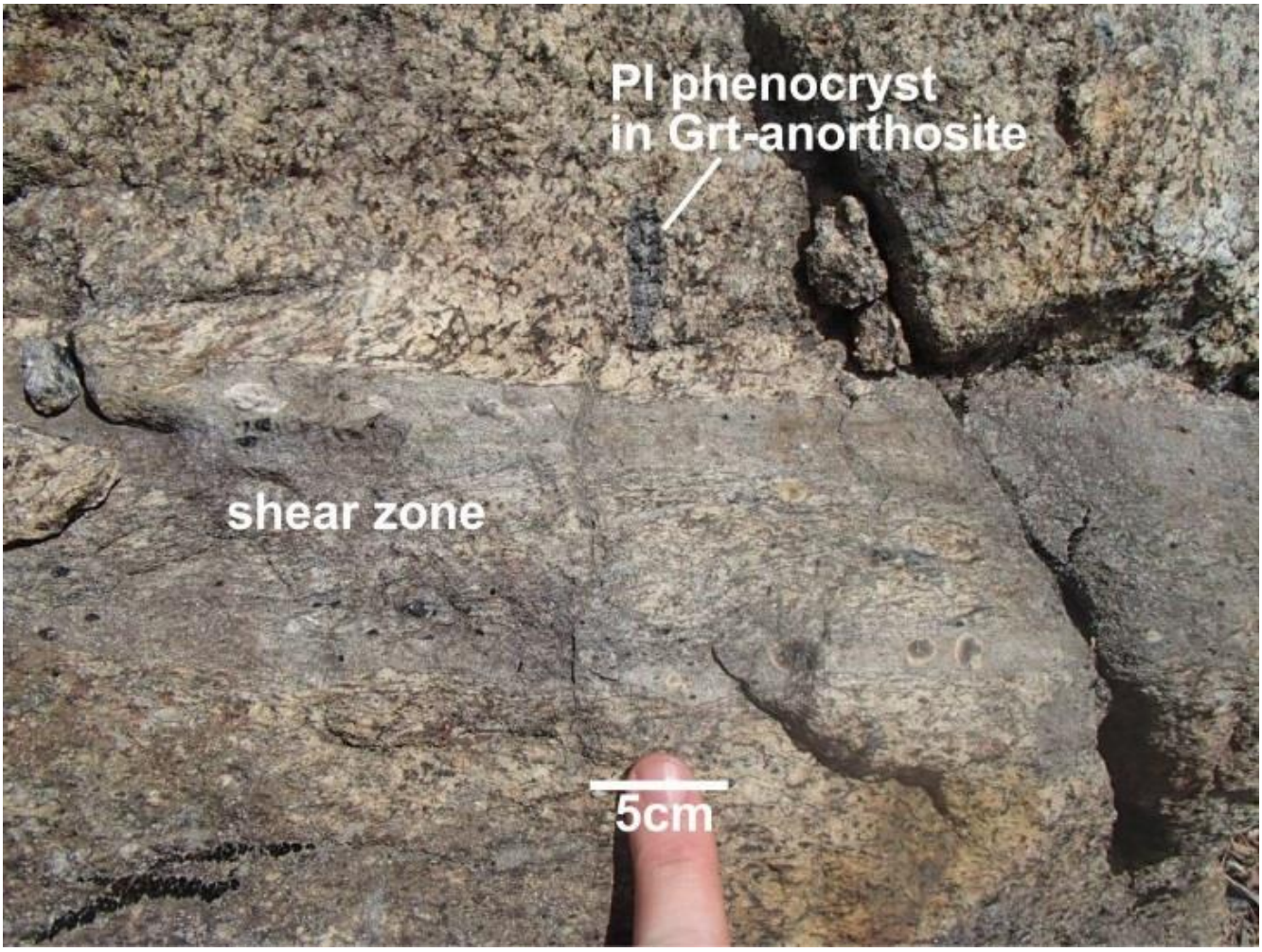

Figure 10.10. Stop 4.5. Garnet-bearing anorthosite with large plagioclase phenocrysts. The rock is largely non deformed apart from localized high-strain zones.

References

Acosta-Góngora, G.P., Gleeson, S.A., Samson, I., Ootes, L., and Corriveau, L., 2015. Gold refining by bismuth melts in the iron oxide-dominated NICO Au-Co-Bi (±Cu±W) deposit, NWT, Canada. Economic Geology, v. 110, p. 291–314.

Aleinikoff, J.N., Selby, D., Slack, J.F., Day, W.C., Pillers, R.M., Cosca, M.A., Seeger, C.M., Fanning, C.M., and Samson, I.M., 2016. U-Pb, Re-Os, and Ar/Ar geochronology of REE-rich breccia pipes and associated host rocks from the Mesoproterozoic Pea Ridge Fe-REE-Au deposit, St. Francois Mountains, Missouri. In: Slack, J., Corriveau, L., and Hitzman, M., eds., Proterozoic iron oxide-apatite (± REE) and iron oxide-copper- gold and affiliated deposits of Southeast Missouri, USA, and the Great Bear magmatic zone, Northwest Territories, Canada. Economic Geology, v. 111, p.1883–1914.

Allard, G.O., 1978. Pétrologie et potentiel économique du prolongement du sillon de roches vertes de Chibougamau dans la Province de Grenville. Ministère des Ressources naturelles du Québec, DPV 604.

Allard, G.O., 1979. Prolongement du Complexe du Lac Doré dans la Province de Grenville, à l'est de Chibougamau. Ministère de l'Énergie et des Ressources, Québec, DPV-685, 21 p.

Allard, G.O. and Carpenter, R.H., 1989. Mineralogical anomalies in metamorphosed terrains, a neglected but promising exploration tool. International Conference on the Geochemical Evolution of the Continental Crust, Pocos de Cladas, Brazil, p. 229–236.

Amelin, Y., Corriveau, L., and Morin, D., 1994. Constraints on the evolution of Grenvillian lithosphere from Nd-Sr-Pb clinopyroxene and garnet and U-Pb zircon study of pyroxenite and mafic granulitic xenoliths. United States Geological Survey Circular, v. 1107, p. 68.

Antonoff, V., Dufréchou, G., Harris, L.B., and La Flèche, M.R., 2007. Preliminary results of geophysical, field, and geochemical studies applied to mineral exploration in the Bondy gneiss complex, Grenville Province, SW Quebec. Richmond Minerals Inc., unpublished reports, 48 p.

Antonoff, V., La Flèche, M.R., Corriveau, L., Dufréchou, G., and Harris, L.B., 2010. Altération argilique avancée métamorphisée au sein du complexe gneissique de Bondy, Province de Grenville, Québec: Métallotecte pour l'exploration de systèmes de type épithermal métamorphisés? Quebec Exploration 2010 Abstract Volume.

Araujo, S.M., Fawcett, J.J., and Scott, S.D., 1995. Metamorphism of hydrothermally-altered rocks in a volcanogenic massive sulfide deposit: The Palmeirópolis, Brazil exemple. Revista Brasileria de Geociencias, v. 25, p. 173–184.

Augland, L.E., Moukhsil, A., Solgadi, F., and Indares, A., 2015. Pinwarian to Grenvillian magmatic evolution in the central Grenville Province: New constraints from ID–TIMS U–Pb ages and coupled Lu–Hf S–MC–ICP–MS data. Canadian Journal of Earth Sciences, v. 52, p. 701–721.

Bailie, R., Gutzmer, J., and Rajesh, H. M., 2010. Lithogeochemistry as a tracer of the tectonic setting, lateral integrity and mineralization of a highly metamorphosed Mesoproterozoic volcanic arc sequence on the eastern margin of the Namaqua Province, South Africa. Lithos, v. 119, p. 345–362.

Baker, J.H. and Hellingwerf, R.H., 1986. Rare-earth elements in lithochemical prospecting for W-Mo-Au mineralized granites and related high- and low-temperature skarns [abs.]: Institute of Geology and Mineral Exploration and Association of Exploration Geologists Internat. South Symposium on Exploration Geochemistry, Athens, program with abstracts, p. 15.

Benavides, J., Kyser, T.K., Clark, A.H., Stanley, C., and Oates, C., 2008. Exploration guidelines for copper-rich iron oxide-copper-gold deposits in the Mantoverde area, northern Chile: the integration of host-rock molar element ratios and oxygen isotope compositions. Geochemistry: Exploration, Environment, Analysis, v. 8, p. 343–367.

Bernier, L.R. and MacLean, W.H., 1993. Lithogeochemistry of a metamorphosed VMS alteration zone at Montauban, Grenville Province. Exploration Mining Geology, v. 2, p. 367–386.

Blein, O. and Corriveau, L., 2017. Recognizing IOCG alteration facies at granulite facies in the Bondy gneiss complex of the Grenville Province. SGA 2017, 14th SGA biennial meeting, Canada, Proceedings, p. 907–910.

Blein, O., La Flèche, M.R., and Corriveau, L., 2003. Geochemistry of the granulitic Bondy gneiss complex: 1.4 Ga arc in the Central Metasedimentary Belt. Grenville Province, Canada. Precambrian Research, v. 120, p. 193–218.

Blein, O., Corriveau, L., and La Flèche, M., 2004. Cordierite-orthopyroxene white gneiss: A key to unveiling pre-metamorphic hydrothermal activity in the Bondy gneiss complex, Grenville Province, Québec. In Tollo, R., Corriveau, L., McLelland, J., and Bartolomew, M., eds., Proterozoic tectonic evolution of the Grenville Province in eastern North America. Geological Society of America, Memoir 197, p. 19–33.

Boggs, K.J.E., 1996. Retrograde cation exchange in garnets during slow cooling of mid crustal granulites and the P-T-t trajectories from the Mont-Laurier region, Grenville Province, Québec. M.Sc. thesis, Université du Québec à Chicoutimi, Chicoutimi, Quebec, 333 p.

Boggs, K.J.E. and Corriveau, L., 2004. Granulite P-T-t paths and retrograde cation diffusion from the Mont-Laurier area, southwestern Grenville Province, Quebec. In Tollo, R., Corriveau, L., McLelland, J., and Bartolomew, M., eds., Proterozoic tectonic evolution of the Grenville Province in eastern North America. Geological Society of America, Memoir 197, p. 35–64.

Boggs, K.J.E., van Breemen, O., Corriveau, L., and Sawyer, E.W., 1994. New insights on metamorphism in the Central Metasedimentary Belt of Québec, Grenville Province. Mineralogical Magazine, v. 58A, p. 105–106.

Bonnet, A.-L. and Corriveau, L., 2007a. Alteration vectors to metamorphic hydrothermal systems in gneissic terranes. In Goodfellow, W.D., ed., Mineral deposits of Canada: A synthesis of major deposit-types, district metallogeny, the evolution of geological provinces, and exploration methods. Geological Association of Canada, Mineral Deposits Division, Special Publication 5, p. 1035–1049.

Bonnet, A.-L. and Corriveau, L., 2007b. Atlas et outils de reconnaissance de systèmes hydrothermaux métamorphisés dans les terrains gneissiques. In Goodfellow, W.D. (ed.) Mineral deposits of Canada: a synthesis of major deposit-types, district metallogeny, the evolution of geological provinces, and exploration methods. Geological Association of Canada, Mineral Deposits Division, Special Publication 5, DVD, 95p.

Bonnet, A.-L., Corriveau, L., and La Flèche, M. R., 2005. Chemical imprint of highly metamorphosed volcanic-hosted hydrothermal alterations in the La Romaine Supracrustal Belt, eastern Grenville Province, Quebec. Canadian Journal of Earth Sciences, v. 42, p. 1783–1814.

Bons, P.D., Druguet, E., Castaño, L.-M., and Elburg, M.A., 2008. Finding what is now not there anymore: Recognizing missing fluid and magma volumes. Geology, v. 36, p. 851–854.

Cadéron, S., Roy, P., Bandyayera, D., and Sharma, K., 2005. Étude métamorphique d'un segment du Front du Grenville. Ministère des Resources naturelles et de la Faune du Québec, RP 2005-03, 12 p.

Campbell, I.H., Lesher, C.M., Coad, P., Franklin, J.M., Gorton, M.P., and Thurston, P., 1984. Rare-earth element mobility in alteration pipes below massive Cu-Zn-sulfide deposits. Chemical Geology, v. 45, p. 181–202.

Carter, N.L. and Tsenn, M.C., 1987. Flow properties of continental

lithosphere. Tectonophysics, v. 136, p. 27–63.
Charbonneau, R. and Robillard, I., 2016. Technical report on WHN-Boisvert property, Upper Laurentians, Quebec, Canada. kintavar.com/wp-content/uploads/2017/04/43-101_WHN.pdf; access July 6th 2017.
Chen, H., 2013. External sulphur in IOCG mineralization: Implications on definition and classification of the IOCG clan. Ore Geology Reviews, v. 51 p. 74–78.
Chiarenzelli, J., Lupulescu, M., Thern, E., and Cousens, B., 2011. Tectonic implications of the discovery of a Shawinigan ophiolite (Pyrites Complex) in the Adirondack Lowlands. Geosphere, v. 7, p. 333–356.
Chiarenzelli, J., Kratzmann, D., Selleck, B., and de Lorraine, W., 2015. Age and provenance of Grenville Supergroup rocks, Trans-Adirondack Basin, constrained by detrital zircons. Geology, v. 43, p. 183–186.
Ciobanu, C.L., Cook, N.J., Damian, F., and Damina, G., 2006. Gold scavenged by bismuth melts: An example from Alpine shear-remobilizates in the Highiş Massif, Romania. Mineralogy and Petrology, v. 87, p. 351–383.
Clark, T., 2003. Métallogénie des métaux usuels, précieux et énergétiques, et des éléments des terres rares, région de Manitou-Wakeham, Moyenne-Côte-Nord. In Brisebois, D. and Clark, T., eds., Synthèse géologique et métallogénique de la partie est de la Province de Grenville. Ministère des Ressources naturelles, Québec, DV 2002-03.
Clark, T., Gobeil, A., and David, J., 2005. Iron oxide–Cu–Au-type and related deposits in the Manitou Lake area, eastern Grenville Province, Quebec: Variations in setting, composition, and style. In Corriveau, L. and Clark, T., eds., The Grenville Province: A geological and mineral resources perspective derived from government and academic research initiatives. Canadian Journal of Earth Sciences, v. 42, p. 1829–1847.
Clark, T., Gobeil, A., and Chevé, S., 2010. Alterations in IOCG-type and related deposits in the Manitou Lake area, Eastern Grenville Province, Québec. In Corriveau, L. and Mumin, A.H., eds., Exploring for iron oxide copper-gold deposits: Canada and global analogues. Geological Association of Canada, Short Course Notes 20, p. 127–146.
Coker, W.B., 2010. Future research directions in exploration geochemistry. Geochemistry: Exploration, Environment Analysis, v. 10, p. 75–80.
Connolly, J.A.D., 2005. Computation of phase equilibria by linear programming: A tool for geodynamic modeling and its application to subduction zone decarbonation. Earth and Planetary Science Letters, v. 236, p. 524–541.
Connolly, J.A.D. and Petrini, K., 2002. An automated strategy for calculation of phase diagram sections and retrieval of rock properties as a function of physical conditions. Journal of Metamorphic Geology, v. 20, p. 697–708.
Corrigan, D. and van Breemen, O., 1997. U-Pb age constraints for the lithotectonic evolution of the Grenville Province along the Mauricie transect, Quebec. Canadian Journal of Earth Sciences, v. 34, p. 299–316.
Corriveau, L., 2007. Fe oxide copper-gold deposits: a Canadian perspective. In Goodfellow, W.D. (ed.) Mineral deposits of Canada: a synthesis of major deposit-types, district metallogeny, the evolution of geological provinces, and exploration methods. Geological Association of Canada, Mineral Deposits Division, Special Publication 5, p. 307–328.
Corriveau, L., 2013. Architecture de la ceinture métasédimentaire centrale au Québec, Province de Grenville: Un exemple de l'analyse de terrains de métamorphisme élevé. Commission Géologique du Canada, Bulletin 586, 252 p.
Corriveau, L., 2017a, Iron-oxide and alkali-calcic alteration ore systems and their polymetallic IOA, IOCG, skarn, albitite-hosted U±Au±Co, and affiliated deposits: A short course series. Part 1: Introduction. Geological Survey of Canada, Scientific Presentation 56, 1 ppt file. doi:10.4095/300241.
Corriveau, L., 2017b, Les systèmes minéralisateurs à oxydes de fer et altération à éléments alcalins (±calciques) et leurs gîtes IOA, IOCG, skarns, U±Au±Co (au sein d'albitites) et affiliés: Une série de cours intensifs. Partie 1: Introduction. Geological Survey of Canada, Scientific Presentation 57, doi:10.4095/300242.
Corriveau, L. and Bonnet, A.-L., 2005. Pinwarian (1.5 Ga) volcanism and hydrothermal activity at the eastern margin of the Wakeham Group, Grenville Province, Quebec. In Corriveau, L. and Clark, T., eds., The Grenville Province: A geological and mineral resources perspective derived from government and academic research initiatives. Canadian Journal of Earth Sciences, v. 42, p. 1749–1782.
Corriveau, L. and Clark, T., 2005. The Grenville Province: A geological and mineral resources perspective derived from government and academic research initiatives. In Corriveau, L. and Clark, T., eds., The Grenville Province: A geological and mineral resources perspective derived from government and academic research initiatives. Canadian Journal of Earth Sciences, v. 42, p. 1637–1642.
Corriveau, L. and Gorton, M.P., 1993. Coexisting K-rich alkaline and shoshonitic magmatism of arc affinities in the Proterozoic: A reassessment of syenitic stocks in the southwestern Grenville province. Contributions to Mineralogy and Petrology, v. 113, p. 262–279.
Corriveau, L. and Jourdain, V., 1992. Terrane characterization in the Central Metasedimentary Belt of the southern Grenville orogen: The Lac Nominingue map area. Geological Survey of Canada, Current Research Paper 92-1C, p. 81–90.
Corriveau, L. and Jourdain, V., 1993. Géologie de la région de Lac Nominingue, Québec (SNRC 31J/6). Geological Survey of Canada, Open File 2641, 1 annotated map.
Corriveau, L. and Leblanc, D., 1995. Sequential nesting of magmas in marble, SW Grenville Province, Québec: From fracture propagation to diapirism. Tectonophysics, v. 246, p. 183–200.
Corriveau, L. and Madore, L., 1994. Géologie de la région de Duhamel, Québec (SNRC 31J/3). Geological Survey of Canada, Open File 2918, 1 annotated map.
Corriveau, L. and Morin, D., 2000. Modelling 3D architecture of western Grenville from xenoliths, styles of magma emplacement and Lithoprobe reflectors. Canadian Journal of Earth Sciences, v. 37, p. 235–251.
Corriveau, L. and Mumin, A.H., 2010. Exploring for iron oxide copper-gold deposits: The need for case studies, classifications and exploration vectors. In Corriveau, L. and Mumin, A.H., eds., Exploring for iron oxide copper-gold deposits: Canada and global analogues. Geological Association of Canada, Short Course Notes 20, p. 1–12.
Corriveau, L. and Rivard, B., 1997. From source to surface: Extraction, transport and emplacement of magmas from a Grenvillian perspective, Quebec. Geological Association of Canada/ Mineralogical Association of Canada, Guidebook B4, 82 p.
Corriveau, L. and Spry, P., 2014. Metamorphosed hydrothermal ore deposits. In Holland, H.D. and Turekian, K.K., eds., Treatise on Geochemistry, Second Edition, Oxford, Elsevier, v. 13, p. 175–194.
Corriveau, L. and van Breemen, O., 2000. Docking of the Central Metasedimentary Belt to Laurentia in geon 12: Evidence from the 1.17–1.16 Ga Chevreuil intrusive suite and host gneisses, Quebec. Canadian Journal of Earth Sciences, v. 37, p. 253–269.
Corriveau, L., Gold, D., Bédard, J., and Bourne, J., 1989. Alkaline and calc-alkaline complexes of southern Québec. Geological Association of Canada/ Mineralogical Association of Canada, Guidebook B3, 129 p.
Corriveau, L., Heaman, L.M., Marcantonio, F., and van Breemen, O., 1990. 1.1 Ga K-rich alkaline plutonism in the southwestern Grenville Province: U-Pb constraints for the timing of subduction-related magmatism. Contributions to Mineralogy and Petrology, v. 105, p. 473–485.
Corriveau, L., Morin, D., and Madore, L., 1994. Géologie et cibles

d'exploration de la partie centre-est de la Ceinture métasédimentaire du Québec, Province de Grenville. Geological Survey of Canada, Current Peseach Paper 94-C, p. 355–365.

Corriveau, L., Morin, D., van Breemen, O., Rivard, B., Tremblay, P., Boggs, K., and Deschênes, G., 1995. Magmatisme et hydrothermalisme dans la Ceinture métasédimentaire du Québec; implications tectoniques et métallogéniques. Fieldtrip guidebook, Friends of Grenville, 28 p.

Corriveau, L., Morin, D., Tellier, M., Amelin, Y., and van Breemen, O., 1996a. Insights on minette emplacement and the lithosphere underlying the southwest Grenville Province of Québec at 1.08 Ga. In LeCheminant, A.N., Richardson, D.G., Dilabio R.N.W., and Richardson, K.A., eds., Searching for diamond in Canada. Geological Survey of Canada, Open File 3228, p. 139–142.

Corriveau, L., Tellier, M.L., and Morin, D., 1996b. Le dyke de minette de Rivard et le complexe gneissique cuprifère de Bondy; implications tectoniques et métallogéniques pour la région de Mont-Laurier, province de Grenville, Québec. Geological Survey of Canada, Open File 3078.

Corriveau, L., Blein, O., and La Flèche, M.R., 1997. Progress report on the Bondy gneiss complex and its cupriferous hydrothermal system, Mont-Laurier area. Ministère des Ressources naturelles, Québec, GM 54804, 133 p., 1 map.

Corriveau, L., Rivard, B., and van Breemen, O., 1998. Rheological controls on Grenvillian intrusive suites: Implications for tectonic analysis. Journal of Structural Geology, v. 20, p. 1191–1204.

Corriveau, L., Perreault, S., and Davidson, A., 2007. Prospective metallogenic settings of the Grenville Province. In Goodfellow, W.D., ed., Mineral deposits of Canada: A synthesis of major deposit-types, district metallogeny, the evolution of geological provinces and exploration methods. Geological Association of Canada, Mineral Deposits Division, Special Publication 5, p. 819–848.

Corriveau, L., Williams, P.J., and Mumin, A.H., 2010. Alteration vectors to IOCG mineralization: From uncharted terranes to deposits. In Corriveau, L. and Mumin, A.H., eds., Exploring for iron oxide copper-gold deposits: Canada and global analogues. Geological Association of Canada, Short Course Notes 20, p. 89–110.

Corriveau, L., Nadeau, O., Montreuil, J.-F., and Desrocher, J.-P., 2014. Report of activities for the Core Zone: Strategic geomapping and geoscience to assess the mineral potential of the Labrador Trough for multiple metals IOCG and affiliated deposits, Canada. Geological Survey of Canada, Open File 7714, 12 p.

Corriveau, L., Lauzière, K., Montreuil, J.-F., Potter, E., Prémont, S., and Hanes, R., 2015. Dataset of new lithogeochemical analysis in the Great Bear magmatic zone, Northwest Territories, Canada. Geological Survey of Canada, Open File 7643, 24 p.

Corriveau, L., Montreuil, J.-F., and Potter, E.G., 2016. Alteration facies linkages among IOCG, IOA and affiliated deposits in the Great Bear magmatic zone, Canada. In Slack, J., Corriveau, L., and Hitzman, M., eds., Proterozoic Iron Oxide-Apatite (± REE) and Iron Oxide-Copper-Gold and Affiliated Deposits of Southeast Missouri, USA, and the Great Bear Magmatic Zone, Northwest Territories, Canada. Economic Geology, v. 111, p. 2045–2072.

Corriveau, L., Potter, E., Acosta-Gongora, P., Blein, O., Montreuil, J.-F., De Toni, A.F., Day, W.C., Slack, J.F., and Ayuso, R.A., 2017. Petrological mapping and chemical discrimination of alteration facies as vectors to IOA, IOCG, and affiliated deposits within Laurentia and beyond. SGA 2017, 14th SGA biennial meeting, Canada, Proceedings, p. 851–854.

Corriveau, L., Potter, E.G., Montreuil, J.-F., Blein, O., Ehrig, K., De Toni, A., 2018. Iron-oxide and alkali-calcic alteration ore systems and their polymetallic IOA, IOCG, skarn, albitite-hosted U±Au±Co, and affiliated deposits: A short course series. Part 2: Overview of deposit types, distribution, ages, settings, alteration facies, and ore deposit models. Geological Survey of Canada, Scientific Presentation 81, 154 p.

Cuney, M. and Kish, L., 2004. Minéralisations uranifères et fusion crustale: l'exemple de Mont Laurier (Québec, Canada). 72ième congrès de l'ACFAS, C-202 Premières journées De Launay, Program with abstracts, accessed at www.acfas.ca, March 25th 2008.

Davidson, A., 1995a. A review of the Grenville orogen in its North American type area. AGSO Journal of Australian Geology and Geophysics, v. 16, p. 3–24.

Davidson, A., 1995b, Tectonic history of the Grenville Province, Ontario. Geological Survey of Canada, Open File 3142, 150 p.

Davidson, A., Easton, R.M., Corriveau, L., and Martignole, J., 2002. Transect of the Southwestern Grenville Province. Field Trip B6 Guidebook, Geological Association of Canada-Mineralogical Association of Canada, Joint Annual Meeting, 119 p.

Davis, D.W. and Nantel, S., 2016. Datations U-Pb dans la partie nord de la Ceinture centrale des métasédiments, Province de Grenville, région de Mont-Laurier. Ministère de l'Énergie et des Ressources du Québec, MB 2016-04, 52 p.

Day, W.C., Aleinikoff, J.N., du Bray, E., and Ayuso, R.A., 2017. Constraints on ages of magmatism and iron oxide-apatite (IOA) and iron oxide-copper-gold (IOCG) mineral deposit formation in the Mesoproterozoic St. Francois Mountains Terrane of Southeast Missouri, USA. SGA 2017, 14th SGA biennial meeting, Canada, Proceedings, p. 855–858.

de Capitani, C. and Petrakakis, K., 2010. The computation of equilibrium assemblage diagrams with Theriak/Domino software. American Mineralogist, v. 95, p. 1006–1016.

de Lorraine, W.F., 2001. Metamorphism, polydeformation, and extensive remobilization of the Balmat zinc orebodies, northwest Adirondacks, New York. Society of Economic Geologists Guidebook Series 35, p. 25–54.

De Toni, A.F., 2016. Les paragénèses à magnétite des altérations associées aux systèmes à oxydes de fer et altérations en éléments alcalins, zone magmatique du Grand lac de l'Ours. Unpublished M.Sc. thesis, Institut National de la Recherche Scientifique, Quebec, Canada, 529 p.

Dickin, A.P., 2000. Crustal formation in the Grenville Province: Nd-isotope evidence. Canadian Journal Earth Sciences, v. 37, p. 165–181.

Dickin, A.P. and McNutt, R.H., 2007. The Central Metasedimentary Belt (Grenville Province) as a failed back-arc rift zone: Nd isotope evidence. Earth and Planetary Science Letters, v. 259, p. 97–106.

Doig, R., 1991. U-Pb zircon dates of Morin anorthosite suite rocks, Grenville Province, Quebec. Journal of Geology, v. 99, p. 729–738.

Dufréchou, G. and Harris, L.B., 2013. Tectonic models for the origin of regional transverse structures in the Grenville Province of SW Quebec interpreted from regional gravity. Journal of Geodynamics, v. 64, p. 15–39.

Dufréchou, G., Harris, L.B., Corriveau, L., and Antonoff, V., 2011. Gravity evidence for a mafic intrusion beneath a mineralized zone in the Bondy gneiss complex, Grenville Province, Quebec - exploration implications. Journal of Applied Geophysics, v. 75, p. 62–76.

Dufréchou, G., Harris, L.B., and Corriveau, L., 2014. Tectonic reactivation of transverse basement structures in the Grenville orogen of SW Quebec, Canada: Insights from gravity and aeromagnetic data. Precambrian Research, v. 241, p. 61–84.

Dufréchou, G., Harris, L.B., Corriveau, L., and Antonoff, V., 2015. Regional and local controls on mineralization and pluton emplacement in the Bondy gneiss complex, Grenville Province, Canada interpreted from aeromagnetic and gravity data. Journal of Applied Geophysics, no. 116, p. 192–205.

Dunning, G. and Indares, A., 2010. New insights on the 1.7–1.0 Ga crustal evolution of the central Grenville Province from the Manicouagan–Baie Comeau transect. Precambrian Research, v. 180, p. 204–226.

Duquet, M. and Easton, M., 2017. Friends of the Grenville 2017 field trip, Renfrew, Ontario. Friends of Grenville Guidebook.

Ehrig, K., McPhie, J., and Kamenetsky, V., 2012. Geology and

mineralogical zonation of the Olympic Dam iron oxide Cu-U-Au-Ag deposit, South Australia. Society of Economic Geologists, Special Publication 16, p. 237–267.

Ehrig, K., Kamenetsky, V., McPhie, J., Apukhtina, O., Ciobanu, C.L., Cook, N., Kontonikas-Charos, A., and Krneta, S., 2017. The IOCG-IOA Olympic Dam Cu-U-Au-Ag deposit and nearby prospects, South Australia. SGA 2017, 14th SGA biennial meeting, Canada, Proceedings, p. 823–826.

Ells, R.W., 1904. Graphite in Canada. Mineral resources of Canada. Geological Survey of Canada Bulletin 1904, 213 p.

Emslie, R.F. and Hunt, P.A., 1990. Ages and petrogenetic significance of igneous mangerite-charnockite suites associated with massif anorthosite, Grenville Province. The Journal of Geology, v. 98, p. 213–231.

Faure, S., 2007. Outils prévisionnels d'exploration dans les terranes de hauts grades métamorphiques: Le parautochtone grenvillien, une zone à fort potentiel. Rapport du projet CONSOREM 2003-2B, 33 p.

Friedman, R. and Martignole, J., 1995. Mesoproterozoic sedimentation, magmatism, and metamorphism in the southern part of the Grenville Province (western Quebec): U-Pb geochronological constraints. Canadian Journal of Earth Sciences, v. 32, p. 2103–2114.

Froese, E., 1985. Anthophyllite-bearing rocks in the Flin Flon-Sherridon area, Manitoba. Geological Survey of Canada, Paper 85-01B, p. 541–544.

Froese, E., 1998. Metamorphism of hydrothermally altered rocks. Geological Survey of Canada, Paper 1998-E, p. 193–196.

Froese, E., 2010. A reaction grid for pelitic and mafic rocks. Geological Survey of Canada, Current Research 2010-13, 14 p.

Frost, B.R., Mavrogenes, J.A., and Tomkins, A.G., 2002. Partial melting of sulfide ore deposits during medium- and high-grade metamorphism. The Canadian Mineralogist, v. 40, p. 1–18.

Fu, W., Corriveau, L., LaFlèche, M.R., and Blein, O., 2003. Birdwing-shaped REE profiles and Nb/Ta, Hf/Sm ratios in the Bondy gneiss complex, Grenville Province, Québec: Sensitive geochemical markers of fossil hydrothermal systems in high- grade metamorphic terrains. CIM Montreal 2003 Mining Industry Conference and Exhibition, Canadian Institute of Mining, Technical Paper, CD-ROM.

Gauthier, M., 1993. L'aspect que prennent les amas sulfurés en terrain métamorphique: Incidences sur la prospection minière. Bulletin de l'APGGQ (Association professionnelle des géologues et des géophysiciens du Québec), v. 10, no. 1, p. 17–22.

Gauthier, M. and Chartrand, F., 2005. Metallogeny of the Grenville Province revisited. In Corriveau, L. and Clark, T., eds., The Grenville Province: A geological and mineral resources perspective derived from government and academic research initiatives. Canadian Journal of Earth Sciences, v. 42, p. 1719–1734.

Gauthier, M., Poirier, G., Bishop, C., and Soever, A., 1988. Gîtes métallifères dans le sud du Grenville - Livret-guide d'excursion. Ministère de l'Énergie et des Ressources du Québec, MB 88-10, 50 p.

Gauthier, M., Corriveau, L., and Chouteau, M., 2004. Metamorphosed and metamorphogenic ore deposits of the Central Metasedimentary Belt, southwestern Québec and southeastern Ontario Grenville Province. DIVEX, Fieldtrip guide book.

Gibson, H. and Galley, A., 2007, Volcanogenic massive sulphide deposits of the Archean, Noranda District, Quebec. In Goodfellow, W.D., ed., Mineral deposits of Canada: A synthesis of major deposit-types, district metallogeny, the evolution of geological provinces, and exploration methods. Geological Association of Canada, Mineral Deposits Division, Special Publication 5, p. 533–552.

Gobeil, A., Brisebois, D., Clark, T., Verpaelst, P., Madore, L., Wodicka, N., and Chevé, S., 2003. Synthèse géologique de la région de Manitou-Wakeham (moyenne-côte-nord). In Brisebois, D. and Clark, T., eds., Géologie et resources minérales de la partie est de la Province de Grenville. Ministère des Ressources naturelles de la Faune et des Parcs, Québec, DV 2002-03, p. 9–58.

Goodwin, A.M., 1996. Chapter 1 - Distribution and tectonic setting of Precambrian crust. In Goodwin, A.M., ed., Principles of Precambrian geology. London, Academic Press, p. 1–50.

Gower, C.F., 2007. Protolith recognition of metamorphosed felsic volcanic/volcaniclastic rocks, with special reference to the Grenville Province in southeast Labrador. Newfoundland and Labrador Department of Natural Resources, Geological Survey, Report 07-1, p. 11–23.

Gower, C.F., Kamo, S.L., Kwok, K., and Krogh, T.E., 2008. Proterozoic southward accretion and Grenvillian orogenesis in the interior Grenville Province in eastern Labrador: Evidence from U–Pb geochronological investigations. Precambrian Research, v. 165, p. 61–95.

Gromet, L.P., Dymek, R.F., Haskin, L.A., and Korotev, R.L., 1984. The "North American shale composite": its compilation, major and trace element characteristics. Geochimica et Cosmochimica Acta, v. 48, p. 2469–2482.

Gross, G.A., 1996. Stratiform iron. In Eckstrand, O.R., Sinclair, W.D. and Thorpe, R.I., eds., Geology of Canadian mineral deposit types. Geological Survey of Canada, Geology of Canada, v. 8, p. 41–54.

Groves, D.I., Bierlein, F.P., Meinert, L.D., and Hitzman, M.W., 2010. Iron oxide copper-gold (IOCG) deposits through earth history: Implications for origin, lithospheric setting, and distinction from other epigenetic iron oxide deposits. Economic Geology, v. 105, p. 641–654.

Guiraud, M., Powell, R., and Cottin, J.-Y., 1996. Hydration of orthopyroxene-cordierite bearing assemblages at Laouni, Central Hoggar, Algeria. Journal of Metamorphic Geology, v. 14, p. 467–476.

Hanes, J.A., Corriveau, L., and McBride, S.L., 1994. Late-stage cooling history of the Central Metasedimentary Belt of Québec in the southwestern Grenville Province from $^{40}Ar/^{39}Ar$ dating of 1083-1060 Ma K-rich alkaline plutons. Geological Association of Canada-Mineralogical Association of Canada, Program with Abstracts, v. 19, p. A46.11

Hanmer, S., Corrigan, D., Pehrsson, S., and Nadeau, L., 2000. SW Grenville Province, Canada: the case against post-1.4 Ga accretionary tectonics. Tectonophysics, v. 319, p. 33–51.

Harris, L., Rivard, B., and Corriveau, L., 2001. Structure of the Lac Nominingue-Chénéville zone in the Mont-Laurier region, Central Metasedimentary Belt, Québec, Grenville Province. Canadian Journal of Earth Sciences, v. 38, p. 787–802.

Hayward, N., Corriveau, L., Craven, J., and Enkin, R., 2016. Geophysical signature of alteration and mineralisation envelope at the Au-Co-Bi-Cu NICO deposit, NT, Canada. In Slack, J., Corriveau, L., and Hitzman, M., eds., Proterozoic iron oxide-apatite (± REE) and iron oxide-copper-gold and affiliated deposits of Southeast Missouri, USA, and the Great Bear magmatic zone, Northwest Territories, Canada. Economic Geology, v. 111, p. 2087–2110.

Hébert, C. and Nantel, S., 1999. Géologie de la région de l'Ascension (SNRC 31J/10). Ministère des Ressources naturelles, Québec, RG 99-03, 31 p.

Hébert, C., Lacoste, P., Nantel, S., and Nadeau, J., 1996. L'Ascension (SNRC 31J/10). Ministère des Ressources naturelles, Québec, carte SI-31J10-C3G-96K, échelle de 1/50 000.

Hedstroem, P., Simeonov, A., and Malmstrom, L., 1989. The Zinkgruvan ore deposit, south-central Sweden; a Proterozoic, proximal Zn-Pb-Ag deposit in distal volcanic facies. Economic Geology, v. 84, p. 1235–1261.

Hetu, R.J. and Corriveau, L., 1995. Levé géophysique aéoporté, Papineau, Québec. Geological Survey of Canada, Open file 2872.

Hikov, A., 2004. Geochemistry of strontium in advanced argillic alteration systems – possible guide to exploration. Bulgarian Geological Society, Annual Scientific Conference 'Geology 2004', p. 29–31.

Hindemith, M., Indares, A., and Piercey, S., 2017. Hydrothermally

altered volcanic rocks metamorphosed at granulite-facies conditions: An example from the Grenville Province. Canadian Journal of Earth Sciences, v. 54, p. 622–638.

Hitzman, M.W., Oreskes, N., and Einaudi, M.T., 1992. Geological characteristics and tectonic setting of Proterozoic iron-oxide (Cu-U-Au-REE) deposits. Precambrian Research, v. 58, p. 241–287.

Hodges, D.J. and Manojlovic, P.M., 1993. Application of lithogeochemistry to exploration for deep VMS deposits in high-grade metamorphic rocks, Snow Lake, Manitoba. Journal of Geochemical Exploration, v. 48, p. 201–224.

Hofstra, A., Aleinikoff, J., Ayuso, R., Bennett, M., Day, W., du Bray, E., Johnson, C., McCafferty, A., Meighan, C., Mercer, C., Neymark, L., Slack, J., and Watts, K., 2017. Magmatic-hydrothermal origin of the Mesoproterozoic Pea Ridge IOA-REE deposit, Southeast Missouri, USA. SGA 2017, 14th SGA biennial meeting, Canada, Proceedings, p. 863–866.

Holland, T.J.B. and Powell, R., 1991. A compensated-Redlich-Kwong (CORK) equation for volumes and fugacities of CO_2 and H_2O in the range 1 bar to 50 kbar and 100-1600°C. Contributions to Mineralogy and Petrology, v. 109, p. 309–343.

Holland, T.J.B. and Powell, R., 1998. An internally consistent thermodynamic data set for phases of petrological interest. Journal of Metamorphic Geology, v. 16, no. 3, p. 309–343.

Holland, T.J.B. and Powell, R., 2011. An improved and extended internally consistent thermodynamic dataset for phases of petrological interest, involving a new equation of state for solids. Journal of Metamorphic Geology, v. 29, no. 3, p. 333–383.

Huston, D.L. and Hussey, K., 2004. Regional geology and metallogeny of the Eastern Arunta: 2004 Chief Government Geologists Conference field guide, Canberra. Geoscience Australia Record 2004/07, 26 p.

Indares, A., 1982. L'évolution des conditions de température et de pressions pendant le métamorphisme catazonal dans la région de Maniwaki, Province de Grenville, bouclier canadien. Mémoire de maitrise, Université de Montréal, Montréal, 255 p.

Indares, A. and Martignole, J., 1984. Evolution of P-T conditions during a high-grade metamorphic event in the Maniwaki area (Grenville Province). Canadian Journal of Earth Sciences, v. 21, p. 853–863.

Indares, A. and Martignole, J., 1990. Metamorphic constraints on the evolution of the gneisses from the allochthonous monocyclic belt of the Grenville Province, western Quebec. Canadian Journal of Earth Sciences, v. 27, p. 371–386.

Irvine, T.N., 1980. Magmatic density currents and cumulus processes. American Journal of Science, v. 280, p. 1–58.

Irvine, T.N., Andersen, J.C.O., and Brooks, C.K., 1998. Included blocks (and blocks within blocks) in the Skaergaard intrusion: geologic relations and the origin of rhythmic modally graded layers. Geological Society of America Bulletin, v. 110, p. 1398–1447.

Ishikawa, Y., Sawaguchi, T., Iwaya, S., and Horiuchi, M., 1976. Delineation of prospecting targets for Kuroko deposits based on modes of volcanism of underlying dacite and alteration haloes. Mining Geology, v. 26, p. 105–117.

Jiang, D., 2010. Flow and finite deformation of surface elements in three dimensional homogeneous progressive deformations. Tectonophysics, v. 487, p. 85–99.

Kelley, D.L., Kelley, K.D., Coker, W.B., Caughlin, B., and Doherty, M.E., 2006. Beyond the obvious limits of ore deposits: The use of mineralogical, geochemical, and biological features for the remote detection of mineralization. Economic Geology, v. 101, p. 729–752.

Kreiner, D.C. and Barton, M.D., 2011. High-level alteration in iron-oxide(-Cu-Au) ('IOCG') vein systems, examples near Copiapo Chile. In Barra, F., Reich, M., Campos, E., and Tornos, F., eds., Proceeding of the 11th Biennal Meeting, Society of Geology Applied to Ore deposits, p. 497–499.

Kretz, R., 1980. Occurrence, mineral chemistry, and metamorphism of Precambrian carbonate rocks in a portion of the Grenville Province. Journal of Petrology, v. 21, p. 573–620.

Kretz, R., 1990. Biotite and garnet compositional variation and mineral equilibria in Grenville gneisses of the Otter Lake area, Quebec. Journal of Metamorphic Geology, v. 8, p. 493–506.

Kretz, R., 1997. Metamorphic crystallization: examples from the Ottawa Valley and Laurentian highlands. Geological Association of Canada-Mineralogical Association of Canada, Guidebook A6, 28 p.

Large, R.R., Gemmel, J.B., Paulick, H., and Huston, D.L., 2001. The alteration box plot: A simple approach to understanding the relationship between alteration mineralogy and lithogeochemistry associated with volcanic-hosted massive sulphide deposits. Economic Geology, v. 96, p. 957–971.

Le Maitre, R.W., Streckeisen, A., Zanettin, B., Le Bas, M.J., Bonin, B., Bateman, P., Bellieni, G., Dudek, A., Efremova, S., Keller, J., Lameyre, J., Sabine, P.A., Schmid, R., Sorensen, H., and Woolley, A.R., 2002. Igneous rocks: A classification and glossary of terms. Recommendations of the International Union of Geological Sciences, Subcommission on the Systematics of Igneous Rocks, Cambridge, Cambridge University Press, 252 p.

Luque, F.J., Crespo-Feo, E., Barrenechea, J.F., and Ortega, L., 2012. Carbon isotopes of graphite: Implications on fluid history. Geoscience Frontiers, v. 3, p. 197–207.

Martignole, J. and Corriveau, L., 1991. Lithotectonic studies in the Central Metasedimentary Belt of the southern Grenville Province: lithology and structure of the Saint-Jovite map area, Québec. Geological Survey of Canada, Paper 91-1C, p. 77–87.

Martignole, J. and Friedman, R., 1998. Geochronological constraints on the last stages of terrane assembly in the central part of the Grenville Province. Precambrian Research, v. 92, p. 145–164.

Martignole, J. and Schriever, K., 1970. Tectonic setting and evolution of the Morin Anorthosite, Grenville Province, Quebec. Bulletin of the Geological Society of Finland, v. 42, p. 165–209.

Martignole, J., Calvert, A.J., Friedman, R., and Reynolds, P., 2000. Crustal evolution along a seismic section across the Grenville Province (western Québec). Canadian Journal of Earth Sciences, v. 37, p. 291–306.

McCausland, P.J., van der Voo, R., and Hall, C.M., 2007. Circum-Iapetus paleogeography of the Precambrian–Cambrian transition with a new paleomagnetic constraint from Laurentia. Precambrian Research, v. 156, p. 125–152.

McEachern, S.J. and van Breemen, O., 1993. Age of deformation within the Central Metasedimentary Belt boundary thrust zone, southwest Grenville orogen: constraints on the collision of the Mid-Proterozoic Elzevir terrane. Canadian Journal of Earth Science, v. 30, p. 1155–1165.

McFarlane, C.R.M., Mavrogenes, J.A., and Tomkins, A.G., 2007. Recognizing hydrothermal alteration through a granulite facies metamorphic overprint at the Challenger Au deposit, South Australia. Chemical Geology, v. 243, p. 64–89.

McLelland, J., Daly, J.S., and McLelland, J.M., 1996. The Grenville orogenic cycle (ca. 1350-1000Ma): An Adirondack perspective. Tectonophysics, v. 265, p. 1–28.

McLelland, J.M., Bickford, M.E., Hill, B.H., Clechenko, C.C, Valley, J.W., and Hamilton, M.A., 2004. Direct dating of Adirondack massif anorthosite by U–Pb SHRIMP analysis of igneous zircon: Implications for AMCG complexes. Geological Society America Bulletin, v. 116, p. 1299–1317.

McLelland, J.M., Selleck, B.W., and Bickford, M.E., 2010. Review of the Proterozoic evolution of the Grenville Province, its Adirondack outlier, and the Mesoproterozoic inliers of the Appalachians. In Tollo, R.P., Bartholomew, M.J., Hibbard, J.P., and Karabinos, P.M., eds., From Rodinia to Pangea: The lithotectonic record of the Appalachian region. Geological Society of America, Memoir 206, p. 21–49.

McLelland, J.M., Selleck, B.W., and Bickford, M.E., 2013. Tectonic evolution of the Adirondack mountains and Grenville orogen inliers within the USA. Geoscience Canada, v. 40, p. 318–352.

McMullen, S.M., 1999. Tectonic evolution of the Bark Lake area,

eastern Central Gneiss Belt, Ontario Grenville: Constraints from geology, geochemistry and U-Pb geochronology. Unpublished MSc thesis, Carleton University, Ottawa, Ontario, 175 p.

Montreuil, J.-F., Corriveau, L., and Grunsky, E.C., 2013. Compositional data analysis of IOCG systems, Great Bear magmatic zone, Canada: To each alteration types its own geochemical signature. Geochemistry: Exploration, Environment, Analysis, v. 13, p. 229–247.

Montreuil, J.-F., Corriveau, L., and Potter, E.G., 2015. Formation of albitite-hosted uranium within IOCG systems: The Southern Breccia, Great Bear magmatic zone, Northwest Territories, Canada. Mineralium Deposita, v. 50, p. 293–325.

Montreuil, J.-F., Corriveau, L., and Davis, W., 2016a. Tectonomagmatic evolution of the southern Great Bear magmatic zone (Northwest Territories, Canada) – Implications on the genesis of iron oxide alkali-altered hydrothermal systems. In Slack, J., Corriveau, L., and Hitzman, M., eds., Proterozoic iron oxide-apatite (± REE) and iron oxide-copper-gold and affiliated deposits of Southeast Missouri, USA, and the Great Bear magmatic zone, Northwest Territories, Canada. Economic Geology, v. 111, p. 2111-2138.

Montreuil, J.-F., Corriveau, L., Potter, E.G., and De Toni, A.F., 2016b. On the relation between alteration facies and metal endowment of iron oxide alkali-altered systems, southern Great Bear magmatic zone (Canada). In In Slack, J., Corriveau, L., and Hitzman, M., eds., Proterozoic iron oxide-apatite (± REE) and iron oxide-copper-gold and affiliated deposits of Southeast Missouri, USA, and the Great Bear magmatic zone, Northwest Territories, Canada. Economic Geology, v. 111, p. 2139–2168.

Moore, J.M. and Waters, D.J., 1990. Geochemistry and origin of cordierite-orthoamphibole/ orthopyroxene-phlogopite rocks from Namaqualand, South Africa. Chemical Geology, v. 85, p. 77–100.

Morin, D., 1998. La brèche intrusive de Rivard - mise en place, nature et origine d'un lamprophyre ultrapotassique grenvillien et de ses xénolites ultramafiques, région de Mont-Laurier, Québec. Unpublished PhD thesis, INRS-Géoressources, Québec, 538 p.

Morin, D. and Corriveau, L., 1996. Fragmentation processes and xenolith transport in a Proterozoic minette dyke, Grenville Province, Québec. Contributions to Mineralogy and Petrology, v. 125, p. 319–331.

Morin, D., Hébert, R., and Corriveau, L., 2005. Mesoproterozoic deep K-magmatism recorded in a megacryst- and xenolith-bearing minette dyke, western Grenville Province. Canadian Journal of Earth Sciences, v. 42, p. 1881–1906.

Morisset, C., Scoates, J., Weiss, D., and Friedman, R., 2009. U-Pb and $^{40}Ar/^{39}Ar$ of the St. Urbain and Lac Allard (Havre–St. Pierre) anorthosites and associated Fe-Ti ores, Quebec: Evidence for slow cooling during the collisional Ottawan orogeny in the Grenville Province. Precambrian Research, v. 174, p. 95–116.

Mosher, S., Levine, J.S.F., and Carlson, W.D., 2008. Mesoproterozoic plate tectonics: A collisional model for the Grenville-aged orogenic belt in the Llano uplift, central Texas. Geology, v. 36, p. 55–58.

Mumin, A.H., Somarin, A.K., Jones, B., Corriveau, L., Ootes, L., and Camier, J., 2010. The IOCG-porphyry-epithermal continuum of deposits types in the Great Bear magmatic zone, Northwest Territories, Canada. In Corriveau, L. and Mumin, A.H., eds., Exploring for iron oxide copper-gold deposits: Canada and global analogues. Geological Association of Canada, Short Course Notes 20, p. 59–78.

Myers, J., Voordoux, J., and Tettelaar, T., 2008. Proterozoic anorthosite-granite Nain batholith: Structure and intrusion processes in an active lithosphere-scale fault zone, northern Labrador. Canadian Journal of Earth Sciences, v. 45, p. 909–934.

Nadeau, L. and van Breemen, O., 1998. Plutonic ages and tectonic setting of the Algonquin and Muskoka allochthons, Central Gneiss Belt, Grenville Province, Ontario. Canadian Journal of Earth Sciences, v. 35, p. 1423–1438.

Nantel, S., 2008. Géologie et aperçu de la géochronologie et des indices métalliques découverts entre 1996 et 2007 dans la partie nord de la Ceinture centrale des métasédiments, Province de Grenville, région de Mont-Laurier. Ministère des Ressources naturelles, Québec, RG2008-04, 17 p.

Nantel, S. and Pinston, H., 2002a. Géologie de la région du lac Dieppe (310/03). Ministère des Ressources naturelles, Québec, RG2001-16.

Nantel, S. and Pintson, H., 2002b. Carte préliminaire de la partie nord de la Ceinture centrale des métasédiments, Province de Grenville, et études connexes. Ministère des Ressources naturelles, Québec, DV 2002-10, 46 p.

Nantel, S. Ouellet, S., Doucet, P., and Lesage, D., 2008. Chapter 1D, Grenville Province. Québec Department of Energy and Natural Resources, DV 2009-02, p. 43–50.

Ohmoto, H., 1996. Formation of volcanogenic massive sulfide deposits: the Kuroko perspective. Ore Geology Reviews, v. 10, p. 135–177.

Passchier, C.W., Myers, J.S., and Kröner, A., 1990. Field geology of high-grade gneiss terrains. Springer Verlag, Germany, 150 p.

Paterson, S.R., Vernon, R.H., and Tobish, O.T., 1989. A review of criteria for the identification of magmatic and tectonic foliations in granitoids. Journal of Structural Geology, v. 11, p. 349–363.

Pattison, D.R.M., 2003. Petrogenetic significance of orthopyroxene-free garnet + clinopyroxene + plagioclase ± quartz-bearing metabasites with respect to the amphibolite and granulite facies. Journal of Metamorphic Geology, v. 21, no. 1, p. 21–34.

Pavlis, T.L., 1996. Fabric development in syn-tectonic intrusive sheets as a consequence of melt-dominated flow and thermal softening of the crust. Tectonophysics, v. 253, p. 1–31.

Pearce, J.A., 1996. Sources and settings of granitic rocks. Episodes, v. 19, p. 120–125.

Peck, W.H., 2012. Reconnaissance geochronology and geochemistry of the Mont-Tremblant gneiss of the Morin terrane, Grenville Province, Québec. Geosphere, v. 8, p. 1356–1365.

Peck, W.H., De Angelis, M.T., Meredith, M.T., and Morin, E., 2005. Polymetamorphism of marbles in the Morin Terrane, Grenville Province, Quebec. Canadian Journal of Earth Sciences, v. 42, p. 1949–1965.

Perkins, D., III, Essene, E.J., and Marcotty, L.A., 1982. Thermometry and barometry of some amphibolite-granulite facies rocks from the Otter Lake area, southern Quebec. Canadian Journal of Earth Sciences, v. 19, p. 1759–1774.

Perreault, S. and Hébert, C., 2003. Review of Fe-Ti±V and Fe-TiP_2O_5±V deposits associated with anorthositic suites in the Grenville Province, Québec. In Duchesne, J.-C. and Korneliussen, A., eds. Ilmenite deposits and their geological environment. Norges geologiske undersokelse, Special Publication 9, p. 83–84.

Perreault, S. and Lafrance, B., 2015. Kwyjibo, a REE-enriched iron oxides-copper-gold (IOCG) deposit, Grenville Province, Québec. In Simandl, G.J. and Neetz, M., eds., Symposium on Strategic and Critical Materials Proceedings, November 13-14, 2015, Victoria, British Columbia. British Columbia Ministry of Energy and Mines, British Columbia Geological Survey Paper 2015-3, pp. 139-145

Philpotts, A.R., 1976, Grenville Township (SE part); Ministère des Richesses Naturelles, Geological Report, RG-156, 51 p. 1 map.

Pirajno, F., 2009. Hydrothermal processes and mineral systems. Springer, Berlin, Germany, 1250 p.

Pollard, P.J., 2000. Evidence of a magmatic fluid source for iron oxide-Cu-Au mineralisation. In Porter, T.M., ed., Hydrothermal iron oxide copper-gold and related deposits: A global perspective, Volume 1. Porter Geoscience Consultancy Publishing, Adelaide, p. 27–41.

Pollard, P.J., 2006. An intrusion-related origin for Cu-Au mineralization in iron oxide-copper-gold (IOCG) provinces. Mineralium Deposita, v. 41, p. 179–187.

Porter, T.M., 2010a. Current understanding of iron oxide associated-alkali altered mineralised systems. Part 1 - An overview. In Porter, T.M., ed., Hydrothermal iron oxide copper-gold and related

deposits. A global perspective, volume 3–Advances in the understanding of IOCG deposits. Porter Geoscience Consultancy Publishing, Adelaide, p. 5–32.

Porter, T.M., 2010b. The Carrapateena iron oxide copper-gold deposit, Gawler Craton, South Australia: A review. In Porter, T.M., ed., Hydrothermal iron oxide copper-gold and related deposits. A global perspective, volume 3–Advances in the understanding of IOCG deposits. Porter Geoscience Consultancy Publishing, Adelaide, p. 191–200.

Puffer, J.H. and Gorring, M.L., 2005. The Edison magnetite deposits in the context of pre-syn-and post-orogenic metallogenesis in the Grenville Highlands of New Jersey. Canadian Journal of Earth Sciences, v. 42, p. 1735–1748.

Ravenelle, J.-F., Dubé, B., Malo, M., McNicoll, V., Nadeau, L., and Simoneau, J., 2010. Insights on the geology of the world-class Roberto gold deposit, Eleonore property, James Bay, Quebec. Geological Survey of Canada Current Research 2010-1, 26 p.

Richmond Minerals Inc., 2010. Report on the geophysical surveying and ground sampling at the Bondy gneiss complex. Ministère des Ressources naturelles, Québec, GM 65497, 16 p.

Rivard, B., Corriveau, L., and Harris, L.B., 1999. Structural reconnaissance of a deep crustal orogen using satellite imagery and airborne geophysics. Canadian Journal of Remote-Sensing, v. 25, p. 258-267.

Rivers, T., 1997. Lithotectonic elements of the Grenville Province: review and tectonic implications. Precambrian Research, v. 86, p. 117–154.

Rivers, T., 2008. Assembly and preservation of lower, mid, and upper orogenic crust in the Grenville Province—Implications for the evolution of large hot long-duration orogens. Precambrian Research, v. 167, p. 237–259.

Rivers, T., Martignole, J., Gower, C.F., and Davidson, A., 1989. New tectonic divisions of the Grenville Province, Southeast Canadian Shield. Tectonics, v. 8, p. 63–84.

Rogers, N., 2001. Preliminary report on the stratigraphy and structure of the Bee Lake greenstone belt, Superior Province, northwestern Ontario. Geological Survey of Canada, Open File Report, v. 2001-C17, 25 p.

Roy, P., Cadéron, S., and Houle, P., 2006. Géologie structurale et typologie des indices de la région des lacs Chevrier et Dollier (32G09-200-0201 et 32G09-200-0202). Ministère des Resources naturelles et de la Faune du Québec, RP 2006-05, 13 p.

Rubin, J.N., Henry, C.D., and Price, J.G., 1993. The mobility of zirconium and other 'immobile' elements during hydrothermal alteration. Chemical Geology, v. 110, p. 29–47.

Saint-Germain, P. and Corriveau, L., 2003. Évolution magmatique et géochimique du Complexe de gabbronorite et de monzonite de Matamec. In Brisebois, D. and Clark, T., eds., Géologie et resources minérales de la partie est de la Province de Grenville. Ministère des Ressources naturelles de la Faune et des Parcs, Québec, DV 2002-03, p. 179–212.

Sappin, A.-A., Constantin, M., Clark, T., and van Breemen, O., 2009. Geochemistry, geochronology, and geodynamic setting of Ni-Cu±PGE mineral prospects hosted by mafic and ultramafic intrusions in the Portneuf-Mauricie domain, Grenville Province, Quebec. Canadian Journal of Earth Sciences, v. 46, p. 331–353.

Sawyer, E.W., 1999. Criteria for the recognition of partial melting. Physics and Chemistry of the Earth, v. 24, p. 269–279.

Schlegel, T.U. and Heinrich, C.A., 2015. Lithology and hydrothermal alteration control the distribution of copper grade in the Prominent Hill iron oxide-copper-gold deposit (Gawler Craton, South Australia). Economic Geology, v. 110, p. 1953–1994.

Schmidt Mumm, A., Bruggera, J., Zhao, C., and Schacht, U., 2010. Fluids in geological processes − The present state and future outlook. Journal of Geochemical Exploration, v. 106, p. 1–7.

Schneider, D.A., Cope, N., and Holm, D.K., 2013. Thermochronology of the Mont Laurier terrane, southern Canadian Grenville Province, and its bearing on defining orogenic architecture. Precambrian Research, v. 226, p. 43–58.

Schreurs, J. and Westra, L., 1985. Cordierite-orthopyroxene rocks: The granulite facies equivalents of the Orijarvi cordierite-anthophyllite rocks in West Uusimaa, southwest Finland. Lithos, v. 18, p. 215–228.

Sharma, K.N.M. and Singhroy, V., 1997. New developments in Grenville geology and remote-sensing, Fort Coulonge region, western Quebec. Geological Association of Canada-Mineralogical Association of Canada, Guidebook B3.

Sharma, K.N.M., Lévesque, J., Hocq, M., and Rive, M., 1993. Excursion des Amis du Grenville au Québec: observations structurales et importance économique, région de Grand- Remous, Maniwaki, Danford Lake. Ministère des Ressources naturelles du Québec, MB 93-50.

Sheepers, D.J. and Cornell, D.H., 1990. Host rock protolithology of metamorphosed ore deposits. In Spry, P. and Bryndzia, L.T., eds., Regional metamorphism of ore deposits and genetic implications. V.S.P. Scientific Publishers, p. 141–160.

Simandl, G.J., Paradis, S., and Akam, C., 2015. Graphite deposit types, their origin and economic significance. In Simandl, G.J. and Neetz, M., eds., Symposium on strategic and critical materials proceedings. British-Columbia Geological Survey Paper 2015-3, p. 163–171.

Skirrow, R., 2010. "Hematite-group" IOCG±U ore systems: Tectonic settings, hydrothermal characteristics, and Cu-Au and U mineralizing processes. In Corriveau, L. and Mumin, A.H., eds. Exploring for iron oxide copper-gold deposits: Canada and global analogues. Geological Association of Canada, Short Course Notes 20, p. 39–58.

Slack, J.F., Palmer, M.R., Stevens, B.P.J., and Barnes, R.G., 1993. Origin and significance of tourmaline-rich rocks in the Broken Hill district, Australia. Economic Geology, v. 88, p. 505–541.

Slack, J., Corriveau, L., and Hitzman, M., 2016. A special issue devoted to proterozoic iron oxide-apatite (± REE) and iron oxide-copper-gold and affiliated deposits of Southeast Missouri, USA, and the Great Bear magmatic zone, Northwest Territories, Canada - Preface. In Slack, J., Corriveau, L., and Hitzman, M., eds., Proterozoic iron oxide-apatite (± REE) and iron oxide-copper-gold and affiliated deposits of Southeast Missouri, USA, and the Great Bear magmatic zone, Northwest Territories, Canada. Economic Geology, v. 111, p. 1803–1814.

Slagstad, T., Culshaw, N.G., Jamieson, R.A., and Ketchum, J.W.F., 2004. Early Mesoproterozoic tectonic history of the southwestern Grenville Province, Ontario: Constraints from geochemistry and geochronology of high-grade gneisses. In Tollo, R.P., Corriveau, L., McLelland, J., and Bartholomew, M., eds., Proterozoic tectonic evolution of the Grenville orogen in North America. Geological Society of America, Memoir 197, p. 209–242.

Slagstad, T., Culshaw, N.G., Daly, J.S., and Jamieson, R.A., 2009. Western Grenville Province holds key to midcontinental Granite-Rhyolite Province enigma. Terra Nova, v. 21, p. 181–187.

Soucy-La Roche, R.S., Gervais, F., Tremblay, A., Crowley, J.L., and Ruffet, G., 2015. Tectono-metamorphic history of the eastern Taureau shear zone, Mauricie area, Québec: Implications for the exhumation of the mid-crust in the Grenville Province. Precambrian Research, v. 257, p. 22–46.

Sparks, H.A., Mavrogenes, J.A., and Frost, B.R., 2007. The secret lives of immiscible metal-rich melts: Two liquid immiscibility in the sulfide-antimony system. Geologian tutkimuskeskus, Opas 53 – Geological Survey of Finland Guide 53, p. 65–70.

Spear, F.S., 1993. Metamorphic phase equilibria and pressure-temperature-time paths. Mineralogical Society of America. Monograph series, 799 p.

Spence, H.S., 1920. Graphite in Canada. Canada Mines Branch, Publication 511, 240 p.

Spry, P.G., Marshall, B., and Vokes, F.M., eds., 2000. Metamorphosed and metamorphogenic ore deposits. Reviews in Economic Geology, v. 11, 310 p.

Streckeisen, A., 1976. To each plutonic rock its proper name. Earth Science Reviews, v. 12, p. 1–33.

Sun, S.S. and McDonough, W.F., 1989. Chemical and isotopic systematics of oceanic basalts: implications for mantle composition and processes. In Saunders, A.D. and Norry, M.J., eds., Magmatism in the ocean basins. Geological Society, Special Publication 42, p. 313–345.

Theart H.F.J., Cornell, D.H., and Schade, J., 1989. Geochemistry and metamorphism of the Prieska Zn-Cu deposit, South Africa. Economic Geology, v. 84, p. 34–48.

Theart, H.F.J., Ghavami-Riabi, R., Mouri, H., and Gräser, P., 2010. Applying the box plot to the recognition of footwall alteration zones related to VMS deposits in a high-grade metamorphic terrain, South Africa, a lithogeochemical exploration application. Chemie Erde-Geochemistry, v. 71, p. 143–154.

Timmermann, H., Parrish, R.R., Jamieson, R.A., and Culshaw, N.G., 1997. Time of metamorphism beneath the Central Metasedimentary Belt boundary thrust zone, Grenville orogen, Ontario: Accretion at 1080 Ma? Canadian Journal of Earth Sciences, v. 34, p. 1023–1029.

Tomkins, A.G., 2007. Three mechanisms of ore remobilisation at the amphibolite facies Montauban Zn-Pb-Au-Ag deposit. Mineralium Deposita, v. 42, p. 627–637.

Tomkins, A.G. and Mavrogenes, J.A., 2002. Mobilization of gold as a polymetallic melt during pelite anataexis at the Challenger gold deposit, South Australia: A metamorphosed Archean gold deposit. Economic Geology, v. 97, p. 1249–1271.

Tomkins, A.G., Pattison, D.R.M., and Frost, B.R., 2007. On the initiation of metamorphic sulfide anatexis. Journal of Petrology, v. 48, p. 511–535.

Tornos, F., 2017. The roots and tops of magnetite-apatite mineralization: Evolving magmatic-hydrothermal systems. SGA 2017, 14th SGA biennial meeting, Canada, Proceedings, p. 831–834.

Tornos, F., Velasco, F., Barra, F. and Morata, D., 2010. The Tropezón Cu–Mo–(Au) deposit, Northern Chile: The missing link between IOCG and porphyry copper systems? Mineralium Deposita, v. 45, p. 313–321.

Trägårdh, J., 1991. Metamorphism of magnesium-altered felsic volcanic rocks from Bergslagen, central Sweden: A transition from Mg-chlorite- to cordierite-rich rocks. Ore Geology Reviews, v. 6, p. 485–497.

Trapy, P.-H., 2018. Modélisation d'équilibre de phase prédictive des faciès d'altération associés aux gîtes à oxydes de fer-cuivre-or dans les terrains de hauts grades métamorphiques. M.Sc. thesis, École Polytechnique, Montréal, 113 p.

Trapy, P.H., Gervais, F., Corriveau, L., and Moukhsil, A., 2015. La modélisation pétrogénétique des gîtes d'oxydes de fer à cuivre-or comme outil d'exploration dans les terrains de haut grade métamorphique: application à la zone de Parent (Haute-Mauricie, Québec). Energie Ressources Québec, MB 2015-05, 52 p.

Tremblay, P., Corriveau, L., and Daigneault, R.A., 1993. Géologie de la réserve faunique de Papineau-Labelle - rallyes géologiques. INRS-Géoressources.

Tremblay, P., Corriveau, L., and Daigneault, R.A., 1996. Si la Terre m'était contée; géologie de la réserve faunique de Papineau-Labelle. INRS-Géoressources, 64 p.

Tremblay, P., Corriveau, L., and Daigneault, R.A., 1997. Un aperçu du Bouclier canadien dans la région de la réserve faunique de Papineau Labelle, Québec, à l'intention des enseignants / An introduction for teachers to the Canadian Shield in the Papineau Labelle wildlife reserve, Quebec. Geological Association of Canada-Mineralogical Association of Canada, Fieldtrip guidebook A3, 29 p.

Vallance, T.G., 1967. Mafic rock alteration and isochemical development of some cordierite-anthophyllite rocks. Journal of Petrology, v. 8, p. 84–96.

Valley, P.M., Hanchar, J.M., and Whitehouse, M.J., 2011. New insights on the evolution of the Lyon Mountain granite and associated Kiruna-type magnetite-apatite deposits, Adirondack Mountains, New York State. Geosphere, v. 7, p. 357–389.

van Breemen, O. and Corriveau, L., 1995. Evolution of the Central Metasedimentary Belt in Quebec, Grenville orogen: U-Pb geochronology. International Conference on Tectonics and Metallogeny of Early/Mid Precambrian Orogenic Belt, Precambrian 1995, Program with Abstracts, p. 137.

van Breemen, O. and Corriveau, L., 2005. U-Pb age constraints on arenaceous and volcanic rocks of the Wakeham Group, eastern Grenville Province. In Corriveau, L. and Clark, T., eds., The Grenville Province: A geological and mineral resources perspective derived from government and academic research initiatives. Canadian Journal of Earth Sciences, v. 42, p. 1677–1697.

van der Pluijm, B., 1991. Marble mylonites in the Bancroft shear zone, Ontario, Canada: microstructures and deformation mechanisms. Journal of Structural Geology, v. 13, p. 1125–1135.

van Ruitenbeek, F.J.A., Cudahy, T.J., van der Meer, F.D., and Hale, M., 2012. Characterization of the hydrothermal systems associated with Archean VMS-mineralization at Panorama, Western Australia, using hyperspectral, geochemical and geothermometric data. Ore Geology Reviews, v. 45, p. 33–46.

Vigneresse, J.L., Barbey, P., and Cuney, M., 1996. Rheological transitions during partial melting and crystallization with application to felsic magma segregation and transfer. Journal of Petrology, v. 37, p. 1579–1600.

Wang, S. and Williams, P.J., 2001. Geochemistry and origin of Proterozoic skarns at the Mount Elliott Cu-Au(-Co-Ni) deposit, Cloncurry district, NW Queensland, Australia. Mineralium Deposita, v. 36, p. 109–124.

Wanhainen, C. and Martinsson, O., 2010. The hybrid character of the Aitik deposit, Norrbotten, Sweden: A porphyry Cu-Au-Ag(-Mo) system overprinted by Fe-oxide Cu-Au hydrothermal fluids. In Porter, T.M., ed., Hydrothermal iron oxide copper-gold & related deposits: A global perspective, volume 4, Advances in the understanding of IOCG deposits. Porter Geoscience Consulting Publishing, Adelaide, p. 415–426.

Wanhainen, C., Billström, K., Martinsson, O., Stein, H., and Nordin, R., 2005. 160 Ma of magmatic/hydrothermal and metamorphic activity in the Gällivare area: Re-Os dating of molybdenite and U-Pb dating of titanite from the Aitik Cu-Au-Ag deposit, northern Sweden. Mineralium Deposita, v. 40, p. 435–447.

Warren, I., Simmons, S.F., and Mauk, J.L., 2007. Whole-rock geochemical techniques for evaluating hydrothermal alteration, mass changes, and compositional gradients associated with epithermal Au-Ag mineralization. Economic Geology, v. 102, p. 923–948

Weihed, P., 2003. A review of major base metal deposits in the Fennoscandian Shield. In Kelly, J.G., Andrew, J.H., Boland, M.B., Earls, G., Fusciardi, L., and Stanley, G., eds., Europe´s major base metal deposits. Irish Association of Economic Geologists, p. 49–86.

Weihed, P. and Eilu, P., 2005. Fennoscandian Shield – Proterozoic VMS deposits. Ore Geology Reviews, v. 27, p. 324–325.

Weihed, P., Arndt, N., Billström, K., Duchesne, J.-C., Eilu, P., Martinsson, O., Papunen, H., and Lahtinen, R., 2005. Precambrian geodynamics and ore formation: The Fennoscandian Shield. Ore Geology Reviews, v. 27, p. 273–322.

Whitney, D.L. and Evans, B.W., 2010. Abbreviations for names of rock-forming minerals. American Mineralogist, v. 95, p. 185–187.

Williams, P.J., 1990. Evidence for a late metamorphic origin of disseminated gold mineralization in Grenville gneisses at Calumet, Quebec. Economic Geology, v. 85, p. 164–171.

Williams, P.J., 1992. Metamorphosed boninitic basalts, arc tholeiites, and cryptic volcanic stratigraphy from the Elzevir Terrane of the Grenville Province, Calumet mine, Quebec. Canadian Journal of Earth Science, v. 29, p. 26–34.

Williams, P.J., 2010. Classifying IOCG deposits. In Corriveau, L. and Mumin, A.H., eds., Exploring for iron oxide copper-gold deposits: Canada and global analogues. Geological Association of Canada, Short Course Notes 20, p. 13–22.

Williams, N.C. and Davidson, G.J., 2004. Possible submarine advanced argillic alteration at the Basin Lake prospect, western Tasmania, Australia. Economic Geology, v. 99, p. 987–1002.

Williams, P.J. and Smith, M.J., 2003. Pb–Zn–(As) enrichments in amphibolites from Broken Hill-type ore systems, NW Queensland: Products of retrograde hydrothermal dispersion. Geochemistry: Exploration, Environment, Analysis, v. 3, p. 245–261.

Williams, P.J., Barton, M.D., Johnson, D.A., Fontboté, L., de Haller, A., Mark, G., Oliver, N.H.S., and Marschik, R., 2005. Iron oxide-copper-gold deposits: Geology, space-time distribution, and possible modes of origin. In Hedenquist, J.W., Thompson, J.F.H., Goldfarb, R.J., and Richards, J.P., eds., Economic Geology 100th Anniversary Volume, Littleton, Society of Economic Geologists, p. 371–405.

Williamson, K., Corriveau, L., Bonnet, A.-L., and Parsons, S., 2003. Reconnaissance de systèmes hydrothermaux métamorphisés dans les terrains de haut grade métamorphique: Outils géologiques diagnostiques et implications pour l'exploration régionale. CIM Montreal 2003, Canadian Institute of Mining, Technical Paper, CD-ROM.

Wodicka, N., Corriveau, L., and Stern, R.A., 2004. Shrimp U-Pb zircon geochronology of the Bondy gneiss complex: evidence for a 1.40 Ga arc magmatism and polyphase Grenvillian metamorphism in the Central Metasedimentary Belt, Grenville Province, Québec. In Tollo, R., Corriveau, L., McLelland, J., and Bartolomew, M., eds., Proterozoic tectonic evolution of the Grenville Province in eastern North America. Geological Society of America, Memoir 197, p. 243–266.

Wynne-Edwards, H.R, Gregory, A.F., Hay, P.W., Giovanella, C.A., and Reinhardt, E.W., 1966. Mont-Laurier and Kempt Lake map-areas, Québec. Geological Survey of Canada, Paper 66, 32 p.

Xavier, R.P., Monteiro, L.V.S., de Souza Filho, C.R., Torresi, I., de Resende Carvalho, E., Dreher, A.M., Wiedenbeck, M., Trumbull, R.B., Pestilho, A.L.S., and Moreto, C.P.N., 2010. The iron oxide copper-gold deposits of the Carajás mineral province, Brazil: An updated and critical review. In Porter, T.M., ed., Hydrothermal iron oxide copper–gold and related deposits: A global perspective, volume 3–Advances in the understanding of IOCG deposits. Porter Geoscience Consultancy Publishing, Adelaide, p. 285–306.

Yardley, B.W.D., 2012. The chemical composition of metasomatic fluids in the crust. In Harlov, D.E. and Austrheim, H., eds., Metasomatism and the chemical transformation of rock. Lecture Notes in Earth System Sciences, p. 17–52.

Zhao, X., Ji, S., and Martignole, J., 1997. Quartz microstructures and c-axis preferred orientations in high-grade gneisses and mylonites around the Morin anorthosite (Grenville Province). Canadian Journal of Earth Sciences, v. 34, p. 819–832.

Zhao, X.-F., Zhou, M.-F., Su, Z.-K., Chen, W.-T., Li, X.-Chun, and Li, J.-W., 2017. Geology, geochronology, and geochemistry of the Dahongshan Fe-Cu-(Au-Ag) deposit, Southwest China: Implications for the formation of iron oxide copper-gold deposits in intracratonic rift settings. Economic Geology, v. 112, p. 603–628.

Amphibolite and garnetite within the Breccia Trail mineral occurrence, Bondy gneiss complex Grenville Province